Site-directed mutagenesis of *Hypericum* benzophenone synthases

Von der Fakultät für Lebenswissenschaften

der Technischen Universität Carolo-Wilhelmina

zu Braunschweig

zur Erlangung des Grades einer

Doktorin der Naturwissenschaften

(Dr. rer. nat.)

genehmigte

D i s s e r t a t i o n

von Sahar Abdelaziz Mohamed Abdelaziz
aus Sharkia, Ägypten

1.Referent: Professor Dr.Ludger Beerhues
2. Referentin Professor Dr.Ursula Bilitewski
eingereicht am: 17.02.2014
mündliche Prüfung (Disputation) am: 08.05.2014

Druckjahr 2014

Vorveröffentlichungen der Dissertation

Teilergebnisse aus dieser Arbeit wurden mit Genehmigung der Fakulät für Lebenswissenschaften, vertreten durch den Mentor der Arbeit, in folgenden Beiträgen vorab veröffentlicht:

Tagungsbeiträge

Abdelaziz, S., Liu, B., & Beerhues, L.: A single amino acid substitution converts benzophenone synthase from *Hypericum sampsonii* into 4-hydroxycoumarin synthase (Vortrag), Tagung der Sektion "Pflanzliche Naturstoffe" der Deutschen Botanischen Gesellschaft im Michaeliskloster Hildesheim ,Germany 30.09-02.10 2012

Acknowledgments

First and foremost, I would like to thank *ALLAH,* the lord of the worlds, the creator of the universe, and the source of knowledge, who gave me patience, support and power to complete this work.

Actually, it is a great pleasure to get this chance for expressing my sincere gratitude, thanks, appreciation and deep respect to my supervisor Professor Dr. *Ludger Beerhues* for giving me this opportunity to be a member in his research group and for the excellent work facilities at the Institute für Pharmazeutische Biologie, Technische Universität Braunschweig. Thank you ever so much for your continuous help, unforgettable support, precious advices and encouragement during this work. Through his positive attitude and heartiness, we felt like a family. I particularly owe him the suggestion of this interesting research point, which let me give my best. I remember that any of us could come to him with any problem or idea without fearing that he would not consider it. In fact, we will not find many people in this position with that kind of modesty and respectful character.

I am heartily thankful to Dr. *Benye Liu* for his continuous guidance, fruitful discussions, and valuable suggestions. I have never known you to say no when asking for help. I really appreciate how your office door was always open for all of us to come by and ask for anything at any time. A lot of thanks to Dr. *Rainer Lindigkeit* for his kind help with any software problems. My special thanks to Dr. *Till Beuerle* for his help with the chemical analysis and constructive discussions and advices during the chemical synthesis. I would like to express my great appreciation to Dr. *Marco Bocola* for performing the modeling work and contributing to the understanding of the mutagenesis results.

I would like to convey my thanks to my *past and present colleagues* and lab mates for the wonderful time we spent together, for their presence and assistance whenever needed. Thank you for being such an amazing group to work with. The variation of skills in our group helped me a lot during my laboratory work. I really appreciate the cooperative environment that we worked in and I will miss the friendship of everyone in the lab. I cannot forget to thank Mrs. *Ines Rahaus* and Mrs. *Doris Glindemann*. Thank you for keeping the funny atmosphere during the hard working days and for your kind help during my work. Thanks a lot for keeping things bright and colorful.

Many thanks to my *professors and colleagues* from the Pharmacognosy Department, Zagazig University, Zagazig, Egypt for offering me this chance to study in Germany. I am greatly thankful to the *Egyptian Government* for funding this mission.

Frankly, no words will be enough to express my greatest thanks and gratitude to everyone in my family especially my *mother* and my *father* for their continuous support and encouragement. Finally, I owe the success of this work to my *husband*, without his motivation it will be so difficult to go on in this journey. My cordial thanks to my *daughters*, they are the light of my eyes and their presence relieves the feeling with any difficulty in this life.

Contents

List of abbreviations

AaOKS	*Aloe arborescens* octaketide synthase
AaPCS	*Aloe arborescens* pentaketide synthase
AmQNS	*Aegle. Marmelos* quinolone synthase
APS	Ammonium peroxydisulfate
bp	Base pair
BSA	Bovine serum albumin
°C	Degree Celsius
cDNA	Complementary deoxyribonucleic acid
CePPS	*Centaurium erythraea* phenylpyrone synthase
CoA	Coenzyme A
DAD	Diode array detector
DNA	Deoxyribonucleic acid
dNTP	Deoxynucleoside triphosphate
eq	equivelant
g	gramme
Gh2PS	*Gerbera hybrida* 2pyrone synthase
h	hour
HaBPS	*Hypericum androsaemum* benzophenone synthase
HaCHS	*Hypericum androsaemum* chalcone synthase
HcBPS	*Hypericum calycinum* benzophenone synthase
H.l VPS	*Humulus lupulus* valerophenone synthase
HpaBPS	*Hypericum perforatum* spp *angustifolium* benzophenone synthase
HPLC	High Performance Liquid Chromatography
HsBPS	*Hypericum sampsonii* benzophenone synthase
HsCHS	*Hypericum sampsonii* chalcone synthase
HusPKS1	*Huperzia. serrata* polyketide synthase 1
IPTG	Isopropyl-β-D-thiogalactopyranoside
K_m	Michaelis-Menten constant
K_{cat}	Turnover number
K_{cat}/K_m	Catalytic efficiency

LB	Luria broth
m	milli
M	Molar
min	minute
ml	milliliter
MsCHS	*Medicago sativa* CHS2
Ni-NTA	nickel-nitrilotriacetic acid
nm	nanometer
OD	Optical density
PAGE	Polyacrylamide gel electrophoresis
PKS	Polyketide synthase
psi	pound per square inch
PsSTS	*Pinus sylvestris* stilbene synthase
RgACS	*Ruta graveolens* acridone synthase
RpALS	*Rheum palmatum* aloesone synthase
RpBAS	*Rheum palmatum* benzalacetone synthase
SDM-PCR	Site directed mutagenesis-Polymerase chain reaction
s	second
SaBIS	*Sorbus aucuparia* BIS
SDS	Sodium dodecyl sulfate
ssp	Sub species
TAE	Tris-acetate-EDTA
TEMED	N,N,N,N`-tetramethylethylenediamine
T_m	Melting temperature (primer)
UV	Ultraviolet

Amino acids

A	Ala	Alanine
C	Cys	Cysteine
D	Asp	Aspartic acid
E	Glu	Glutamic acid
F	Phe	Phenylalanine
G	Gly	Glycine
H	His	Histidine
I	Ile	Isoleucine
K	Lys	Lysine
L	Leu	Leucine
M	Met	Methionine
N	Asn	Asparagine
P	Pro	Proline
Q	Gln	Glutamine
R	Arg	Arginine
S	Ser	Serine
T	Thr	Threonine
V	Val	Valine
W	Trp	Tryptophan
Y	Tyr	Tyrosine

Nucleotides

A	Adenine
C	Cytosine
G	Guanine
T	Thymine
U	Uracil

1 Introduction

Recently plant type III-polyketide synthases (PKSs) became the target of numerous mutational studies, especially after crystal structure determination of some PKSs which showed an academic importance in addition to the essential role for the reasonable reconfiguration of these enzymes for the production of novel compounds (Staunton and Weissman, 2001; Lukacin et al., 2005). Several factors are related to the molecular variation of the polyketide products such as the choice of the starter substrate, the number of polyketide chain elongations, and the cyclization and aromatization reaction mechanism. Interestingly, only a few modifications of the active site appear to be needed to generate a remarkable functional diversity of the type III PKSs (Morita et al., 2001; Raja Abdul Rahman et al., 2012). In this study, site-directed mutagenesis of benzophenone synthase (BPS) from selected *Hypericum* species was carried out. BPS is one of the CHS-like enzymes which belong to plant PKSs. *Hypericum androsaemum* BPS (HaBPS) was the first BPS for which a cDNA was cloned from elicitor-treated cell cultures (Liu et al., 2003). Recently, BPSs from *Garcinia mangostana* and *Hypericum sampsonii* were published (Huang et al., 2012; Nualkaew et al., 2012). In addition, our work group isolated cDNAs for the enzymes from, the *Hypericum perforatum* ssp *angustifolium* and *Hypericum calycinum* (Zodi, 2011; Tocci, 2013). All these BPSs prefer benzoyl-CoA as a starter substrate, forming 2,4,6 trihydroxybenzophenone. Benzoyl-CoA is considered as a rare starter substrate for type III PKSs and it is used by microbial type I and II PKSs to form soraphen A and enterocin respectively (Moore, 2005). Using biochemical and molecular genetic studies in addition to homology modeling, efforts were carried out to investigate the effect of mutations on the substrate and product specificities of the BPSs from *H. sampsonii, H. androsaemum, H. perforatum* ssp *angustifolium* and *H. calycinum.*

1.1 Site-directed mutagenesis (SDM)

Site-directed mutagenesis is the targeted change of a gene to give a protein with a particular modification in its amino acid sequence. Actually, SDM is considered as a very powerful tool for the determination of the importance of specific amino acid residues in an enzyme. Comparative studies of the mutant enzymes with one another and with the wild-type provide valuable information about the role of particular amino acid residues in substrate binding, catalysis and enzyme stability. SDM is widely employed in studying protein structure-function relationships but one has to define which position in the wild-type should be mutated

and which mutations of this amino acid should be done. The residues to be mutated are chosen to clarify specific points about the mechanism of the enzymatic reaction or to make particular modifications in the properties of the enzyme. It is very vital to have a detailed 3D-structure of the enzyme or at least of an intimately linked enzyme on which the enzyme of interest should be modeled. Depending on the 3D-structure, some amino acids are essential for substrate binding or may have a role in catalysis and these amino acids would be the targets of mutation. Eventually amino acid sequence alignments provide precious information about the highly conserved amino acids which were supposed to play significant roles in structure or function of the enzyme. Upon amino acid replacements it should be taken into account that the substitution of an original amino acid with a smaller one will not source much interference in the overall protein structure while larger amino acids may cause steric interference (Price and Stevens, 1982).

1.1.1 Types of mutations

Many divergent ways could be used for modifying DNA leading to different mutation types. Some examples are point, neutral, silent, and nonsense mutations. Point mutation is a single amino acid exchange in which one base in a codon is displaced with another. Usually, base-exchange in the first and second codon positions results in the exchange of the amino acid and so eventually the function or structure of the protein. Neutral mutation is a mutation in which the base-exchange leads to the incorporation of an amino acid which is chemically related to the original one. Silent mutation leads to generation of a codon encoding the same amino acid and this kind of mutation is mainly used in molecular cloning experiments in order to create or remove a recognition site for restriction enzymes. Nonsense mutation is a change in which the single base substitution converts a sense codon into a nonsense (termination) codon. For example, TGG (tryptophane) to TGA (stop).This kind of mutation is considered harmful to the cell and may impair the cell function as it leads to earlier termination of the protein synthesis and accordingly formation of shortened proteins, which may not function at all. Briefly, all of the previously mentioned mutations are substitution mutations However; there is also insertion mutation, which means the addition of one or more base pairs into the gene of interest. The last type is deletion mutation, which means loss or removal of a DNA section (The University of California 2010; Rodnina et al., 2011).

1.1.1.1 Point mutation

In the current study, we only worked with point mutation, which leads to incorporation of a different amino acid residue in a particular position. Performing this procedure requires the

designing of two specific, modified, and relatively long primers to be able to specifically bind to the required position in which mutation should be done in the SDM-PCR reaction. Practically, several protocols are followed to get the desired mutations and all of them are based mostly on the QuikChange site-directed mutagenesis protocol (Stratagene, 2005). These protocols differ in their ways of designing the mutant primers and are mentioned in details in section (3.1.1).

1.2 Polyketides

1.2.1 History of polyketide research

Orcinol was the first famous polyketide isolated by Collie (1893) and a rough mechanism for the synthesis of orcinol and similar compounds was suggested based on their structure. As they are divergent from the previously described chemical classes, they are placed in a novel class called polyketides. Its compounds are characterized by the repetitive existence of (-CH_2-CO-) which was entitled as ketide. The ketide groups found in polyketides originate from acetate units derived from the primary metabolism of the producing organism and this was confirmed by radio labeling techniques (Frandsen, 2010).

1.2.2 Polyketide natural products

Polyketides are an amazing group of natural products displaying a fabulous variety of functional and structural diversity in addition to significant medicinal activities including antibiotic, antifungal, anti-parasitic, anticancer, and immunosuppressive properties. Over the last 50 years, the polyketide secondary metabolites and their semi-synthetic derivatives have executed a tremendous role notably in the medicinal field. Polyketides, and their synthesizing enzymes which are polyketide synthases (PKSs), represent an important study area attracting a lot of scientists principally in the biopharmaceutical research field due to the diversity in their biological activities. Noteworthy, the total market for polyketide natural products surpasses $10 billion annually and the defiance to find new drug candidates becomes a must notably after the resistance of organisms to many kinds of known molecules (Staunton and Weissman, 2001).

1.2.3 Polyketide synthases

Despite the great variation in the polyketide constructions all of them share a general approach in biosynthesis. They are synthesized by PKSs which are a group of enzymes structurally and functionally similar to fatty acid synthases (FASs). Both PKSs and FASs have a β-keto synthase (KS) activity that stimulates the successive head-to-tail addition of two-carbon

acetate units into a developing polyketide chain. In contrast to FASs, which carry out reduction and dehydration reactions on each formed β-keto carbon to yield an inert hydrocarbon, PKSs skip or change some of these latter reactions, and so resulting in a diversity of the polyketide chain. PKS enzymes selectively manipulate the reactivity of polyketide intermediates to support intramolecular cyclization, producing a remarkably varied yield of end products from basic acetyl precursors (Austin and Noel, 2003; Ainasoja, 2008).

1.2.4 Types of polyketide synthases

PKSs divide into type I, II, and III based on their number of subunits and mode of synthesis. Type I PKSs resemble the yeast and animal FASs, consisting of multi-domain polyproteins that form large multi-functional biosynthetic complexes and act in either a modular or iterative mode. Erythromycin biosynthesis in the bacterium *Saccharopolyspora erythraea* is an example of a modular type I PKS, while the biosynthesis of 6-methylsalicylic acid (6-MSA) in the fungus *Penicillium patulum* is carried out by an iterative, homotetrameric type I PKS (Austin and Noel, 2003). Principally, type II PKSs are multienzyme complexes composed of separated proteins, like the FAS type II systems found in plants and bacteria. In spite of the fact that type II polyketide enzymes are disconnected, and not certainly encoded in a linear mode within the genome, they are assumed to form complexes in vivo, similar to those of the type I PKS systems. Actinorhodin biosynthesis in *Streptomyces coelicolor* is catalyzed by a typical type II PKS (Austin and Noel, 2003; Frandsen, 2010). On the contrary, type III or CHS-like PKS enzymes, which are discussed in details in the following section, sustain a simple architecture, a homodimer of corresponding KS monomeric domains, making them much more liable to in vitro inspection and manipulation in addition to structural analyses. From recent structural studies it was suggested that type III PKS enzymes evolved by earning function from the structurally identical homodimeric KAS III which stimulates type II FAS biosynthesis by adding a single acetate unit to a small starter molecule by decarboxylative condensation with malonyl-ACP (Austin and Noel, 2003). Despite the similarity of the biosynthesis mechanism of type III PKSs with that of the modular type I and the dissociated type II PKSs, there are several significant differences. Most importantly, the simple homodimeric type III PKSs carry out a complete series of decarboxylation, condensation, cylization and aromatization reactions within a single active site cavity by using CoA-linked substrates without participation of the acyl carrier protein (ACP) which is mainly used by type I and II PKSs to shuttle substrates and intermediates among active sites (Staunton and Weissman, 2001).

1.2.5 Plant type III polyketide synthases

This group of enzymes generates the main skeleton of a large number of plant secondary metabolites with fascinating biological activities such as flavonoids, phloroglucinols, resorcinols, benzophenones, biphenyls, chromones, isocoumarins, 4-hydroxycoumarins, acridones, pyrones, curcuminoids, stilbenes, etc. They share 30–95% amino acid sequence identities with each other, but only 21–31% identity with type III PKSs of bacterial origin (Abe, 2008; Liu et al., 2010; Jeya et al., 2012). Type III plant PKSs are usually known as the chalcone synthase (CHS) superfamily as they were detected after the CHS enzyme. They catalyze the condensation of a CoA-ester starter with extender molecules mostly malonyl-CoAs to give a linear polyketide intermediate which is properly folded for cyclization to the end product. The starter substrate selection, the number of condensations, and the particular folding type lead to the great functional diversity of type III PKSs (Lukacin et al., 2005). Investigation of the biosynthesis variability of this group of enzymes suggests new procedures for expanding the resistance of plants to different infections in addition to the possible production of pharmaceutical drugs in genetically modified plants (Jez et al., 2001). A large number of functionally different plant type III PKSs have been cloned and characterized including stilbene synthase (STS) (Morita et al., 2001; Austin et al., 2004), acridone synthase (ACS) (Lukacin et al., 1999; Lukacin et al., 2001; Morita et al., 2007; Wanibuchi et al., 2007), benzalacetone synthase (BAS) (Abe et al., 2001; Abe et al., 2003; Abe et al., 2007; Shimokawa et al., 2010), 2-pyrone synthase (2PS) (Eckermann et al., 1998; Jez et al., 2000), aloesone synthase (ALS) (Abe et al., 2004; Abe et al., 2006), benzphenone synthase (BPS) (Liu et al., 2003; Huang et al., 2012; Nualkaew et al., 2012), biphenyl synthase (BIS) (Liu et al., 2004; Liu et al., 2007; Liu et al., 2010), and quinolone synthase (QNS) (Resmi et al., 2013). In addition, various bacterial type III PKSs were also cloned and characterized such as 1,3,6,8-tetrahydroxynaphthalene synthase (THNS or RppA) from *Streptomyces coelicolor* and *Streptomyces griseus* (Izumikawa et al., 2003) and PhlD from *Pseudomonas fluorescens* which catalyzes the formation of phloroglucinol from three molecules of malonyl-CoA (Zha et al., 2006). Most of the previously cited type III PKSs, especially those which are referred to in the current study will be discussed in more details in the next sections.

1.2.5.1 Type III PKSs preferring aromatic starters

- **Chalcone synthase (CHS)**

Chalcone synthase is the most famous member of type III PKSs in plants, of course due to its main role in initiating flavonoids biosynthesis as it provides chalcone to a group of downstream enzymes, which modify it to produce a large number of flavonoids end products. These metabolites are important biologically active compounds used as antimicrobial phytoalexins, anthocyanin pigments, UV photo-protectant, and inducers of symbiotic root nodulation by *Rhizobium* bacteria leading to nitrogen fixation (Jez et al., 2000; Austin and Noel, 2003). Flavonoids are the majority ample polyphenols present in the human diet and are the main components of many herbal products. A lot of studies have suggested that a high intake of flavonoids may help in decreasing the risk of cancer, coronary diseases, and osteoporosis in addition to its antiallergenic, antiviral, anti-inflammatory, vasodilating, and antioxidant activities (Pietta, 2000; Zhang et al., 2004; Raja Abdul Rahman et al., 2012). CHS catalyzes the iterative condensation of one starter molecule of *p*-coumaroyl-CoA with three extender molecules of malonyl-CoA in the same active site, followed by intramolecular cyclization and aromatization which result in chalcone formation (Fig. 1). The crystal structure of CHS2 alone and complexed with substrates and products was determined by Ferrer et al. (1999), and these structures provide the basis for understanding the biosynthesis of various polyketides.

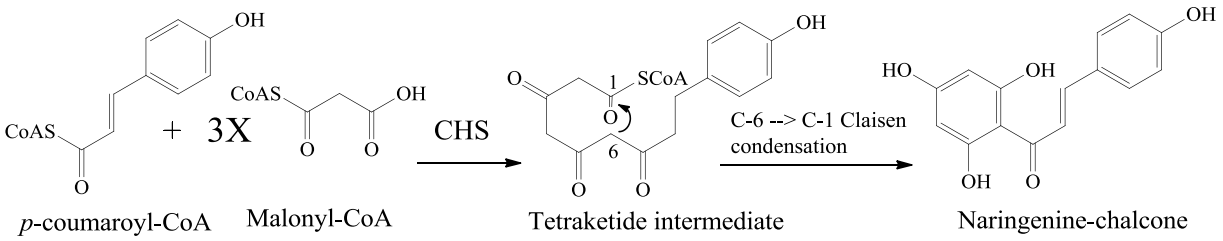

Fig. 1 Chalcone synthase (CHS) reaction mechanism

- **Benzophenone synthase (BPS)**

This enzyme is the focus of the present study, so it will be explained in more details. The pivotal reaction in xanthones and benzophenones biosynthesis is the formation of the C_{13} skeleton which is catalyzed by benzophenone synthase (BPS). Liu et al. (2003) cloned and characterized the first BPS from *Hypericum androsaemum* (Clusiaceae) cell cultures (EC

2.3.1.151). It is a homodimer with a molecular mass of 42.8 kDa catalyzing iterative condensations of one molecule of benzoyl-CoA with three molecules of malonyl-CoA to form a linear tetraketide intermediate which is cyclized into 2,4,6-trihydroxybenzophenone by C6→C1 intramolecular Claisen condensation (Fig. 2) (Liu et al., 2003). In contrast, BPS from *Centaurium erythraea* (Gentianaceae) accepts and prefers 3-hydroxybenzoyl-CoA as a starter substrate catalyzing the formation of 2,3',4,6-tetrahydroxybenzophenone after three malonyl-CoA extensions (Beerhues, 1996). Recently *G. mangostana* and *H. sampsonii* BPSs were found to also accept 2-hydroxybenzoyl-CoA as a minor substrate forming 4-hydroxycoumarin (Huang et al., 2012; Nualkaew et al., 2012). This observation is similar to *Sorbus. aucuparia* biphenyl synthases with salicoyl-CoA as starter substrate (Liu et al., 2010). Trihydroxy and tetrahydroxybenzophenones (Fig. 3) are the building blocks of xanthones and prenylated benzophenone derivatives which are considered as an important group of phenolic natural products with fascinating pharmacological activities such as anti-HIV, antimicrobial, anti-inflammatory, and antioxidant properties of guttiferone F in addition to the anticancer activity of garcinol (Fig. 3). These polyprenylated benzophenones are restricted in their occurrence to the family Guttiferae = Clusiaceae (Liu et al., 2003; Klundt et al., 2009). Other structurally complicated benzophenone derivatives are sampsoniones (Fig. 3) which were isolated from the Chinese medicinal plant *Hypericum sampsonii*. They showed cytotoxic activity and are characterized by unique caged tetracyclic skeletons (Hu and Sim, 2000). In addition to polyprenylation, intramolecular cyclization of benzophenones to form xanthones is a second choice, as tetrahydroxybenzophenone could be converted to 1,3,5- and 1,3,7-trihydroxyxanthones by regiospecific oxidative phenol coupling catalyzed by cytochrome P450 enzymes (Peters et al., 1997). 1,3,5-Trihydroxyxanthone is the precursor of psorospermine which is found in the African medicinal plant *Psoropermum febrifugum* and shows significant activity against drug resistant human leukaemia cell lines and AIDS-related lymphoma (Habib et al., 1987; Kwok and Hurley, 1998). This DNA-alkylating topoisomerase II agent is considered as a lead in the design of new anti-cancer drugs. 1,3,7-Trihydroxyxanthone is the precursor of rubraxanthone (Fig. 3) which was isolated from *Garcinia mangostana* and showed antibacterial activity against methicillin-resistant *Staphylococcus aureus* even higher than the antibiotic vancomycin (Liu et al., 2003). Ultimately, gambogic acid (GA) is a famous example of a bridged polycyclic xanthone. Recently, it was reported that GA has anticancer effect and inhibits the growth of multiple types of human cancer cells in vitro and in vivo. It is isolated from approved Chinese herbs that are used for clinical trials in cancer patients by the Chinese Food and Drug

Administration. GA efficiently inhibits tumor growth with minimal side effects and with little toxicity on the immune system (Klundt et al., 2009; Li et al., 2013). Transformation of BPS into a functional phenylpyrone synthase (PPS) was done by point mutation in the active site cavity (Thr135Leu) (Klundt et al., 2009). The *H. androsaemum* T135L mutant (PPS) catalyzed formation of 4-hydroxy-6-phenyl-pyrane-2-on after two malonyl-CoA extensions of benzoyl-CoA followed by C5-oxy→C1 lactonization (Fig. 2). PPS may be a promising biotechnological implement for manipulating benzoate-primed biosynthetic pathways for the production of new compounds (Klundt et al., 2009).

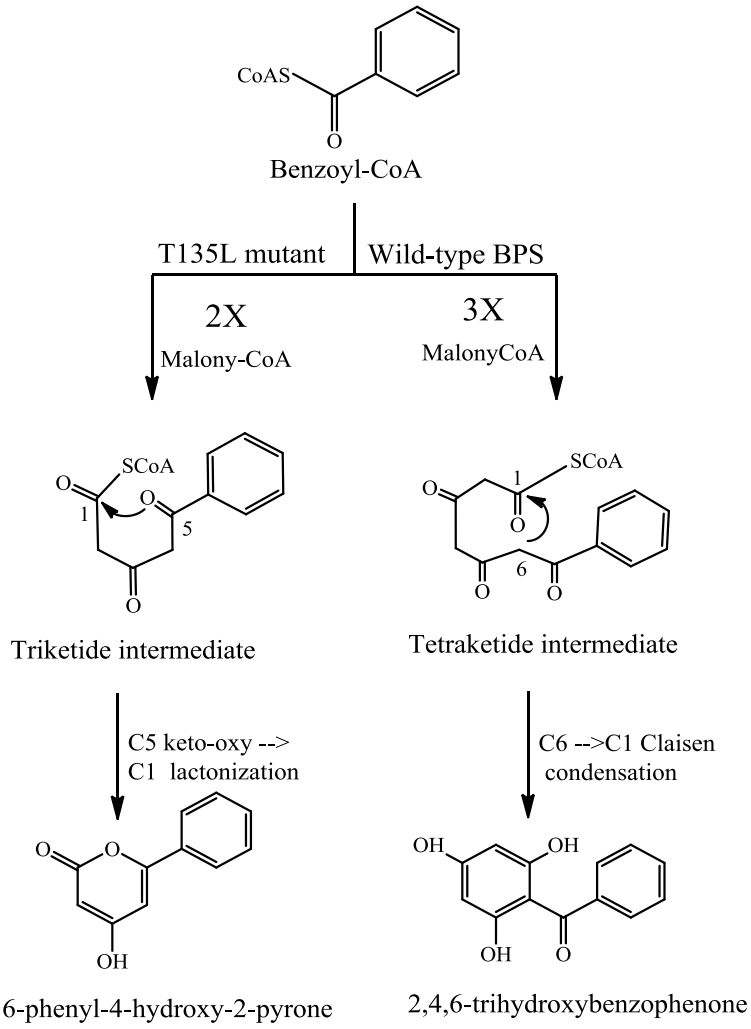

Fig. 2 Reaction mechanism of *H.androsaemum* benzophenone synthase (HaBPS) wild-type and the HaT135L mutant (PPS)

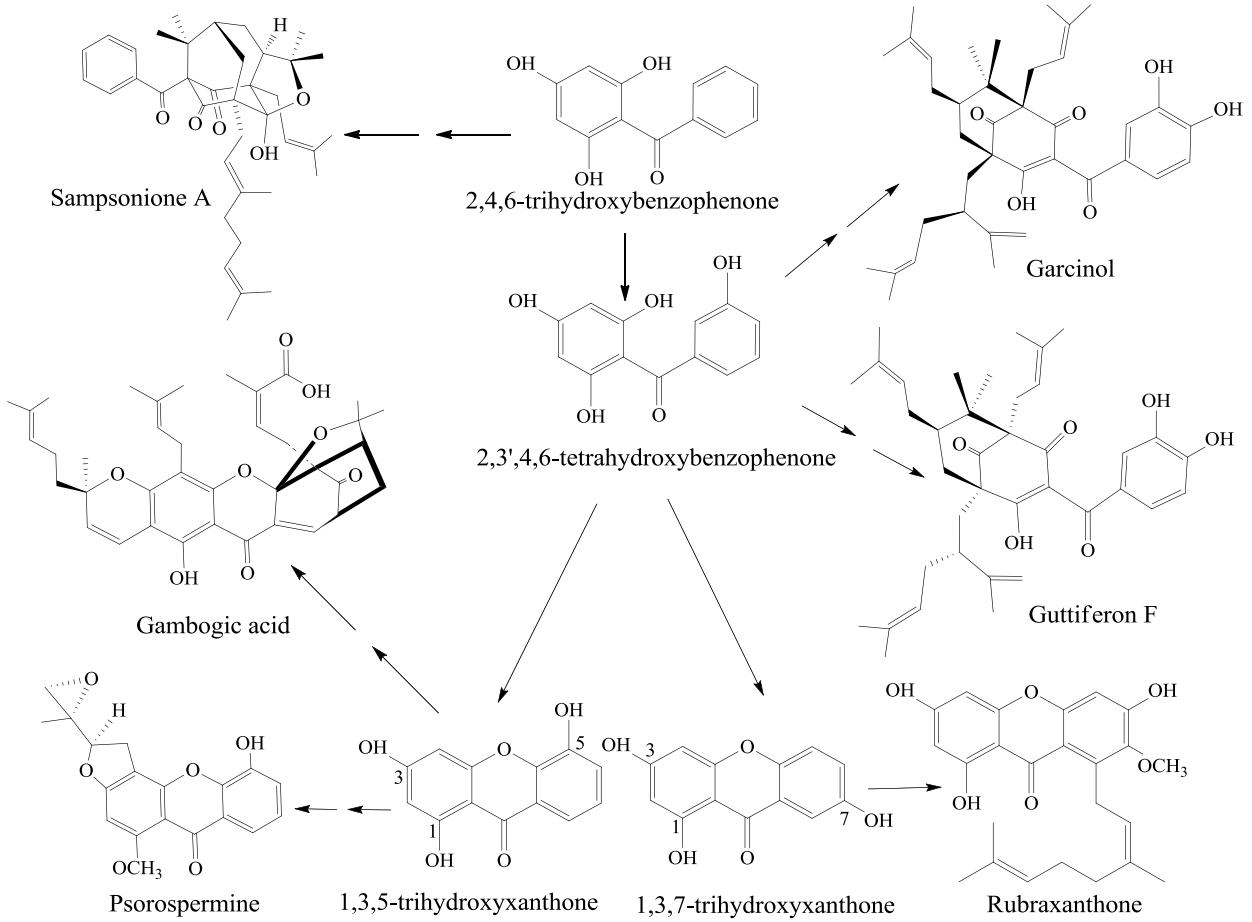

Fig. 3 Examples of biologically active benzophenone derivatives modified from; Liu et al., (2003); Klundt et al., (2009).

- **Biphenyl synthase (BIS)**

BIS is the second type III PKS, which accepts and prefers the rare starter substrate, benzoyl-CoA, after the previously mentioned BPS. It is the key enzyme responsible for the synthesis of the C_{12} skeleton of bipehnyls and dibenzofurans. It shares 53–66% amino acid sequence identity with other plant type III PKSs. The BIS activity was first detected in yeast-extract-treated *S. aucuparia* cell cultures (Liu et al., 2004). The cDNA for biphenyl synthase was also cloned and characterized by Liu et al., (2007). The enzyme catalyzes the iterative condensation of benzoyl-CoA with three malonyl-CoAs to form a tetraketide intermediate which undergoes intramolecular C2→C~~7~~ aldol condensation with the removal of a carboxyl group to yield 3,5-dihydroxybiphenyl (Fig. 4, A). This product is considered as the precursor of all biphenyls and dibenzofurans, which are the phytoalexins of the Pyrinae (formerly Maloideae), a subtribe of the economically important Rosaceae. This family includes valuable fruit trees such

as apple and pear. 3-Hydroxybenzoyl-CoA was also accepted but the product formed was 3-hydroxybenzoyl diacetic acid lactone after two malonyl-CoA extensions. In contrast, upon replacement of benzoyl-CoA with salicoyl-CoA as a starter substrate the enzyme catalyzes a single decarboxylative condensation with malonyl-CoA to form an intermediate diketide, which undergoes intramolecular cyclization via nucleophilic attack of the phenol group on the CoA- or cysteine-tethered C-1 thioester, yielding 4-hydroxycoumarin after enolization (Fig. 4, B). Subsequently, two cDNAs encoding additional isoenzymes (BIS2, BIS3) were cloned and characterized (Liu et al., 2010). They prefer salicoyl-CoA over benzoyl-CoA as a starter substrate. Notably, no 4-hydroxycoumarin was identified in the cell cultures of *S. aucuparia* possibly due to the unavailability of salicoyl-CoA as endogenous substrate. 4-Hydroxycoumarin could be detected only after feeding of the cell cultures with salicoyl-NAC, with N-acetylcysteamine (NAC) mimicking the activation by coenzyme A (Fig.4, C). This showed that formation of 4-hydroxycoumarin in vivo could be one of the BIS functions in the plant and is not only a side reaction of BIS with a non-physiological starter substrate (Schröder, 2009; Liu et al., 2010), as these derailment reactions are well-known for type III PKSs. The role of BIS in 4-hydroxycoumarin formation is significant because some plant species of the Apiaceae (*Ferula communis*) and Asteraceae (*Gerbera jamesonii*) contain 4-hydroxycoumarin or its derivatives independent of the action of microorganisms. It is a good idea that plant type III PKSs might be involved (Schröder, 2009; Liu et al., 2010). Finally, the BIS reaction corresponds to the benzalacetone synthase (BAS) reaction that is recommended as a prospect for a type III PKS activity in the quinolone alkaloids biosynthesis, which was proved recently by cloning and characterization of *Aegle marmelos* quinolone synthase (QNS) which will be discussed in details in a later section (Abe et al., 2006; Resmi et al., 2013).

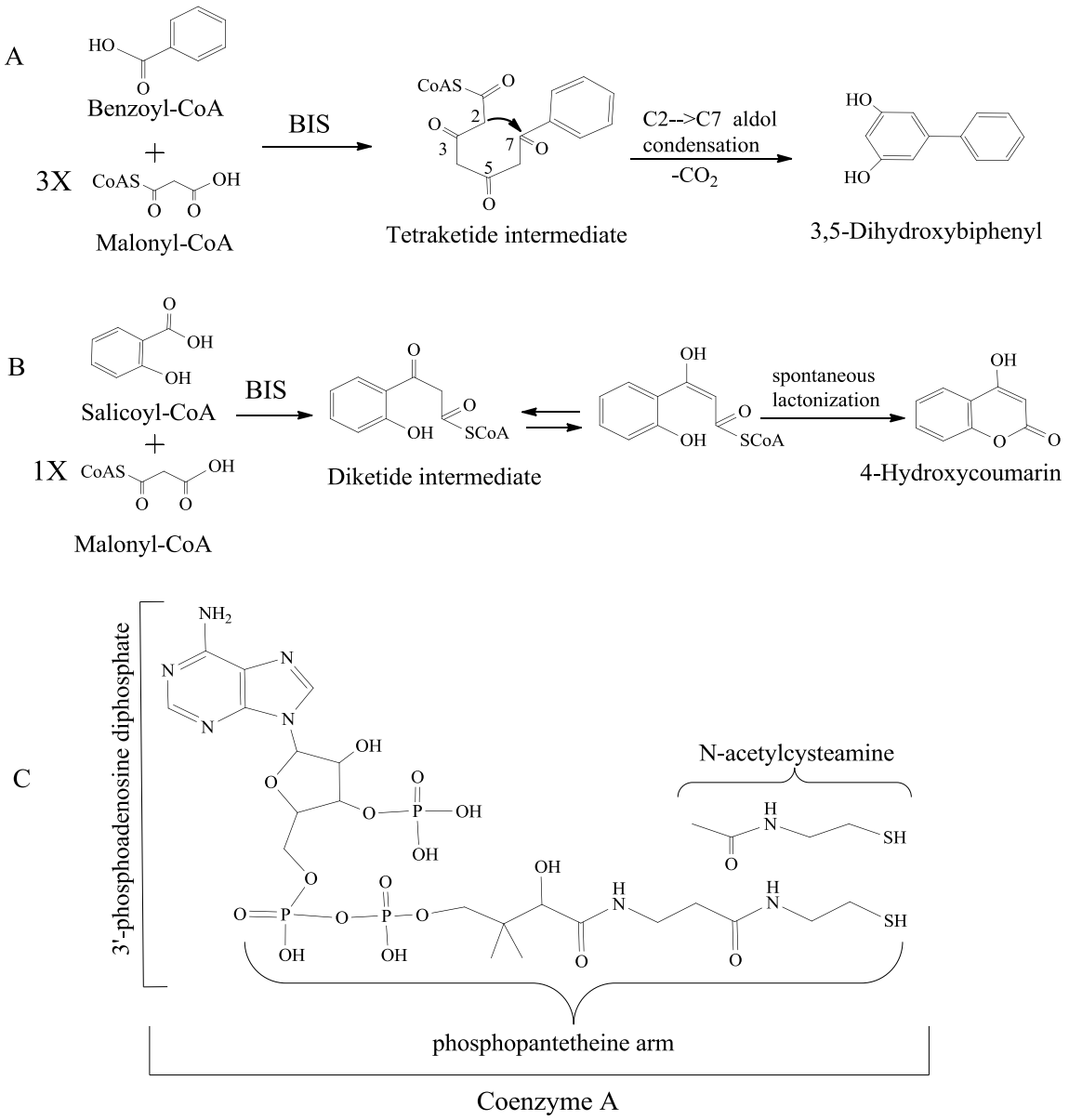

Fig. 4 Reaction mechanism of biphenyl synthase, A: with benzoyl-CoA, B: with salicoyl-CoA (Liu et al., 2010), C: Structure comparison of coenzyme A and *N*-acetylcysteamine 'NAC' (Austin and Noel, 2003).

- **Stilbene synthase (STS)**

Stilbene synthases (STSs) are CHS-like enzymes which synthesize an identical linear tetraketide intermediate (from *p*-coumaroyl-CoA and three malonyl-CoAs) as CHS. However, where CHS cyclizes this intermediate using an intramolecular Claisen condensation between carbons C6→C1 (numbering from the cysteine thioester), STS forms resveratrol via linking C2→C7 by intramolecular aldol condensation with additional decarboxylative loss of the C1 carbon as CO_2 (Fig. 5). Both STS and CHS displayed over 50% amino acid sequence identity

besides the presence of the same amino acid residues in the active site and around the substrate entrance cavity although catalyzing the formation of different products from the same tetraketide intermediates (Austin and Noel, 2003; Abe and Morita, 2010; Gleason and Chollet, 2012). The first STS protein purification was carried out from induced cell suspension cultures of peanut (*Arachis hypogaea*). Subsequently, STS genes and cDNAs were cloned from grape (*Vitis vinifera*) and scots pine (*Pinus sylvestris*). Resveratrol (3,4',5-trihydroxystilbene) belongs to a category of polyphenolic compounds called stilbenes which are produced in some plants in response to injury, stress, fungal infection, or UV radiation. They are widespread but not universally distributed in higher plants and have antioxidant activity, prevent blood platelet aggregation and lipid peroxidation, and exhibit anti-inflammatory activity, vasodilation, and anti-cancer properties (Higdon, 2008). This class of polyphenolic compounds became a hot research area especially after the first report about the presence of resveratrol in red wine, which led to the famous postulation that resveratrol might be the explanation of the so-called 'French Paradox' which is the low mortality rate by coronary heart diseases in France despite high saturated fats dietary levels (Gleason and Chollet, 2012). In addition, stilbenes are known for their agricultural properties like increased resistance to fungal infection of transgenic plants encoding STS gene (Austin and Noel, 2003).

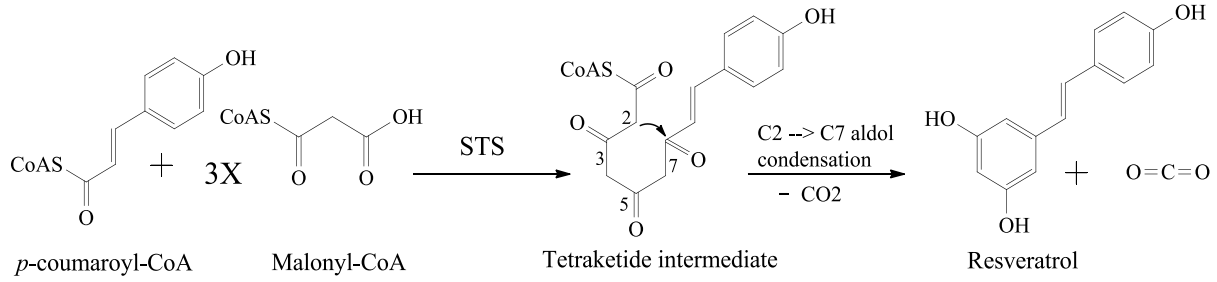

Fig. 5 Reaction mechanism of stilbene synthase (STS).

- **Benzalacetone synthase (BAS)**

Benzalacetone synthase (BAS) is another interesting example of plant type III PKSs. It is the key enzyme in the biosynthesis of the C6–C4 skeleton of the biologically active phenylbutanoids, such as raspberry ketone (*p*-hydroxyphenylbutan-2-one, pHPB) (Fig. 6, A), which grants the specific aroma of raspberries, *Rubus idaeus* (Borejsza-Wysocki and Hrazdina, 1996) and the anti-inflammatory glucoside lindleyin (Fig. 6, A) in rhubarb, *Rheum palmatum* (Abe et al., 2001). Up to date, cloning of five BAS-encoding cDNAs have been reported: *Rheum*

palmatum RpBAS (Abe et al., 2001), *Wachendorfia thyrsiflora* WtPKS1 (Brand et al., 2006), *Rubus idaeus* RiPkS4 (Zheng and Hrazdina, 2008), and *Polygonum cuspidatum* PcPKS1 and PcPKS2 (Ma et al., 2009; Ma et al., 2009). BAS catalyzes a single decarboxylative condensation of malonyl-CoA with *p*-coumaroyl-CoA to give a linear diketide intermediate which after decarboxylation produces *p*-hydroxyphenylbut-3-en-2-one (*p*-hydroxybenzalacetone), which undergoes hydrogenation of the aliphatic double bond by a NADPH-dependent benzalacetone reductase to form pHPB (Fig. 6, A). RpBAS showed broad substrate specificity as it accepts various non-physiological substrates to produce a set of chemically and structurally diverse unnatural polyketides such as 1-(4-hydroxyphenyl) pent-1-en-3-one which is an unnatural novel diketide produced from condensation of methyl-malonyl-CoA as extender substrate with 4-coumaroyl-CoA as starter (Fig. 6, B) (Abe et al., 2002). Notably, RpBAS also accepts methylmalonyl-CoA as a sole substrate to form a methylated C9 triketide pyrone, 6-ethyl-4-hydroxy-3,5-dimethyl-2-pyrone as a single product from three molecules of methylmalonyl-CoA (Fig. 6, C) (Abe et al., 2006). Most notable is the formation of 4-hydroxy-2(1*H*)-quinolones (Fig. 6, D) by RpBAS from the condensation of *N*-methylanthraniloyl-CoA with one molecule of either malonyl-CoA or methylmalonyl-CoA. The RpBAS enzymatic reaction with the anthraniloyl starter proceeds without the decarboxylation step as amide formation takes place immediately after the condensation reactions with malonyl-CoA. Remarkably, the best yield was obtained with the combination of *N*-methylanthraniloyl-CoA and methylmalonyl-CoA. The steady-state kinetics for the formation of 4-hydroxy-1,3-dimethyl-2(1*H*)-quinolone revealed a K_m = 23.7 μM and a K_{cat} =1.48 min−1 for *N*-methylanthraniloyl-CoA, which were comparable to those for the formation of benzalacetone. This suggests the presence of an unidentified novel type III PKS that produces quinolones from the CoA thioester of anthranilic acid (Abe et al., 2006).

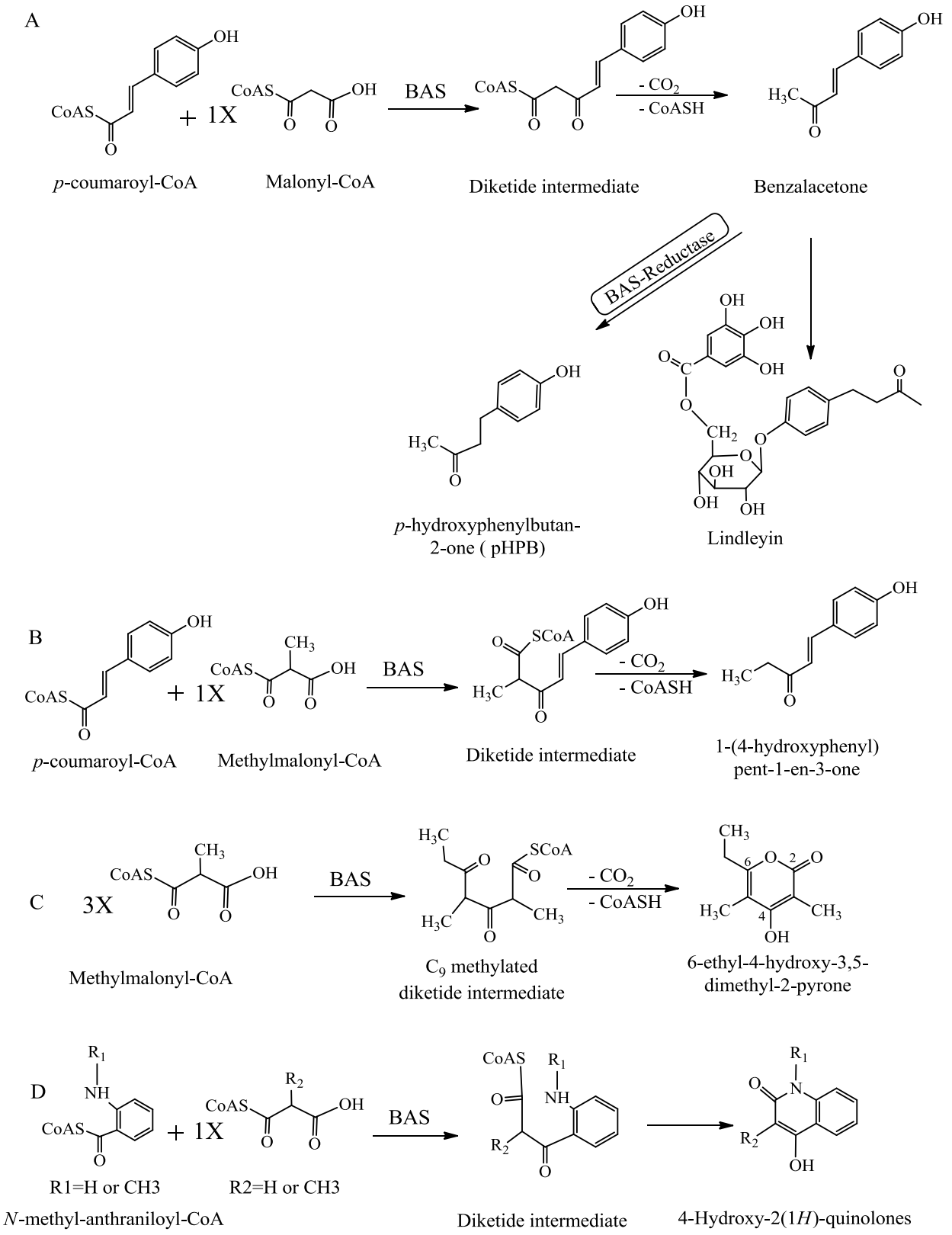

Fig. 6 The proposed mechanisms for A: benzalacetone formation by *R. palmatum* BAS, B: C_6–C_5 diketide formation, C: formation of methylated C_9 triketide pyrone, D: diketide quinolones formation. adapted from Abe, (2012).

- **Acridone synthase (ACS)**

Acridone alkaloids derived from anthranilic acid are considered as an interesting class of secondary metabolites due to their important biological activities and their biosynthesis mechanism. This group of secondary metabolites including around 100 naturally known acridone alkaloids, such as melicopicine, acronycine and rutacridone (Fig. 7, C) is mainly present in the family Rutaceae (Austin and Noel, 2003; Schröder, 2009). Recently, this group of alkaloids is being intensively studied as potent anticancer drugs due to their planar structure which facilitates DNA and RNA strands intercalation, in addition to their hydrophilic-lipophilic balance which helps in crossing the biological membranes to reach the nucleus in which they perform their effect. In vitro results of this group of compounds are promising; however, their clinical application may be restricted due to their significant side effects. They also showed various biological activities such as anti-bacterial, anti-protozoal, and anti-HIV activities (Cholewinski et al., 2011; Srikanth G. et al., 2013). The key enzyme which is responsible for the synthesis of the acridone skeleton is acridone synthase (ACS), which is another CHS-like enzyme. ACS catalyzes three malonyl-CoA condensations with one molecule of *N*-methylanthraniloyl-CoA starter, followed by Claisen condensation reaction of the formed tetraketide intermediate and C–N linkage by a nucleophilic addition reaction, dehydration and enolization leading to formation of the stable aromatic 1,3-dihydroxy-*N*-methylacridone (Fig. 7, A) (Dewick, 2002; Austin and Noel, 2003; Schröder, 2009). Several ACS isoenzymes have been cloned from either elicited or irradiated cell cultures or immature flowers of *R. graveolens*, after the purification of the first ACS from the cell suspension culture of the same plant. Determination of the amino acid residues which are responsible for substrate specificity difference between ACS and CHS requires many efforts. Noteworthy, the ACS wild-type showed around 15% CHS-like activity in vitro forming naringenin chalcone from *p*-coumaroyl-CoA while *N*-methylanthraniloyl-CoA was not accepted as a substrate for RgCHS nor any other known CHS or STS. While there were around 100 different amino acid residues between ACS and CHS only three of them were lining the active site cavity. Due to the ACS side activity with *p*-coumaroyl-CoA it was quite easy to increase its CHS-like side activity by mutation of these three amino acids in the ACS active site to their CHS corresponding amino acids (S132T, A133S and V265F). This effort completely transformed ACS to a functional CHS with relatively low side ACS activity while the corresponding reverse CHS triple mutant was not successful. It is important to mention that, the RsACSV265F single mutant impaired the ACS-like activity and did not improve the CHS-like

activity. The MsCHSF215S mutant was surprising in accepting *N*-methylanthraniloyl-CoA as a substrate and carrying out three condensation reactions with malonyl-CoA but it formed *N*-methylanthraniloyltriacetic acid lactone (Fig. 7, A) instead of acridone as the unsuccessful CHS-type ring-folding usually results in a pyrone-type product. Due to the enlargement of the active site entrance the MsCHSF215S mutant accepted the bulky *N*-methylanthraniloyl-CoA substrate (Jez et al., 2002; Austin and Noel, 2003; Schröder, 2009). Ultimately, Wanibuchi et al. (2007) cloned HusPKS1 from the Chinese club moss *Huperzia serrata* (Huperziaceae) which is a new multifunctional type III PKS that accepts bulky starter substrates like 4 methoxycinnamoyl-CoA and *N*-methylanthraniloyl-CoA forming 4-methoxy-2',4',6'-trihydroxychalcone and 1,3-dihydroxy-*N*-methylacridone respectively after three malonyl-CoAs condensation. Remarkably, this is the first enzymatic formation of acridone alkaloid by a type III PKS from a non-Rutaceae plant. As mentioned before, ACS from *R. graveolens* is the only characterized type III PKS that accepts *N*-methylanthraniloyl-CoA and forms acridone alkaloids which restrict to plants of the family Rutaceae. *H. serrata* PKS1 shared only 44-66% identity with other plant type III PKSs and showed in vitro broad substrate specificity as it accepts aromatic and aliphatic substrates but not all of the products showed the completed CHS-type ring folding. Nearly all kinds of pyrone products after one, two or three condensation reactions were detected. Notably, *H. serrata* PKS1 produces *N*-methylacridone after three malonyl-CoA condensations with *N*-methylanthraniloyl-CoA and in addition the diketide quinolone (4-hydroxy-1-methyl-2(1*H*)-quinolone) beside triketide and tetraketide lactone derailment products (Fig. 7, B). It is probable that *H. serrata* PKS1 has a larger starter substrate binding pocket as active site and guides the Claisen-type aromatic ring formation reaction of the tetraketide intermediate.

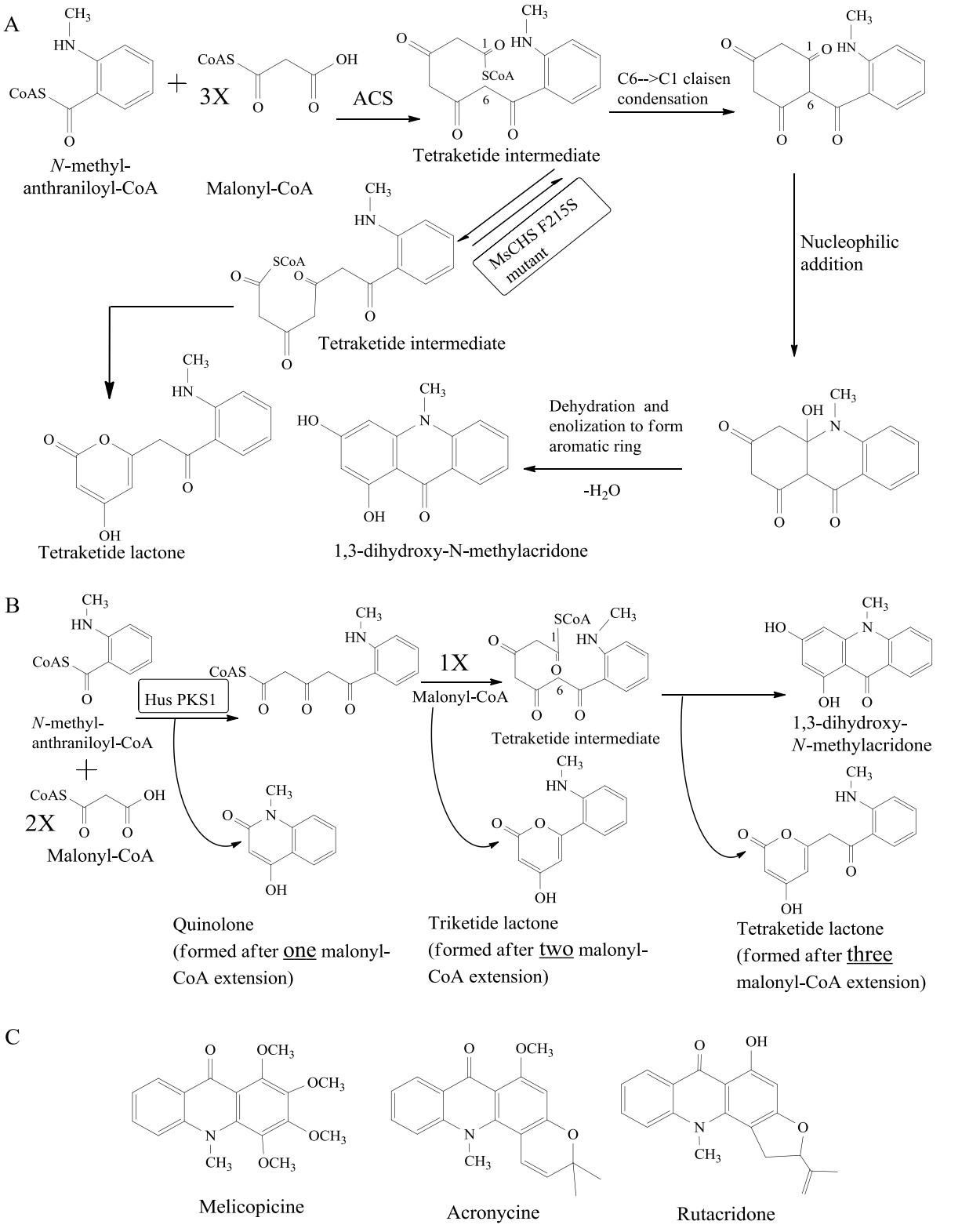

Fig. 7 Reaction mechanisms of A: acridone synthase (ACS) and the *M. sativa* CHS F215S mutant, B: *H.serrata* PKS1. C: Examples of some acridone alkaloid derivatives.

- **Quinolone synthase (QNS)**

Very recently, Resmi et al. (2013) cloned and characterized a new type III PKS from *Aegle marmelos* (Rutaceae) which is named quinolone synthase (QNS) depending on its activity. It catalyzes decarboxylative condensation of malonyl-CoA with *N*-methylanthraniloyl-CoA to form an intermediate which cyclized spontaneously by amide formation to form 4-hydroxy-2(1*H*)-quinolone (main product 89%) and acridone (minor product 11%). QNS also accepts *p*-coumaroyl-CoA and forms benzalacetone. The whole reactions catalyzed by QNS enzyme are summarized in (Fig. 8). Interestingly, besides the diketide condensation the QNS wild-type displays a minor tetraketide condensation leading to acridone formation like ACS. But under most of the experimental conditions, QNS favours stopping of the chain extension at the diketide stage and quinolone alkaloid formation which supports a different reaction mechanism of this novel PKS (Resmi et al., 2013). The most interesting point is that RpBAS also accepts *N*-methylanthraniloyl-CoA and forms quinolone alkaloids but up to date no quinolone alkaloids have been isolated from *R. palmatum* (Polygonaceae) they are mainly restricted to Rutaceae. So the physiological role of BAS in quinolone alkaloid biosynthesis still open. Meanwhile the QNS from *A. marmelos* which is a Rutaceous plant rich in quinolone and acridone alkaloid derivatives is a more physiologically new type III PKSs catalyzing quinolone biosynthesis. In *A. marmelos* QNS T132, S133 and F265 amino acid residues lining the active site of MsCHS are replaced by S132, A133, and V265 in QNS. These amino acids line the active site cavity of QNS and are not conserved in other PKSs except ACS. Replacement of S132 to T and A133 to S in a QNS double mutant (S132T/A133S) completely transformed QNS into a functional CHS which completely lost the ability to accept *N*-methylanthraniloyl-CoA. This could be postulated as an active site cavity constriction by the introduction of a methyl group in T132 residue. The smaller size of the substrate-binding pocket of the double mutant when compared to the wild QNS did not allow for bulky starter substrate binding and consequently prevented quinolone or acridone formation. Eventually, this new type III PKS which is involved in quinolone formation is similar to SaBISs which perform the same mechanism with salicoyl-CoA and form 4-hydroxycoumarin after only one malonyl-CoA condensation reaction and that expands the extent of functional diversity of type III PKSs family members (Liu et al., 2010).

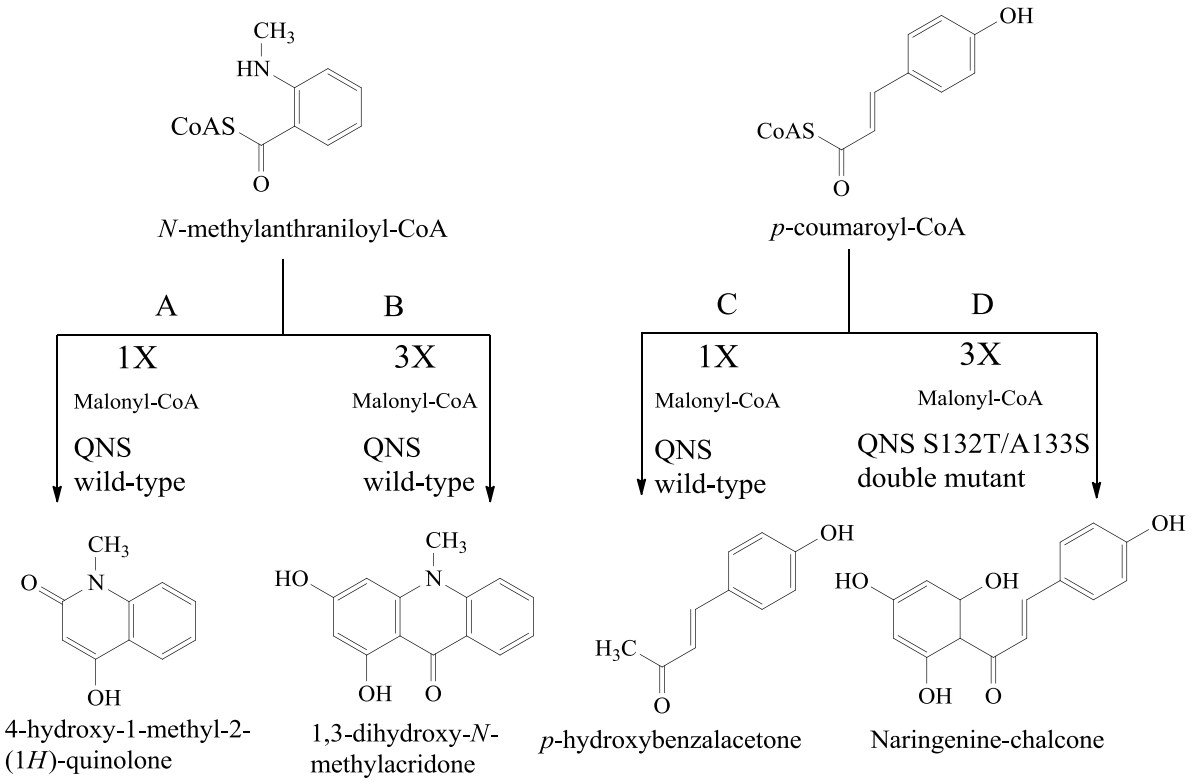

Fig. 8 Reactions catalyzed by quinolone synthase (QNS).

1.2.5.2 Type III PKSs preferring aliphatic starters

- **Valerophenone synthase (VPS)**

Humulus lupulus (hop) used since long time in beer preparation as a stabilizing agent due to its bitter acids constituents such as humulone (Fig. 9) and lupulone. VPS is the key enzyme responsible for the bitter acids skeleton formation in hop. It is another example of a type III PKS that accepts aliphatic starter substrates such as isovaleryl or isobutyryl-CoAs catalyzing their condensation with three molecules of malonyl-CoA to form a tetraketide intermediate which undergoes C6→C1 Claisen condensation and formation of phlorisovalerophenone or phlorisobutyrophenone respectively (Fig. 9). The enzyme products undergo stepwise prenylation reactions and formation of the bitter acids natural products. Unlike CHS enzymes which accept isovaleryl-CoA in vitro forming a mixture of phlorisovalerophenone and a triketide lactone as a side product, hop VPS did not accept *p*-coumaroyl-CoA as a starter substrate (Zuurbier et al., 1998; Austin and Noel, 2003). Amino acid sequence comparison of the cloned VPS from hop and CHS showed important differences near the starter substrate-binding pocket such as replacement of threonines at positions 132 and 197 which are conserved in CHSs with glycine

and isoleucine respectively in VPS. However, VPS cloned from *Psilotum nudum* (a primitive vascular plant) has serines at positions 132 and 197 and a valine at position 338 which is serine in CHSs hops VPS, and all other plant type III enzymes which catalyze the CHS-like intramolecular Claisen cyclization (except BPS). So it seems that the VPS reaction proceeds based on various active site configurations (Austin and Noel, 2003).

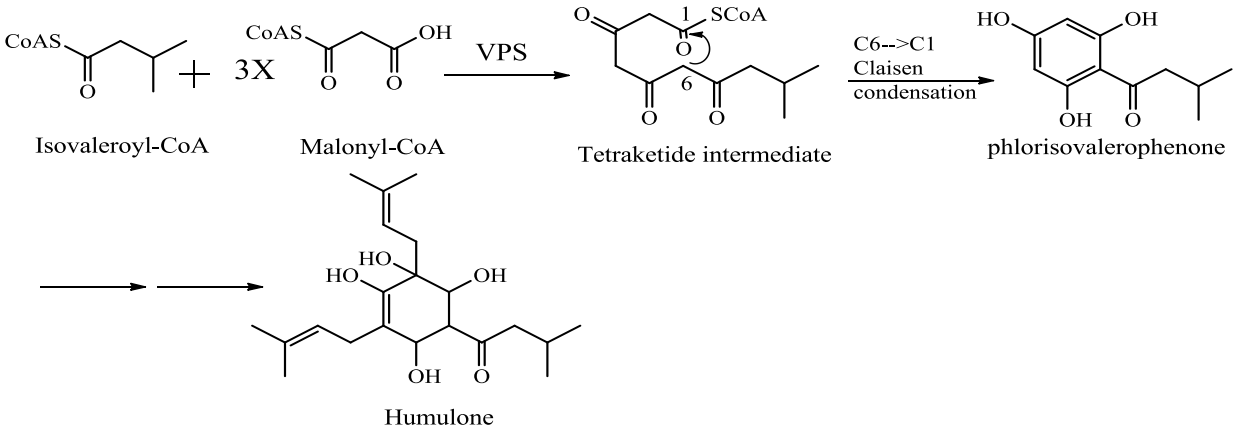

Fig. 9 Reaction mechanism of valerophenone synthase (VPS).

- **Isobutyrophenone synthase (BUS)**

Hyperforin which is a polyprenylated acylphloroglucinol derivative and its homologue adhyperforin (Fig. 10) are present mainly in the aerial parts especially flowers and fruits of *H. perforatum* and exhibit similar pharmacological properties. Their biosynthesis is still open at least at the molecular level. Feeding experiments revealed that a type III PKS with either isobutyryl-CoA (hyperforin) or 2-methylbutyryl-CoA (adhyperforin) synthesizes the phloroglucinol part (Karppinen et al., 2007; Schröder, 2008). BUS is considered as the key enzyme in the formation of the hyperforin and adhyperforin skeletons and it was detected in cell-free extracts of *H. calycinum* cell cultures (Klingauf et al., 2005). The enzyme catalyzes the condensation of one molecule of the starter isobutyryl-CoA or 2-methylbutyryl-CoA with three molecules of the extender malonyl-CoA to give phlorisobutyrophenone or 2-methylbutyrophenone respectively (Fig. 10). These intermediates then undergo stepwise prenylation to give hyperforin and adhyperforin. It seems that 2-methylbutyryl-CoA is the preferred starter substrate in cell cultures of *H. calycinum* as they mainly contain adhyperforin (Klingauf et al., 2005). VPS (1.2.5.2) is the enzyme which is functionally similar to BUS. As mentioned, VPS is responsible for the biosynthesis of the backbone of bitter acids in *H. lupulus*.

In both species, *H. lupulus* and *H. calycinum* the PKS products undergo stepwise prenylation to give bitter acids and hyperforins respectively so it will be interesting after BUS sequence determination to compare it with the VPS sequence from hop (*H. lupulus*) which also accepts isobutyryl-CoA as a starter substrate.

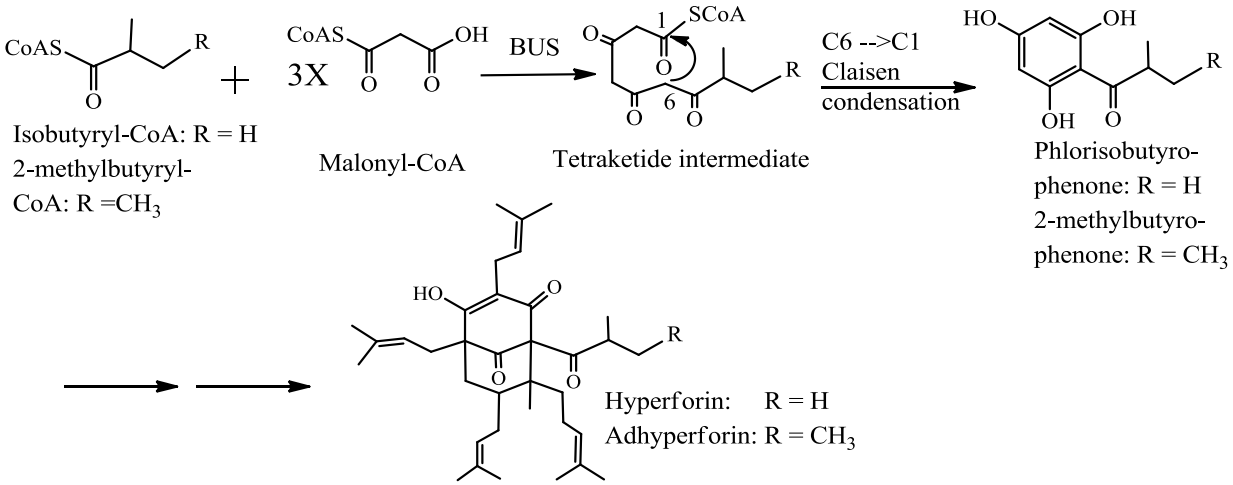

Fig. 10 Reaction mechanism of isobutyrophenone synthase (BUS).

- **2-Pyrone synthase (2-PS)**

Pyrone synthases are considered as a subfamily of type III PKSs with limited distribution between plants (Gleason and Chollet, 2012). Although they share around 74% sequence identity with CHS they differ in the starter substrate, number of malonyl-CoA condensations and the type of cyclization (Austin and Noel, 2003). The basic pyrone synthase that was cloned from the ornamental plant *Gerbera hybrida* (Asteraceae) is the key enzyme in pyrone derivatives biosynthesis. The recombinant enzyme is a polyketide synthase that catalyzes iterative condensation of one molecule of acetyl-CoA and two malonyl-CoAs to form a linear triketide intermediate that undergoes C5-oxy→C1 lactonization and formation of 6-methyl-4-hydroxy-2-pyrone (triacetic acid lactone, TAL) (Fig. 11) which is the precursor of pyrone derivatives like gerberin and parasorboside glucosides. These metabolites are natural products with reduced pyrone skeleton and related to pathogen and insect resistance by inhibiting bacterial and fungal growth. The enzyme also accepts benzoyl-CoA which then undergoes lactonization after two malonyl-CoA condensations to synthesize 6-phenyl-4-hydroxy-2-pyrone which composes the skeleton of some HIV-1 protease inhibitors (Helariutta et al., 1995; Eckermann et al., 1998; Austin and Noel, 2003). The sequence comparison suggests that CHS and pyrone synthase are

different in four amino acids: Thr197, Ile254, Gly256 and Ser338 which were replaced with Leu, Met, Leu and Ile respectively in Gh2-PS (numbering from MsCHS). Only three of them which contribute to the size and shape of the active site namely Thr197, Gly256 and Ser338 were sufficient to alter CHS into a functional 2PS (Schröder, 2008).

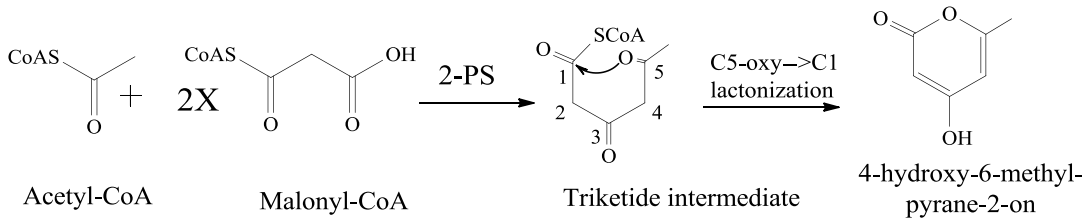

Fig. 11 Reaction mechanism of 2-pyrone synthase (2-PS).

- **Pentaketide chromone synthase (PCS)**

From the young roots of aloe (*Aloe arborescens*) which is a medicinal plant rich in aromatic polyketides such as chromones and anthraquinones, a cDNA encoding a novel type III PKS named pentaketide chromone synthase (PCS) was cloned (Abe et al., 2005). The cloned enzyme shares 50-60% identity to CHS enzymes and 50% identity with *R. palmatum* ALS. The products of the recombinant enzyme with malonyl-CoA is 5,7-dihydroxy-2-methylchromone (Fig. 12, A) which is the precursor in the biosynthesis of the anti-asthmatic furochromones khellin and visnagin (Fig. 12, A). *A. arborescens* PCS showed broad substrate specificity as it also accepts aromatic and aliphatic CoA-esters as starters and performs two and three condensations with malonyl-CoA to form triketide and tetraketide pyrones. Sequence comparison displayed that the catalytic triad and most of the CHS active site residues are conserved in *A. arborescens* PCS but one of the most important character of *A. arborescens* PCS is that the CHS active site residues Thr197, Gly256, and Ser338 (numbering in *M. sativa* CHS) are replaced with Met, Leu, and Val respectively. Interestingly, the three residues are also changed in the heptaketide-forming *R. palmatum* ALS (T197A/G256L/ S338T) and in *G. hybrida* 2-PS (T197L/G256L/S338I) that also selects acetyl-CoA as a starter to produce a triketide pyrone. A CHS triple mutant (T197L/G256L/S338I) transformed CHS into 2-PS, indicating the responsibility of these three residues for the starter substrate specificity. Ultimately, a single amino acid substitution in the active site of *A. arborescens* PCS, M207G, completely transformed it into an octaketide synthase which forms the aromatic octaketides

SEK4 and SEK4b after seven malonyl-CoA condensations (Fig. 12, B; Abe et al., 2005; Morita et al., 2006; Morita et al., 2007; Schröder, 2009).

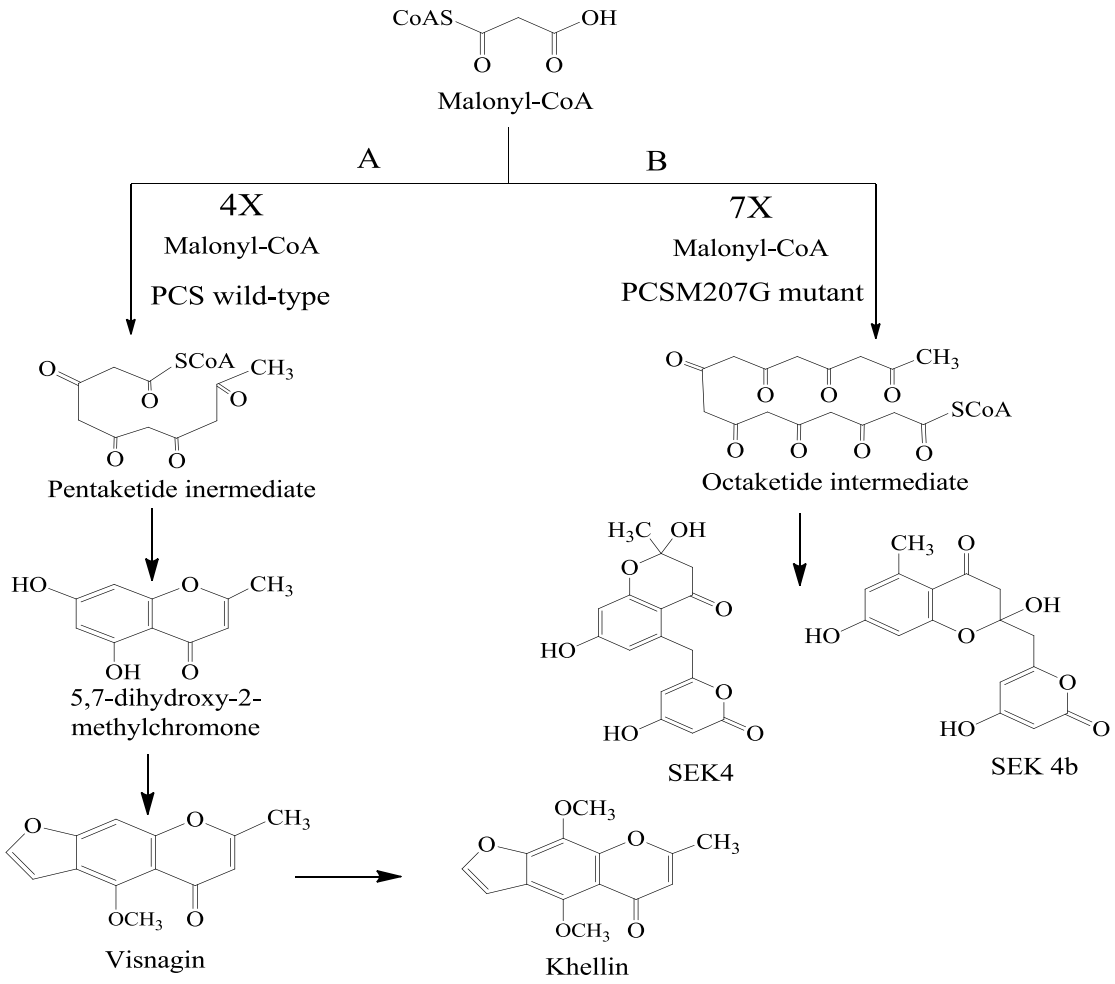

Fig. 12 Reactions catalyzed by pentaketide chromone synthase (PCS) wild-type (A) and the PCS M207G mutant (B).

- **Aloesone synthase (ALS)**

ALS was the first plant type III PKS enzyme which catalyzes more than three condensation reactions. It was cloned from young roots of rhubarb (*R. palmatum*) a medicinal plant rich in aromatic polyketides such as chromones, naphthalenes, phenylbutanones, and anthraquinones and later from *A. arborescens*. ALS catalyzes the formation of an aromatic heptaketide called aloesone (2-acetonyl-7-hydroxy-5-methylchromone) (Fig. 13) by iterative condensation of one acetyl-CoA and six molecules of malonyl-CoA followed by cyclization of the heptaketide intermediate with the removal of a carboxyl group. The enzyme shared 60% amino acid

sequence identity with CHSs and nearly maintained the conserved amino acids lining the active site of plant type III PKSs including the CoA binding sites and the catalytic triad. It also shares the overall fold like CHS. The most interesting point is the replacement of the CHS active site residues lining the initiation/elongation cavity Thr197, Ile254, Gly256 and Ser338 with Ala, Met, Leu and Thr in RpALS. Remarkably, a large number of mutants were constructed to elucidate the roles of specific residues responsible for the substrate and product specificities of this enzyme compared to other type III PKSs. Only replacement of Ala197 to Thr transformed heptaketide synthase (RpALS) into a pentaketide synthase which forms 2,7-dihydroxy-5-methylchromone instead of aloesone (Abe et al., 2004; Abe et al., 2006; Schröder, 2009).

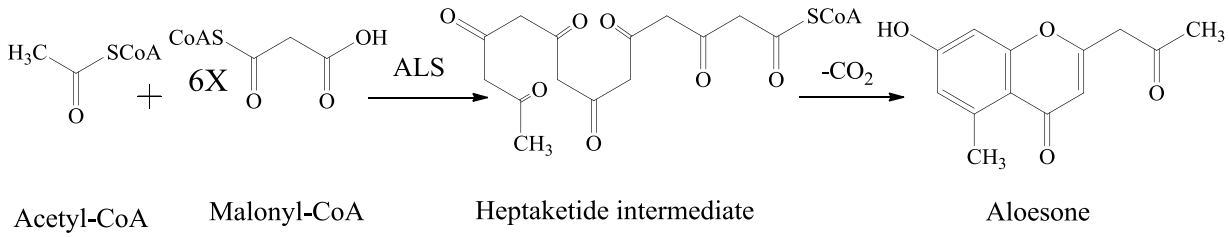

Fig. 13 Reaction mechanism of aloesone synthase (ALS).

- **Oktaketide synthas (OKS)**

From young roots of *A. arborescens* a cDNA encoding the octaketide synthase (OKS) was cloned. The enzyme showed 50-60% identity to type III plant PKSs and more than 90% identity with *A. arborescens* PCS (Abe et al., 2005). The enzyme accepts malonyl-CoA as a starter substrate catalyzing seven condensations with malonyl-CoA to yield the aromatic octaketides SEK4 and SEK4b the longest polyketides synthesized by plant type III PKSs (Fig. 14). However, the Aloe plant does not produce these substances but forms anthrones and anthraquinones that are probably derived from octaketides. Despite of accepting the suggested starter substrate and carrying out the correct condensation number with malonyl-CoA the right cyclization of the linear polyketide intermediate to the predicted final products failed *in vitro* and only the formation of the shunt products SEK4 and SEK4b takes place. This may be due to misfolding of the protein in the *E. coli* expression system or because of the absence of interactions with a yet unidentified tailoring enzyme such as ketoreductase. The involvement of tailoring enzymes is supported by the fact that SEK4 and SEK4b are also formed as shunt products by a type II PKS of *Streptomyces coelicolor* involved in actinorhodin antibiotic

biosynthesis when the enzyme is incubated in the absence of ketoreductase (Fu et al., 1994). *A. arborescens* OKS showed broad substrate specificity as it also accepts, in addition to malonyl and acetyl-CoAs, aromatic and long-chain fatty acyl-CoA esters as starters and performed sequential condensations with malonyl-CoA to produce triketide and tetraketide pyrones (Mizuuchi et al., 2009). Sequence comparison of *A. arborescens* OKS with other PKSs showed absolute conservation of the catalytic triad and most of the CHS active-site residues except CHS's Thr197, Gly256 and Ser338 which are substituted with Gly, Leu, and Val in AaOKS respectively (Fig. 84 appendix). As mentioned earlier, these three residues are changed in a number of type III PKSs such as heptaketide synthase from *R. palmatum*, ALS (T197A/G256L/S338T) (Abe et al., 2004), pentaketide synthase from *A. arborescens*, PCS (T197M/G256L/S338V) (Abe et al., 2005), and triketide synthasee from *G. hybrida*, 2PS (T197L/G256L/S338I) (Eckermann et al., 1998; Jez et al., 2000). It has been proposed that these inert active site residues control the starter substrate selectivity and polyketide chain length by steric modulation of the initiation/elongation cavity (Abe et al., 2005). Replacement of Gly207 in AaOKS by the Met207 of AaPCS led to an enzyme similar to PCS i.e. it produces a pentaketide. However, it was not the expected 5,7-dihydroxy-2-methylchromone but the isomeric 2,**7**-dihydroxy-**5**-methylchromone (Fig. 14, B). Thus, a single change in direction to PCS was sufficient to convert the octaketide synthase into a pentaketide synthase but the difference in the products indicates that the enzymes are in this case not properly inter-convertible.

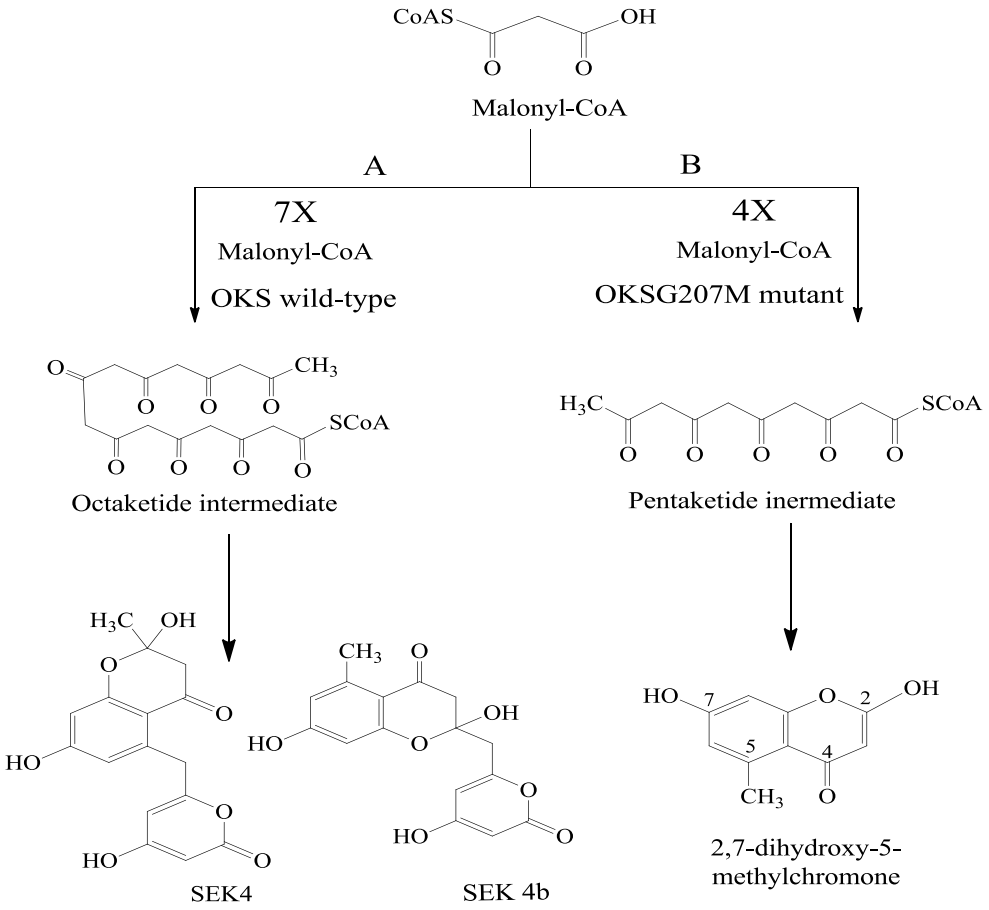

Fig. 14 Reaction mechanisms of A: octaketide synthase (OKS) wild-type, B: OKS G207M mutant.

1.2.6 Active site of plant type III polyketide synthases

For a better understanding of the function of each amino acid used in this study, amino acid sequences alignment for selected type III PKSs (Fig. 84) is provided. Recent crystallographic and site-directed mutagenesis studies on plant and bacterial enzymes provide valuable structural and functional details of this class of enzymes which are structurally simple small homodimeric proteins of approximately 40–45 kDa that share almost the same three-dimensional overall fold and common active-site architecture with an absolutely conserved Cys, His and Asn catalytic triad. The first resolved PKS structure was that of *M.sativa* (alfalfa) CHS alone and complexed with substrate and product analogues which showed that the active site of CHS2 consists of three inter-connected cavities which are the CoA-binding tunnel, a coumaroyl-binding pocket and a cyclization pocket. Each type III PKS monomer utilizes the triad within an internal active site cavity which is connected to the outer aqueous environment by a narrow CoA-binding tunnel. This partition of the active site separated pockets represents the structural basis for the capability of the CHSs-like enzymes to catalyze different reactions within a single

buried active site cavity. Multiple sequences alignments displayed high sequence similarity between divergent type III PKS proteins. Nearly 30–95% similarity was noticed between CHSs and plant type III PKSs. This high similarity suggested a strict conservation between CHSs from plant species. Around 21–31% similarity was observed in fungal and bacterial type III PKSs meanwhile the non-CHS proteins showed more than 70% similarity (Abe et al., 2001; Jeya et al., 2012, Radhakrishnan EK, 2009; Mallika et al., 2011).

1.2.6.1 Catalytic residues

Structural insights into the catalytic machinery of *M. sativa* CHS revealed the conservation of four amino acid residues (Cys164, Phe215, His303 and Asn336 numbering from MsCHS) except in *R. palmatum* BAS (which is a non-CHS protein) where Phe215 is replaced with Leu. In addition there is a substitution of the conserved Asn336 with Ala in *Persea americana* (Avocado) CHS (Q9ZU06) (Mallika et al., 2011). The conserved catalytic triad (Cys164, His303 and Asn336) is positioned at the top of the active site cavity (Fig. 15, A) where it acts on substrates incorporated into the active site by the pantetheine arm of the CoA-linked molecules. Interestingly, the catalytic cysteine (Cys164) which is strictly conserved in all thiolase-fold enzymes is situated at the amino terminal end of one of a pair of buried α-helices that make the buried central α-layer of the thiolase-fold architecture (Fig. 15, B). Phe215 is located at the bottom of the binding pocket (Fig. 15, A). It is one of two ‘gatekeeper’ phenylalanines which block the lower portion of the opening between the CoA-binding tunnel and the active site cavity. It is stated that ‘Phe215’ is implicated in the decarboxylation of malonyl-CoA and may help in the orientation of substrates and reaction intermediates at the active site. The conformational flexibility of these gate keeper residues (deduced from comparison of several crystal structures) may grant the ability of CHS to restrict the access of water to the active site while harboring substrates and intermediates of variable size (Jez and Noel, 2000; Austin and Noel, 2003; Mallika et al., 2011).

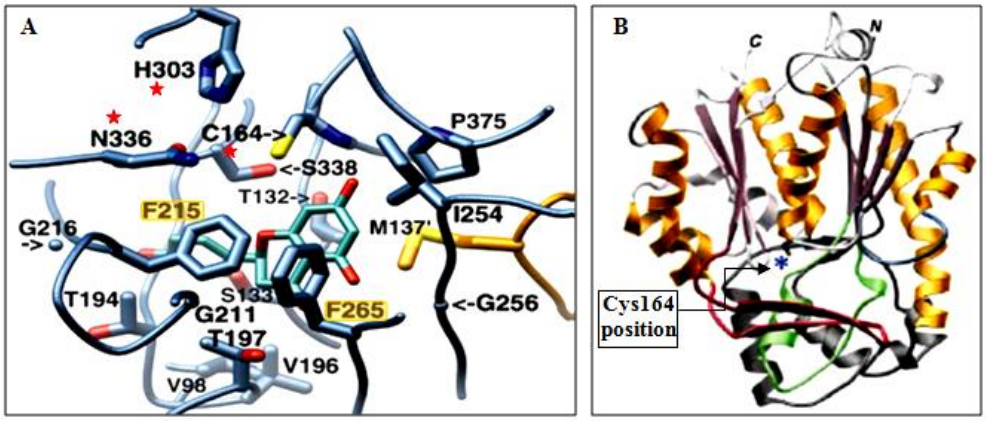

Fig. 15 A: Buried active site cavity of CHS with naringenin bound. View is from the outside looking through the CoA-binding tunnel. The interface of the active site cavity and the CoA-binding tunnel is mediated by the 'gatekeeper' phenylalanines at positions 215 and 265. Other active site residues discussed in the text are also shown, B: position of the catalytic cysteine at the N-terminal end of one of a pair of buried α-helices that make the buried central α-layer of the thiolase-fold architecture, modified from; Austin and Noel, (2003).

1.2.6.2 Substrate binding pocket residues

Despite of the fact that PKSs have broad substrate specificity, the amino acid residues forming the substrate binding pocket were found to have steric and mechanistic effects on the substrate selectivity (Brand et al., 2006). Ser133, Glu192, Thr194, Thr197 and Ser338 (numbering from MsCHS) are the amino acid residues located at the substrate binding pocket and presented high degree of conservation with a number of exceptions. Ser133 was replaced with Thr in all fungal and bacterial type III PKSs in addition to *P. sylvestris* STS and *R. palmatum* ALS. In *G. hybrida* 2-PS, *R. palmatum* BAS, *R. graveolens* ACS and *A. marmelos* QNS Ser133 was substituted with Ala. Also in *A. arborescens* PCS and OKS Ser133 was replaced with Cys. Glu192 showed absolute conservation while Thr194, Thr197 and Ser338 displayed variations. Like the replacement of Thr194 with Cys in most of the fungal and bacterial type III PKSs and with Gly, Ile, Thr, and Val in selected *Hypericum* BPSs and *S. aucuparia* BIS, *Gerbera hybrida* 2-PS, *R. palmatum* ALS, *A. arborescens* PCS and OKS respectively (Mallika et al., 2011). Thr197 showed variation especially in non-CHSs enzymes like SaBIS, Gh2PS, HlVPS, RpBAS, RpALS, AaPCS and OKS where it was replaced with Phe, Leu, Ile, Cys, Ala, Met and Gly respectively. It was reported that Ser at position 338 played a role in the starter substrate selectivity and is mainly substituted in non-CHSs for a special function (Abe et al., 2006). For example, Ser338 was replaced with Ile and Thr in Gh2PS and.

RpALS, respectively. In SaBIS and selected *Hypericum* BPSs it was replaced with Gly. Finally, Val replaces Ser338 in AaPCS and OKS

1.2.6.3 Cyclization pocket residues

Thr132, Met137, Phe215, Ile254, Gly256, Phe265, and Pro375 are the amino acid residues that form the cyclization pocket. They show high degree of conservation in CHSs but with a number of exceptions in other type III PKSs and they are essential for providing the required steric guidance to the linear polyketide (Austin and Noel, 2003). Thr132 which is our amino acid of interest during this study was conserved in CHSs from all plants with an exception of *C. erythraea* PPS which is a natural phenylpyrone synthase (Gaid, unpublished results). In *Zingiber officinale* CHS, Thr132 was replaced with Ile (Radhakrishnan EK, 2009; Mallika et al., 2011). In most of non-CHS enzymes like RpBAS, SaBIS and HlVPS, Thr132 was replaced with Leu, Ala, and Gly respectively. In RgACS, AmQNS, AaPCS and OKS it was substituted with Ser. Finally Thr132 was replaced with Cys in most of the fungal and bacterial type III PKSs (Mallika et al., 2011). Met137 is strictly conserved except in PsSTS where it was substituted with Leu. Pro375 amino acid residue displayed stringent conservation across different type III plant PKSs. Position 254 mainly contains Ile but in SaBIS it was replaced with Val while in Gh2PS and RpALS it was substituted with Met. Gly256 is conserved in most of CHSs while in non-CHSs like SaBIS and selected *Hypericum* BPSs it was replaced with Ala while in Gh2PS, RpAlS, AaPCS and OKS it was substituted with Leu. Position 265 occupied with the second gatekeeper Phe in most of CHSs. But it was replaced with Tyr in SaBIS and selected *Hypericum* BPSs while in CePPS, RgACS and in AmQNS it was substituted with Val. Ultimately, Pro138, Gly163, Gly167, Leu214, Asp217, Gly262, Pro304, Gly305, Gly306, Gly335, Gly374, Pro375 and Gly376 are conserved amino acid residues maintaining the overall architecture of the MsCHS enzyme. Interestingly, minor changes in the amino acid residues lining these pockets may have profound effects on the reaction mechanism leading to metabolic divergence (Abe et al., 2001; Radhakrishnan EK, 2009).

1.2.7 Proposed type III PKS reaction mechanism

All polyketide synthases have a conserved catalytic triad consisting of His, Cys, and Asn residues in their active sites. The (His) imidazole-N acts as a base and removes a proton from the (Cys) sulfhydryl group generating a reactive thiolate anion. This anion attacks the carbonyl carbon of starter-CoA and displaces the CoA moiety. The second substrate, malonyl-CoA binds near the (Asn) residue. The (Asn) amide-NH2 forms a H-bond with the carbonyl oxygen of

malonyl-CoA facilitating its decarboxylation. The produced acetyl carbanion attacks the carbonyl carbon of the starter-Cys complex and produces a diketide intermediate which rebounds to the Cys by thiolate nucleophilic attack on carbonyl thioester of the diketide The second equivalent of malonyl-CoA is attached to the Asn residue, decarboxylated and added to the diketide. The resulting triketide intermediate undergoes another elongation round by binding to the active site (Cys) and acetate addition to yield a tetraketide intermediate. Cyclization and aromatization of the teraketide intermediate occur while it is still bound to the enzyme to produce the final product (Fig. 16). Briefly, the reaction of polyketide formation is started by loading the starter substrate at the active site Cys, followed by malonyl-CoA decarboxylation, elongation of the polyketide chain, and ultimate cyclization of the polyketide intermediate to the final product (Staunton and Weissman, 2001; Austin and Noel, 2003; Gleason and Chollet, 2012). However, further analysis of the flexibility and catalytic potential of the functionally divergent plant type III PKSs pledge to reveal fine structural details of the enzyme-catalyzed processes and so enriching the field of structure-based engineering of this class of enzymes will of course lead to the production of structurally and chemically variable novel polyketide compounds with possibly important pharmacological activities (Abe, 2008).

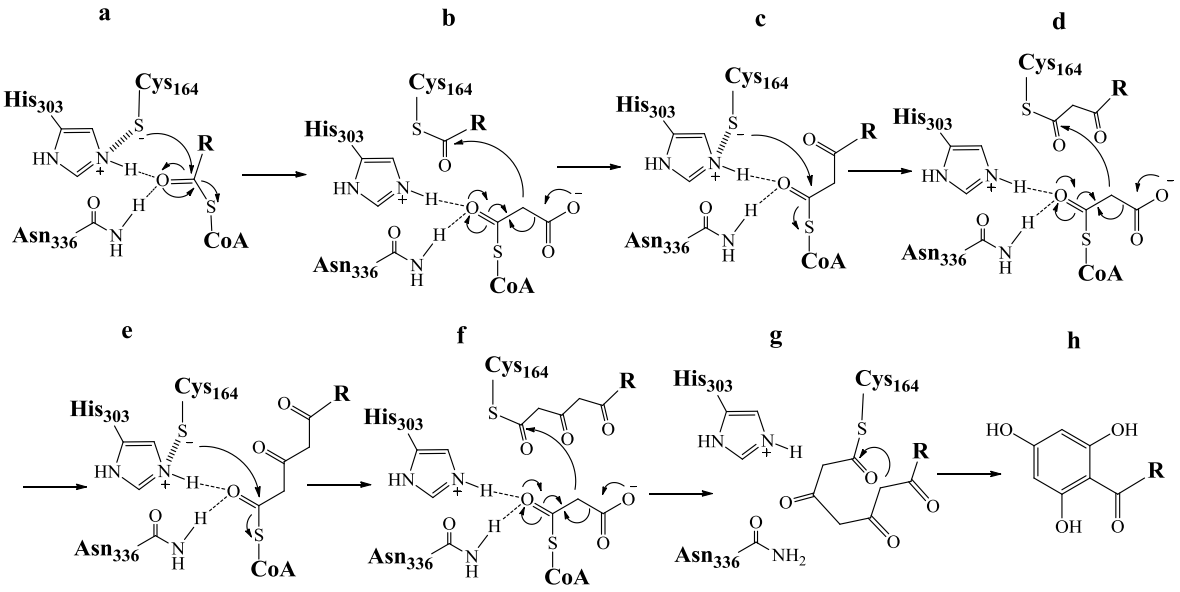

Fig. 16 Proposed reaction mechanism of type III polyketide synthases. a: starter substrate loading, b: first malonyl decarboxylation and condensation with the growing ketide chain (polyketide extension), c: reloading of the diketide intermediate, d: second malonyl decarboxylation and condensation with the growing ketide chain (polyketide extension), e: reloading of the triketide intermediate, f: third malonyl decarboxylation and condensation with the growing ketide chain (polyketide extension), g: reloading of the tetraketide intermediate, h: cyclization, aromatization and then release of the final product from the active site modified from; Abe, (2008).

1.3 *Hypericum*

The genus *Hypericum* is the largest genus of the family Hypericaceae previously classified as Guttiferae or Clusiaceae (Stevens, 2007). This family contains nine genera (*Hypericum, Cratoxylum, Eliea, Harungana, Lianthus, Santomasia, Thornea, Triadenum* and *Vismia)* (Wikipedia, 2013). *Hypericum* as a genus consists of about 500 species of shrubs, herbs and a few trees classified into 36 taxonomical sections and containing approximately 80 % of the diversity of Hypericaceae (Ocak et al., 2013). Plants of this genus are widely distributed all over the world mainly in the temperate regions and present in almost all kinds of temperate habitats (Nürk 2011). A general overview of the taxonomy of the genus and the distribution of relevant secondary metabolites is presented in Crockett and Robson (2011). The plants of this genus contain a wide range of structurally different and biologically active secondary metabolites belonging to at least ten different classes (Menichini et al., 2013) with preponderance of naphthodianthrons 'hypericin and pseudohypericin', phloroglucinols 'hyperforin', flavonoids 'rutin, hyperoside, isoquercitrin, quercitrin, quercetin, amentoflavone' and phenylpropanoids 'chlorogenic acid' (Bruni et al., 2005) in addition to xanthones. However, great variations in contents have been reported for wild populations worldwide from Australia (Southwell and Campbell, 1991) to Turkey (Çirak et al., 2006) and this may explain its various supposed therapeutic indications like wound healing, anti-inflammatory, and antiseptic activities, treatment of anxiety and sleep disorders in addition to its sedative or tonic effects (Usai et al., 2003). The name *Hypericum* possibly comes from the Greek words hyper (above) and eikon (picture) and this indicates that using this plant over Gods pictures may keep the owner from evil (Czygan, 2003). *Hypericum* species have received significant interest due to the increasing market requirements (Usai et al., 2003). So the economic value of plants of this genus to the herbal industry is one of various factors that motivated research into phytochemical diversity of *H. perforatum* specifically and of other members of the genus in general (Crockett and Robson, 2011). Extracts of the inflorescences and upper stem leaves of *H. perforatum* are prescribed for many years in Europe and are available as dietary supplements in the United States to treat mild to moderate depression (Crockett and Robson, 2011). High efficacy and tolerability of the herb's extract is unimpeachable, while its clinical activity is comparable to other antidepressants (Woelk, 2000). *H. perforatum* also shows promising antiviral and anti-inflammatory activities and is being studied for its prospect benefit to AIDS patients. It has long been used as a cure for

uterine spasm, bedwetting, and anxiety. St. John's wort is also used internally and externally for pain relief (Hobbs, 2013).

1.3.1 *H .perforatum* ssp *angustifolium* (Hpa)

According to the Flora of Italy by Pignatti (1982), there are three different subspecies: *perforatum*, *veronense* and *angustifolium* distinguished by the size of their sepals (Dukovčić et al., 2012). *H. perforatum* ssp *angustifolium* (Fig. 18, 4) has linear lanceolate leaves and found to be the highest in hypericin content which is accumulated in the black globules that are present in all the aerial parts of the plant (Males et al., 2006). The extract of *H. perforatum* ssp *angustifolium* showed an efficacy which was similar to that obtained with the treatment with the classical antidepressant imipramine or *H. perforatum* ssp perforatum. Furthermore, *H. perforatum* ssp angustifolium extract was active at doses eight times lower than those necessary to produce a comparable activity with *H. perforatum* ssp *perforatum* extracts (Usai et al., 2003).

1.3.2 *Hypericum calycinum* (Hc)

H. calycinum L. (rose of Sharon; Fig., 18, 3) is a common ornamental plant in the United States. It is a deciduous shrub. Its flowers and leaves are much larger than those of *H. perforatum*. Since it accepts a wide range of soil types including sand and showed adaptation to different habitats, *H. calycinum* used by gardeners for ground cover and rock gardens and to stabilize hillsides. *H. calycinum* bears yellow flowers that resemble wild roses. This hardy shrub is free of most serious plant diseases and has no insect problem that affects its existence (Spengler, 2013). Interestingly, antibiotic substances isolated from *H. calycinum* are comparable in their activity to those in *H. perforatum* (Shakirova, 1970; Hobbs, 1998), in addition to its fungicidal activity against *Cladosporium cucumerinum*, in vitro antimalarial and anticancer activity (Decosterd et al., 1989; Decosterd et al., 1991). Ozturk (1997) stated that the alcoholic extract of *H. calycinum* has antidepressant properties while other tested species like *H. hyssopifolium* ssp. *elongatum* var. *elongatum* were free of antidepressant effects.

1.3.3 *Hypericum androsaemum* (Ha)

Hypericum androsaemum L. (Guttiferae, Fig. 18, 2) is a medicinal plant growing in West Europe in shady or clammy places. Investigation of this species includes only the separation and identification of its constituents like flavonoids, phenolic acids in addition to xanthones which occur mainly in roots but minor amounts can also be present in leaves (Nielsen and Arends, 1979; Schmidt et al., 2000; Valentão et al., 2003). These phenolic compounds may be

responsible for the properties and pharmacological activities of this plant. In traditional medicine *H. androsaemum* leaves were used in preparation of teas with diuretic and antihepatotoxic activities (Valentão et al., 2002; Klundt, 2008). The lyophilized infusion of *H. androsaemum* showed antioxidant activity against superoxide radical, hydroxyl radical and hypochlorous acid which is probably due to the predominance of several quercetin glycosides in this species (Valentão et al., 2002). In addition to the hepatoprotective activity of *H. androsaemum* infusion which may be due to the phenolic compounds, 5-O-caffeoylquinic acid, and quercetine derivatives that inhibited lipid peroxidation (Valentão et al., 2004).

1.3.4 *Hypericum sampsonii* (Hs)

H. sampsonii Hance (Fig. 18, 1) is a small evergreen shrub distributed and cultivated in the north and south of China. Its fruits are used in the treatment of lung disease and whooping cough while roots used in case of rheumatism, cough and back pain (Healthcare, 2011). It is the most closely related species of St. John's wort in China which has been used in traditional medicine for many diseases like snakebites, menstrual irregularity hematemesis, epistaxis, external traumatic injury, and swellings. Recent studies have shown that *H. sampsonii* possesses anti-cancer activity however, how *H. sampsonii* exerts its various biological effects remains substantially unknown (Zeng et al., 2006). There is also antibacterial activity against multidrug-resistant (MDR) strains of *Staphylococcus aureus* (Xiao et al., 2010). Due to its important bioactivities prolonged phytochemical studies showed that *H. sampsonii* contains a lot of polyprenylated phloroglucinol derivatives with complex caged tetracyclic skeletons (Fig. 17) which exhibited moderate antibacterial and cytotoxic activities (Xiao et al., 2007; Xiao et al., 2010; Xin et al., 2011). Recently, sampsonols A and B (Fig. 17) are new polyprenylated phloroglucinol derivatives isolated from the arial parts of the petroleum ether extract of *H. sampsonii* and showed significant cytotoxicity against human breast, hepatoma, colon and lung tumor cell lines. These compounds may serve as lead compounds with interesting therapeutic potential as antitumor and anti-inflammatory agents (Xin et al., 2012). Despite their important pharmacological activities especially as anti-cancers biosynthesis of these benzophenone derivatives is still poorly understood. The main nucleus of these compounds is a benzophenone which is biosynthesized by benzophenone synthase (Beerhues and Liu, 2009). The first published BPS (HaBPS) cDNA was cloned from elicitor-treated *H. androsaemum* cell cultures, which served as a model system for studying benzophenone metabolism (Liu et al., 2003). The second BPS cDNA was cloned and characterized from *Garcinia mangostana* (Nualkaew et al.,

2012). Recently, cloning and functional characterization of a cDNA encoding BPS from *H.sampsonii* was carried out in addition to the analysis of the organ-specific expression pattern by quantitative PCR (Huang et al., 2012).

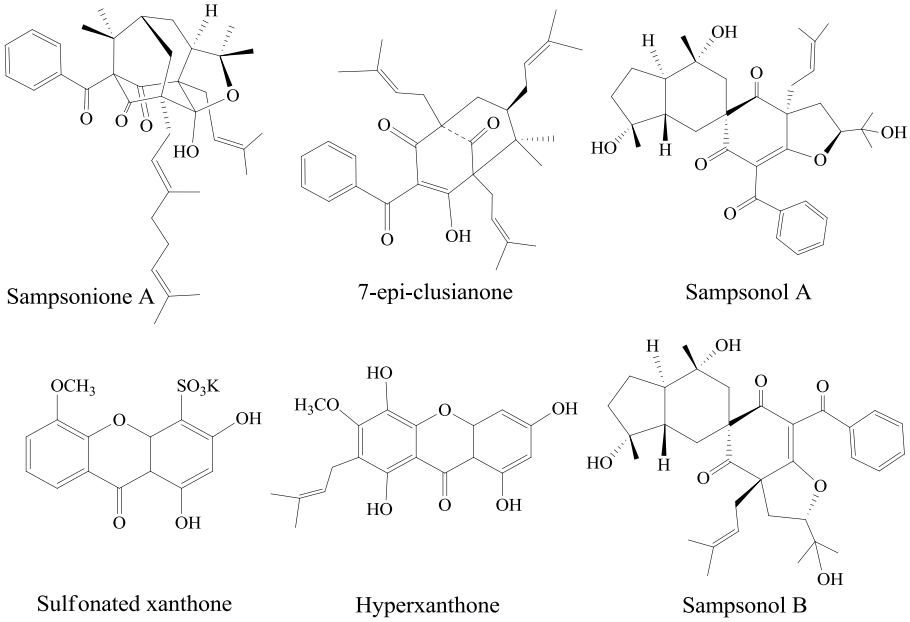

Fig. 17 Structures of some isolated polyprenylated phloroglucinol derivatives and xanthones from *Hypericum sampsonii*.

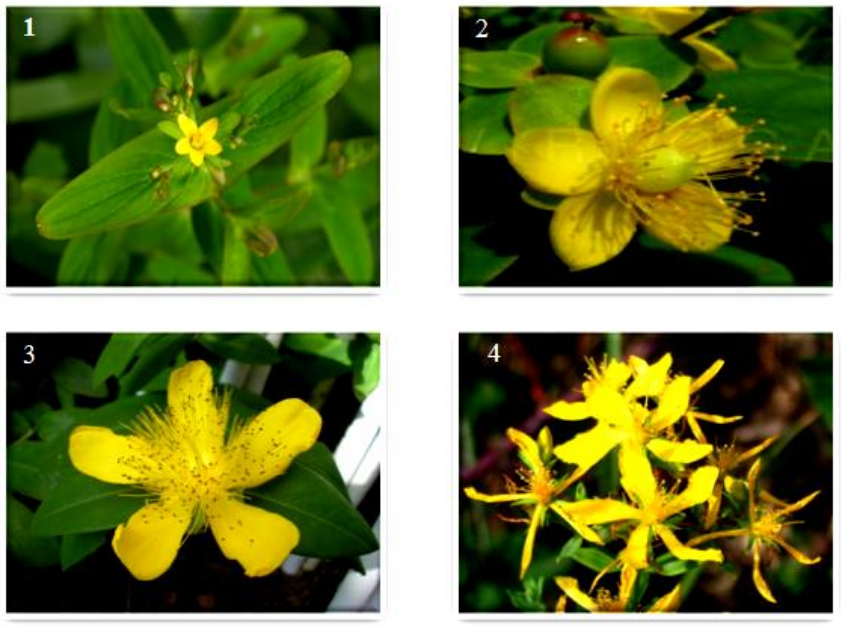

Fig. 18 Selected *Hypericum* species 1: *H. sampsonii* (Herbarium, 2013), 2: *H. androsaemum* (Germer, 2008), 3: *H. calycinum* (Flicksi, 2011), 4: *H. perforatum* ssp. *angustifolium* (Lleida, 2010).

1.4 Homology modeling

Despite of the increasing number of known 3D structures of proteins but they still cover a tiny part of the identified proteins. Therefore comparative homology models for proteins with unknown 3D structures are one of the most essential approaches for studying protein structure/function relationships and guiding mutation experiments. Homology modeling is a technique which generates the 3D-structure of an unknown protein (target) from its amino acid sequence based on the known structure of a closely related protein (template). This method depends on the fact that homologous proteins evolved from a common ancestor have conserved 3D structures. The accuracy of the model based mainly on the sequence identity between the target protein and the selected template. More than 50% sequence identity usually results in reliable models (Chothia and Lesk, 1986). Simply, few steps should be followed to generate a homology model including (i) selection of the template which shows highest similarity to the target protein from PDB (protein data bank), (ii) amino acid sequences alignment of the template and the target protein, and (iii) generation of the model and checking its validity. The computer work done in the current study was a kind cooperation with Dr. Marco Bocola (Head of computational biology, Institute of Biotechnology, RWTH Aachen).

1.5 Research strategies and objectives

The functional behavior of *H.androsaemum* BPS was dramatically changed by a single amino acid substitution in the active site cavity of the enzyme (T135L) (Klundt et al., 2009). The most interesting point on which this work is based is the replacement of Leu with other amino acids such as Gly, Ala, Val, Ile, Asn, and Tyr which gave catalytically inactive proteins while Ser and Phe gave mutants which were similar to the wild type but with lower activities (Klundt et al., 2009). As mentioned before, Thr135 is one of the amino acids which form the cyclization pocket of type III PKSs and play an important role in providing the required steric guidance to the linear polyketide in the active site (Austin and Noel, 2003). Thr135 is conserved in most plant PKSs with some exceptions such as CePPS, SaBIS, and RpBAS in which Thr was replaced with Ile, Ala, and Leu respectively. The amino acids lining the active site cavities of the BPSs from *H. sampsonii, H. androsaemum, H. calycinum and H. perforatum* ssp. *angustifolium* are identical, especially Thr135.

The main objectives of this study were:

- Screening the effects of the other 19 amino acids in position 135 in *H. sampsonii* BPS.
- Investigation of the effect of Leu in position 135 in BPSs of selected *Hypericum* species other than *H. androsaemum*.
- Functional and kinetic characterization of the BPS mutants that showed novel activities.
- Homology modeling of the enzyme mutants that exhibited dramatic changes in the product and substrate specificities (in cooperation with Dr. Bocola, Aachen).
- Analysis of structure-function-relationships.

2 Materials

2.1 Chemicals, nutrient media, solutions and buffers

2.1.1 Chemicals

Chemicals unless otherwise mentioned were purchased from the following companies: Roth, Sigma-Aldrich, Applichem, Fischer Scientific and Fluka. Deionized water was supplied from Milli-Q water purification system (Sartorius, Germany), and used in preparing all aqueous solutions used in the study. All solutions were autoclaved by 120°C for 20 min. Solutions of thermolabile compounds were sterile filtered and added to autoclaved solutions under sterile conditions. All salts required for the plant or bacterial culture media were supplied from Roth or Applichem.

Chemical	**Supplier**
For bacterial culture medium	
Yeast	Applichem
Peptone (casein)	Roth
NaCl	Roth
Agar	Applichem
KH_2PO_4	Roth
K_2HPO_4	Roth
$MgSO_4.7H_2O$	Roth
Glycerol	Roth
Stationary phases used in protein desalting and affinity purification	
PD_{10}-cartridge Sepharose G-25 columns	GE Healthcare
Nickel-nitrilotriacetic acid	Qiagen
Substrates used for enzyme assays	
Benzoyl-CoA, malonyl-CoA	Sigma-Aldrich
Anthraniloyl-CoA	Synthesized according to (Stöckigt and Zenk, 1975; Beuerle and Pichersky, 2002)
2-Hydroxybenzoyl-CoA	Synthesized according to (Stöckigt and Zenk,

	1975; Beuerle and Pichersky, 2002)
3-Hydroxybenzoyl CoA	Synthesized by Dr. M. Gaid (our work group)
4-Hydroxybenzoyl CoA	Synthesized by Dr. B. Liu (our work group)
2-Methoxybenzoyl-*N*-acetylcysteamin	Synthesized according to (Suo et al., 2000)
2-Mercaptobenzoyl-*N*- acetylcysteamin	Synthesized according to (Suo et al., 2000)
Phlorbenzophenone	ICN Biomedicals Inc.
Reagents for biochemistry and molecular biology	
IPTG	Applichem
dNTPs	Thermo Scientific
Imidazole	Roth
Tris-HCl	Roth
Antibiotics	
Ampicillin	Roth
Chloramphenicol	Applichem
Reagents for gel electrophoresis	
peqGold universal agarose	Peqlab
Ethidium bromide	Roth
Acrylamide/Bisacrylamide 30%	Bio-Rad
TEMED	Bio-Rad
Ammonium persulfate	Roth
SDS	Roth
β-mercaptoethanol	Roth
Bromophenol blue	Sigma-Aldrich
Commassie-blue R250 and G250	Merck
Solvents for HPLC	
Methanol, Acetonitrile	Fischer Scientific
Orthophosphoric acid	Roth
Ladder	
Gene Ruler DNA ladder Mix	Thermo Scientific
Page Ruler Unstained Protein Ladder	Thermo Scientific

2.1.2 Nutrient media for Bacterial culture

Medium	Composition	
LB medium	Peptone (casein)	10 g/l
	Yeast extract	5 g/l
	NaCl	10 g/l
For solid medium	Agar	1%
SOC Medium	Peptone (casein)	20 g/l
	Yeast extract	5 g/l
	1 M NaCl	10 ml/l
	1M KCl	10 ml/l
	Autoclave and then add the sterile filtered solution of	
	2 M Mg^{2+}	10 ml/l
	2 M glucose	10 ml/l
For induction of protein expression	IPTG (Isopropyl-β-D-thiogalactopydranoside)	0.12 g/ml (0.5 M)
	Final concentration in bacterial culture	0.5mM
Antibiotic for selection of transformed bacteria	Ampicillin (0.269 M) (100 mg /ml aqueous soln.)	
	Chloramphenicol (0.093 M) (30 mg/ml soln. in ethanol)	
For preservation of bacterial culture	Glycerol:LB (Medium 60:40)	250 µl
	Bacterial culture	750 µl

2.1.3 Buffers and solutions

2.1.3.1 Buffers for DNA- gel electrophoresis

50X TAE buffer	Tris-HCl	2 M
	EDTA	0.05 M
	Adjust pH to 8 with glacial acetic acid	

To examine DNA products less than 300 bp, 2% agarose gel was prepared; for larger sizes, 1% agarose gel was prepared.

2.1.3.2 Buffers for protein electrophoresis (SDS-PAGE)

Staking gel (for 2 small gels)	Water	2.72 ml
	1 M Tris-HCl (pH 6.8)	504 µl
	30% Acrylamide/Bis	664 µl
	10% (w/v) SDS	40 µl
	10% (w/v) APS	40 µl
	TEMED	4 µl
Resolving gel (for 2 small gels)	Water	2.3 ml
	1.5 M Tris-HCl (pH 8.8)	1.75 ml
	30% acrylamide/Bis	2.8 ml
	10% (w/v) SDS	70 µl
	10% (w/v) APS	70 µl
	TEMED	2.8 µl
Protein loading buffer (2X)	Water	2.7 ml
	0.5 M Tris-HCl (pH 6.8)	1.0 ml
	Glycerol	2.0 ml
	10% (w/v) SDS	3.3 ml
	β-mercaptoethanol	0.5 ml
	0.5% (w/v) bromophenolblue	0.5 ml
SDS-electrode buffer (10X)	Tris base	15 g
	Glycine	72 g
	SDS	5 g
	Water	ad 500 ml
Staining solution	Coomassie blue R-250	1 g
	Mathanol	500 ml
	Acetic acid	75 ml
	Water	ad 1000 ml
Destaining solution	Methanol	200 ml
	Acetic acid	76 ml
	Water	ad 1000 ml

2.1.3.3 Buffers for extraction and purification of His_6-tagged fusion protein

Lysis buffer	50 mM Na_2HPO_4	3.44 g
	30 mM NaCl	0.87 g
	20 mM Imidazole	0.68 g
	Water	ad 500 ml
Washing buffer	50 mM Na_2HPO_4	3.44 g
	1.5 mM NaCl	0.04 g
	50 mM Imidazole	1.7 g
	Water	ad 500 ml
Elution buffer	50 mM Na_2HPO_4	3.4 g
	300 mM NaCl	8.76 g
	250 mM Imidazole	8.51 g
	Water	ad 500 ml

2.1.3.4 Buffers for plasmid isolation (miniprep)

Buffer I (pH 8)	Tris-HCl	50 mM	1.5 g/250 ml
	EDTA	10 mM	0.93 g/250 ml
	RNase A	10µl/ml	
	RNase A was added freshly before use		
Buffer II	NaOH	0.2 M	2 g/250 ml
	SDS	1% (w/v)	2.5 g/250 ml
Buffer III (pH 5.5)	K acetate	2.55 M	62.57 g/250 ml
	Glacial acetic acid to adjust pH		

2.1.3.5 Solution to determine the protein amount

Bradford-dye solution	Coomassie-Brilliant blue G-250 100 mg Ethanol 96% 50 ml *o*-phosphoric acid 85% w/v 100 ml water ad 1000 ml	The Coomassie-Brilliant blue G250 powder was dissolve in ethanol by stirring. Orthophosphoric acid was added, and then the volume was completed with water. The solution was filter till no blue color could be seen It was kept protected from light in an amber glass bottle by 4°C.

2.1.3.6 Solutions for PD_{10} washing and Ni-NTA agarose regeneration

PD_{10} washing solution NaOH (0.15 M)	Wash with 25 ml (5x column volume) then wash with water till getting a neutral eluent.
Ni-NTA agarose washing and regeneration solution. Wash with the following solutions in the same order.	0.2 M acetic acid 30% glycerol Deionized water

2.1.3.7 Buffer for enzyme assay

Buffer KH_2PO_4	100 mM dH_2O pH adjusted by KOH	1.36 g ad 100 ml

2.1.4 Materials used for molecular biology

2.1.4.1 Host cells

E. coli	**Purpose**	**Genotype**
DH5α	Deliver high yield plasmid preparation for downstream applications, chemically competent	*F'φ80δlacZ9M15endA1hsdR17(rk-mk+)supE44thi1 λgyrA96relA19 (lacZYA-argFV169) deoR*
BL21(DE3) pLysS	For protein overexpression (Invitrogen), chemically competent	*F-, ompT hsdSB (rB- mB-) gal dcm (DE3) pLysS (CamR)*

2.1.4.2 Cloning vector

pRSET-B vector (protein expression)	Invitrogen

2.1.4.3 Enzymes

Name	**Purpose**	**Supplier**
Pfu DNA polymerase	High fidelity amplification of DNA	Thermo Scientific
Phusion Hot Start II High fidelity DNA polymerase	High fidelity amplification of DNA	Thermo Scientific
Dpn I	Digest the parental DNA template and to select for mutation containing synthesized DNA	Thermo Scientific
Kpn I	Endonucleolytic cleavage of DNA to give specific double-stranded fragments	Thermo Scientific

	with terminal 5'-phosphates	
RNase A	Digestion of RNA by plasmid isolation	Thermo Scientific

2.1.4.4 Primers

All the primers were synthesized in HPSF (High Purity Salt Free) quality at MWG-Biotech AG (Ebersberg, Germany).

- **HaBPS mutation primers**

Designed according to (Zheng et al., 2004)

HaBPSE54D Sen	T_m 64.2°C	5'- CAC ATG ACC GAt CTC AAG GAG AAA TTT AAA C-3'
Ha BPSE54D Ant	T_m 70.8°C	5'- CTC CTT GAG aTC GGT CAT GTG CTC GCT GTT G-3'
HaBPSV146A Sen	T_m 75°C	5'- GCA GAC TAC Gct ATC ACC CGC CTC CTC GGC C-3'
HaBPSV146A Ant	T_m >75°C	5'- GCG GGT GAT agC GTA GTC TGC CCC GGG CAT C-3'
HaBPSV359L Sen	T_m 74.8°C	5'- G AGC TCC AAG cTC AAC GGG AAG CCC ACC ACC-3'
HaBPSV359L Ant	T_m 70.8°C	5'- C TT CCC GTT GAg CTT GGA GCT CTT CCT AAG C-3'
HaBPSN360S Sen	T_m >75°C	5'-CC AAG GTC Agt GGG AAG CCC ACC ACC GGC-3'
HaBPSN360S Ant	T_m 72.3°C	5'-GGG CTT CCC acT GACCTT GGA GCT CTT CC-3'
HaBPSC230G Sen	T_m >75°C	5'- C ATC GGG GCA gGC CCT GAC GTT GCT TCT GGG -3'
HaBPSC230G Ant	T_m >75°C	5'- C GTC AGG GCc TGCCCC GAT GAT CAG AGCAGC -3'
HaBPSS235A Sen	T_m 75°C	5'- GAC GTT GCT gCT GGGGAG CGC GCA GTG TTC-3'
HaBPSS235A Ant	T_m >75°C	5'- GCG CTC CCC AGc AGCAAC GTC AGG GCA TGC-3'

- **HsBPST135L mutation primers**

Designed according to (Stratagene, 2005)

HsBPST135L Sen	T_m >75°C	5'-GAT CAC CCA CGT GGT GTT TGC GAC Cct cTC CGG GTT CAT GAT GCC CGG C-3'
HsBPST135L Ant	T_m >75°C	5'-GCC GGG CAT CAT GAA CCC GGA gag GGT CGC AAA CAC CAC GTG GGT GAT C -3'

- **HsBPS mutation primers**

Designed according to (Zheng et al., 2004)

HsBPST135A Sen	T_m>74.5°C	5'- GTG TTT GCG ACC gcc TCC GGG TTC ATG ATG CC-3'
HsBPST135A Ant	T_m >75°C	5'- GAA CCC GGA ggc GGT CGC AAA CAC CAC GTG G -3'
HsBPST135G Sen	T_m 74.6°C	5'-GTG TTT GCG ACC ggc TCC GGG TTC ATG ATG CC -3'
Hs BPST135GAnt	T_m >75°C	5'-GAA CCC GGA gcc GGT CGC AAA CAC CAC GTG GG -3'
HsBPST135D Sen	T_m 73.3°C	5' –GTG TTT GCG ACC gac TCC GGG TTC ATG ATG CC-3'
HsBPST135D Ant	T_m >75°C	5'-GAA CC GGA gtc GGT CGC AAA CAC CAC GTG GG -3'
HsBPST135K Sen	T_m 72.1°C	5'- GTG TTT GCG ACC aag TCC GGG TTC ATG ATG CC -3'
HsBPST135K Ant	T_m 74.6°C	5'- GAA CCC GGA ctt GGT CGC AAA CAC CAC GTG GG -3'
HsBPST135W Sen	T_m 73.3°C	5'-GTG TTT GCG ACC tgg TCC GGG TTC ATG ATG CC -3'
HsBPST135W Ant	T_m >75°C	5'-GAA CCC GGA cca GGT CGC AAA CAC CAC GTG GG -3'
HsBPST135Y Sen	T_m 72.1°C	5'-GTG TTT GCG ACC tac TCC GGG TTC ATG ATG CC-3'
HsBPST135Y Ant	T_m 74,6°C	5'-GAA CCC GGA gta GGT CGC AAA CAC CAC GTG GG -3'
HsBPST135I Sen	T_m 72.1° C	5'-GTG TTT GCG ACC atc TCC GGG TTC ATG ATG CC-3'
HsBPST135I Ant	T_m 74.6° C	5'-GAA CCC GGA gat GGT CGC AAA CAC CAC GTG GG-3'
HsBPST135V Sen	T_m 73.3°C	5'-GTG TTT GCG ACC gtc TCC GGG TTC ATG ATG CC-3'
HsBPST135V Ant	T_m >75°C	5'-GAA CCC GGA gac GGT CGC AAA CAC CAC GTG GG-3'
HsBPST135M Sen	T_m 72.1°C	5'-GTG TTT GCG ACC atg TCC GGG TTC ATG ATG CC-3'
HsBPST135M Ant	T_m 74.6°C	5'-GAA CCC GGA cat GGT CGC AAA CAC CAC GTG GG-3'
HsBPST135F Sen	T_m 72.1°C	5'-GTG TTT GCG ACC ttc TCC GGG TTC ATG ATG CC-3'
HsBPST135F Ant	T_m 74.6°C	5'-GAA CCC GGA gaa GGT CGC AAA CAC CAC GTG GG-3'
HsBPST135H Sen	T_m 73.3°C	5'-GTG TTT GCG ACC cac TCC GGG TTC ATG ATG CC-3'
HsBPST135H Ant	T_m >75°C	5'-GAA CCC GGA gtg GGT CGC AAA CAC CAC GTG GG-3'

- **HpaBPS mutation primers**

Designed according to (Zheng et al., 2004)

HpaBPST135L Sen	T_m 73.3	5'- GTG TTT GCG ACC ctC TCC GGG TTC ATG ATG CC-3'
HpaBPST135L Ant	T_m >75°C	5'- GAA CCC GGA Gag GGT CGC AAA CAC GAC GTG GG-3'
HpaBPST135I Sen	T_m 72.1° C	5'-GTG TTT GCG ACC atc TCC GGG TTC ATG ATG CC-3'
HpaBPST135I Ant	T_m 74.6° C	5'-GAA CCC GGA gat GGT CGC AAA CAC CAC GTG GG-3'
HpaBPST135K Sen	T_m 72.1°C	5'- GTG TTT GCG ACC aag TCC GGG TTC ATG ATG CC -3'
HpaBPST135K Ant	T_m 74.6°C	5'- GAA CCC GGA ctt GGT CGC AAA CAC CAC GTG GG -3'

- **HcBPS mutants primers**

  Designed according to (Liu and Naismith, 2008)

HcBPST135L Sen	T_m >75°C	5'- GCT ACG ctC TCC GGG TTC ATG ATG CCA GGC GCG GAC TAC G -3'
HcBPST135L Ant	T_m >75°C	5'- CCC GGA Gag CGT AGC GAA CAC AAC GTG GGT GAT CTT GGA G -3'
HcBPST135I Sen	T_m >75°C	5'-GCT ACG atC TCC GGG TTC ATG ATG CCA GGC GCG GAC TAC G -3'
HcBPST135I Ant	T_m >75°C	5'-CCC GGA Gat CGT AGC GAA CAC AAC GTG GGT GAT CTT GGA G -3'
HcBPST135K Sen	T_m >75°C	5'-GCT ACG Aag TCC GGG TTC ATG ATG CCA GGC GCG GAC TAC G -3'
HcBPST135K Ant	T_m >75°C	5'-CCC GGA ctT CGT AGC GAA CAC AAC GTG GGT GAT CTT GGA G -3'

2.2 Instruments

Instrument	**Model**	**Company**
Balance LA 230S Sartorius	Germany	Balance LA 230S Sartorius
Autoclave	Vx-120 Systec GmbH	Labor-systemtechni Systec
pH Meter	Digital pH meter 325	WTW
Centrifuge	Universal 32R	Hettich
	Biofuge 13	Heraeus Sepatech
	Avanti®- J-E Centrifuge	Beckman Coulter
	Sigma 1-15K	Sigma Centrifuges
-80°C Freezer	Hera Freeze	Heraeus
Spectrophotometer	Ultrospect 1000	Pharmacia Biotech
Incubator shaker	HT	Infors HT
Thermo block Dri	Block DB-3	Techne
Water purification system	Arium 611 VF	Sartorius, Germany
Clean bench	LaminarAir HLB 2472	Heraeus
	Laminar Air HBB 2460	Heraeus

Instrument	**Model**	**Company**
Heating circulator water bath	MW-4	Julabo
Magnetic rotator	VF2	IKA-Labortechnik (Janke & Kunkel)
Ultrasonic Cell- Disruptor PCR cycler Gel documentation MultiImage TM	Sonifier 250 T-Proffessional Gradient Light Cabient	Branson (G. Heinemann) Biometra Alpha In. Corp
Electrophoresis	Mini-Sub Cell Sub Cell GT Protein Chamber	BioRad BioRad Biometra
LC-MS (ESI-MS)	3200 Q TRAP, Analyst version 1.4.2 software, N2 collision gas.	Applied Biosystems Sciex
EI-MS	double focussing sectorfield, Resolution: 2000 (10% valley definition), Source Temp.: 180 °C, Electron energy: 70 eV	Thermofinnigan MAT (Bremen, Germany)
HPLC	Elite LaChrom series • L-2200 auto sampler • quaternary L-2130 Pump equipped with low-pressure gradient • L-2455 diode array detector • EZ Chrome Elite software	VWR-Hitachi
	Hyper Clone ODS column (C18, 250 x 4.6 mm, 3µm)	Phenomenex

3 Methods

3.1 General molecular biology methods

3.1.1 Design of mutant primers

3.1.1.1 Primers design according to the QuickChange® SDM protocol

The QuickChange® site-directed mutagenesis System (QCM) developed by Stratagene 'La Jolla, CA' (Zheng et al., 2004; Stratagene, 2005) is the simplest and most broadly usable protocol with this approach; the mutation is introduced in a single PCR with one pair of complementary primers containing the mutation of interest. The mutagenic primers for use in this protocol must be designed individually according to the desired mutation. The following considerations should be made for designing mutagenic site and selection primers: 1- Both of the mutagenic primers must contain the desired mutation and anneal to the same sequence on opposite strands of the plasmid. 2- Primers should be between 25 and 45 bases in length and the melting temperature (T_m) of the primers should be greater than or equal to 78°C. 3- The desired mutation should be in the middle of the primer with ~10–15 bases of correct sequence on both sides. 4- The primers optimally should have a minimum GC content of 40% and should terminate in one or more C or G bases. In this protocol (Fig. 19) the wild type and the two mutant primers are used. During the temperature cycling *Pfu* DNA polymerase extends the primers (containing the desired mutation). Annealing of the mutant primers produces a mutated plasmid containing staggered nicks. After the PCR reaction the product is treated with *Dpn* I. restriction enzyme which is specific for methylated and hemimethylated DNA. *Dpn* I is used for parental DNA template digestion and selection for mutation containing synthesized DNA. DNA isolated from almost all *E. coli* strains is methylated and digested by *Dpn* I. The last step is the transformation of the nicked plasmid containing the required mutations in DH5α competent cells. To decrease the possibility of random mutations through the PCR reaction, it is essential to use small amount of the template, high fidelity of the *Pfu* DNA polymerase, and decrease the number of thermal cycles.

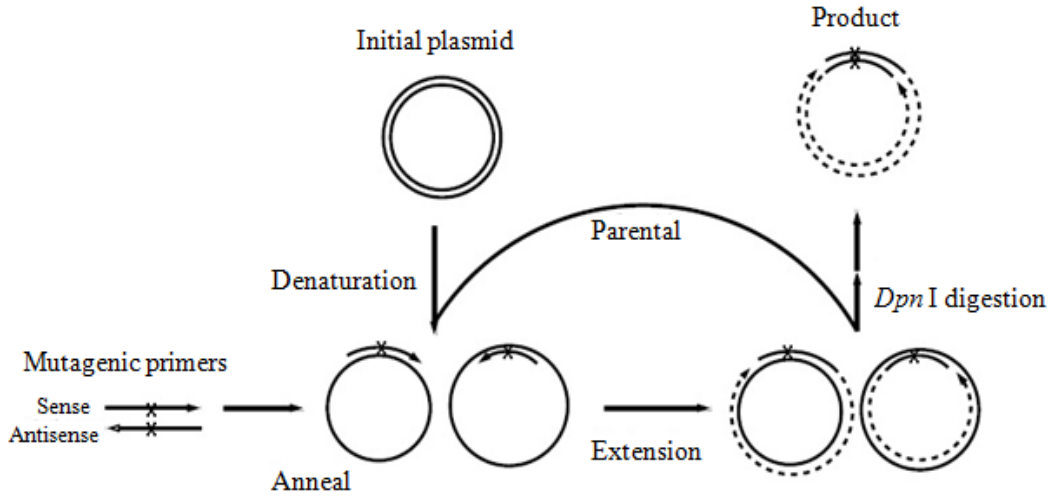

Fig. 19 Schematic representation of the QuikChange® site-directed mutagenesis method modified from; Loening, (2005).

3.1.1.2 Primer design according to (Zheng et al., 2004)

In this protocol, they developed a new primer design method based on the QuickChange® SDM protocol which significantly improves the PCR amplification efficiency. This design method minimizes primer dimerization and ensures the priority of primer-template annealing over primer self-pairing during the PCR. The simple and efficient modification for QCM stated in this protocol overcomes and eliminates the problems associated with primer pair self-annealing. With this modification the primer can be designed as for routine PCR experiments since the T_m value of the primer does not appear to be a strict determining factor anymore. Partial overlapping automatically enlarges the T_m difference between primer to template annealing and primer-pair self-annealing. A few rules should be considered during designing the mutant primers based on this protocol. 1- At least eight non-overlapping bases should be introduced at the 3' terminus of the primer. 2- The targeted mutation (s) should be included into both primers, and a silent mutation should be present in at least one of them. 3- At least one G or C should be placed at the end of each terminus.

3.1.1.3 Primer design according to (Liu and Naismith, 2008)

They have developed a site-directed mutagenesis protocol that conserved the one step simple procedure of the QuikChange® site-directed mutagenesis and at the same time enhances its efficiency. This modified protocol used a new primer design that enhanced primer-template annealing by removing primer dimerization and allowed the newly synthesized DNA to be used

as the template in subsequent amplification cycles. These two factors are the fundamental reasons for the enhanced amplification efficiency. This modified protocol mainly increased the efficiency of single and multiple mutations in a single experiment an option discordant with the standard QuikChange®. Moreover, the new protocol required significantly less parental DNA which supported the *Dpn*I digestion after the PCR amplification and enhanced the overall efficiency and reliability.

3.1.2 Site-directed mutagenesis PCR (SDM-PCR)

In this work, different approaches were used to get the mutant enzymes and all of them depend mainly on the simple one-step procedure of the QuickChange® site-directed mutagenesis protocol from Stratagene. In this protocol the PCR technique was performed in order to make a point mutation in a DNA fragment that was inserted in a super coiled double-stranded DNA vector. Two synthetic oligonucleotide primers either completely or partially overlapping containing the desired mutation were designed (see 3.1.1). During extension of the mutagenic primers in PCR cycles catalyzed by *Pfu* or *Phusion* DNA polymerase a mutated plasmid containing nicked circular strands was generated and so the product of the reaction is never used as a template. This mean that, this is a linear amplification technique (except in case of the primers designed according to Liu and Naismith, (2008) in which the PCR product could be used as a template because the non-overlapping part is long enough to bridge the formed nick. A schematic presentation of the SDM-PCR amplification process is illustrated in (Fig.20).

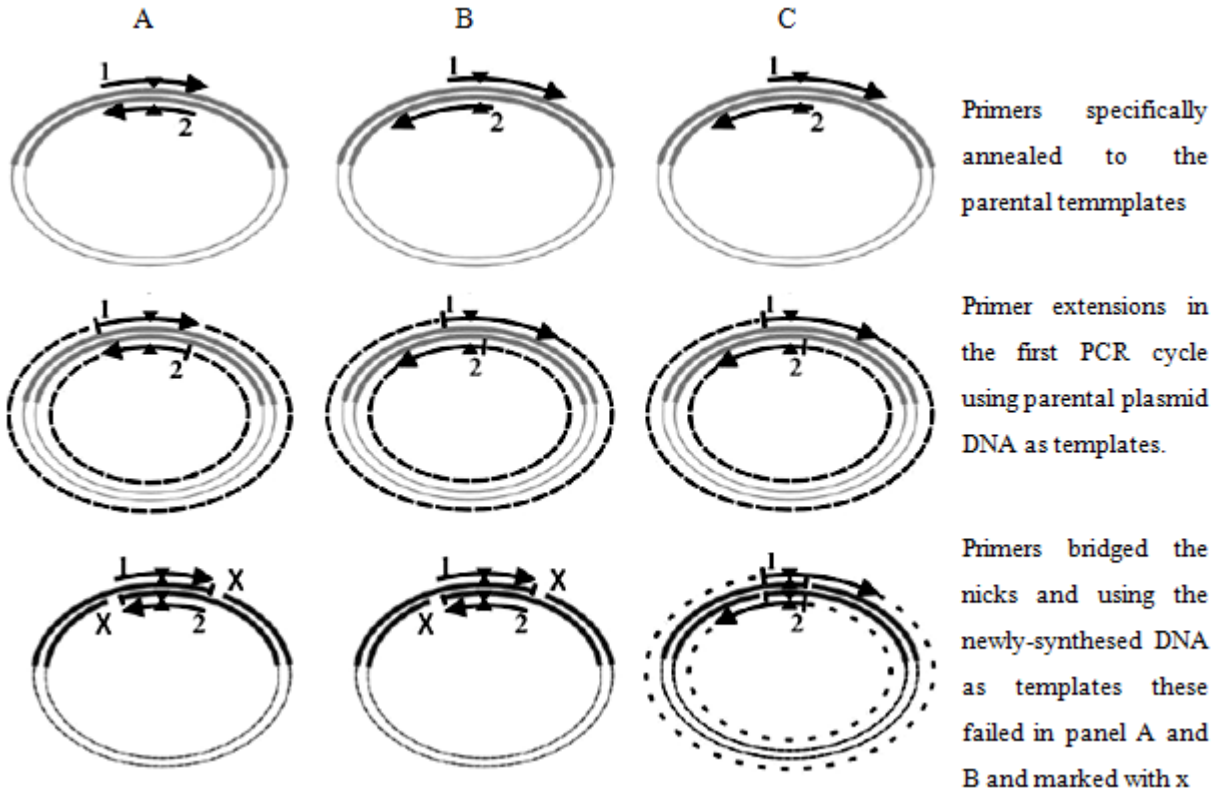

Fig. 20 Schematic representation of mutagenesis PCR amplification processes, A: using the primers designed as recommended in the QuickChange® protocol. PCR extension fails when primers annealed to the newly synthesized 'nicked' DNA. B: using primers designed according to Zheng et al., (2004). C: using the primer designed according to Liu and Naismith, (2008) to generate single-site mutation. The gray cycles represent the parental plasmid DNA, the cycles of dash lines represent the DNA amplified using the parental DNA as templates while the cycles of gapped dash line are the DNA amplified using the newly-synthesized DNA as templates. Arrows indicate the numbered primers; Triangles indicate the location of the mutations; Short bars indicate the 'nicks' in the newly synthesized DNA molecules.

3.1.3 PCR program and reaction composition used for HsBPS mutants production

The program used and the composition of each PCR reaction is slightly variable with each group of amino acids as follows:

3.1.3.1 HsThr135Leu mutant

The amounts used in the PCR reaction and the program are summarized in The following (Tab. 1).

Tab. 1 PCR reaction conditions and program used for HsT132L mutant production

PCR reaction constituents		**PCR program**		
10 pmol Sense mutagenic primer	1.5 µl	**Temp., °C**	**Time**	**Step**
10 pmol Anti-sense mutagenic primer	1.5 µl	Lid Temp. 99		preheating on
Template DNA Plasmid	1 µl	95	Pause	
10 x *Pfu* buffer	5 µl	95	4 min	Initial denaturation
10 mM dNTP mix	1.5 µl	70	pause	
3 U/µl *Pfu* DNA polymerase	0.5 µl	95	30 sec	Denaturation
Up to 50 µl PCR water	x µl	60	45 sec	Annealing
		72	10 min 4 25	Extension
		72	15 min	Final extension
		15	pause	

3.1.3.2 HsThr135Ala, Asp, Gly, Lys, Trp and Tyr mutants

The same previous conditions were used but the mutagenic primers were designed according to (Zheng et al., 2004).

3.1.3.3 HsThr135Glu, Phe, His, Ile, Met and Arg mutants

Also the (Zheng et al., 2004) method was used for designing the primers but we added 10µl enhancer mixture prepared according to (Ralser et al., 2006) which is an effective, low-cost and concentration-dependent PCR enhancer. It is a combination of betaine, dithiothreitol, and dimethyl sulfoxide that broadly enhanced the quantitative and/or qualitative output of PCRs especially in case of poor amplification of GC-rich DNA sequences.

3.1.3.4 HsThr135Cys, Asn, Pro, Gln, Ser, and Val mutants

For the production of this group of mutants, a different enzyme was used in addition to different PCR reaction composition and program, which are summarized in (Tab. 2).

Tab. 2 PCR reaction and program used for HsT135C, HsT135N, HsT135P, HsT135Q, HsT135S, and HsT135V mutants production

PCR reaction constituents		**PCR program**		
10 pmol Sense mutagenic primer	1.5 µl	**Temp., °C**	**Time**	**Step**
10 pmol Antisense mutagenic primer	1.5 µl	Lid temp. 99		preheating on
Template DNA Plasmid	1 µl	98	Pause	
5 x *Phusion* GC buffer	10 µl	98	1 min	Initial denaturation
10 mM dNTP mix	1.5 µl	98	30 sec	Denaturation
2 U/µl *Phusion* Hot Start II High fidelity DNA polymerase	0.5 µl	68	30 sec	Annealing
Up to 50 µl PCR water	x µl	72	2 min 3 34	Extension
		72	10 min	Final extension
		15	pause	

3.1.3.5 HaBPS, HpaBPS and HcBPS mutants

The same previous reaction constituents were used with some PCR program modifications as shown in (Tab. 3).

Tab. 3 PCR program used for HaBPS, HpaBPS, and HcBPS mutants

Temperature (°C)	**Time**	**Step**
Lid temp.99 °C		preheating on
98	Pause	
98	2.30 min	Initial denaturation
98	20 sec	Denaturation
68	45 sec	Annealing
72	3 min 3 34	Extension
72	10 min	Final extension
15	pause	

All the SDM-PCR products were treated with *Dpn*I to digest the parental DNA template and to select mutation-containing synthesized DNA. The *Dpn*I enzyme is specific for methylated and hemimethylated DNA. After 2 h of incubation at 37°C, five µl of *Dpn*I treated DNA was used for transformation in DH5α competent cells (3.1.6.1).

3.1.4 Agarose gel electrophoresis

This method is used for analysis and separation of DNA and RNA based on their size and charge. Small DNA molecules migrate faster than larger molecules through the agarose matrix under effect of electric current. Based on the size range of DNA molecules in the sample agarose gel is prepared in ranges of 0.5-2% agarose in TAE buffer. The higher the proportion of agarose the smaller the pore sizes of the matrix and the slower the migration rate. In this study 1% agarose gel was used. Ethidium bromide is used for visualization of bands. It intercalates nucleic acid molecules and its fluorescence increases 20-fold after this binding. According to the number of samples, the corresponding volume of TAE buffer and agarose weight were mixed and boiled in a microwave. After cooling down ethidium bromide was added and then poured in the gel tray and left to solidify at room temperature. Samples were loaded on the gel after mixing with loading dye along with DNA or RNA ladder. Then samples were run in a gel chamber filled with TAE buffer and under electric current (220 V). The gel was developed till the visible dyes in the loaded sample migrate 2/3 the distance. The bands in the gel are visualized under UV-equipped transilluminator.

3.1.5 Preparation of competent cells

The foreign DNA-plasmid can be taken in *E.coli* cells treated with calcium ions (competent cells) to produce large quantities of the plasmid in a process known as transformation. Calcium ions increase the permeability of the cell membrane to the foreign DNA. Preparation of the competent cells was done according to modified methods (Mandel and Higa, 1970; Cohen et al., 1972; Dagert and Ehrlich, 1979). A single colony from an overnight agar plate or a sterile loopful from frozen culture was inoculated into 5 ml of LB medium and incubated at 37°C with shaking at 225 rpm overnight. One ml of this fresh culture was transferred to 50 ml LB medium. Incubated at 37°C with shaking at 225 rpm until the OD_{600} reached 0.6-0.8. The culture was then chilled for 10 min on ice and the cells were harvested by centrifugation at 3000 rpm and 4°C for 10 min. The bacterial pellet was washed with 50 ml of ice-cold 0.1M $CaCl_2$. Cells were harvested by centrifugation as above and re-suspended in 20 ml of 0.1M $CaCl_2$. The cell suspension was then kept in ice for 20 minutes. After centrifugation and removing of the supernatant the pellets were re-suspended in 940 µl of 0.1M $CaCl_2$ solution. After 15 min incubation on ice 140 µl glycerol was added. Afterwards, the competent cells were stored at -80°C as 50 µl aliquots until further use.

3.1.6 Transformation of plasmid DNA in *E.coli*

3.1.6.1 Transformation into DH5α

This strain of *E. coli* was used for plasmid maintenance; because it has high transformation efficiency and high plasmid yields. The following procedure was used: 50 µl *E. coli* DH5α competent cells from a -80 °C storage (3.1.5) were incubated 5 minutes in ice then addition of 1 µl of foreign plasmid DNA, mixing and incubation of the mixture on ice for 25 minutes. Heat shock at 42 °C for 45 seconds was applied to force the foreign plasmid into the cells followed directly by 5 minutes incubation at 4 °C. In order to maximize transformation efficiency cells were allowed to grow in 250 µl SOC medium with continuous shaking at 37°C for 90 min. The whole bacterial suspension is plated on LB-agar medium containing ampicillin (100 µg/ ml).

3.1.6.2 Transformation into BL21 (DE3) pLysS

E. coli BL21 is mainly used for high-level of gene expression and production of recombinant protein in a bacterial system. The transformation procedure was the same as with DH 5α (3.1.6.1) except that the heat shock time was for 20 seconds and 700 µl SOC medium was used for growing bacterial culture. After one hour of incubation at 37°C about 100 µl of bacterial suspension was finally plated on LB-agar medium containing ampicillin (100 µg/ml) and chloramphenicol (60 µg/ml). Ampicillin resistance is acquired from the expression vector and chloramphenicol resistance is acquired from the host cells. Bacterial cultures containing plasmids with target insert were stored at -80°C in autoclaved solution of 20% glycerol/LB-medium. This continuous culture from *E. coli* BL21 (DE3) containing the desired gene can be used as a permanent supply to start protein expression.

3.1.7 Plasmid DNA isolation by minipreparation

Plasmid isolation by alkaline hydrolysis was carried out as described by Birnboim and Doly (1979). A single colony of the transformed DH5α plate was inoculated into 5 ml LB medium containing 20µg/ml ampicillin and grown over night at 37°C. In the second day, 2ml culture were centrifuged at 5000 rpm for 5 min. Bacterial pellets were resuspended in ice-cooled buffer I (300 µl) containing RNase A. Then buffer II (300µl) was added and the bacterial suspension was mixed by inverting cautiously 6 times and incubate at room temperature for maximum 5 min. Lysis of the cell wall took place in addition to denaturation of large

chromosomal DNA. RNA is destroyed by RNase I. Precipitation of proteins and denaturation of large chromosomal DNA were done by adding ice-cooled buffer III (300 µl), gentle mixing by inversion upside-down 6 times and incubation on ice for 20 min. Centrifugation at 13.000 rpm for 10 min was done to exclude the denatured proteins and DNA. The clear supernatant containing the DNA solution (800 µl) was transferred to a new Eppendorf tube. Residual contaminants and hydrolysed protein were extracted by vortex with 800 µl chloroform followed by centrifugation at 13.000 rpm for 10 min. The aqueous layer was transferred to a new Eppendorf tube. Isopropanol (0.7 volume) was added, mixed and followed by centrifugation at 13000 rpm for 30 min to precipitate plasmid DNA. The pellets were washed with 70% ethanol (500 µl) followed by centrifugation at 13.000 rpm for 10 min. The supernatant is discarded and the plasmid pellets are dried by 37°C and then dissolved in 50 µl distilled water. This purified plasmid can be directly used after measuring the concentration as described in (3.1.8) for transformation (3.1.6) restriction analysis (3.1.9) or stored at -20 °C for further usage.

3.1.8 Determination of the concentration of nucleic acids

Nucleic acids concentration was determined spectrophotometrically by measuring the absorbance value of the DNA or RNA samples at wavelength 260 nm. 10 µl samples were diluted (50×) in water and measured in a 0.5 ml quartz cuvette. The concentration is determined by using the following equation (Sambrook et al., 2001). Concentration (C) = A_{260} x absorbance x dilution factor. Where A_{260} is the absorbance coefficient which equals 40 ng/µl for single-stranded RNA or 50 ng/µl for double-stranded DNA. Purity of RNA was determined by measuring the ratio of absorbance at the wavelength 280 nm and 260 nm. Pure samples should have a ratio >1.5. Contaminations with proteins or phenolics would reduce this value due to their absorbance at 280 nm.

3.1.9 Restriction analysis

Restriction enzymes (endonucleases) are a group of enzymes which recognize a particular sequence of DNA bases and catalyze the cleavage of the double-stranded DNA. Plasmid DNA obtained from a normal spin mini preparation (3.1.7) was digested by *Kpn*I restriction enzyme using the following restriction protocol.(Tab. 4).

Tab. 4 Restriction protocol used for *Kpn*I digestion

Plasmid DNA	2 µl
10x restriction *Kpn*I buffer	2 µl
Restriction enzyme	0.5 µl

The reaction was incubated at 37°C for 2 hours, the sample was loaded on an Agarose gel (3.1.4), the size of the band was visualized and confirmed under UV-light and the plasmid with target DNA was prepared for sequencing.

3.1.10 Heterologous expression of recombinant protein in *E. coli*

pRSET-B vector containing wild-type or mutated BPS was transformed in *E. coli* BL21-Codon Plus (DE3) which was grown on agar plates containing ampicillin and chloramphenicol for selection. 10 ml LB medium containing 150 µg/ml ampicillin and 45 µg/ml chloramphenicol was inoculated with one colony and incubated on a shaker (225 rpm) at 37°C over-night (18 h). About 4 ml of the overnight culture was inoculated into 100 ml of the LB medium containing ampicillin (100 µg/ml). The cultures were grown at 37°C until OD_{600} of 0.6-0.8 was reached. one ml sample was immediately taken before induction (non-induced control), centrifuged at 5000 rpm for 5 min and the pellets were stored at -20°C until SDS-PAGE analysis. IPTG was added at final concentration of 0.5 mM in order to induce the production of the recombinant protein. The culture was then incubated in dark by shaking at 23°C for 20 h and then a second one ml sample (induced control) was collected, centrifuged and stored at -20°C until SDS-PAGE analysis. Bacterial cells after IPTG induction were harvested by centrifugation at 5000 rpm and 4°C each 100 ml into two halves (50 ml). and stored at -20°C for further use. Protein expression was done at low temperature to slow the metabolic processing of the bacteria and giving the chance for the protein to be folded in the right way. The aliquots of induced and control cultures were then analyzed for expression of the recombinant protein by SDS-PAGE analysis.

3.1.11 Extraction of expressed proteins from *E. coli* cells

Sonication (mechanical disruption of the cell wall) is a common method for breaking the cell wall and isolating the soluble protein. The frozen cell pellet from 50 ml culture (3.1.10) was re-suspended in 5 ml of lysis buffer with 20 mM imidazole, pH 8 at 4°C. Sonication of the cells was carried out on ice for 5 min at duty cycle 40% and output control of 1.5 using a Branson Sonifier B15. Cell debris was separated by centrifugation at 12000 rpm and 4ºC for 10 min. An

aliquot of the supernatant, after centrifugation had been taken as expressed protein control and stored at -20°C until SDS-PAGE analysis.

3.1.12 Purification of His_6 -tagged proteins by affinity chromatography

Affinity chromatography principle is based on the specific interaction between the tagged protein needed to be purified and the affinity matrix. So that the over-expressed protein binds specifically to the matrix while the other proteins are washed away and the target protein will be eluted thereafter with a special buffer. In this study, the cDNA of BPS is cloned into a pRSET B vector which is constructed so that the N-terminus of the expressed enzyme is a sequence of six histidine residues which has high affinity for divalent cations such as Ni^{+2}. So the supernatant which contained either His_6-BPS wild-type or its mutants as described in (3.1.11) was purified by using the nickel-nitrilotriacetic acid (Ni-NTA) protein purification system. 200 µl Ni-NTA were added to 3 ml cleared supernatant and the mixture was incubated with shaking at 4 °C for one hour to allow binding of the protein to the Ni ions. The slurry is transferred to an empty column and left to drop out the buffer. Unbound protein is eluted using washing buffer 4 ml (4 times 1 ml each). The His_6-tagged-fusion protein was eluted by using 2.5 ml (0.5 ml each) elution buffer which contained high concentration of imidazole.

3.1.13 Buffer change and desalting of protein samples

Desalting (removal of imidazole used in elution buffer from the protein) was done by gel filtration through PD_{10} column equilibrated with 25 ml (5 x elution volume of column) of 0.1 M potassium dihydrogen phosphate buffer pH 7. Then 2.5 ml of the protein sample was loaded onto a PD_{10} column. Soluble proteins were eluted with 3.5 ml 0.1 M potassium dihydrogen phosphate buffer pH 7.

3.1.14 SDS-PAGE gel electrophoresis

SDS-PAGE (sodium dodecyl sulfate polyacrylamide gel electrophoresis) is the most common analytical technique used to separate and characterize proteins according to their molecular masses (Laemmli, 1970). It is also used to confirm the successful expression of cloned cDNAs in heterologous expression systems. Polyacrylamide gel consists of a polymerized mixture of acrylamide and bisacrylamide. Acrylamide alone forms linear polymers. The bisacrylamide introduces crosslinks between polyacrylamide chains. The 'pore size' is determined by the ratio of acrylamide to bisacrylamide and by the concentration of acrylamide.

Induction of polymerization is done by addition of ammonium per-sulfate (APS) which spontaneously decomposes to form free radicals and N,N,N′,N′-tetramethylethylenediamine (TEMED) which is a free radical stabilizer and usually included to induce and accelerate polymerization. Sodium dodecyl sulfate (SDS) is a detergent which has an anionic head group and a lipophilic tail. It binds non-covalently to proteins and causes proteins to denature and disassociate from each other. It also gives protein negative charge. In the presence of SDS the actual charge of a protein is masked. During SDS-PAGE all proteins migrate toward the anode. SDS-treated proteins have very similar charge-to-mass ratios and similar shapes. During PAGE the rate of migration of SDS-treated proteins depends only on the molecular mass. Glycerol in the sample buffer helps the samples to sink and settle down in the wells. Bromophenol blue is a small size dye whose particles migrate faster than any protein and will help in tracing the development of the gel. The protein samples are denaturated in the presence of the sample loading buffer (ratio 1:1) at 95°C for 5 min. SDS-PAGE gel consists of 2 gels, stacking and resolving gels. In the stacking gel, proteins migrate through large pores and so no separation occurs only all the proteins in a sample will collect as a thin compact band at front of the resolving gel. The resolving gel has a narrower pore size and proteins will be separated according to their masses. Low molecular weight proteins will run faster than large molecular weight proteins. The ingredients of the resolving gel are mixed together in a flask. Then poured between the glass plates of the instrument and then water added to the surface to avoid air bubble and unsmooth surface formation. After 30 min, the gel polymerized and water is removed with a filter paper. The same procedure is carried out for the stacking gel except the addition of a comb to create the sample wells and no water is used. Protein samples are prepared as mentioned before. Bacterial pellets (from 1 ml bacterial suspension) are suspended in sample buffer (100 µl). Denatured in the same way as protein samples. Samples are loaded on the gel and run at 35 mA/200 V max supplied by a Standard Power Pack P25 (Biometra). The gel was run until the dye front reached the bottom. After electrophoresis, the protein bands of interest must be located in the gel by staining. The gel is stained by immersing in coomassie blue solution with gentle shaking for 30 min then de-stained by immersing in de-staining solution overnight.

3.2 Biochemical methods

3.2.1 Determination of protein concentration by dye-binding assay

This is a photometric protein assay which was carried out using the Bradford assay (Bradford, 1976). The principal of this assay depends on the interaction of Coomassie® Brilliant Blue G-250 with aromatic and basic amino acids of the protein. The negative charged sulfonate anions of the dye give charges to cationic amino acids which results in exposure of the hydrophobic part of the protein which by van der Waals forces interact with the phenyl residues of the dye. After this interaction with protein, the absorption maximum of the dye shifts from 465 nm (red, free form) to 595 nm (blue, bound form). 10 µl of a protein sample was mixed gently with 90 µl buffer and 900 µl Bradford-dye solution, incubated for 5 minutes at room temperature and measured for the absorbance at 595 nm. The assay was performed in a cuvette of one cm width at 595 nm in an UV/VIS spectrophotometer. Protein concentrations were calculated from a calibration curve which was prepared using serial dilutions (from 1 µg/ml to 10 µg/ml) of bovine serum albumin (BSA) stock solution (1 mg/ml).

3.2.2 Enzyme assays

3.2.2.1 Benzophenone synthases (BPSs) wild-types and mutants assays

The standard assay was carried out in a final volume of 250 µl and contained the amounts summarized in (Tab. 5) for the starter and the extender CoAs (which equals 2.5 x their reported K_m values) protein amounts, and buffer. After incubation at 35 °C for 10 min for all BPSs except HsBPS (30 °C) the reaction was stopped with 27.0 µl 50% acetic acid and the products were extracted twice with 250 µl ethyl acetate by vigorous mixing for 1 min and centrifugation at 13.000 rpm for 10 min. The organic phases were dried under vacuum and the residue was dissolved in 50 µl of methanol for HPLC. Analysis of the enzymatic products was performed by HPLC. The detection wavelength was 306 nm (benzophenones), 317, 325 nm (phenylpyrones) and 279 nm (4-hydroxycoumarin). Standard solutions of reference compounds served for quantification. For LC-MS analysis of the new enzymatic products (quinolone alkaloid and 4-hydroxycoumarin) the reaction volume, incubation time and the protein amount were increased to 500 µl, 60 min and 10 µg purified recombinant protein respectively. The reaction was stopped with 58 µl 50% acetic acid and the products were extracted three times with 500µl ethyl acetate by vigorous mixing for 1 min and centrifugation at 13.000 rpm for 10 min. The organic phases were collected in glass vials and dried under air. The products are dissolved 300 µl methanol and

purified using HPLC analytical column (Hyper Clone ODS column (C18, 250 x 3µm). The purified enzymatic products were analyzed using ESI MS/MS (3.3.2.1).

Tab. 5 Benzophenone synthases assay

	Starter-CoA	**Extender-CoA**	**Protein amount**	**Buffer**	**Temp.** °C	**Incubation Time min.**
HsBPS (Huang et al., 2012)	40 µM	232 µM	2 µg	0.1M KH_2PO_4 (pH 7.0)	30	10
HaBPS (Liu et al., 2003)	22 µM	79 µM			35	10
HcBPS (Zodi, 2011)	27 µM	39 µM			35	10
HpaBPS (Tocci, 2013)	10 µM	36 µM			35	10

3.2.3 HPLC analysis of enzyme assays

Analysis of enzymatic products including benzophenones, phenylpyrones, 4-hydroxycoumarin and quinolone alkaloids were carried out on HPLC. The mobile phase consisted of water containing 0.1% phosphoric acid (A) and methanol (B). The HPLC method gradient and the detection wave lengths are represented in (Tab.6).

Tab. 6 HPLC method gradient and detection wavelengths

Gradient		**Compounds analyzed**	**Detection (λ_{max}, nm)**
Time (min)	**Methanol (%)**		
0	30	Benzophenones	306
2	30		
15	80	Phenylpyrones	317, 325
18	90		
20	95	4-Hydroxycoumarins	279
23	95		
25	30	Quinolones	270
33	30		

3.2.4 Characterization of the over-expressed proteins

3.2.4.1 Determination of pH and temperature optima

The incubations were carried out as in (3.2.2.1) at pH values from 5.5 - 9 in 0.1M KH_2PO_4 buffer with 2 µg purified protein at 37°C for 10 min. Then the enzymatic products were analyzed by HPLC and the optimum pH was determined. At the optimum pH value another series of incubations were performed at different temperatures between 20 to 50 °C.

3.2.4.2 Determination of substrate specificity

At the pH and temperature optima, BPS mutants assays were performed using malonyl-CoA as extender substrate and a series of starter substrates: benzoyl-CoA, 2-hydroxybenzoyl-CoA, 3-hydroxybenzoyl-CoA, *p*-hydroxybenzoyl-CoA, anthraniloyl-CoA, *N*-methylantheraniloyl-CoA, 2-mercaptobenzoyl-*N*-acetylcysteamine, 2-methoxybenzoyl-*N*-acetylcysteamin. After incubation (at 30 °C for 5 min in KH_2PO_4 buffer pH 7.0) the products were extracted and analyzed by HPLC.

3.2.4.3 Linearity with protein amount and incubation time

The amount of the formed enzymatic products was determined as a function of the protein amount in the standard assay (0.145 -14.5µg) and incubation time (2, 4, 6, 10, 15, 20, 25, and 30 min).

3.2.4.4 Determination of kinetic data

The kinetic properties of BPS mutants were determined using different concentrations of benzoyl-CoA or 2-hydroxybenzoyl-CoA at a saturating concentration of malonyl-CoA or using different concentrations of malonyl-CoA at a saturating concentration of benzoyl-CoA or 2-hydroxybenzoyl-CoA. The used concentrations of these substrates were summarized in (Tab. 7). The protein amount used was 1.5 µg per assay and the incubation time for HsBPS mutants was 5 min. 2 µg protein and 10 min incubation time were chosen for HaBPS mutants so that the reaction velocity was linear during the assay period. The apparent K_m values for the HsBPS mutants substrates were calculated using Hyper 32, a hyperbolic regression program for the analysis of enzyme kinetic data (http://homepage.ntlworld.com/john.easterby/software.html).

Tab. 7 Concentrations of starter and extender -CoAs used for the determination of the kinetic data of BPS mutants

Mutant	2-Hydroxybenzoyl-CoA (mM)	Benzoyl-CoA (mM)	Malonyl-CoA (mM)
HsT135K	0.003- 0.144		0.149- 4.46
HsT135L		0.002- 0.061	0.149- 2.25
HsT135I		0.003- 0.129	0.112- 3.5
HaV146A/T135K	0.003- 0.252		0.037- 2.35
HaE54D		0.005- 0.044	0.037- 0.3
HaV146A		0.005- 0.202	0.037-0.374
HaC230G		0.003- 0.044	0.02- 0.3
HaV359L		0.005- 0.044	0.037- 0.3
HaN360S		0.005- 0.055	0.037- 0.3

3.3 Chemical methods

3.3.1 Chemical synthesis of acyl-CoAs, 2-hydroxy- and 2-aminobenzoyl-CoAs

Synthesis of 2-hydroxybenzoyl-CoA (salicoyl-CoA) and 2-aminobenzoyl-CoA (anthraniloyl-CoA) was performed according to (Lapidot et al., 1967; Stöckigt and Zenk, 1975). The synthesis consists of two steps. In the first step synthesis of *N*-hydroxysuccinimide ester (NHS) intermediate was done and in the second step transesterification of NHS ester with the free CoASH was performed.

3.3.1.1 Synthesis of NHS ester of 2-hydroxy and 2-aminobenzoic acid

2-Hydroxybenzoic acid (2.07 g, 15 mM) or 2-amino benzoic acid (2.06 g, 15 mM) was dissolved under heating (50 °C) in 75 ml dichloromethane then 1.73 g (15 mM) of *N*-hydroxysuccinimide (NHS) was added. The previous solution was cooled to 30 °C and then 3.5 g (17 mM) of *N*,*N* dicyclohexylcarbodiimide (DCC) were added. The reaction mixture was left for 16 hours at room temperature (with continuous gentle stirring for the first 6 hours then left stagnant). Dicyclohexyl urea was removed by filtration twice. The filtrate (CH_2CL_2) was washed with 1 M (21 g/250 ml H_2O) sodium bicarbonate ($NaHCO_3$) three times (75 ml each) and then three times with water (75 ml each). The wash was rejected. The filtrate (CH_2CL_2) was dried over anhydrous sodium sulfate and evaporated under vacuum. The resulting residue contained *N*-hydroxysuccinimide ester of 2-hydroxy or 2- amino benzoic acid. These intermediates was purified on a silica gel column (60 g, 20 x 2.5 cm). Elution was done using petroleum ether: ethyl acetate 7:3 (to remove all impurities) followed by CH_2CL_2 to elute the target compound.

Fractions of 100 to 250 ml were collected and monitored by using silica gel plates solvent system petroleum ether: ethyl acetate: methanol (6:2.5:1.5) as developer and UV light for detection of the spots. Fractions containing the intermediate ester were collected and evaporated to dryness before the ester was identified by mass spectrometry (Fig. 45, 46).

3.3.1.2 Transesterification of 2-hydroxy and 2-aminobenzoic-NHS esters

In 5 ml water 55 mg $NaHCO_3$ (to adjust pH 7.5-8) and 50 mg free CoA was dissolved. 80 mg of intermediate ester was dissolved in 4 ml acetone and add to the previous solution. In order to get a high yield of the product the previous mixture should be in a single phase by addition of excess amounts of acetone which also maintain the homogeneity of the solution (Al-Arif and Blecher, 1969). N_2 gas was applied for two minutes then the solution was kept for 18 h at 4° with continuous gentle stirring. 245 µl (1:10) formic acid was added at the end of the reaction to precipitate the product and all of the excess reactants. Acetone was evaporated under vacuum at room temperature. The aqueous phase was extracted with ethyl acetate three times (5 ml each). Discard ethyl acetate which contains the unreacted esters. The remaining aqueous phase was measured.

3.3.1.3 Purification of the CoA esters

Purification of 2-hydroxy and 2-aminobenzoyl-CoA esters was carried out according to (Beuerle and Pichersky, 2002) by using LC-18 solid-phase extraction cartridges (SPE) (Supelco, 1 g). The column was washed with 10 ml methanol, dH_2O and then with 4% ammonium acetate solution to remove any traces of water (5 column volumes each). The previously measured water phase was mixed with equal volume of 8% ammonium acetate to a final concentration of 4%. The mixture was loaded on the preconditioned column. The column was washed with 4% ammonium acetate solution until the effluent showed no free CoASH (determined by spectrophotometer at λ_{max} 261nm). The CoA esters were eluted by distilled water. Fractions containing the CoA esters were detected by their UV spectrum and then lyophilized overnight. LC-MS analysis was performed for the lyophilized product.

3.3.1.4 Electrospray ionization-mass spectrometry for 2-aminobenzoyl-CoA

Purified 2-aminobenzoyl (anthraniloyl)-CoA (0.1 mM) was analyzed using ESI–MS/MS by direct infusion with a flow rate of 10 µl/min. Mass spectrometric analysis was performed in the ESI negative Enhanced MS mode (EMS^-). MS/MS experiments were carried out using Enhanced Product Ion Scan in –ESI negative mode (EPI^-). Instrument setting and mass

standardization during the whole fragmentation pattern was dependent on the molecular ion peak $[M–H]^{-\cdot}$ The method parameters are summarized in (Tab. 8).

Tab. 8 Method parameters used in ESI-MS and ESI-MS/MS for 2-aminobenzoyl (anthraniloyl)-CoA

Parameter/Experiment	**EMS$^-$**	**EPI$^-$**
Curtain Gas	10 psi	10 psi
Collision Gas	high	high
Ion Spray Voltage	–4500 V	–4500 V
Heater	–	–
Ion Source Gas 1	10 psi	10 psi
Ion Source Gas 2	–	–
Declustering Potential	–100 V	–100 V
Entrance Potential	–10 V	–10 V
Collision Energy	–10 V	–48 V
Collision Cell Entrance potential	–19.06 V	–44.41 V

3.3.2 Synthesis of 2-methoxy and 2-mercaptobenzoyl-NAC esters

Synthesis of these two compounds as -NAC thioesters was carried out according to (Suo et al., 2000). (1 eq) of 2-methoxybenzoic acid or 2-mercaptobenzoic acid was dissolved in 10 ml tetrahydrofuran (THF). (1.2 eq) 1-hydroxybenzotriazole dissolved in another 10 ml THF. DCC (1.2 eq) is also dissolved in 10 ml THF. The three solutions were mixed together in one flask. 5 eq *N*-acetylcysteamin was added. The reaction mixture was stirred for 1 h at room temperature then K_2CO_3 (1eq) was added and the stirring continued for another 2 hours. The solution was filtered and the filtrate was evaporated to dryness under vacuum. The resulting residue was dissolved in 15 ml ethyl acetate, washed with 15 ml 10% $NaHCO_3$ solution once and then washed with 15 ml distilled water twice. The solution was dried over anhydrous Na_2SO_4 and concentrated under vacuum. The residue was purified using a silica gel column (60 g, 20 x 2.5 cm). Elution was carried out using 1-5% $MeOH/CH_2CL_2$ to give –NAC thioester. The identity of the product was checked by EI mass spectrometry.

3.3.2.1 Electrospray ionization mass spectrometry for enzymatic products

HPLC purified enzymatic products (10 µg/ml) of HsBPS wild type, HsT135K and HsT135L mutants were analyzed using ESI-MS/MS. Mass spectrometric analysis was performed in the ESI positive Enhanced MS mode (EMS^+) for the whole compounds. For further confirmation of 4-hydroxy-1-methyl-2(1*H*)-quinolone product the ESI negative Enhanced MS mode (EMS^-) was done. MS/MS experiments were carried out using Enhanced Product Ion Scan

in +ESI positive mode (EPI^+) for the whole compounds and -ESI negative mode (EPI^-) for 4-hydroxy-1-methyl-2(1*H*)-quinolone confirmation. Instrument setting and mass standardization during the whole fragmentation pattern was dependent on the molecular ion peak. The method parameters are summarized in (Tabs. 9, 10).

Tab. 9 Method parameters of ESI-MS used for enzymatic products identification

Parameter/Experiment	**EMS^+**	**EPI^+**
Curtain Gas	10 psi	10 psi
Collision Gas	high	high
Ion Spray Voltage	5500 V	5500 V
Heater	–	–
Ion Source Gas 1	14 psi	14 psi
Ion Source Gas 2	–	–
Declustering Potential	51 V	51 V
Entrance Potential	5.5 V	5.5 V
Collision Energy	10 V	Depend on the compound
Collision Cell Entrance potential	14.34 V	
Compound	**Collision Energy**	**Collision Cell Entrance potential**
1: 2,4,6 Trihydroxybenzophenone	30	16.61
2: 6-Phenyl-4-hydroxy-2-pyrone	30	15.43
3: 2,3',4,6-Tetrahydroxy-benzophenone	35	17.06
4: 6-(3-Hydroxy-phenyl)-4-hydroxy-2-pyrone	30	15.88
5: 4-Hydroxycoumarin	35	14.71
6: 4-Hydroxy-2(1*H*)-quinolone	35	14.68
7:4-Hydroxy-1-methyl-2(1H)-quinolone	52	15.07

Tab. 10 Method parameters of ESI-MS used for 4-hydroxy-1-methyl-2(1*H*)-quinolone confirmation

Parameter/Experiment	**EMS^-**	**EPI^-**
Curtain Gas	10 psi	10 psi
Collision Gas	high	high
Ion Spray Voltage	-4500 V	-4500 V
Heater	–	–
Ion Source Gas 1	14 psi	14 psi
Ion Source Gas 2	–	–
Declustering Potential	-20 V	-20 V
Entrance Potential	-10 V	-10 V
Collision Energy	-10V	-10V
Collision Cell Entrance potential	-17.21 V	-18.09 V

4 Results

4.1 Site-directed mutagenesis of *Hypericum sampsonii* BPS (HsBPS)

HsBPS is one of the plant type III PKSs. In most of these PKSs, threonine residues occupy three active site positions (135, 197, and 200 corresponding to alfalfa CHS2 132, 194, and 197) (Austin et al., 2004). The hydroxyl groups of threonines in these three positions are supposed to help driving and trapping polyketide intermediates using polar and/or hydrogen bonding interactions along the growing polyketide chain (Ferrer et al., 1999; Austin and Noel, 2003) It was shown that threonines in position 132 and 197 are involved in cyclization specificity in STS (Austin et al., 2004) and CHS respectively (Jez et al., 2000). Recently (Klundt et al., 2009) reported that replacement of Thr135 by leucine transformed HaBPS into phenylpyrone synthase (PPS) but the replacement of the Thr135 residue with glycine, alanine, valine, isoleucine, asparagine, and tyrosine instead of a leucine gave catalytically inactive proteins. Basically in this work we are interested in the position Thr135 in additional BPSs from different *Hypericum* species like *Hypericum sampsonii* (HsBPS) (Huang et al., 2012), *Hypericum calycinum* (HcBPS) (Zodi, 2011) and *Hypericum perforatum* ssp *angustifolium* (HpaBPS) (Tocci, 2013) which were recently cloned in our work group. All of these *Hypericum* BPSs are identical in the amino acids lining the active site cavity especially in the amino acid of interest (Thr135) which is conserved in all of them. The amino acids which are different between these *Hypericum* BPSs are located away from the active site. Initially we started with HsBPS to test different amino acids instead of Thr in position 135.

4.1.1 Detection of enzyme activity of wild-type HsBPS

First we had to reproduce the results of Huang et al. (2012) which were published about the activity of wild-type HsBPS. The highest activity was found with benzoyl-CoA (Fig. 21, a). It forms 2,4,6-trihydroxybenzophenone as a major product. In addition, a small amount of 4-hydroxy-6-phenylpyran-2-one as a side product was detected. HsBPS also accepts 3-hydroxybenzoyl-CoA as the second best substrate (Fig. 21, b) forming 2,3',4,6-tetrahydroxybenzophenone as major product and 4-hydroxy-6-(3-hydroxy) phenylpyran-2-one as a side product which is formed by only two decarboxylative condensations with malonyl-CoA. It also accepts 2-hydroxybenzoyl-CoA, anthraniloyl-CoA and *N*-methylanthraniloyl-CoA forming small amounts of 4-hydroxycoumarin, 4-hydroxy-2(1*H*)-quinolone and 4-hydroxy-1-methyl-2(1*H*)-quinolone (Fig. 21, c, d and e) respectively. All the results were confirmed by the UV

spectra, Rt values and LC–MS/MS (4.1.7) analysis for the major enzymatic products. Quantification of the products was done by using standard solutions of the available respective authentic reference compounds. HsBPS is inactive with 4-hydroxybenzoyl-CoA, 2-mercaptobenzoyl-*N*-acetylcysteamine and 2-methoxybenzoyl-*N*-acetylcysteamine. Control incubations with boiled enzyme lacked the respective enzymatic products.

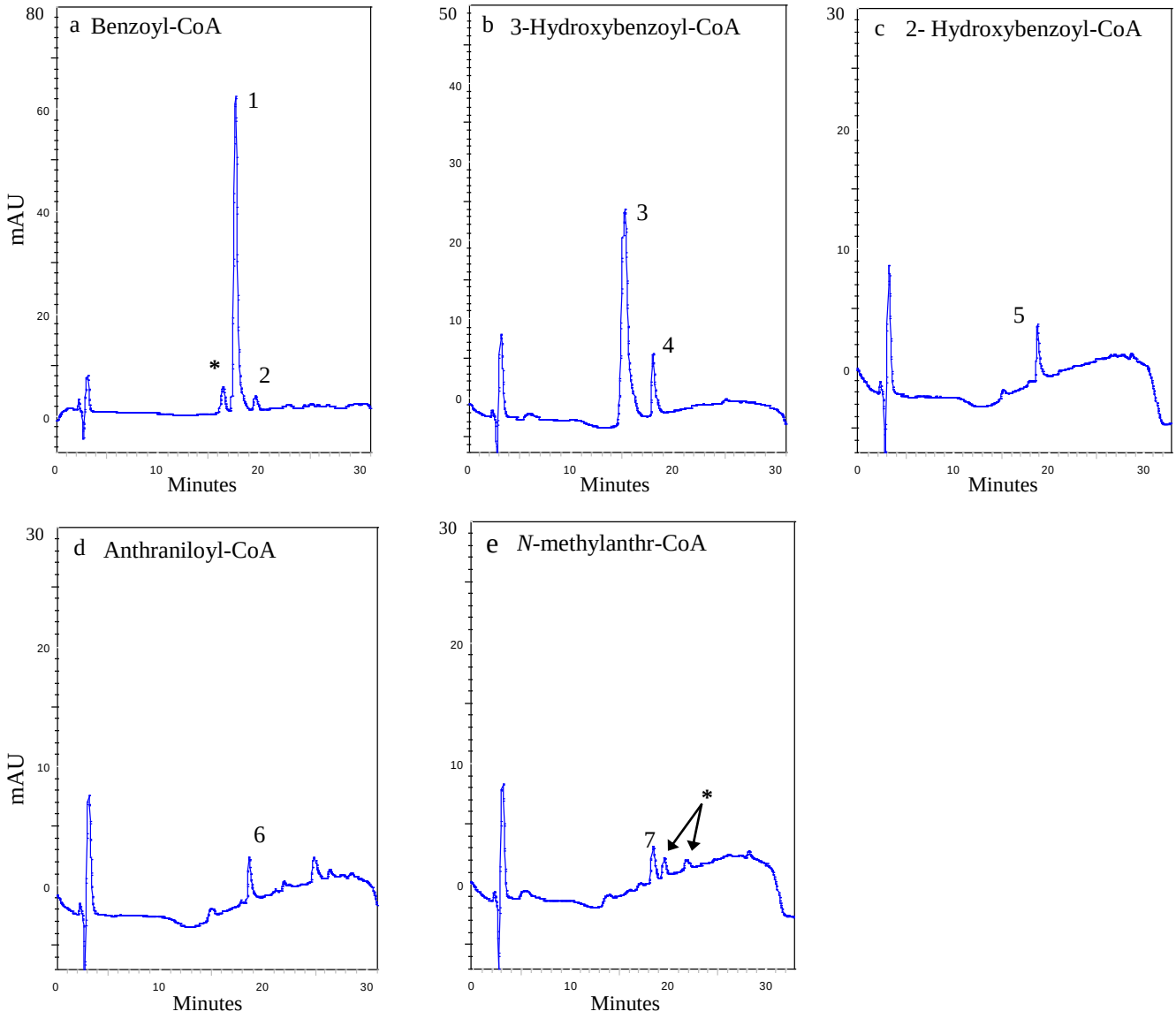

Fig. 21 HPLC analysis of wild-type HsBPS assays with a- benzoyl-CoA, b- 3-hydroxybenzoyl-CoA, c- 2-hydroxybenzoyl-CoA, d: anthraniloyl-CoA, e: *N*-methylantraniloyl-CoA.

1: 2,4,6-trihydroxybenzophenone. 2: 6-phenyl-4-hydroxy-2-pyrone, * unidentified peaks.
3: 2,3',4,6-tetrahydroxybenzophenone, 4: 6-(3-hydroxy-phenyl)-4-hydroxy-2-pyrone,
5: 4-hydroxycoumarin, 6: 4-Hydroxy-2(1*H*)-quinolone, 7: 4-hydroxy-1-methyl-2(1*H*)-quinolone,

4.1.2 Single mutations of wild-type HsBPS

H. sampsonii wild-type BPS accepts and prefers benzoyl-CoA as starter substrate and catalyzes its condensation with three molecules of malonyl-CoA forming 2,4,6-trihydroxybenzophenone as main product and a small amount of 4-hydroxy-6-phenylpyran-2-one as side product. The first aim was investigating the effect of replacement of Thr135 with the other 19 amino acids (Fig. 86 appendix) on the catalytic activity, substrate and product specificities of *H.sampsonii* BPS.

4.1.2.1 SDM-PCR to produce HsThr135Leu mutant

The polar amino acid threonine in position 135 in HsBPS was changed to non polar leucine by site-directed mutagenesis (Fig. 22, a). The resulting mutation is identified in that the first letter indicates the original amino acid at the corresponding position in the wild-type HsBPS protein and the last letter indicates the newly introduced amino acid. Under the PCR conditions described in (3.1.3.1) and the HsBPS mutagenic primers based on the QuickChange® site-directed mutagenesis protocol (Stratagene, 2005) were used. Actually, primers designed using this protocol were successful only with leucine and failed with other amino acids due to the high GC content of HsBPS especially in the mutation part. In addition, primer dimer formation is favored due to the complete overlapping between the primer pairs.

4.1.2.2 SDM-PCR to produce HsThr135Asp, Gly, Lys, Trp, Tyr and Ala mutants

In order to get this group of mutants (Fig. 22, c), six partially overlapping mutant primers were designed following the Zheng et al. (2004) method. This partial overlapping minimizes primer-self annealing, emphasizes primer-template annealing and will thus improve the PCR amplification efficiency.

4.1.2.3 SDM-PCR to produce HsThr135Glu, Phe, His, Ile, Met and Arg mutants

For this group of enzyme mutants (Fig. 22, e) we also designed a group of partially overlapping primers following the method mentioned by Zheng et al. (2004) but we were not able to get any product except by addition of 10 µl of enhancer mixture (Ralser et al., 2006). This is a low-cost concentration-dependent PCR enhancer which consists of a combination of betaine, dithiothreitol, and dimethyl sulfoxide and widely enhances the PCR yield especially in high GC content genes.

4.1.2.4 SDM-PCR to produce HsThr135Cys, Asn, Pro, Gln, Ser, and Val mutants

A lot of trials were done to get this group of mutants (Fig. 22, g) although the primers were designed using the same method (Zheng et al., 2004). No product was detected after the SDM-PCR amplification reaction. The only successful trial was achieved by changing the enzyme from *Pfu* DNA polymerase to *Phusion* Hot Start II DNA polymerase.

4.1.3 *Dpn*I digestion of the sequences for the 19 HsBPS mutants

The resulting 19 SDM-PCR amplification products (which contained the remaining wild-type strand) used as a template and the newly formed mutated plasmids with staggered nicks were subjected to *Dpn*I digestion. This is an endonuclease (target sequence 5´-Gm6ATC-3´) specific for methylated and hemimethylated DNA and is used to remove the wild-type DNA template.

4.1.4 Transformation, plasmid isolation and restriction analysis of HsBPS mutant sequences

Transformation of the HsBPS mutant sequences in *E coli* DH5α was performed as described in (3.1.6.1) followed by plasmid isolation (3.1.7) and then restriction analysis (3.1.9) for size confirmation (Fig. 22, b, d , f, and h). All the mutated plasmids with target DNAs were confirmed by sequencing.

4.1.5 Expression of sequences encoding HsBPS and its mutants

Confirmation of the over-expression of HsBPS wild-type and its mutants (HsThr135Asp, Gln, Pro, Lys, Ile and Leu) was done by means of SDS-PAGE analysis (3.1.14). The following fractions were analyzed: crude bacterial protein extracts before and after induction, the soluble portion of the protein extract after induction and the affinity-purified proteins (Fig. 23, A, B, and C). Protein bands were stained with Coomassie brilliant blue. Both the HsBPS wild-type and the mutants had subunit molecular masses of about ~43 kDa however, the Hs T135D, T135Q and T135P mutants did not show any over-expression in the host cells

Agarose gel electrophoresis of SDM PCR amplification products.

Agarose gel electrophoresis of the mutated sequences after *Kpn*I digestion.

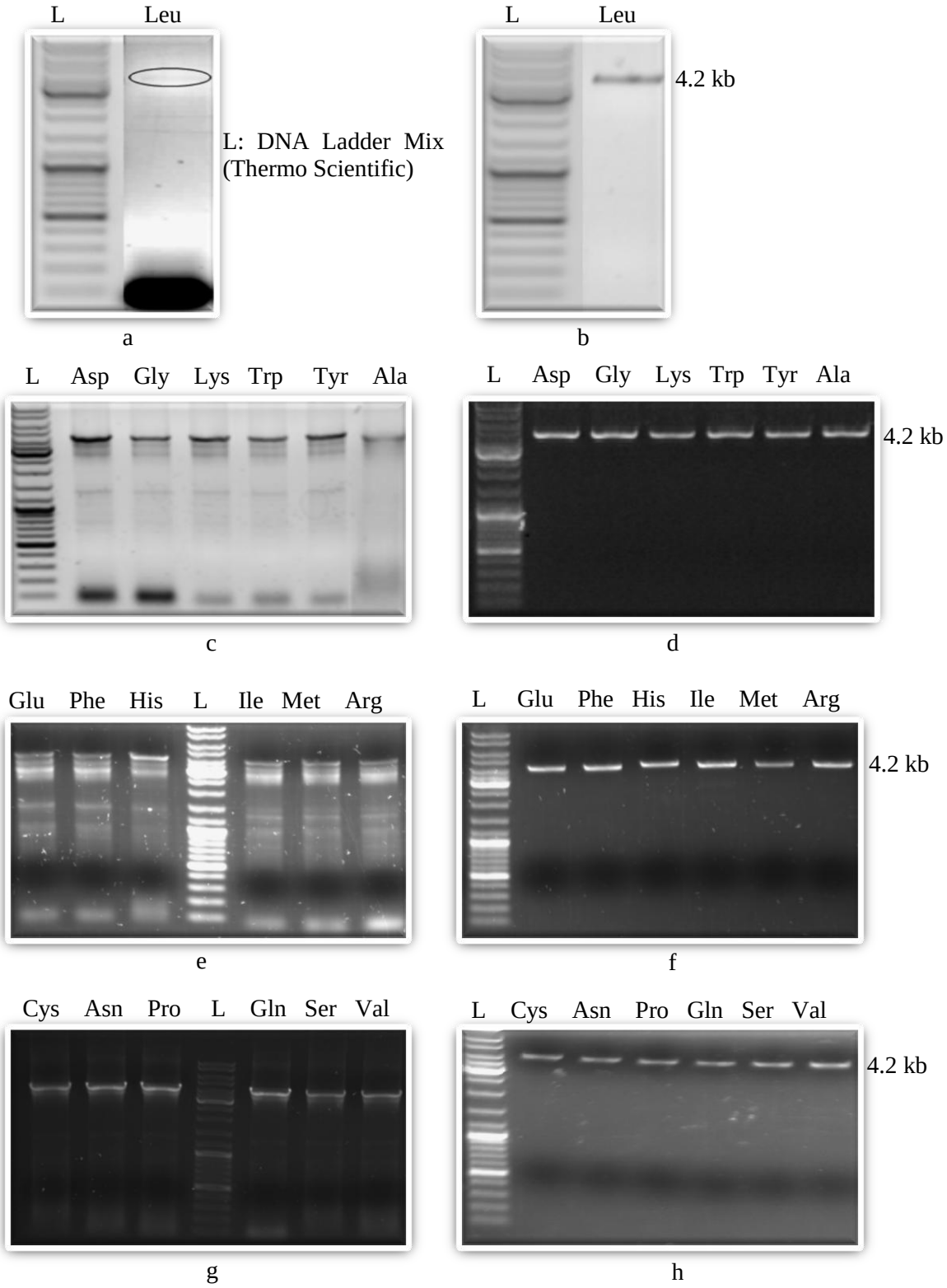

Fig. 22 SDM-PCR amplification products of HsBPS mutants **a:** Leu. **c:** Asp, Gly, Lys, Trp, Tyr, and Ala. **e:** Glu, Phe, His, Ile, Met, and Arg. **g:** Cys, Asn, Pro, Gln, Ser, and Val. *Kpn*I digestion for size confirmation of HsBPS sequences with single mutations, **b:** Leu. **d:** Asp, Gly, Lys, Trp, Tyr, and Ala. **f:** Glu, Phe, His, Ile, Met, and Arg. **h:** Cys, Asn, Pro, Gln, Ser, and Val.

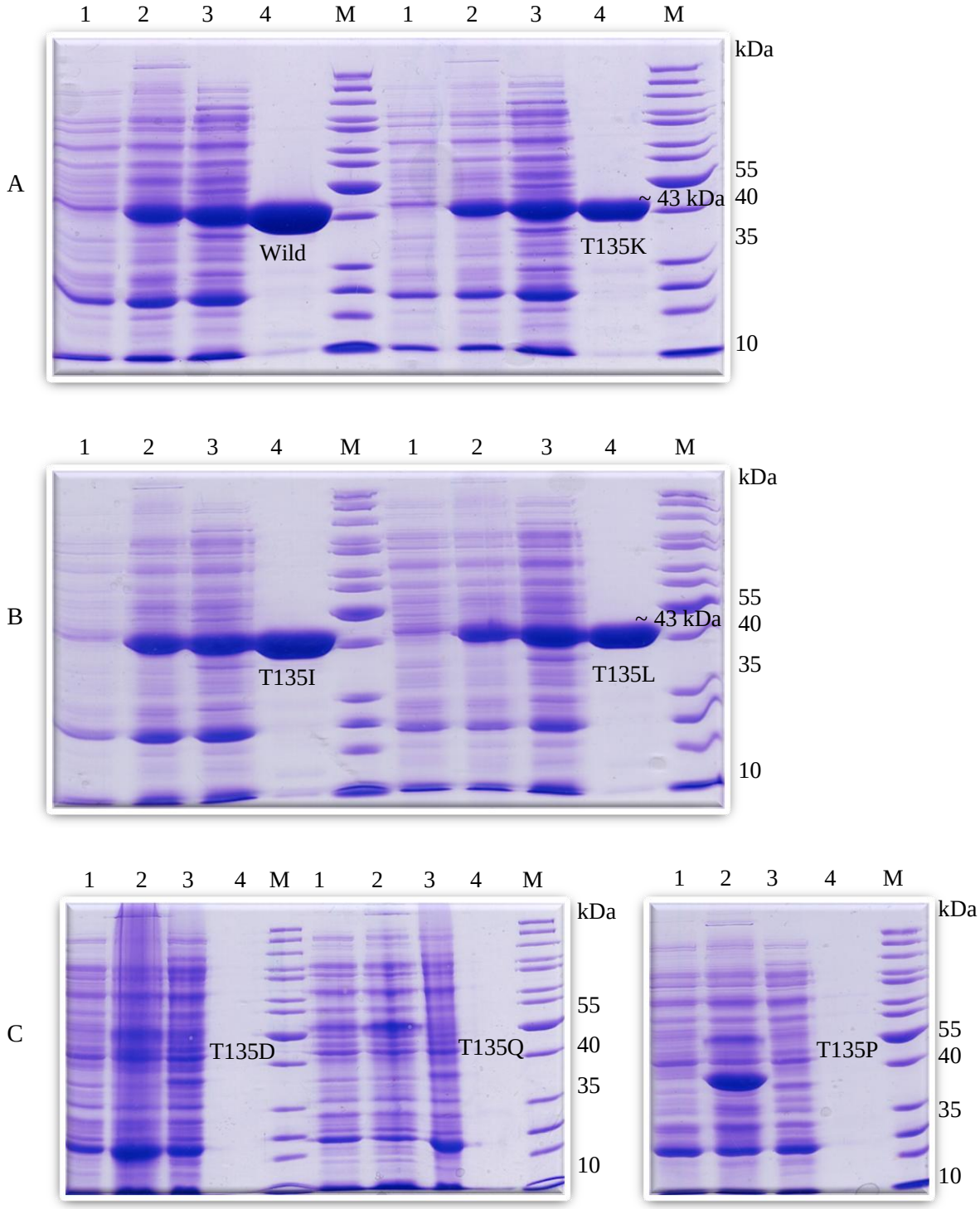

Fig. 23 SDS-PAGE demonstrating the purification by the Ni-NTA system, A: HsBPS wild-type and HsT135K, B: HsT135I and T135L mutants, C: HsT135D, HsT135Q and HsT135P mutants.
M: protein marker, 1: pre-induction, 2: post-induction, 3: soluble protein, 4: affinity-purified protein (10 µg).

4.1.6 Testing the activities of the HsBPS single mutants

Each PCR-mutated plasmid was transferred in *E.coli* BL21 as described in (3.1.6.2) for protein over-expression. The Ni-NTA system was used for the purification of the His_6-tagged HsBPS mutants (3.1.12) which were then subjected to BPS assays (3.2.2.1) using HPLC (3.2.3) to characterize their catalytic activity and substrate specificity (3.2.4). The activities of the affinity-purified single mutants with various starter substrates were determined in (ng/assay) and compared with those of HsBPS wild-type. All the results are summarized in (Tab. 11). From the tested 19 amino acids, three of them showed no over-expression in the host cells (HsT135D, HsT135Q and HsT135P) and the others either decreased the activity markedly (HsT135E, HsT1135R, HsT135G, HsT135W, and HsT135Y) when compared to the wild-type HsBPS or they gave mutants which were more or less similar to the wild-type in their activity with different starter substrates. HsT135K, HsT135L and HsT135I mutants showed dramatic changes in the product and substrate specificities. Notably, the HsT135K mutant preferred 2-hydroxybenzoyl-CoA as a starter substrate forming 4-hydroxycoumarin as main product (Fig. 24, c). It catalyzes a single decarboxylative condensation with malonyl-CoA to form an intermediate diketide which undergoes intramolecular cyclization and enolization yielding 4-hydroxycoumarin (Liu et al., 2010). The HsT135L and HsT135I mutants prefer benzoyl-CoA forming 4-hydroxy-6-phenylpyran-2-on as main product (Figs. 25, a and 26, a). They catalyze iterative condensation of one benzoyl-CoA with two malonyl-CoAs forming a triketide intermediate which undergoes cyclization via C-5 keto-enol oxygen to C-1 and thus lactonization into phenylpyrone (Klundt et al., 2009). Interestingly, anthraniloyl and *N*-methylanthraniloyl-CoAs were accepted as substrates forming 4-hydroxy-2(1*H*) quinolone and 4-hydroxy-1-methyl-2(1*H*)-quinolone products respectively (Fig. 25, d and e). Nothing was reported about the acceptance of BPSs to anthraniloyl and *N*-methylanthraniloyl-CoA substrates and formation of quinolone alkaloids. Remarkably, HsT135K, HsT135L and HsT135I mutants showed higher activity with anthraniloyl-CoA than with *N*-methylanthraniloyl-CoA unlike benzalacetone synthase (BAS) from *Rheum palmatum* (Polygonaceae). This is a diketide-producing PKS and can efficiently catalyze condensation of *N*-methylanthraniloyl-CoA or anthraniloyl-CoA with malonyl-CoA or methylmalonyl-CoA to produce 4-hydroxy-2(1*H*)-quinolones. It was reported that the activity with *N*-methylanthraniloyl-CoA and anthraniloyl-CoA is 80% and 4%, respectively (Abe et al., 2006). Incubation with heat-denatured protein failed to show any activity indicating the enzymatic origin of the formed products. Identification of the enzymatic

products was done in comparison to authentic reference compounds by co-chromatography, UV spectroscopy and LC-MS/MS (4.1.7) analysis of the major enzymatic products. All the HPLC chromatograms of the HsT135K, HsT135L, and HsT135I assays are represented in (Figs. 24, 25, and 26).

Tab. 11 Effect of replacement of Thr135 in HsBPS with different amino acids on the product formation profiles with various starter substrates. Amounts of the products were calculated in ng/assay. The final volume of the assay was 125 µl, and 2 µg protein and 10 min incubation time at 30 °C were used. Interesting changes compared to the wild-type are highlighted in bold.

		Benzoyl-CoA		**3-Hydroxybenzoyl-CoA**		**Salicoyl-CoA**
	Enzyme mutant	**2,4,6-trihydroxy-benzophenone**	**6-phenyl-4-hydroxy-2-pyrone**	**2,3',4,6-tetrahydroxy-benzophenone**	**6-(3-hydroxy-phenyl)-4-hydroxy-2-pyrone**	**4-hydroxy-coumarin**
1	T135D (aspartic acid)	No expression				
2	T135Q (glutamine)	No expression				
3	T135P (proline)	No expression				
4	HsBPS wild-type	**135**	**5**	**95.6**	**4.3**	**7**
5	T135E (glutamic acid)	No product	10.9	No product	4.5	No product
6	T135R (argenine)	No product	2.1	No product	1.5	No product
7	T135G (glycine)	2.1	2	1.5	3	7.8
8	T135W (tryptophane)	No product	3	No product	2.5	15.3
9	T135Y (tyrosine)	2	13.9	No product	2.7	5.7
10	T135A (alanine)	62.3	45.3	20.2	67.9	12.3
11	T135V (valine)	29	36.6	18.3	68.5	6.9
12	T135L (leucine)	4.4	**226.6**	5.8	**160.4**	7.4
13	T135I (isoleucine)	3.6	**250.8**	No product	**102**	7
14	T135K (lysine)	No product	4.8	No product	1.7	**175.8**
15	T135M (methionine)	32.9	76	No product	85	44.6
16	T135F (phenylalanine)	No product	12.5	No product	3.5	30.8
17	T135H (histidine)	No product	21.5	No product	14.7	12.9
18	T135N (aspragine)	22.3	2.8	29.7	18.4	3
19	T135S (serine)	124.7	18.2	69.2	40.7	13
20	T135C (cysteine)	50.8	17.6	40.1	42.1	5.9

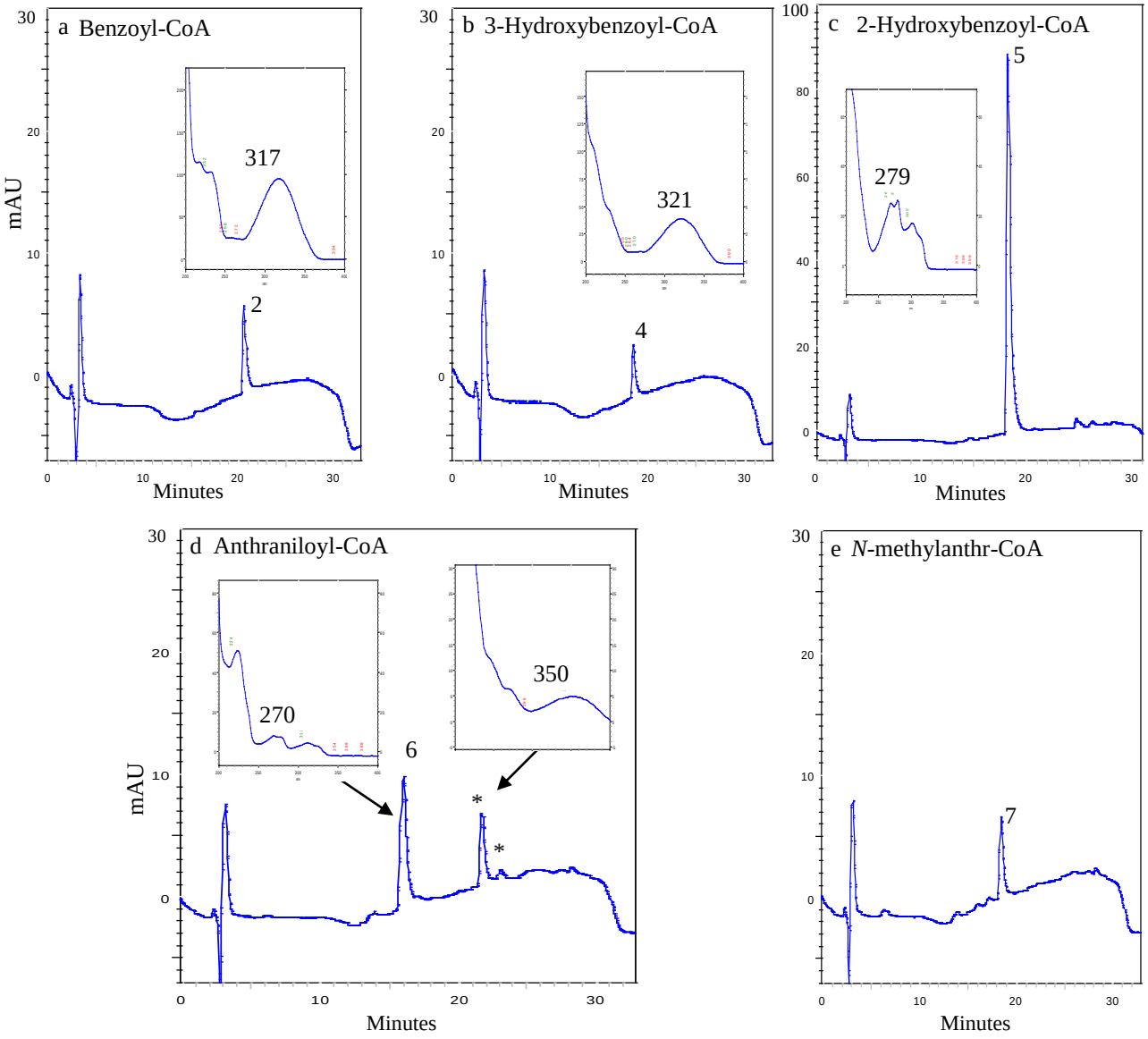

Fig. 24 HPLC analysis of HsT135**K** assays with, a: benzoyl-CoA, b: 3-hydroxybenzoyl-CoA, c: 2-hydroxybenzoyl-CoA, d: anthraniloyl-CoA, e: *N*-methylantraniloyl-CoA.
2: 6-phenyl-4-hydroxy-2-pyrone, 4: 6-(3-hydroxy-phenyl)-4-hydroxy-2-pyrone, 5: 4-hydroxycoumarin, 6: 4-hydroxy-2(1*H*)-quinolone, 7: 4-hydroxy-1-methyl-2(1*H*)-quinolone, *: unidentified peaks.

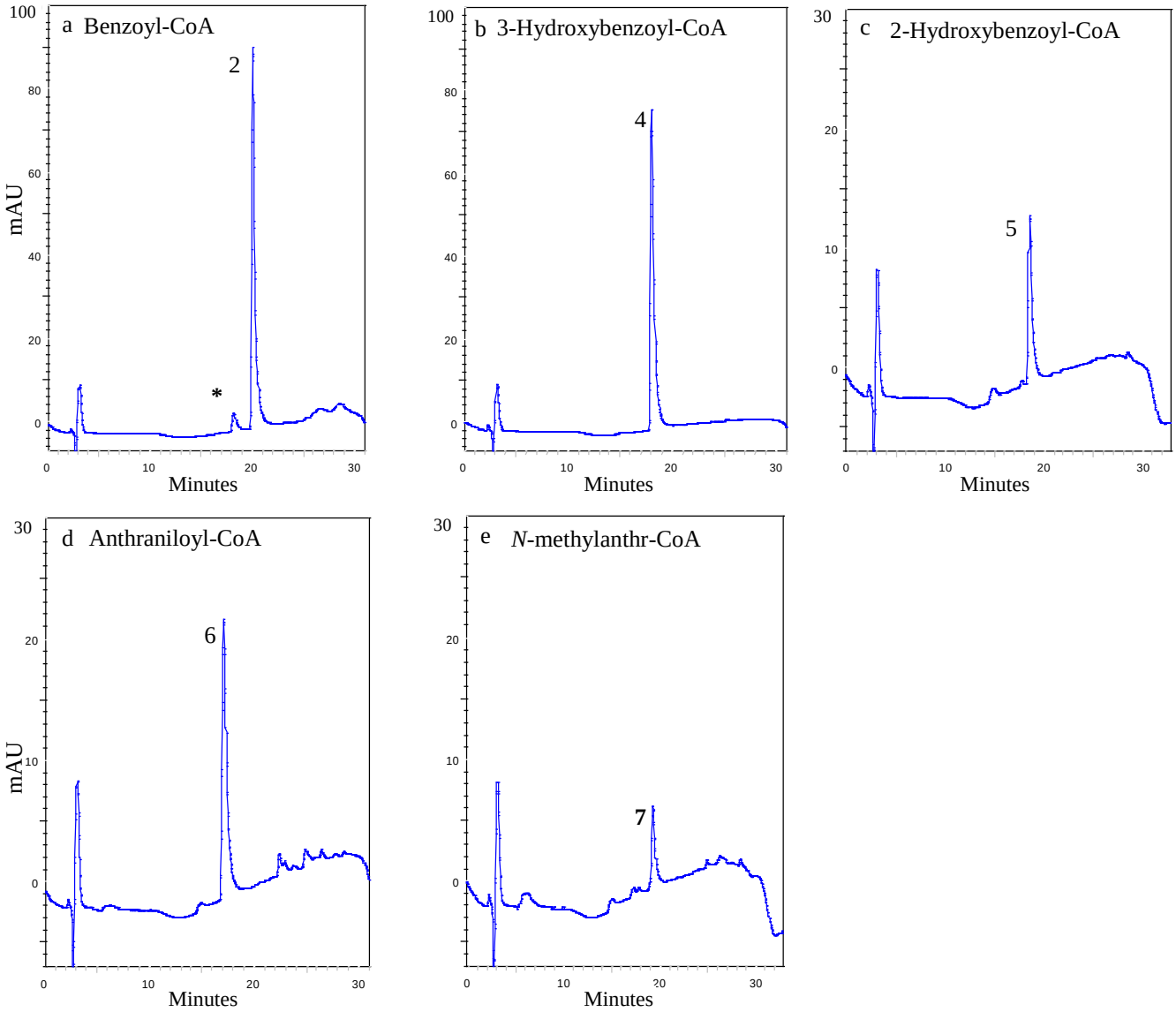

Fig. 25 HPLC analysis of HsT135**L** assays with a: benzoyl-CoA, b: 3-hydroxybenzoyl-CoA, c: 2-hydroxybenzoyl-CoA, d: anthraniloyl-CoA, e: *N*-methylantraniloyl-CoA.

2: 6-phenyl-4-hydroxy-2-pyrone. 4: 6-(3-hydroxy-phenyl)-4-hydroxy-2-pyrone, 5: 4-hydroxycoumarin, 6: 4-hydroxy-2(1*H*)-quinolone, 7: 4-hydroxy-1-methyl-2(1*H*)-quinolone, *: unidentified peak.

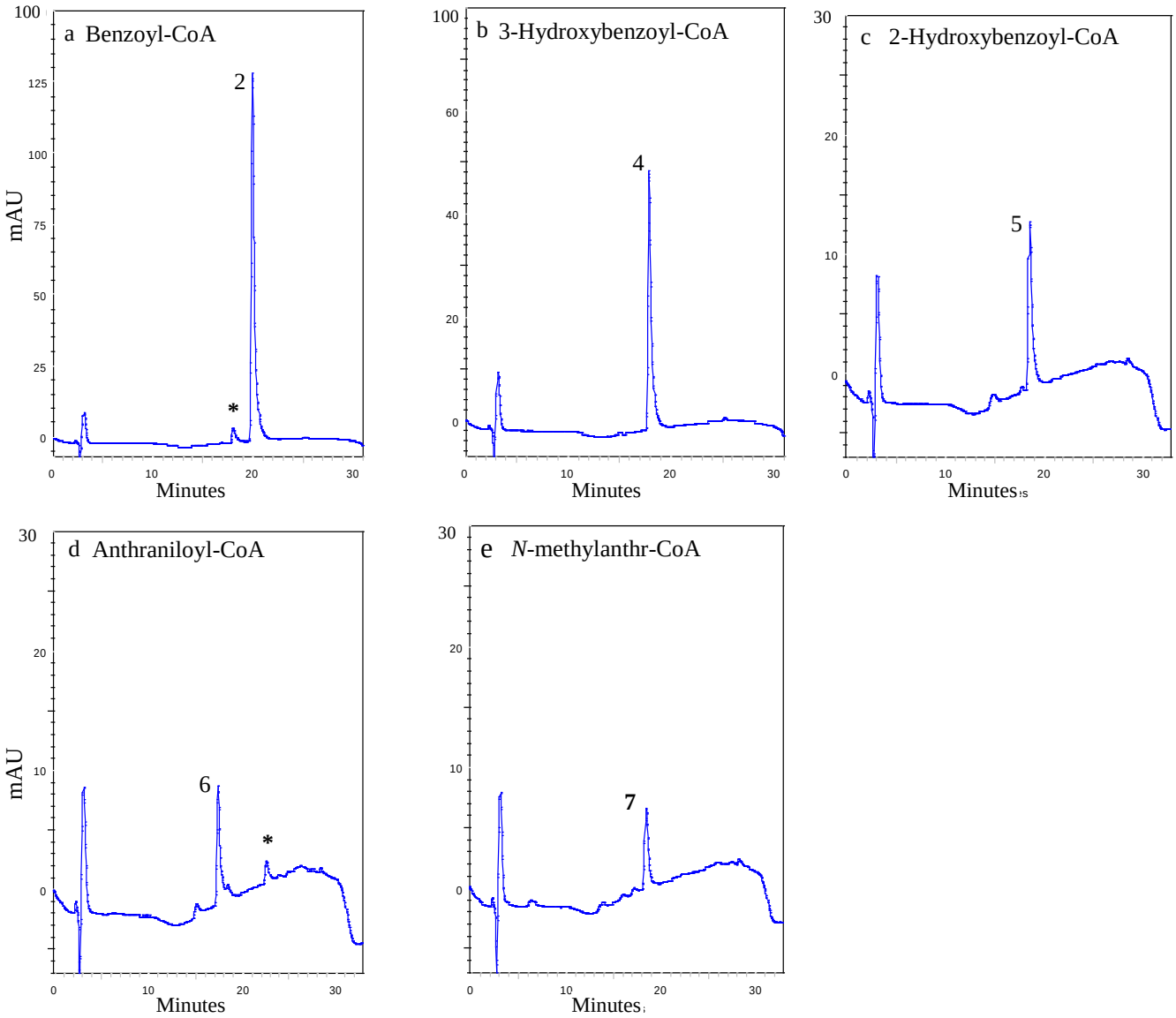

Fig. 26 HPLC analysis of HsT135**I** assays with a: benzoyl-CoA, b: 3-hydroxybenzoyl-CoA, c: 2-hydroxybenzoyl-CoA, d: anthraniloyl-CoA, e: *N*-methylantraniloyl-CoA.
2: 6-phenyl-4-hydroxy-2-pyrone. 4: 6-(3-hydroxy-phenyl)-4-hydroxy-2-pyrone, 5: 4-hydroxycoumarin, 6: 4-hydroxy-2(1*H*)-quinolone, 7: 4-hydroxy-1-methyl-2(1*H*)-quinolone, *: unidentified peaks.

4.1.7 Results of LC-MS/MS analysis of enzymatic products

The structures of the major HPLC-purified enzymatic products of *H. sampsonii* wild-type and its mutants (HsT135K and HsT135L) were confirmed by LC-MS/MS 'Positive Full-Scan Mode analysis' using the enzymatic products themselves and authentic reference compounds. This type of scan displays one mass unit higher than the initial mass of the tested compounds $[M+H]^+$. The x-axis shows the expanding mass-to-charge (m/z) ratio whereas the y-axis represents the relative abundance of each ion which is associated to the number of times that an ion of that m/z ratio hits the detector. The mass spectra of the major enzymatic products and the corresponding reference compounds (4-hydroxycoumarin, 4-hydroxy-2(1*H*)-quinolone, 4-hydroxy-1-methyl-2(1*H*)-quinolone, 6-phenyl-4-hydroxy-2-pyrone, 6-(3-hydroxy-phenyl)-4-hydroxy-2-pyrone, 2,4,6-trihydroxybenzophenone and 2,3',4,6-tetrahydroxybenzophenone) are illustrated in (Figs. 27-39). LC-MS/MS 'Negative Full-Scan Mode analysis' was also done for 4-hydroxy-1-methyl-2(1*H*)-quinolone to compare the spectrum to the published results (Resmi et al., 2013).

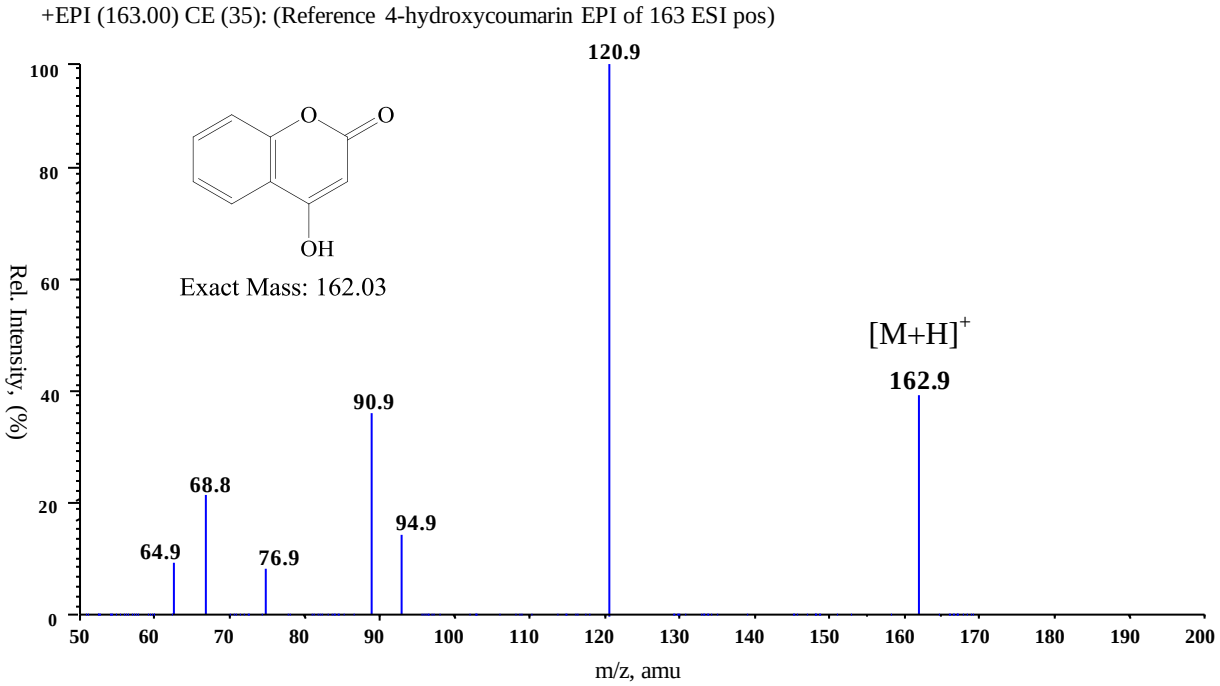

Fig. 27 Mass spectrum (EPI^+) of authentic 4-hydroxycoumarin reference.

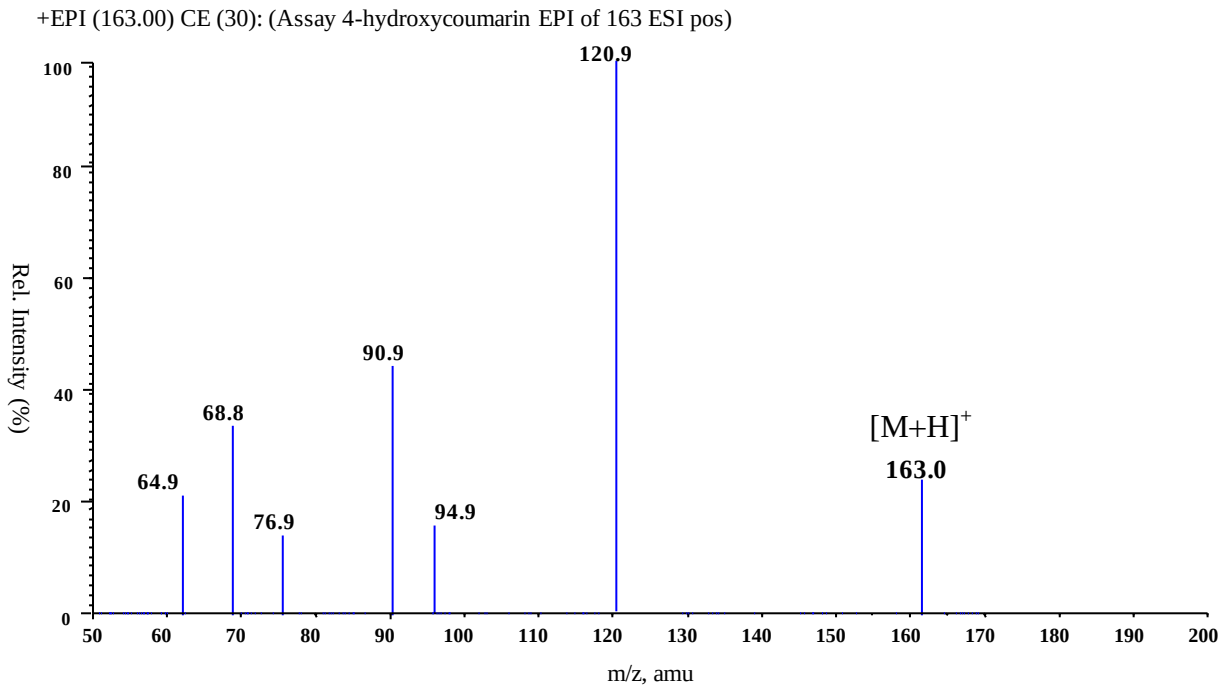

Fig. 28 Mass spectrum (EPI$^+$) of 4-hydroxycoumarin enzymatic product.

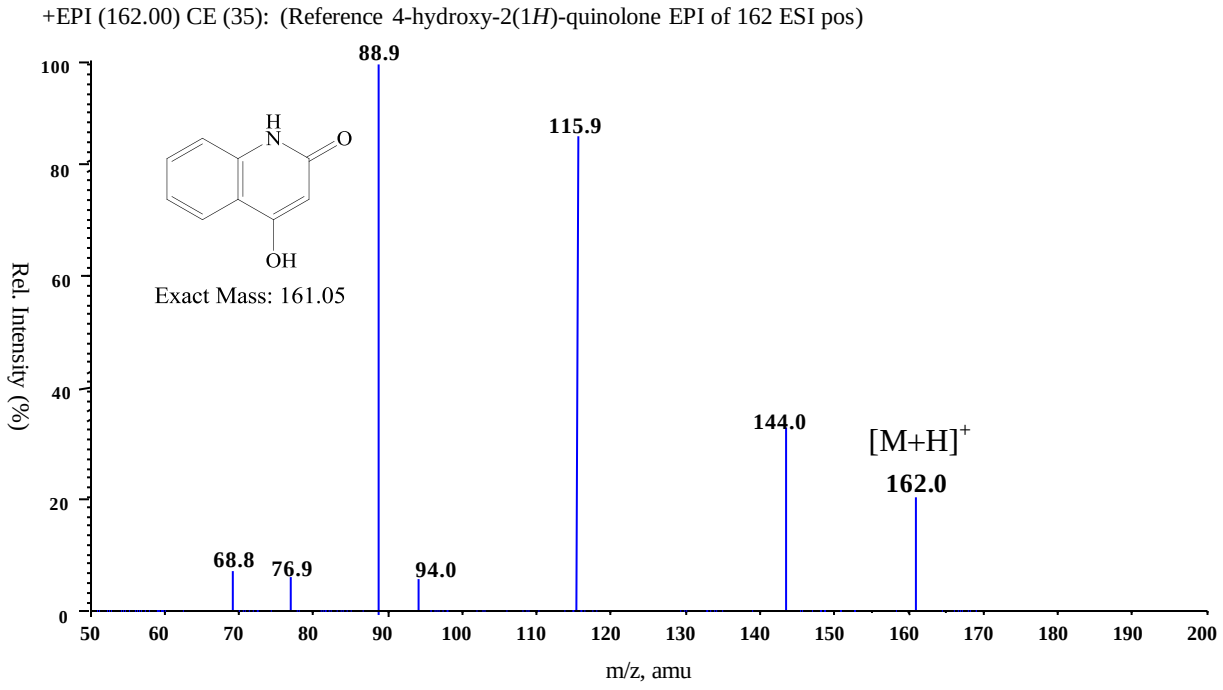

Fig. 29 Mass spectrum (EPI$^+$) of authentic 4-hydroxy-2(1*H*)-quinolone reference.

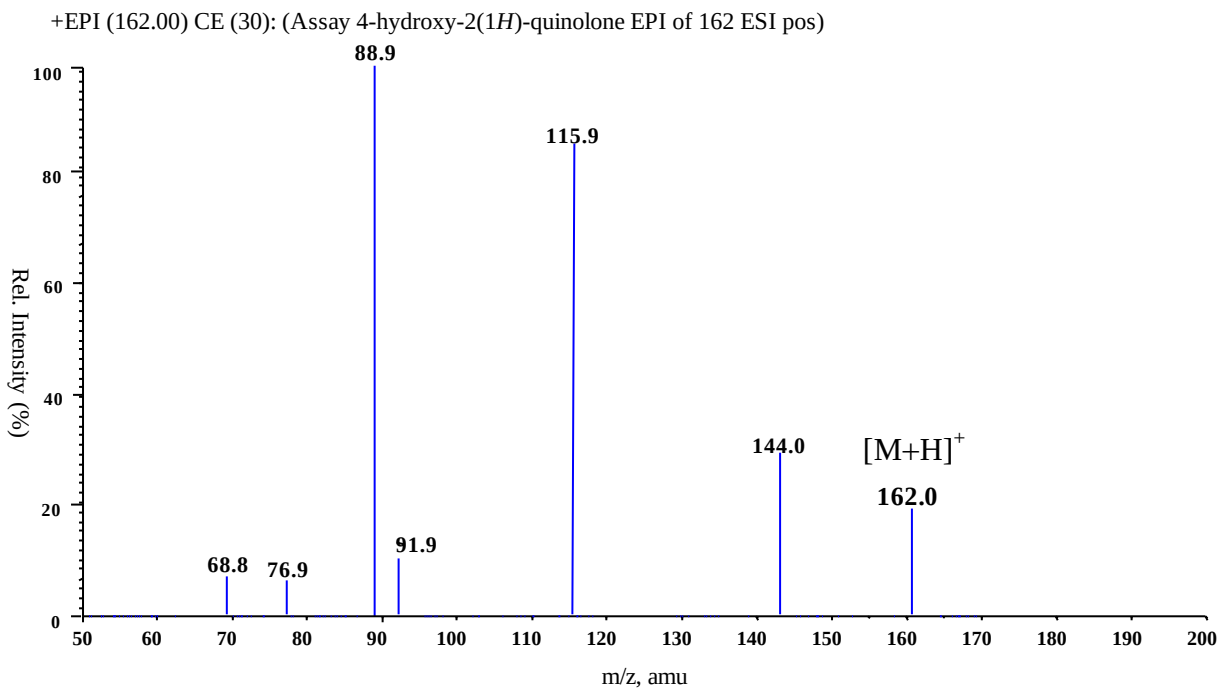

Fig. 30 Mass spectrum (EPI$^+$) of 4-hydroxy-2(1*H*)-quinolone enzymatic product.

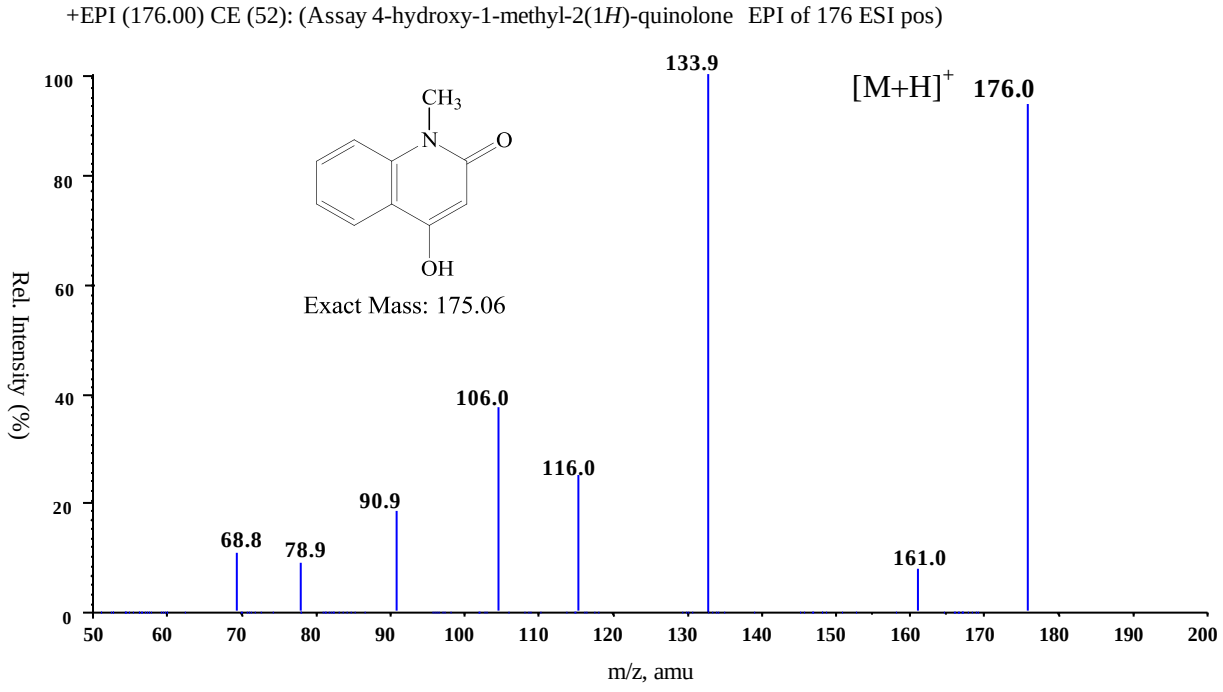

Fig. 31 Mass spectrum (EPI$^+$) of 4-hydroxy-1-methyl-2(1*H*)-quinolone enzymatic product.

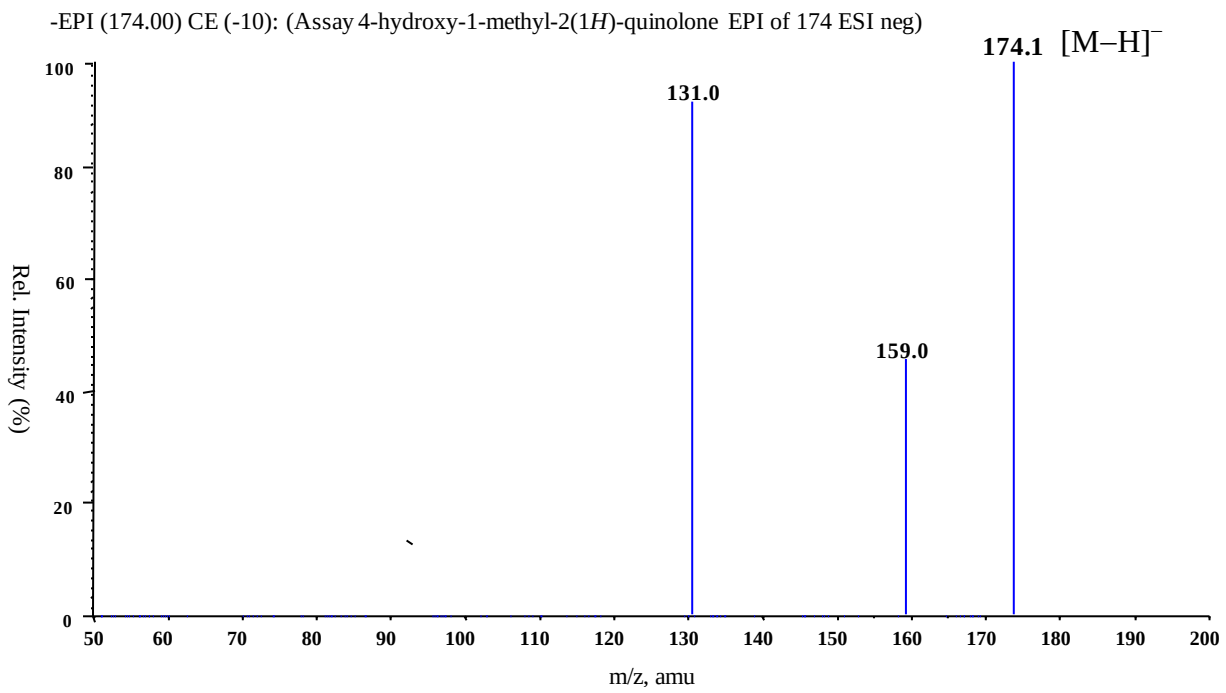

Fig. 32 Mass spectrum (EPI⁻) of 4-hydroxy-1-methyl-2(1*H*)-quinolone enzymatic product.

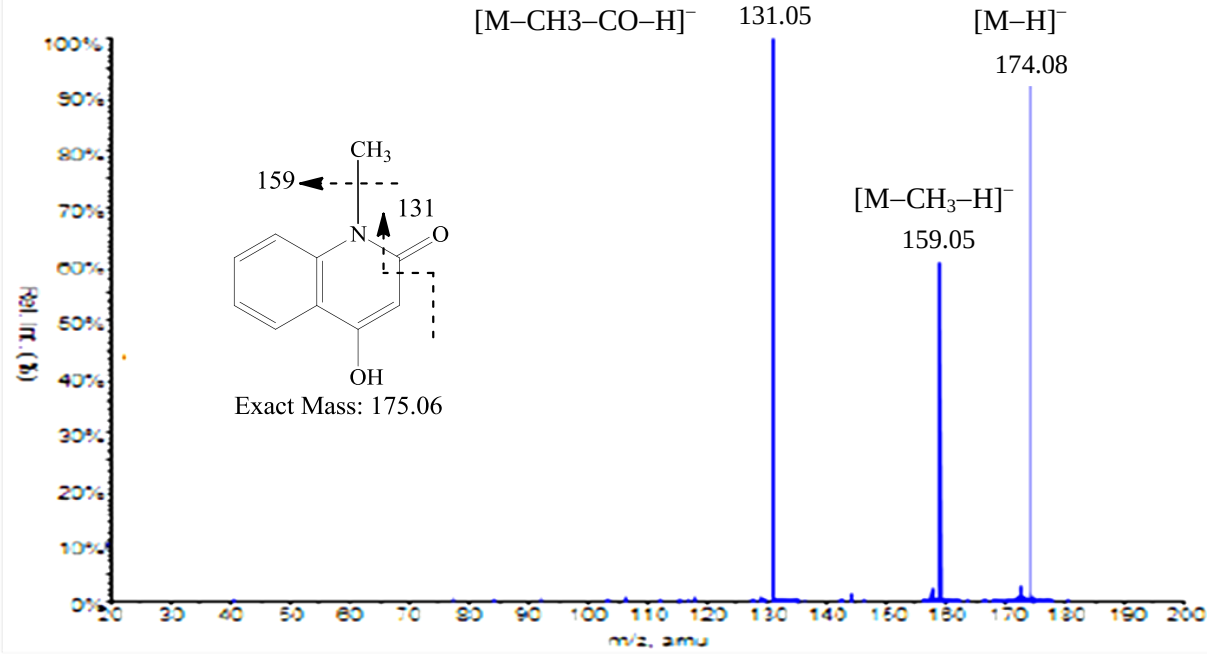

Fig. 33 Mass spectrum (EPI⁻) of 4-hydroxy-1-methyl-2(1*H*)-quinolone enzymatic product formed by *Aegle marmelos* QNS (Resmi et al., 2013).

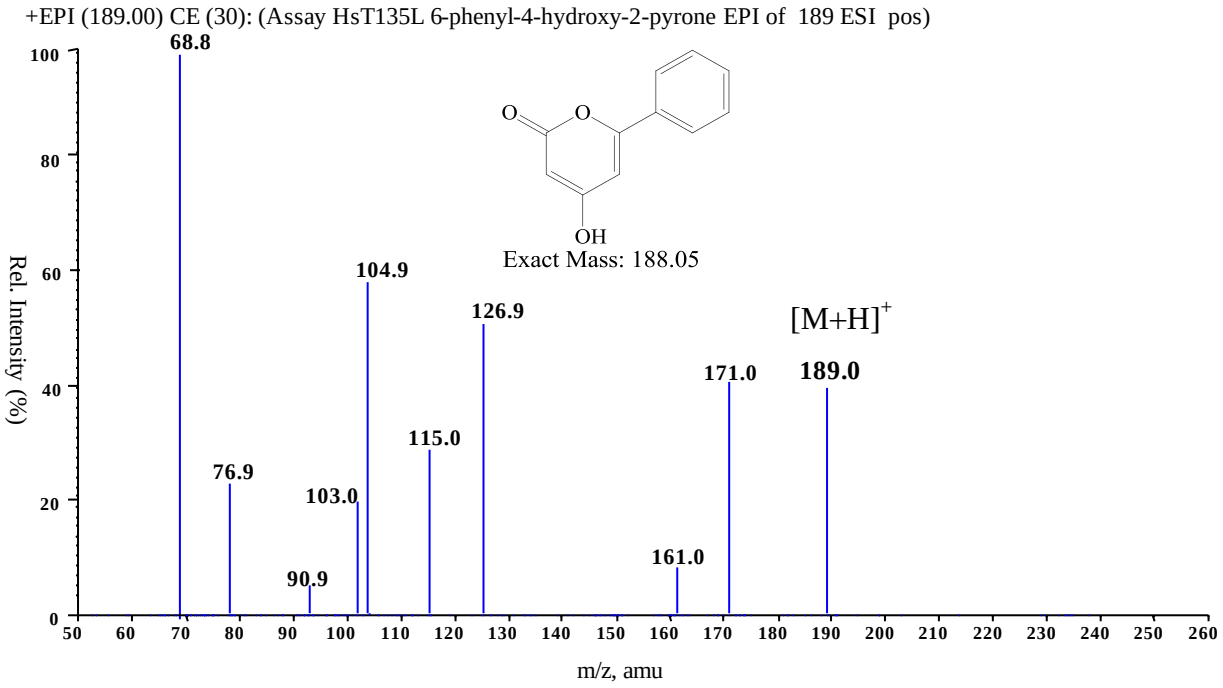

Fig. 34 Mass spectrum (EPI$^+$) of 6-phenyl-4-hydroxy-2-pyrone enzymatic product.

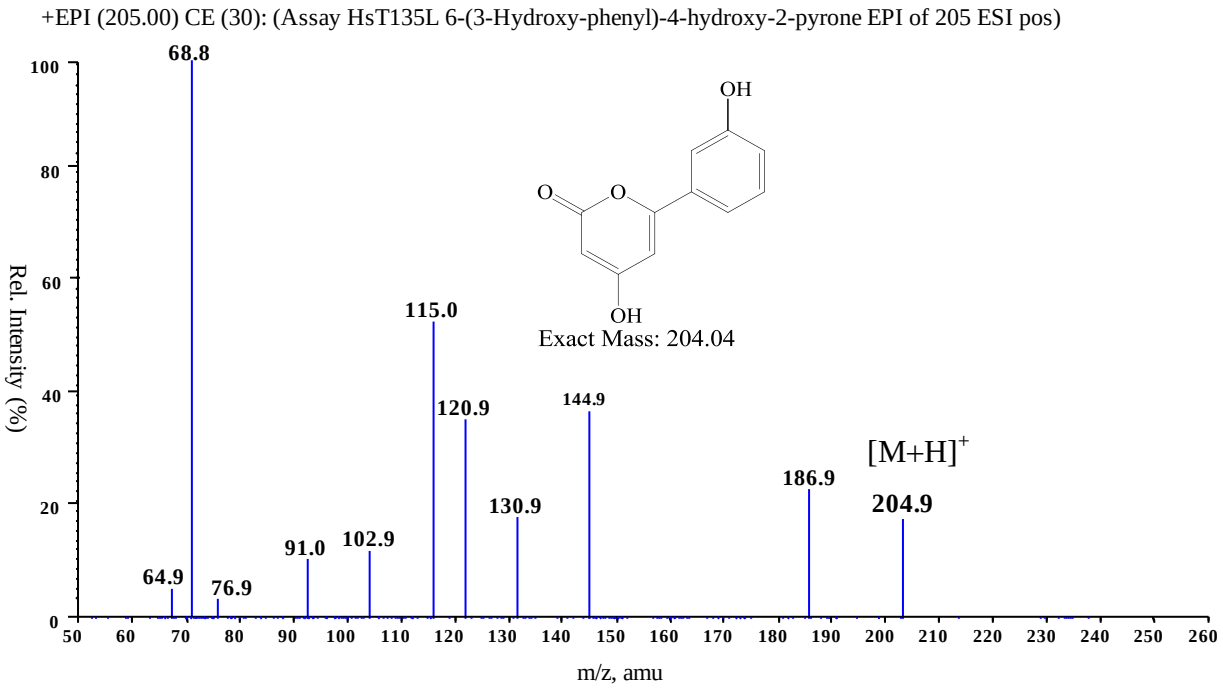

Fig. 35 Mass spectrum (EPI$^+$) of 6-(3-hydroxy-phenyl)-4-hydroxy-2-pyrone enzymatic product.

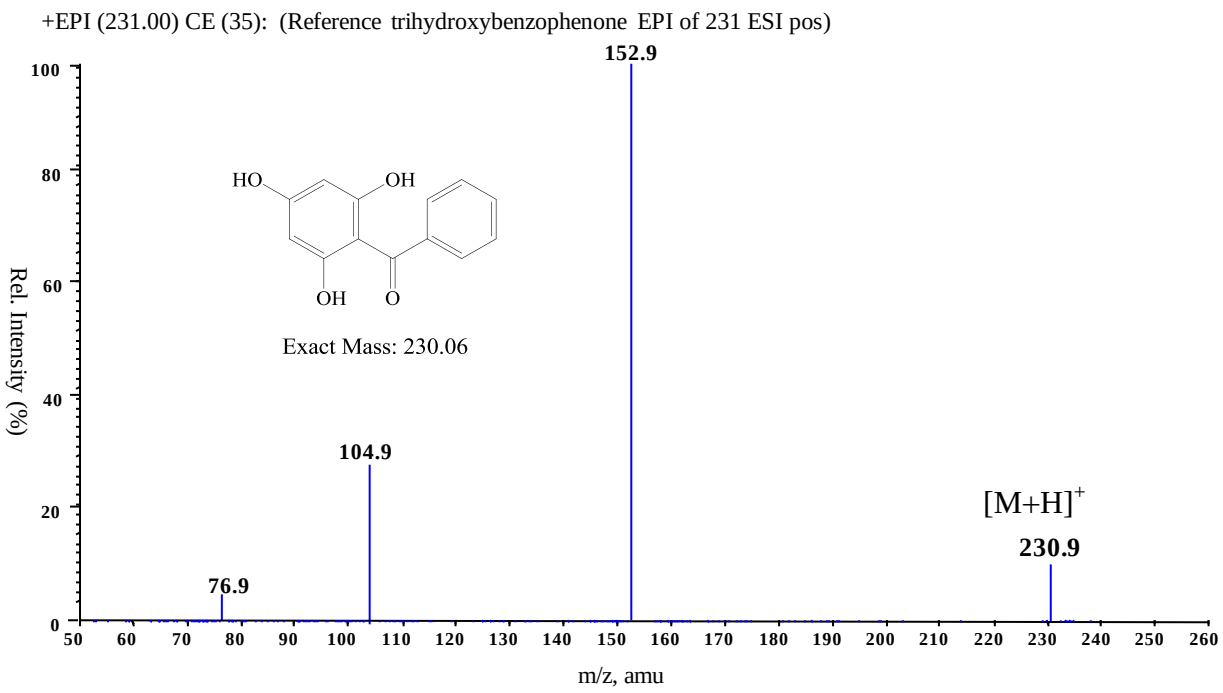

Fig. 36 Mass spectrum (EPI$^+$) of authentic 2,4,6-trihydroxybenzophenone reference.

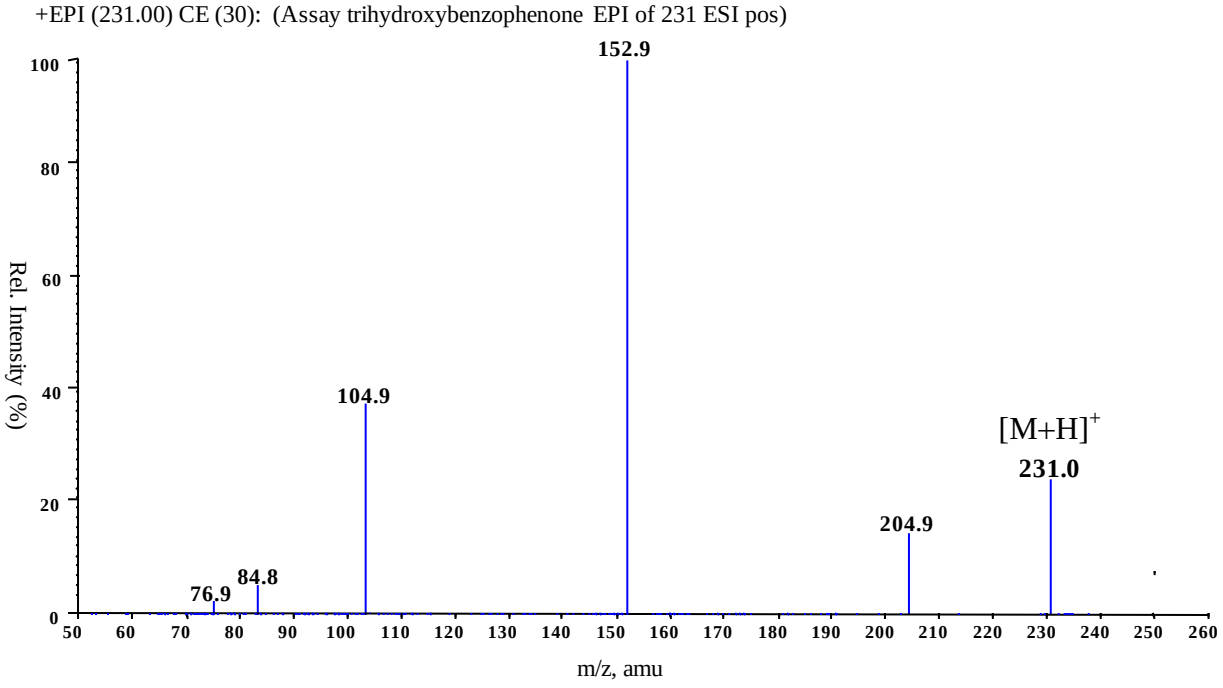

Fig. 37 Mass spectrum (EPI$^+$) of 2,4,6-trihydroxybenzophenone enzymatic product.

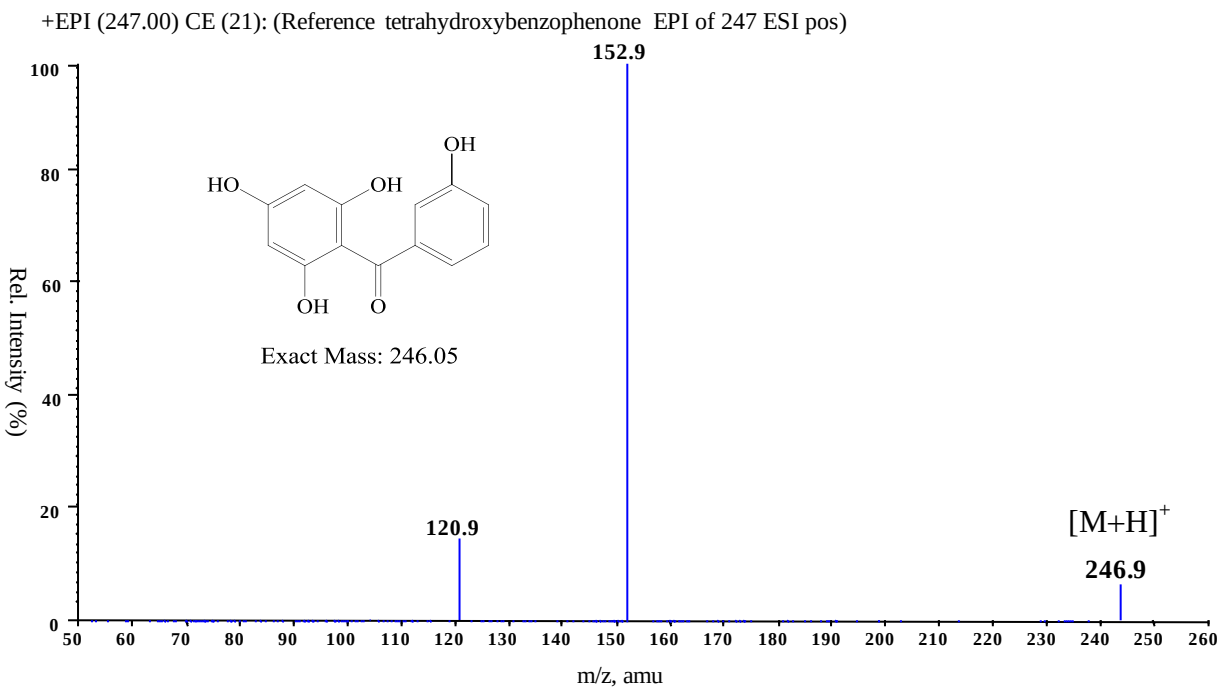

Fig. 38 Mass spectrum (EPI$^+$) of authentic 2,3',4,6-tetrahydroxybenzophenone reference.

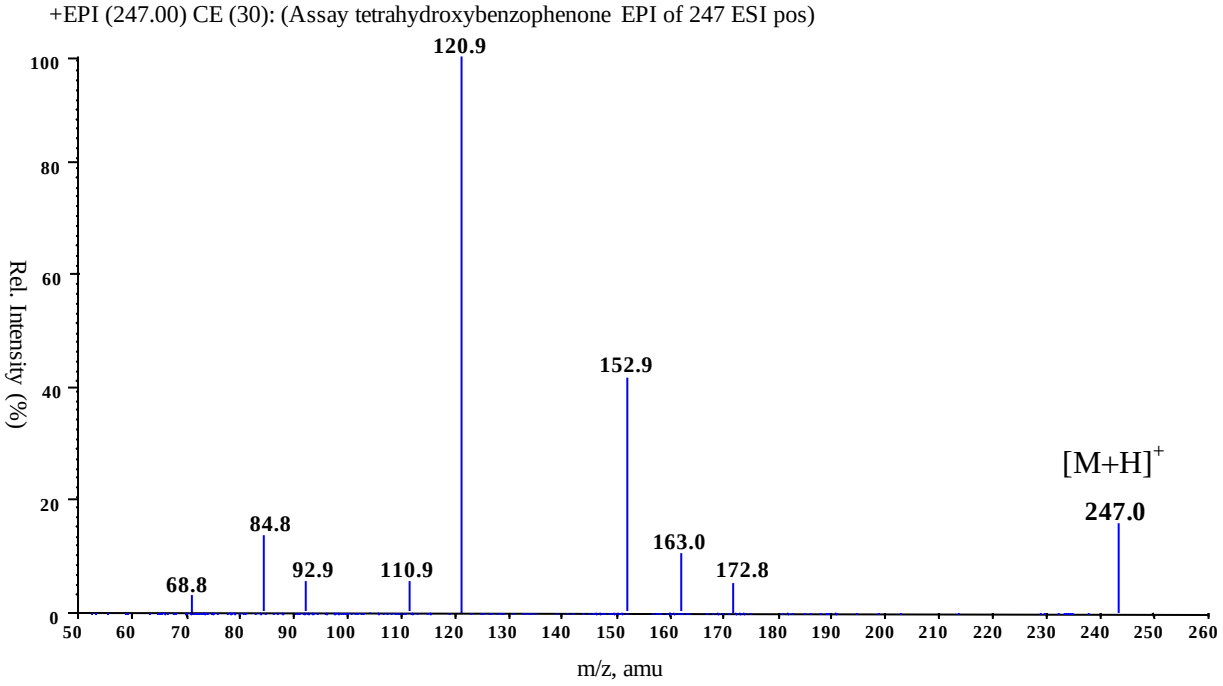

Fig. 39 Mass spectrum (EPI$^+$) of 2,3',4,6-tetrahydroxybenzophenone enzymatic product.

4.1.8 Characterization of the HsT135Lys, Leu and Ile mutants

The upshot of screening 19 enzyme mutants altered in position Thr135 of HsBPS is that lysine was the only amino acid which produced an enzyme mutant that preferred 2-hydroxybenzoyl-CoA as a starter substrate. It forms 4-hydroxycoumarin as the main product after a single malonyl-CoA extension. Salicoyl-CoA is a poor substrate for the wild-type HsBPS. The mutant was nearly inactive with benzoyl-CoA and 3-hydroxybenzoyl-CoA which are the preferred substrates for the wild-type HsBPS. In addition to lysine, leucine and isoleucine were able to convert HsBPS into functional phenylpyrone synthases (PPSs), like the *H. androsaemum* T135L mutant (Klundt et al., 2009). Lysine, leucine and isoleucine produced mutants with dramatically different substrate and product specificities compared to the wild-type HsBPS. Therefore, characterization of these three enzyme mutants was carried out.

4.1.8.1 pH optima of HsT135Lys, Leu and Ile mutants

Each enzyme has its specific pH optimum. Extremely low or high pH values lead to changes in the ionization state of some amino acid residues which are either lining the active site cavity or maintaining the three dimensional structure of the enzyme. An unsuitable pH may also cause changes in the substrate ionization state. These effects of low or high pH may change the properties of the enzyme, interfere with the binding of the substrate to its active site, or even cause loss of the enzyme's catalytic activity. Determination of the activity of the HsBPS mutants was carried out in the pH range 5.5 to 9 and the dependence of the activities on the pH was illustrated in (Fig. 40, A, B and C). The data shown are mean values of two independent experiments. The optimum pH for all three mutants HsT135K, HsT135L, and HsT135I, was 7.0 and they were characterized by relatively broad pH optima. All subsequent tests were performed at pH 7.0 in potassium phosphate (KH_2PO_4) buffer.

4.1.8.2 Temperature optima of the HsT135Lys, Leu and Ile mutants

The rate of the enzyme-catalyzed reaction increases with temperature to a maximal level which is the optimum temperature for the given enzyme. Above this temperature the rate decreases because of thermal denaturation of the enzyme due to disruption of non-covalent bonds such as hydrogen bonds, hydrophobic and ionic interactions. High temperature thus affects the 3-D structure of the enzyme. At low temperature there is not enough energy to overcome the energy barrier between the reactants and the product and so the reaction will not start. At the optimum pH value of 7.0 standard assays were done as duplicates at 5 °C intervals

from 20 °C to 50 °C. Average values of the product amounts were determined (Fig. 41, A, B and C). The optimum temperature for all three mutants HsT135K, HsT135L and HsT135I was 30 °C. In contrast to lysine, both leucine and isoleucine in position 135 increased the stability of the enzymes at higher temperatures.

4.1.8.3 Linearity of product formation with time

The rate of product formation of the enzyme-catalyzed reaction changes by time. At the beginning of the reaction the rate is fast. If the amount of the product is plotted against the time the curve will be linear. Later, enzyme instability and substrate depletion may occur. In addition, product accumulation may cause any inhibition. All of these factors lead to changes in the rate with time and it is critical to measure the rate at the linear part of the curve at a time point which gives detectable product amount. The amounts of the products formed by HsT135K, HsT135L, and HsT135I were determined as a function of time in the standard assay (Fig. 42, A, B and C). Product formation was linear up to 15 min with HsT135K and HsT135I and up to 10 min with HsT135L.

4.1.8.4 Linearity of product formation with enzyme concentration

Before determination of the kinetic constants it is also critical to examine the suitable concentration of the enzyme to be used for the assay. If too low the amount of the product formed will be small and difficult to detect. On the other hand, high concentrations may result in steric hindrance and hence deviation from linearity. Thus, a concentration that yields high product amounts within the linearity is favorable. Product formation by HsT135K, HsT135L and HsT135I mutants were plotted against the various enzymes concentrations (Fig. 43, A, B and C). It was linear up to 3 µg protein/assay with HsT135L and HsT135I and up to 2 µg with HsT135K.

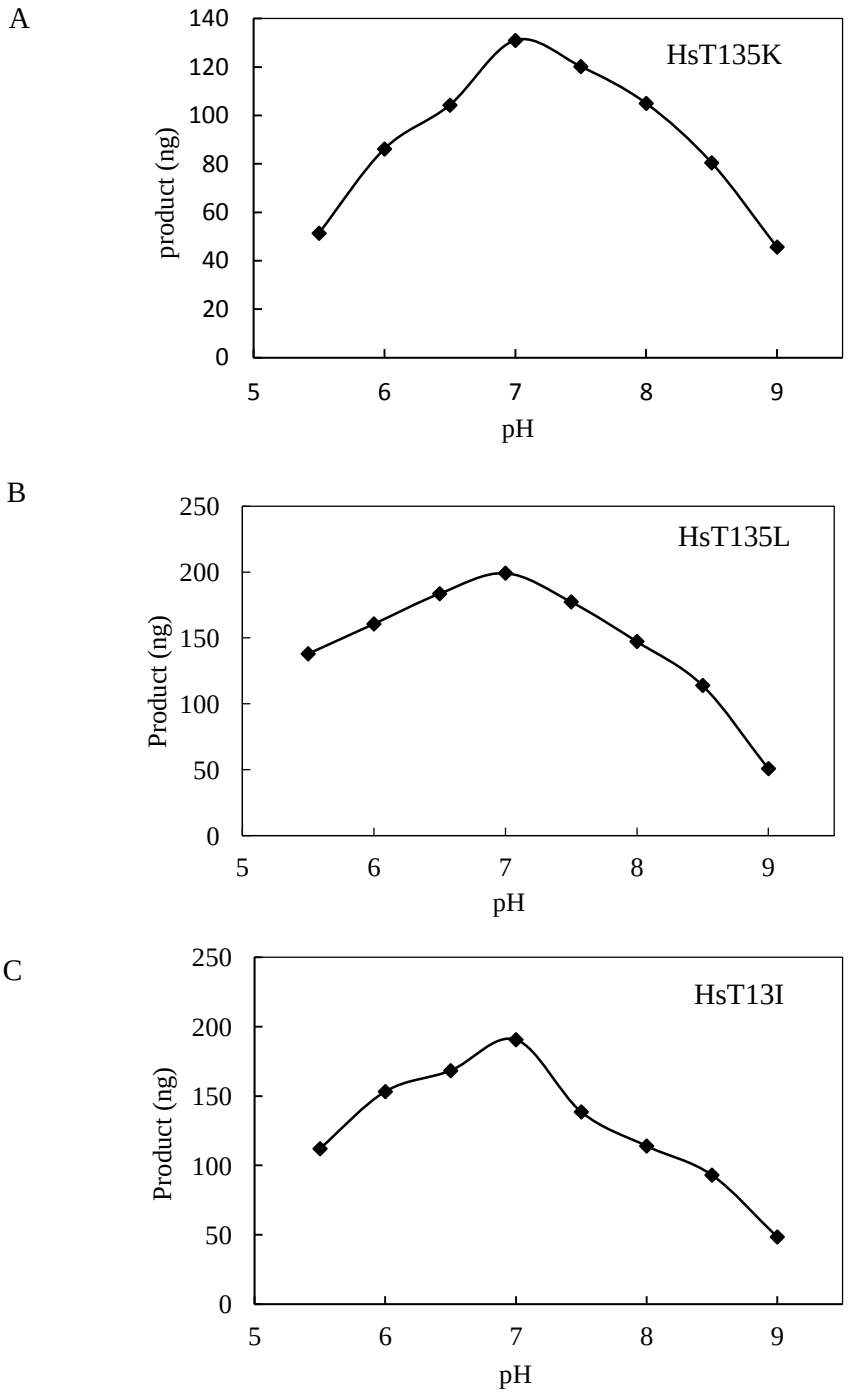

Fig. 40 pH optima of A: HsT135K, B: HsT135L and C: HsT135I mutants. Data are mean values of two independent experiments. pH 7 is the optimum pH for the three mutants.

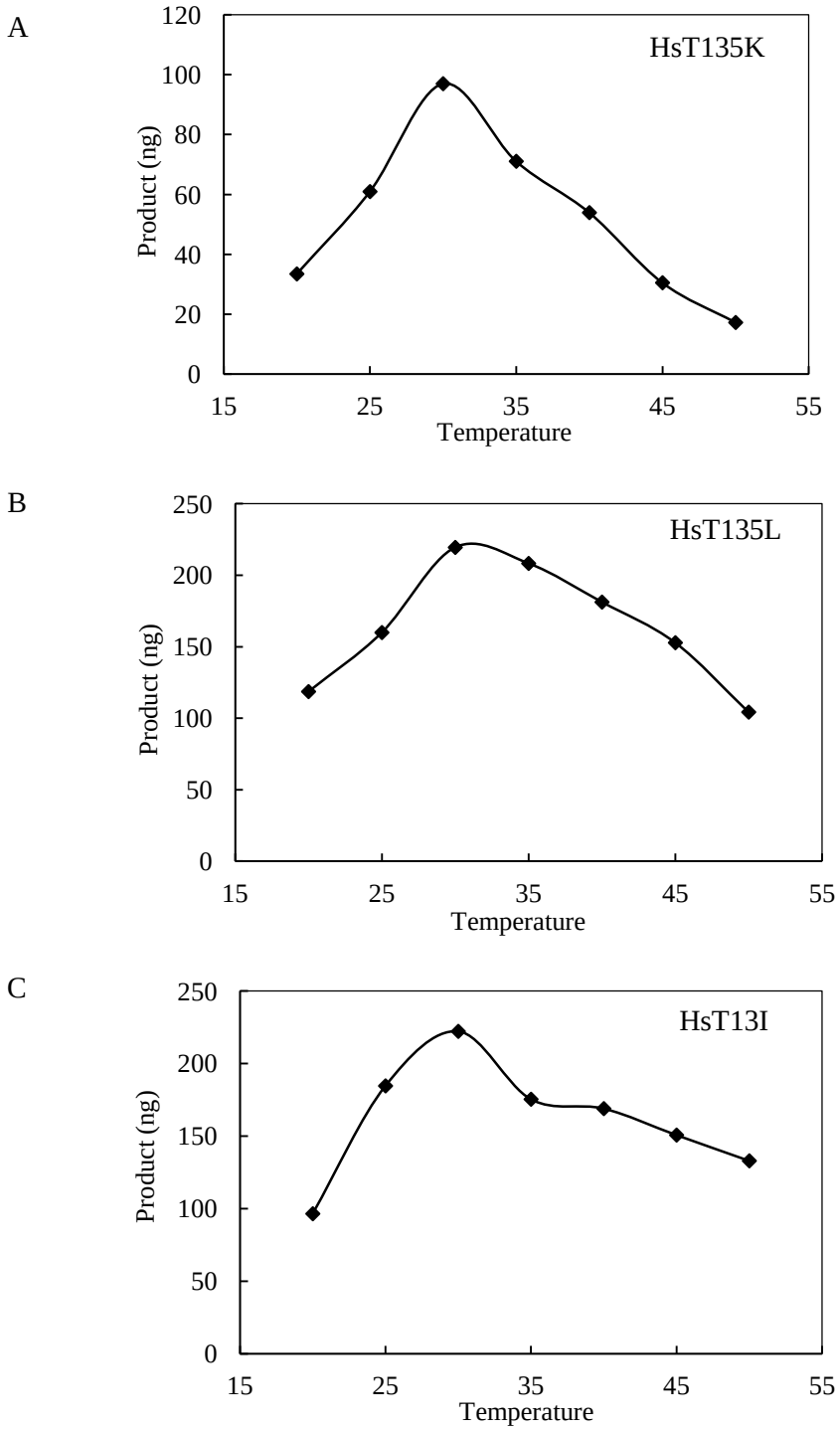

Fig. 41 Temperature optima of, A: HsT135K, B: HsT135L and C: HsT135I mutants. Data are mean values of two independent experiments. The optimum temperature for the three mutants is 30 °C.

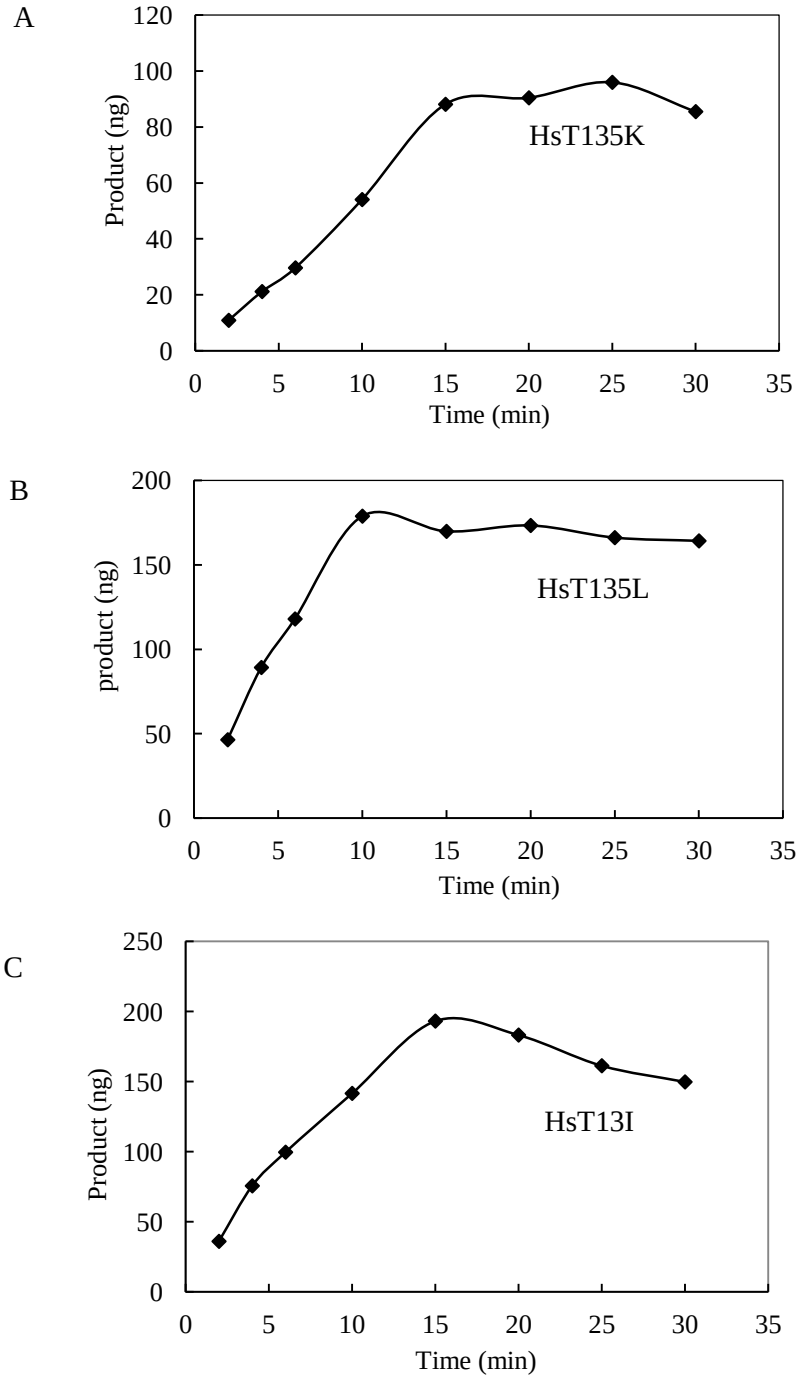

Fig. 42 Dependence of the activity of, A: HsT135K, B: HsT135L and C: HsT135I mutants on time (min). Data are mean values of two independent experiments. The product formation stays linear up to 15 min in case of HsT135K and HsT135I and for 10 min in case of HsT135L.

A

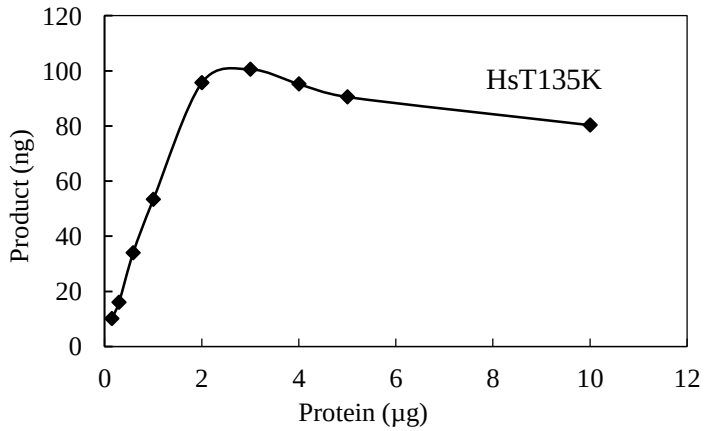

B

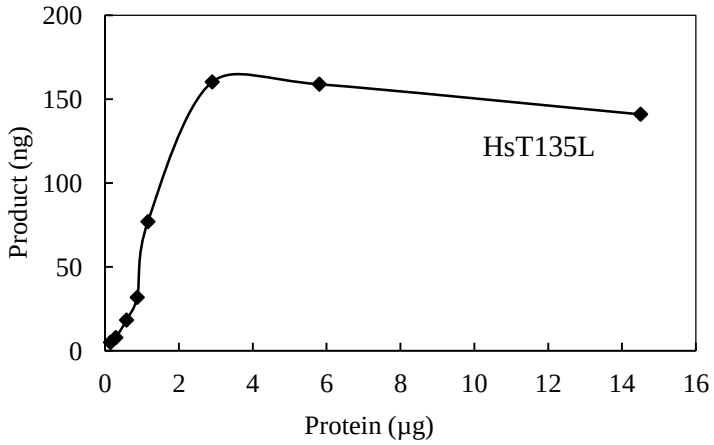

C

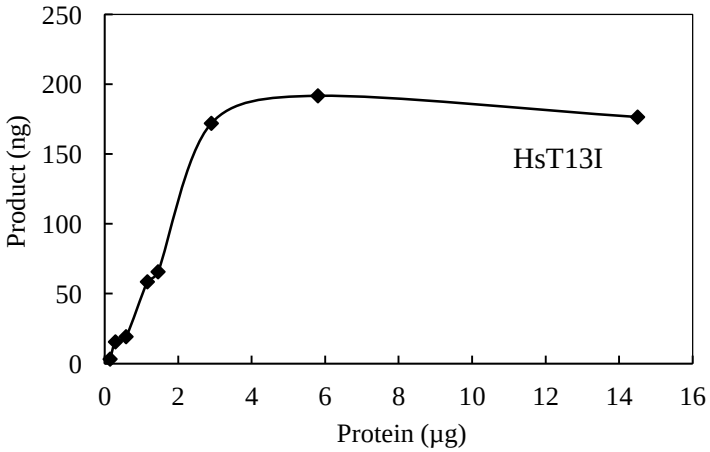

Fig. 43 Dependence of the activity of, A: HsT135K, B: HsT135L and C: HsT135I mutants on the protein amount. Data are mean values of two independent experiments.

4.1.9 Synthesis and use of alternative starter substrates

In the current study the HsT135K mutant accepts 2-hydroxybenzoyl-CoA as a starter substrate. Therefore, synthesis of this substrate was carried out during this work in addition to the synthesis of alternative starter substrates like anthraniloyl-CoA, 2-mercaptobenzoyl-NAC and 2-methoxybenzoyl-NAC as described in (3.3.1, 3.3.2). The objective was to detect activity of the new mutant 'HsT135K' with these potential substrates.

4.1.9.1 2-Hydroxy and 2-aminobenzoyl-CoAs

Synthesis of 2-hydroxybenzoyl-CoA (salicoyl-CoA) and 2-aminobenzoyl-CoA (anthraniloyl-CoA) was performed according to the literature (Lapidot et al., 1967; Stöckigt and Zenk, 1975). The synthesis consists of two steps; in the first step synthesis of *N*-hydroxysuccinimide (NHS) ester intermediate (Fig. 44, A) was done. These esters are stable to be purified and stored at low temperature. NHS esters are prepared by mixing the acid of interest with NHS in an anhydrous solvent. NHS acts as an activating agent. *N*,*N* dicyclohexylcarbodiimide (DCC) is a coupling reagent which forms a highly unstable activated acid intermediate (*O*-acyl urea derivative) which then reacts with NHS and forms a more stable activated acid. If the yield of the reaction is low this may be due to the rearrangement of *O*-acyl urea derivatives to form *N*-acyl urea derivative which is very stable and could not react with NHS. Experimental data for 2-hydroxybenzoyl-*N*-hydroxysuccinimide ester (Fig. 45) were as follows. EI-MS (70 eV), m/z (rel. abundance): 235 $[M]^+$ (7), 121 (100; 2-hydroxybenzoyl), 120 (12.5), 93 (11; hydroxyphenyl), 69 (4), 65 (12). Experimental data for 2-aminobenzoyl-*N*-hydroxysuccinimide (Fig. 46) were as follows. EI-MS m/z (rel. abundance): 234 $[M]^+$ (14.3), 121(8), 120 (100; 2-hydroxybenzoyl), 119 (5), 99 (6) 92 (19; hydroxyphenyl), 65 (10) 56 (5).
Exchange of NHS with Coenzyme A (Fig. 44, B) was performed in the second step (transesterification) in the presence of a base ($NaHCO_3$) as a catalyst as described in section (3.3.1.2). LC-MS analysis was carried out for the purified 2-aminobenzoyl-CoA and data are represented in (Fig. 47, B). It is characterized by the presence of the molecular ion peak $[M–H]^–$ at m/z 885.2. This single charged anthraniloyl-CoA ion was selected for further fragmentation and the product ions were recorded in negative ion mode. $MS/MS^–$ analysis showed characteristic fragments of CoA and phosphoadenosine-containing compounds like $[ADP]^–$ at m/z 426, and $[ADP\text{-}H_2O]^–$ at m/z 408.2 together with fragments containing parts of the

anthraniloyl moiety such as $[M\text{-}AMP]^-$ at m/z 556.5, $[M\text{-}AMP\text{–}H_2O]^-$ at m/z 538.5, $[M\text{–}H_2PO_3]^-$ at m/z 805.7.

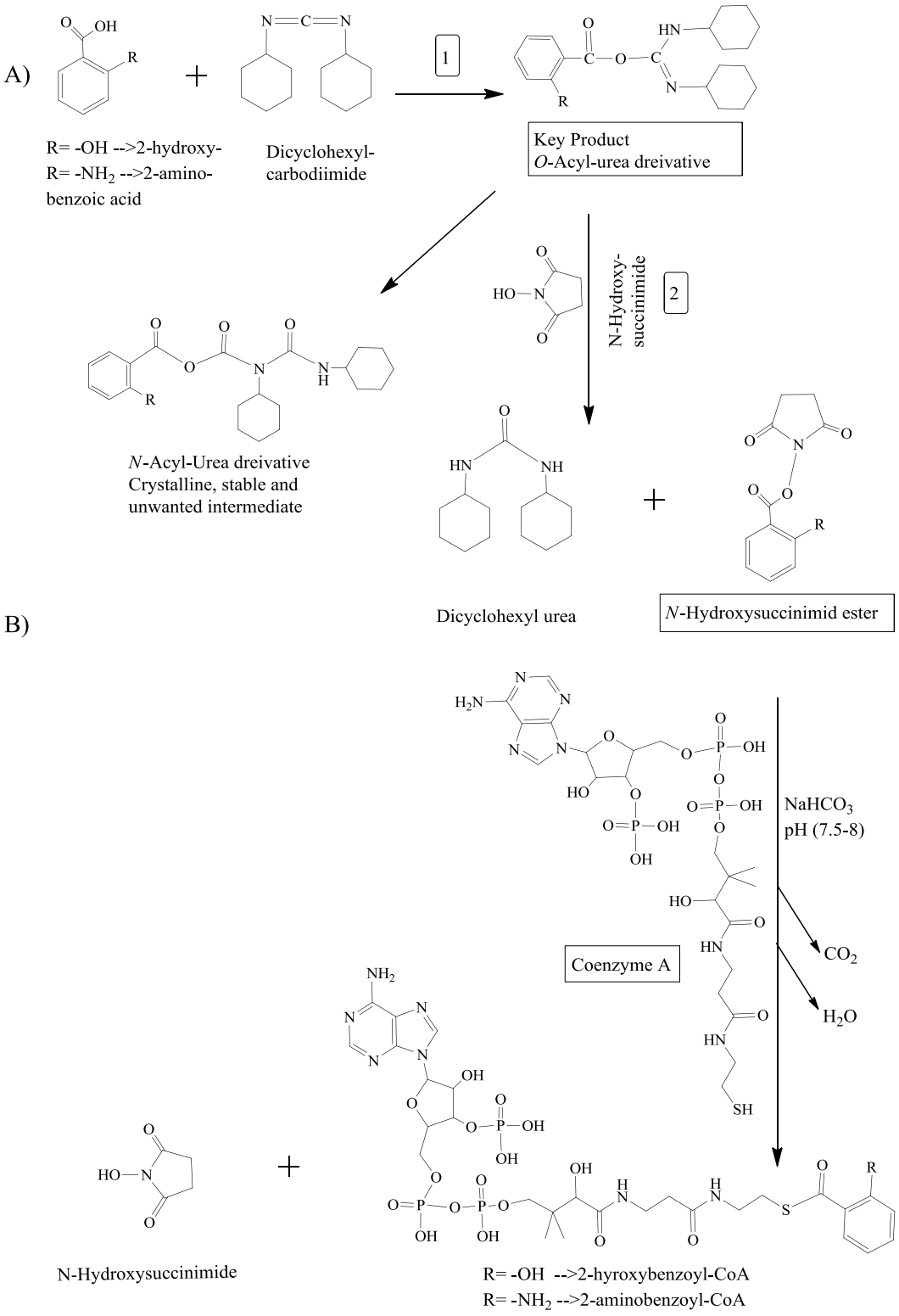

Fig. 44 Synthesis scheme of acyl-CoA esters of 2-hydroxy- or 2-aminobenzoic acid, modified from; Gaid (unpublished results).

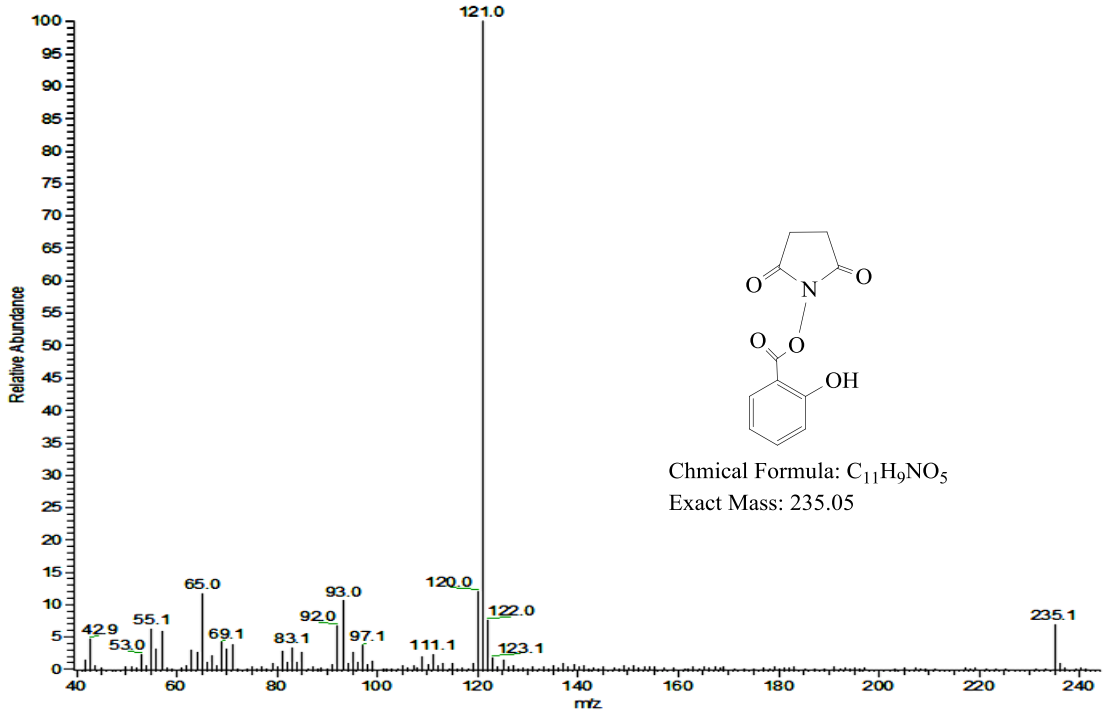

Fig. 45 Mass spectrum of 2-hydroxybenzoyl-*N*-hydroxysuccinimide ester.

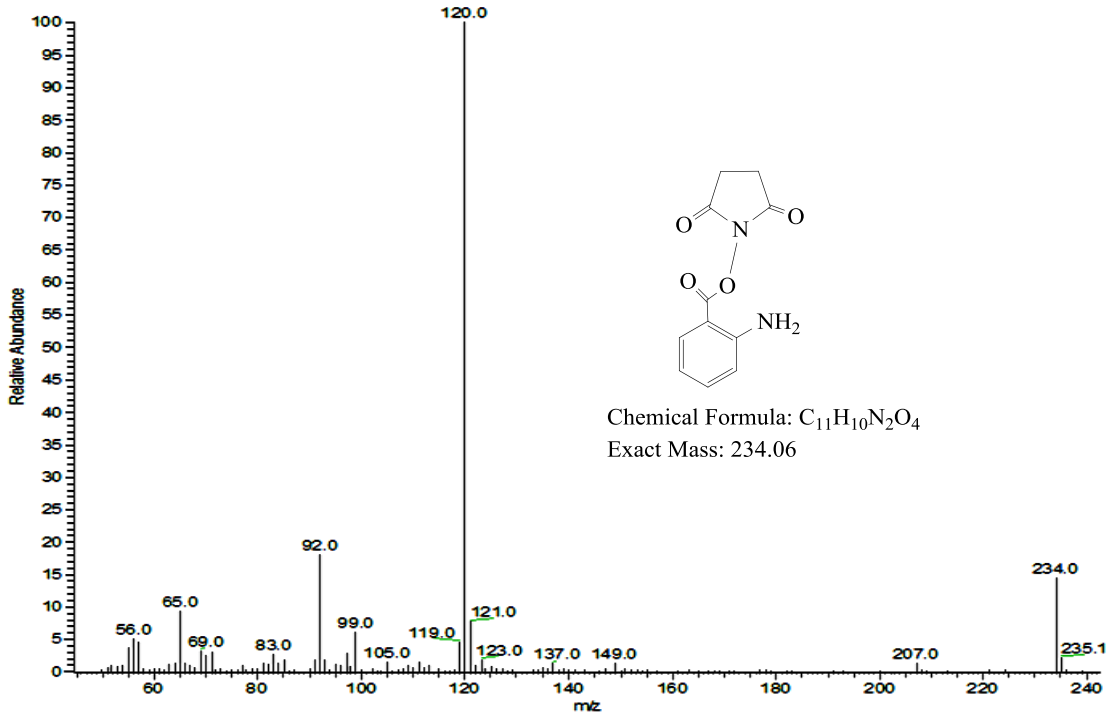

Fig. 46 Mass spectrum of 2-aminobenzoyl-*N*-hydroxysuccinimide ester.

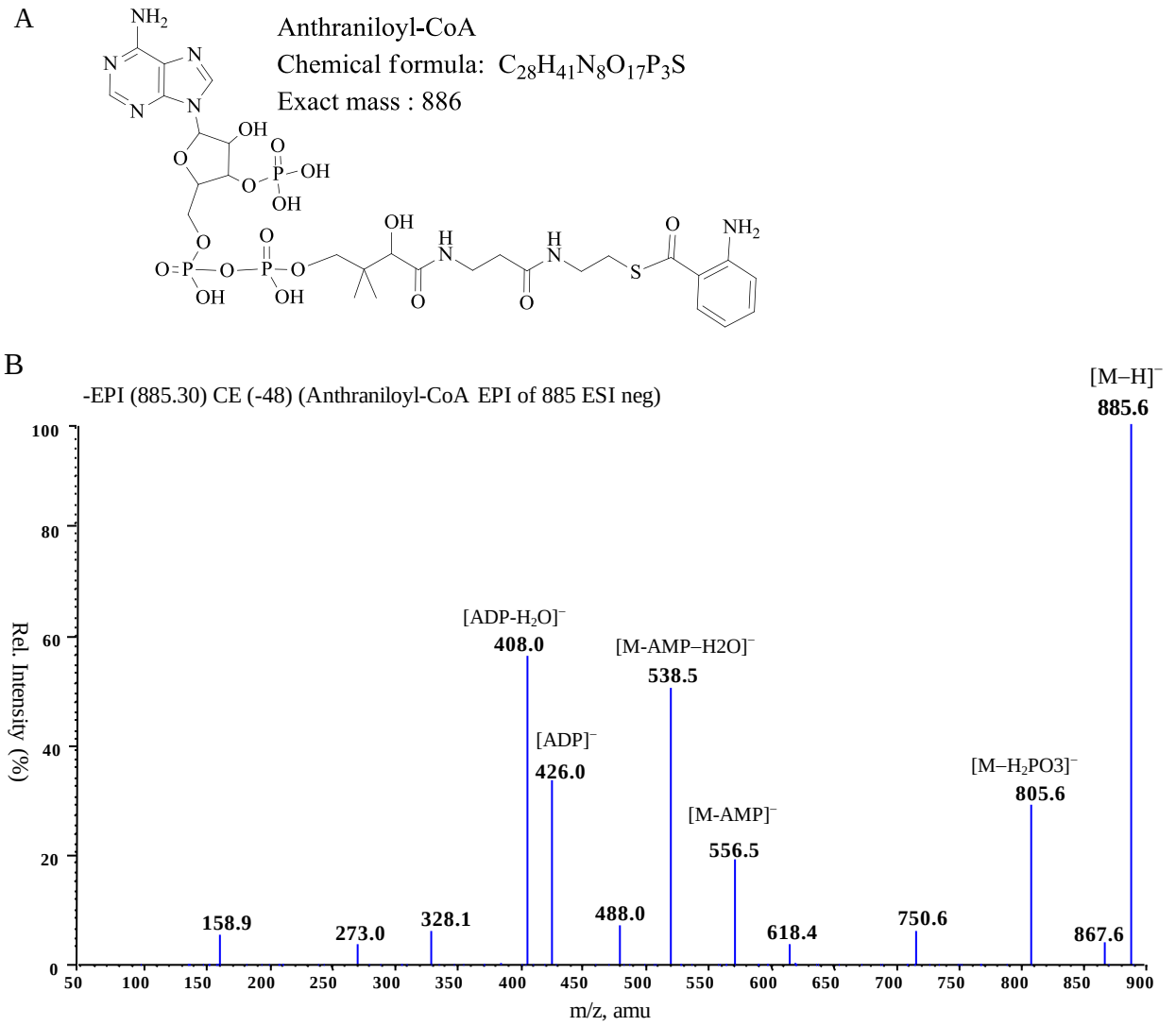

Fig. 47 Structure of anthraniloyl-CoA (A) and the MS/MS⁻ spectrum (EPI⁻) of purified anthraniloyl-CoA (B).

4.1.9.2 2-Methoxy and 2-mercaptobenzoyl-NAC esters

Synthesis of these two substrates as CoA esters was not successful. Only their *N*-hydroxysuccinimide intermediates were obtained, as shown by their mass spectra (Figs. 107 and 108 appendix). However, the transesterification step with CoASH failed and the final product was not detected in the LC-MS/MS analysis. It was reported that the *N*-acetylcysteamine (NAC) thioesters were successfully used as starter substrates instead of CoA thioesters for type III PKSs (Oguro et al., 2004), thus provoked the idea of synthesizing these two compounds as -NAC thioesters. The synthesis was carried out according to Suo et al. (2000). In this reaction 1-hydroxybenzotriazole activates the aromatic carboxylic acid in the presence of the coupling

reagent DCC and then transesterification with the *N*-acetylcysteamin follows. The reaction was carried out as described in (3.3.2). Experimental data for 2-methoxybenzoyl-NAC (Fig. 49) were as follows. EI-MS (70 eV), m/z (rel. abundance): 253 $[M]^+$ (2), 210 (2), 136 (11), 135 (100, 2-methoxybenzoyl), 92 (5), 77 (10). Experimental data for 2-mercaptobenzoyl-NAC (Fig. 50) were as follows. EI-MS (70 eV), m/z (rel. abundance): 255 $[M]^+$ (2), 136 (100, 2-mercaptobenzoyl), 224.2 (11), 167.9 (5), 143.1 (9), 109 (17), 99.1 (10), 87 (41), 81.9 (12), 68.9 (19), 60 (41), 56.1 (20), 42.8 (30).

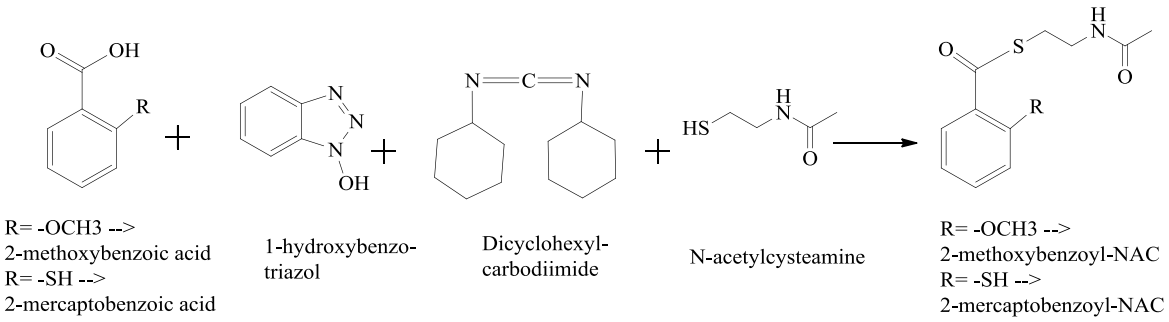

Fig. 48 Synthesis scheme of 2-methoxy and 2-mercaptobenzoyl-NAC thioesters.

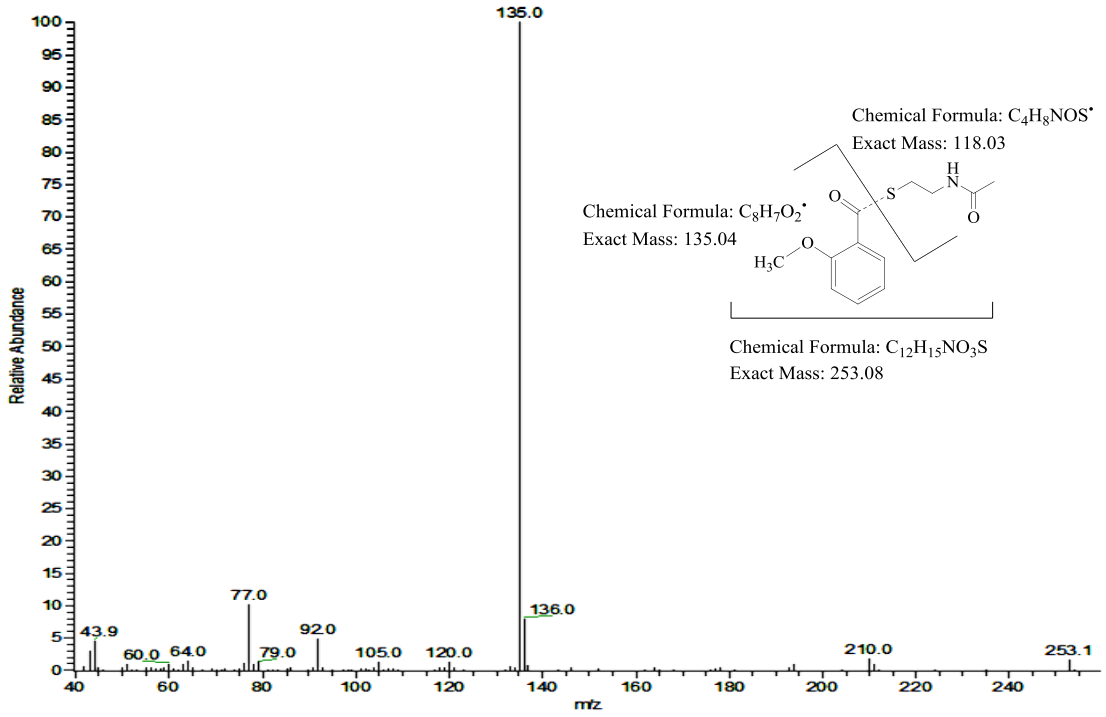

Fig. 49 Mass spectrum of 2-methoxybenzoyl-NAC.

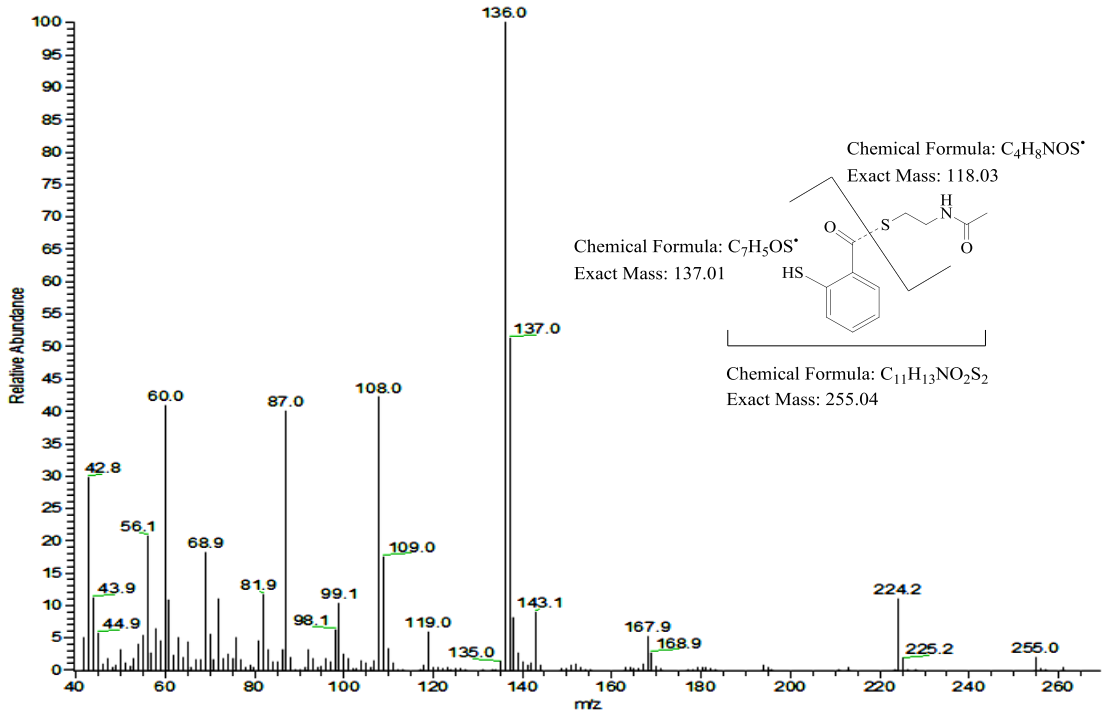

Fig. 50 Mass spectrum of 2-mercaptobenzoyl-NAC.

4.1.10 Substrate and product specificities of HsBPS wild-type and its three mutants

Using the above-determined optimized conditions enzyme assays were done to test the ability of the HsT135K, HsT135L and HsT135I mutants to use different starter substrates. The products formed were examined by HPLC. The detection wavelengths were 306 nm (2,4,6-trihydroxybenzophenon, 2,3',4,6-tetrahydroxybenzophenon), 317 and 321 nm (4-hydroxy-6-phenylpyran-2-one, 4-hydroxy-6-(3-hydroxy)-phenylpyran-2-one respectively), 279 nm (4-hydroxycoumarin), 270 nm (4-hydroxy-2(1*H*)-quinolone) and 272 nm (4-hydroxy-1-methyl-2(1*H*)-quinolone). The HsT135K, HsT135L, HsT135I mutants were incubated in the presence of malonyl-CoA with benzoyl-CoA, 2-hydroxybenzoyl-CoA (salicoyl-CoA), 3-hydroxybenzoyl-CoA, 4-hydroxybenzoyl-CoA, anthraniloyl-CoA, *N*-methylanthraniloyl-CoA, 2-mercaptobenzoyl-*N*-acetylcysteamine and 2-methoxybenzoyl-*N*-acetylcysteamine. The identity of the products formed was established by UV-spectroscopy and co-chromatography with authentic reference compounds. All the enzymatic products were quantified using standard solutions of the respective authentic reference compounds. The substrate and product specificity results are summarized in (Tab. 12). In contrast to HsBPS wild-type (Huang et al., 2012) the HsT135K mutant preferred 2-hydroxybenzoyl-CoA as a starter substrate forming 4-hydroxycoumarin as main product. The HsT135L and HsT135I mutants preferred benzoyl-CoA

forming 4-hydroxy-6-phenylpyran-2-one as main product. Interestingly, 3-hydroxybenzoyl-CoA was the second best substrate of HsT135L and HsT135I forming 4-hydroxy-6-(3-hydroxy)-phenylpyran-2-one as main product in good yield unlike the HaT135L mutant from *H. androsaemum* which was nearly inactive with this substrate (Klundt et al., 2009). The HsT135K, HsT135L and HsT135I mutants also accepted anthraniloyl and *N*-methylanthraniloyl-CoAs, forming 4-hydroxy-2(1*H*)-quinolone and 4-hydroxy-1-methyl-2(1*H*)-quinolone alkaloids respectively like benzalacetone synthase from *Rheum palmatum* (RpBAS) (Abe et al., 2006). All of the three mutants were inactive with *p*-hydroxybenzoyl-CoA, 2-mercaptobenzoyl-*N*-acetylcysteamine and 2-methoxybenzoyl-*N*-acetylcysteamine.

Tab. 12 Substrate and product specificities of HsBPS wild-type and the HsT135K, HsT135L and HsT135I mutants

Substrate	**Relative activity (%)***			
	HsBPS wild-type	**HsT135L**	**HsT135I**	**HsT135K**
Benzoyl-CoA	100[a]	100[c]	100[c]	3.3
3-Hydroxybenzoyl-CoA	66.2[b]	64.2[d]	40.7[d]	1.8
2-Hydroxybenzoyl-CoA	6.3	8.9	16.8	100[e]
4-Hydroxybenzoyl-CoA	0	0	0	0
Anthraniloyl-CoA	7.1[f]	42.8[f]	20.3[f]	15.1[f]
N-Methylantraniloyl-CoA	11.6[g]	8.4[g]	5.3[g]	6.1[g]
2-Methoxybenzoyl-NAC**	0	0	0	0
2-Mercaptobenzoyl-NAC**	0	0	0	0

* Data are mean values of two independent experiments

** -*N*-acetylcysteamine

[a] 2,4,6-Trihydroxybenzophenone [b] 2,3´,4,6-Tetrahydroxybenzophenone

[c] 4-Hydroxy-6-phenylpyran-2-one [d] 4-Hydroxy-6-(3-hydroxy)-phenylpyran-2-one

[e] 4-Hydroxycoumarin [f] 4-Hydroxy-2(1*H*)-quinolone

[g] 4-Hydroxy-1-methyl-2(1*H*)-quinolone

4.1.10.1 Activity of HsT135K mutant and HsBPS wild-type with salicoyl and benzoyl-NACs

As mentioned before some starter substrates such as anthraniloyl-CoA, 2-methoxy- and 2-mercaptobenzoyl-NACs were synthesized during this study. The aim was to get new products such as thiocoumarins or substituted benzophenones. However, only anthraniloyl-CoA was accepted and the highest activity was found with HsT135L mutant. 2-Methoxy and 2-mercaptobenzoyl-NACs were accepted as starter substrates neither by HsBPS wild-type nor by its mutants. So testing the activity of these enzymes with salicoyl and benzoyl-NACs as positive controls was performed. HsT135K mutant did not accept salicoyl-NAC as a starter substrate as shown in (Fig. 51, b). In contrast to the CoA-esters the NAC-esters are extractable into the ethyl acetate phase. HsBPS wild-type which showed around 5% activity with salicoyl-CoA efficiently accepts salicoyl-NAC as a starter substrate forming 4-hydroxycoumarin (Fig. 52, b). Also HsBPS wild-type efficiently accepts benzoyl-NAC as benzoyl-CoA forming 2,4,6 trihydroxybenzophenone (Fig. 52, d). Thus, it could be concluded that HsT135K mutant does not accept the NAC-activated starter substrates. The challenge was that synthetic activation of 2-methoxy and 2-mercaptobenzoic acids as CoA esters failed. Therefore, another trial should be done to synthesize them as -CoAs for testing with the HsT135K mutant.

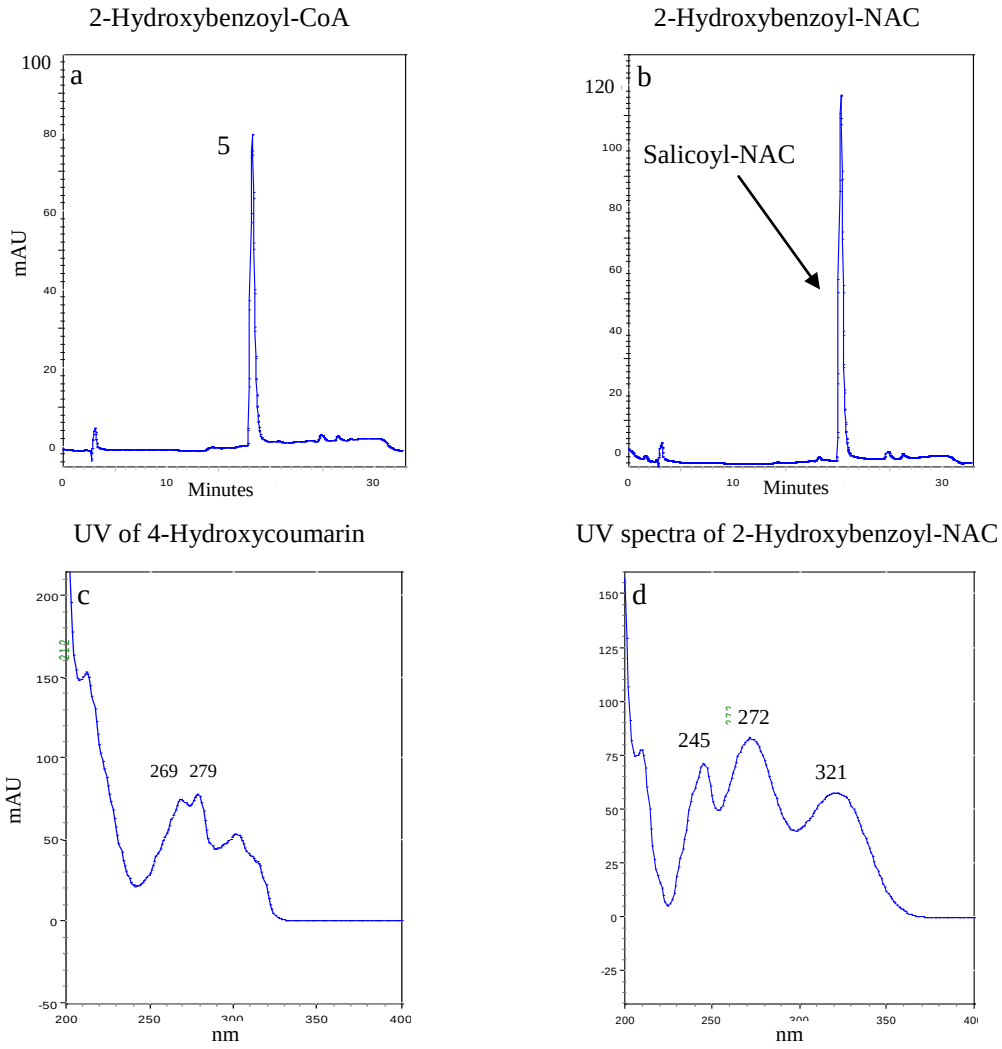

Fig. 51 HPLC chromatograms of assays of HsT135**K** mutant with a: 2-hydroxybenzoyl-CoA, and b: 2-hydroxybenzoyl-NAC; c: UV spectrum of 4-hydroxycoumarin, d: UV spectrum of 2-hydroxybenzoyl-*N*-acetylcysteamine.

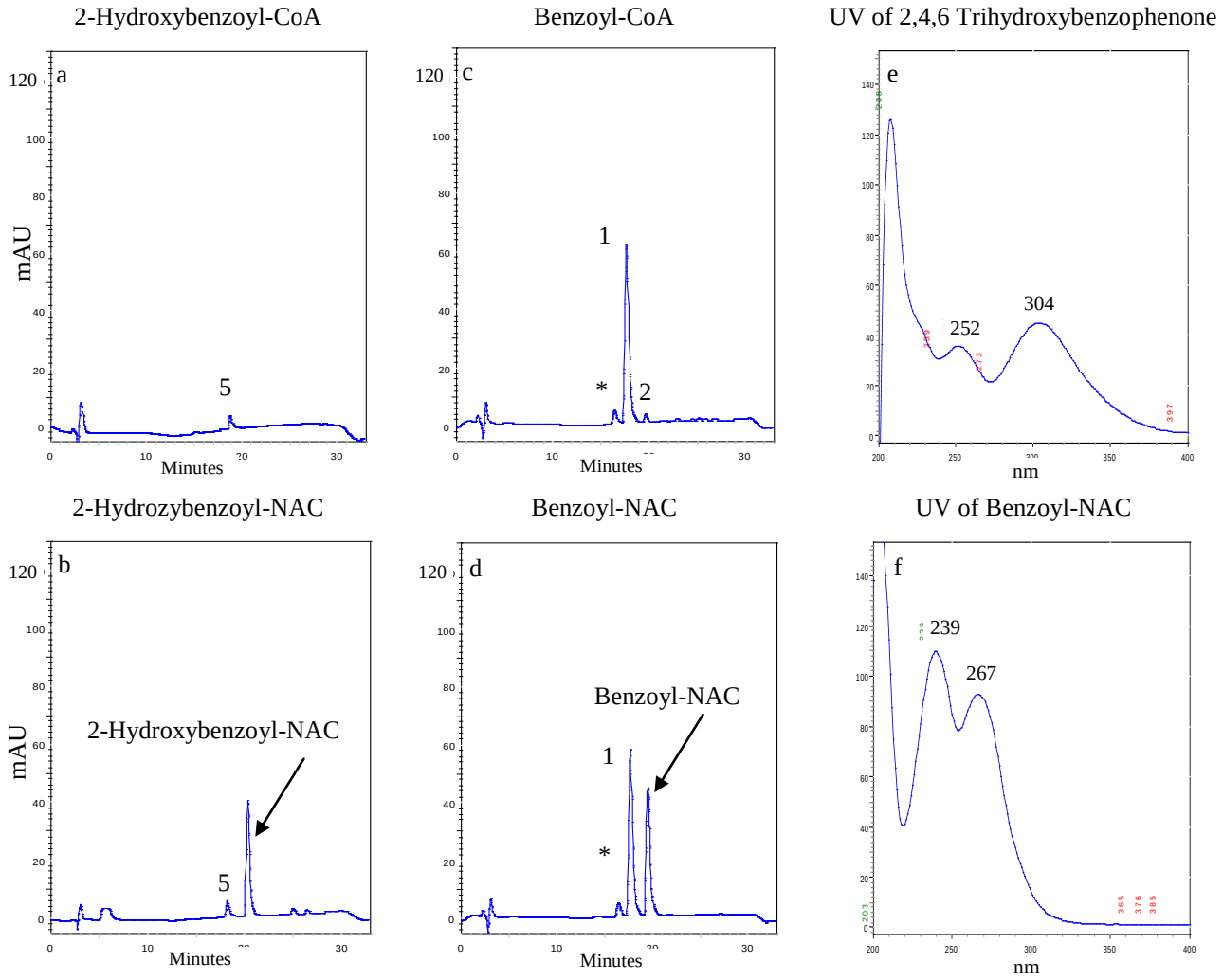

Fig. 52 HPLC chromatograms of assays of HsBPS wild-type with a: 2-hydroxybenzoyl-CoA, b: 2-hydroxybenzoyl-NAC, c: benzoyl-CoA, and d: benzoyl-NAC; e: UV spectrum of 2,4,6 trihydroxybenzophenone, f: UV spectrum of benzoyl-*N*-acetylcysteamine.

4.1.11 Determination of the kinetic parameters of HsThr135Lys, Leu, and Ile mutants

At the optimum reaction conditions, i.e. pH 7.0, temperature 30°C, 1.5 µg protein/assay and 5 min incubation time, the kinetic constants of HsT135K, HsT135L and HsT135I mutants were determined. The increase in reaction rate with increasing concentrations of substrates (salicoyl-CoA and malonyl-CoA in case of HsT135K and benzoyl-CoA and malonyl-CoA in case of the HsT135L and HsT135I mutants) obeyed Michaelis-Menten kinetics. The Michaels constants (K_m) of the mutants were calculated from Lineweaver-Burk plot which is a linear regression of the Michaelis-Menten equation. The kinetic parameters of the *H. sampsonii* mutants are summarized in (Tab. 13) and illustrated in (Figs. 53, 54, and 55). K_m is an important characteristic of the interaction between the enzyme and its substrate and defined as the substrate concentration which results in half of the maximum velocity of the enzymatic reaction. It is considered as an inverse measure of the affinity or strength of binding between the enzyme and its substrate. The K_{cat} value (turn over number) is the maximum number of substrate molecules that converted into product per active site per unit time when the enzyme is fully saturated. (K_{cat}/K_m) is the rate constant (specificity constant) for the interaction of substrate and enzyme. It is used as a measure of the catalytic efficiency as it provides information about how fast the reaction is when the substrate is bound to the enzyme (K_{cat}) and how much of the substrate is required to achieve half of the maximum rate (K_m) and so can characterize the kinetics of the enzyme under similar cellular conditions.

Tab. 13 Steady-state kinetic parameters of HsBPS wild-type and the HsT135K, HsT135L and HsT135I mutants from *H. sampsonii* [a]

Benzoyl-CoA				**Salicoyl-CoA**			**Malonyl-CoA**
Enzyme	K_{cat} **[sec^{-1}]**	K_m **[µM]**	K_{cat}/K_m **[M^{-1}sec^{-1}]**	K_{cat} **[sec^{-1}]**	K_m **[µM]**	K_{cat}/K_m **[M^{-1}sec^{-1}]**	K_m **[µM]**
HsBPS (Huang et al., 2012)	0.391	15.8	25028				92.5
HsT135K				1.181	43.92	26889	747
HsT135L	0.4431	18.03	24575				387
HsT135I	0.4373	24.95	17529				938

[a] Data are mean values of two independent experiments

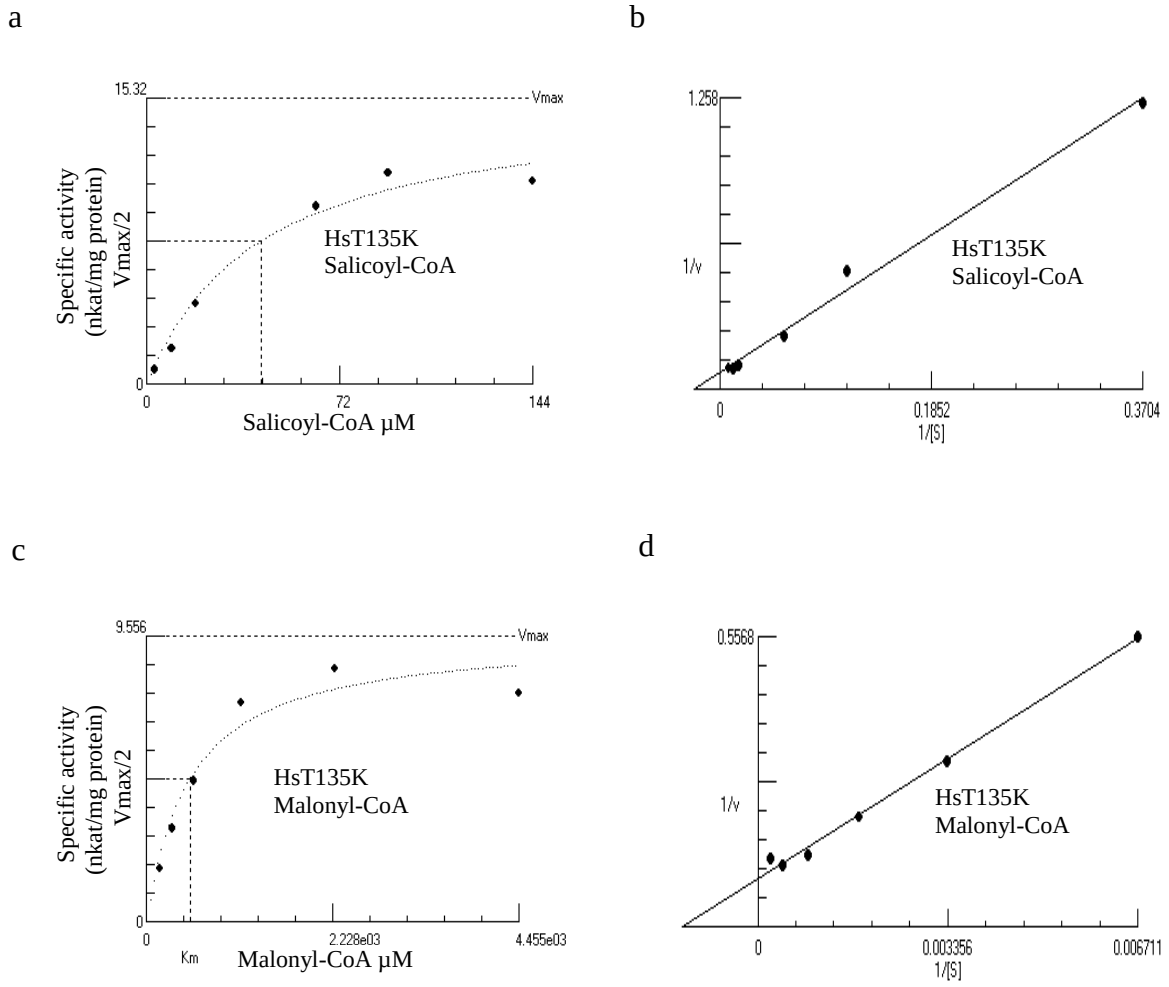

Fig. 53 a: Dependence of HsT135K activity on salicoyl-CoA concentration.
b: Determination of the K_m value for salicoyl-CoA via Lineweaver-Burk plot.
c: Dependence of HsT135K activity on the malonyl-CoA concentration.
d: Determination of the K_m value for malonyl-CoA via Lineweaver-Burk plot.

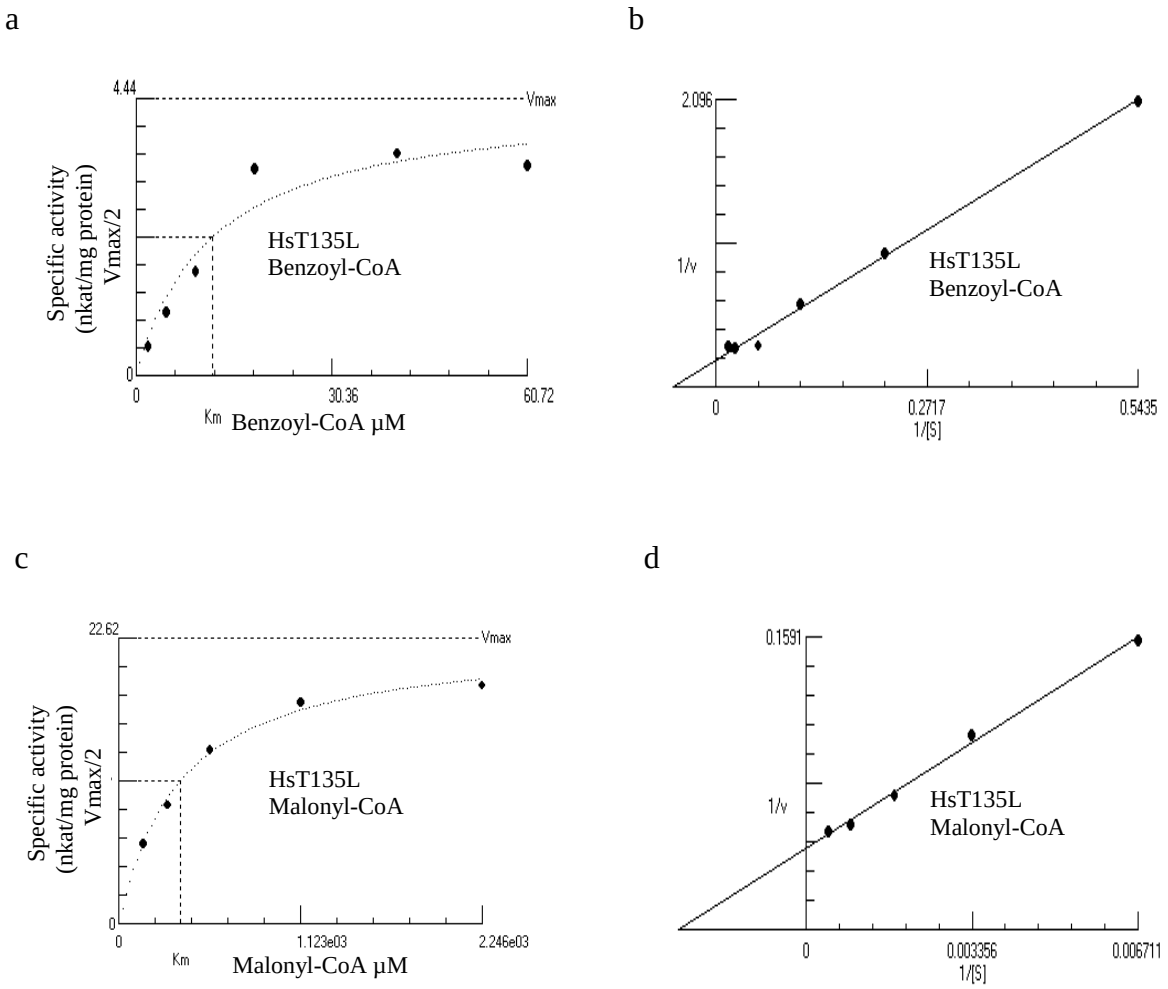

Fig. 54 a: Dependence of HsT135L activity on benzoyl-CoA concentration
b: Determination of K_m value for benzoyl-CoA via Lineweaver-Burk plot
c: Dependence of HsT135L activity on malonyl-CoA concentration
d: Determination of K_m value for malonyl-CoA via Lineweaver-Burk plot

a

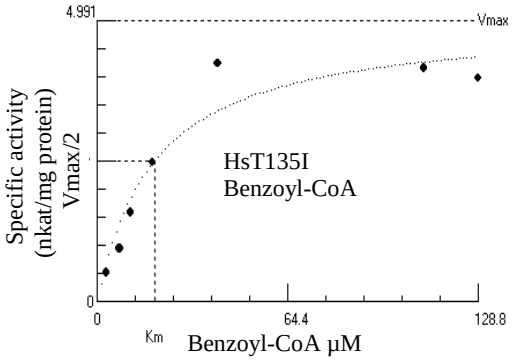

b

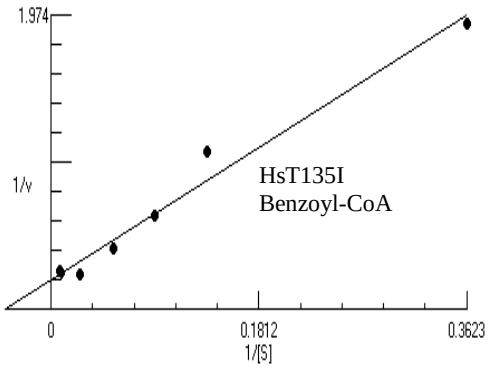

c

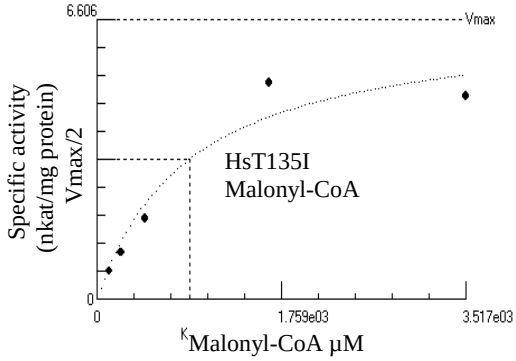

d

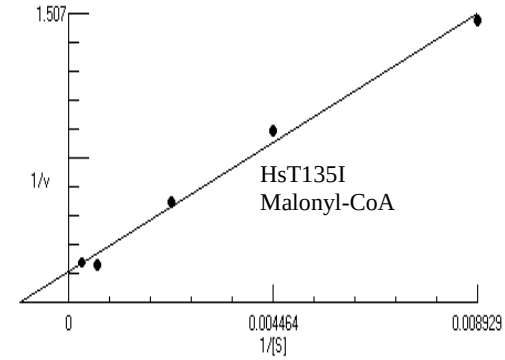

Fig. 55 a: Dependence of HsT135I activity on benzoyl-CoA concentration
b: Determination of K_m value for benzoyl-CoA via Lineweaver-Burk plot
c: Dependence of HsT135I activity on malonyl-CoA concentration
d: Determination of K_m value for malonyl-CoA via Lineweaver-Burk plot

4.2 Site-directed mutagenesis of *H. androsaemum* BPS (HaBPS)

H. androsaemum benzophenone synthase (HaBPS) was transformed into a functional phenylpyrone synthase (PPS) by a single amino acid substitution in the active site cavity namely T135L (Klundt et al., 2009). In the above studies we screened 19 amino acid residues in the same position of *H.sampsonii* (HsBPS), also occupied with Thr, and found that lysine instead of threonine in position 135 (HsT135K) converts HsBPS into a functional 4-hydroxycoumarin synthase (HCS). Thus, it was tempting to investigate the effect of lysine in position 135 in HaBPS and to study the effect of this point mutation on the substrate and product specificities and the catalytic activity of the enzyme.

4.2.1 Single mutation of the *H. androsaemum* BPS wild-type

Threonine in position 135 of HaBPS was converted to lysine by SDM-PCR (3.1.2) using two mutated partially overlapping primers designed according to Zheng et al., (2004) (Fig. 87, A). The resulting PCR amplification product was incubated with *Dpn*I restriction enzyme for 2 h at 37 °C to remove the un-mutated plasmid followed by DH5α transformation (3.1.6.1), plasmid isolation (3.1.7) and then restriction analysis using *Kpn*I for size confirmation (Fig. 87, B). The HaT135K mutant was confirmed by sequencing.

4.2.1.1 Production and isolation of the HaT135K mutant

Confirmation of the over-expression of the HaT135K mutant in *E.coli* was done by means of SDS-PAGE analysis (3.1.14) (Fig. 87, C). Protein bands were stained with Coomassie brilliant blue. The HaT135K mutant has a subunit molecular mass of about ~43 kDa.

4.2.1.2 Testing the activities of HaBPS wild-type and HaT135K mutant

First of all the activity of HaBPS wild-type was determined with benzoyl, 3-hydroxybenzoyl and 2-hydroxybenzoyl-CoAs according to Liu et al., (2003) and Klundt et al., (2009) and the highest activity of HaBPS was found with benzoyl-CoA (Fig. 88, a). It forms 2,4,6-trihydroxybenzophenone and a small amount of 4-hydroxy-6-phenylpyran-2-one as major and side products respectively. The other peaks one of them are non-enzymatic and the second is not identified and might be a tetraketide lactone product like that identified in *G. mangostana* BPS (Nualkaew et al., 2012). HaBPS also accepts 3-hydroxybenzoyl-CoA as a second best substrate (Fig. 88, c) forming 2,3',4,6-tetrahydroxybenzophenone as major product and 4-hydroxy-6-(3-hydroxy) phenylpyran-2-one as a side product. What is worth mentioning is the

acceptance by the HaBPS wild-type of 2-hydroxybenzoyl-CoA as a starter substrate forming a small amount of 4-hydroxycoumarin (Fig. 88, e). It was previously stated that this enzyme did not accept this substrate (Liu et al., 2003; Klundt et al., 2009). When the HaT135K mutant was tested with the previous substrates, this mutation was able to convert HaBPS wild-type into 4-hydroxycoumarin synthase (HaHCS) which prefers 2-hydroxybenzoyl-CoA as a starter substrate forming 4-hydroxycoumarin as a single product (Fig. 88, f). The product amount was around 3 times higher than that formed by the wild-type (HaBPS). The mutant was nearly inactive with benzoyl and 3-hydroxybenzoyl-CoAs (Figs. 88, b and d) which are the best substrates for HaBPS wild-type. This result is quite similar to that obtained with the HsT135K mutant but at lower activity. A lot of trials were carried out to improve the activity of the HaT135K mutant such as changing the pH, temperature, and protein amount but all these trials were not successful. However, the important observation is the low activity of HaBPS wild-type with 2-hydroxybenzoyl-CoA and the confirmation of the ability of lysine in position 135 to dramatically change the specificities of HaBPS wild-type and to transform it into HCS which is similar to HsT135K.

4.2.2 *H. sampsonii* BPS-based mutations of HaBPS

The amino acid sequence alignments (Fig. 56) indicate only 6 different amino acids between these two enzymes. Despite this high degree of similarity (98.2 %) the K_m value for malonyl-CoA of HsBPS wild-type which equals 92.5 µM (Huang et al., 2012) is around 3 times higher than that of HaBPS wild-type (31.3 µM). It was interesting to find out which of these six amino acid residues (which are all away from the active site cavity) may be responsible for this high HsBPS malonyl-CoA K_m value. Six mutated and partially overlapping primers are designed according to (Zheng et al., 2004). SDM-PCR was done and the resulting PCR amplification product (Fig. 89, A) was incubated with *Dpn*I restriction enzyme for 2 h at 37 °C to remove the un-mutated plasmid followed by DH5α transformation (3.1.6.1), plasmid isolation (3.1.7) and then restriction analysis using *Kpn*I for size confirmation (Fig. 89, B). The HaE54D, HaV146A, HaC230G, HaS235A, HaV359L and HaN360S mutants were confirmed by sequencing.

4.2.2.1 Production and isolation of six *H.androsaemum* single mutants

Confirmation of the over-expression of the HaE54D, HaV146A, HaC230G, HaS235A, HaV359L and HaN360S mutants was done by means of SDS-PAGE analysis (3.1.14). (Fig. 89,

C and D). Only five mutants were over-expressed in the *E.coli* host cells while the HaS235A mutant failed to be over-expressed.

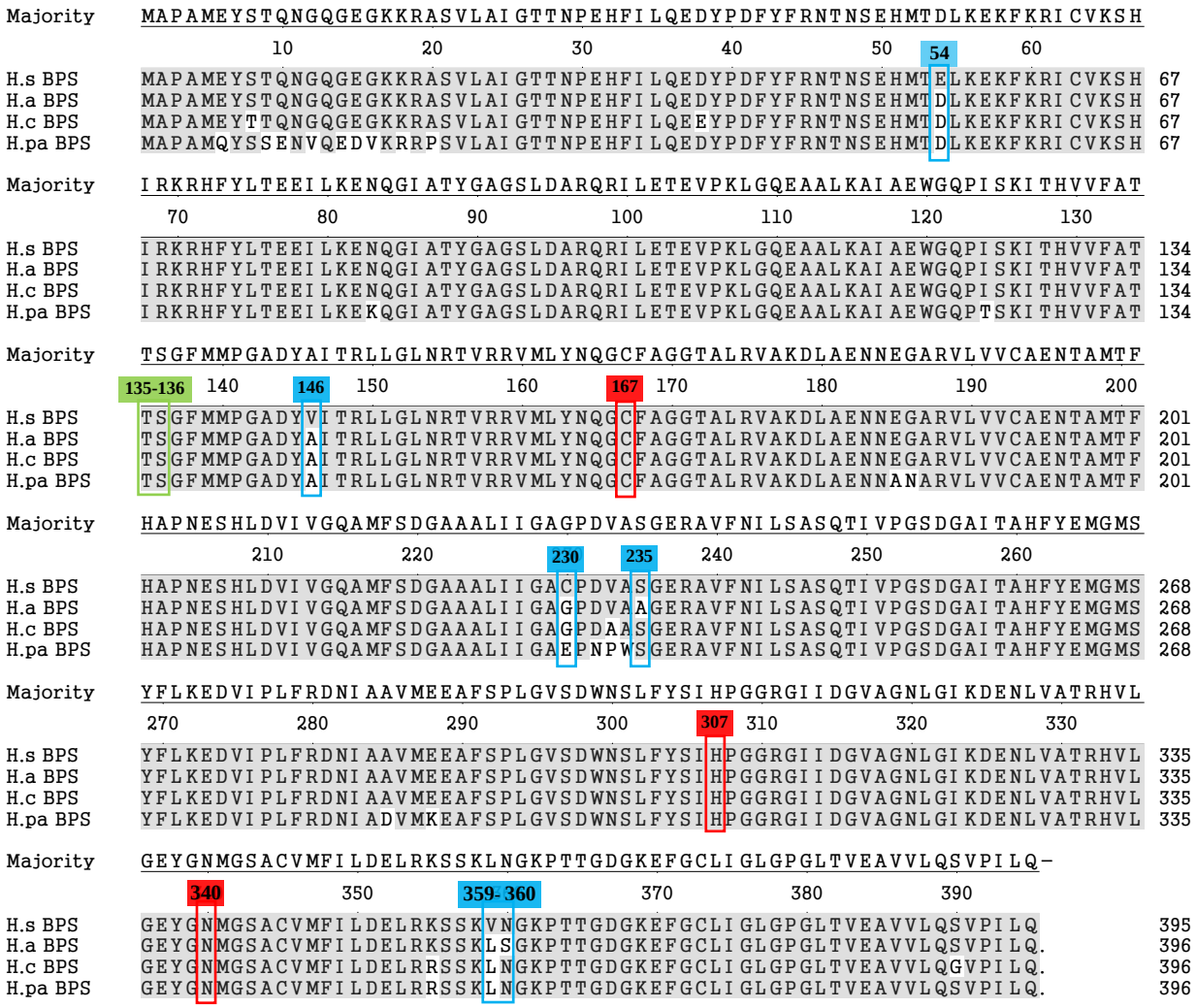

Fig. 56 Alignment of BPS amino acid sequences of *H. sampsonii* (HsBPS), *H. androsaemum* (HaBPS), *H. calycinum* (HcBPS) and *H. perforatum* ssp. *angustifolium* (HpaBPS).

4.2.2.2 Testing the activities of *H.androsaemum* single mutants

Transformation of the PCR-mutated plasmids of *H.androsaemum* BPS in *E.coli* BL21 was done as described in (3.1.6.2). Protein over-expression and purification of the His_6-tagged HaBPS single mutants using the Ni-NTA system (3.1.12) was performed and all of the purified mutants were then subjected to BPS assays (3.2.2.1) to characterize their specificities (3.2.4.4). The activities of the affinity-purified single mutants with various starter substrates were determined and compared with those of HaBPS wild-type (Fig. 57). All of these five active single mutants accepted and preferred benzoyl-CoA as a starter substrate forming 2,4,6-trihydroxybenzophenone

and a small amount of 4-hydroxy-6-phenylpyran-2-one as main product and side product respectively. The second best substrate was 3-hydroxybenzoyl-CoA and the products were 2,3',4,6-tetrahydroxybenzophenone and 4-hydroxy-6-(3-hydroxy) phenylpyran-2-one as main and side product respectively. All of them also accepted 2-hydroxybenzoyl-CoA forming small amounts of 4-hydroxycoumarin.

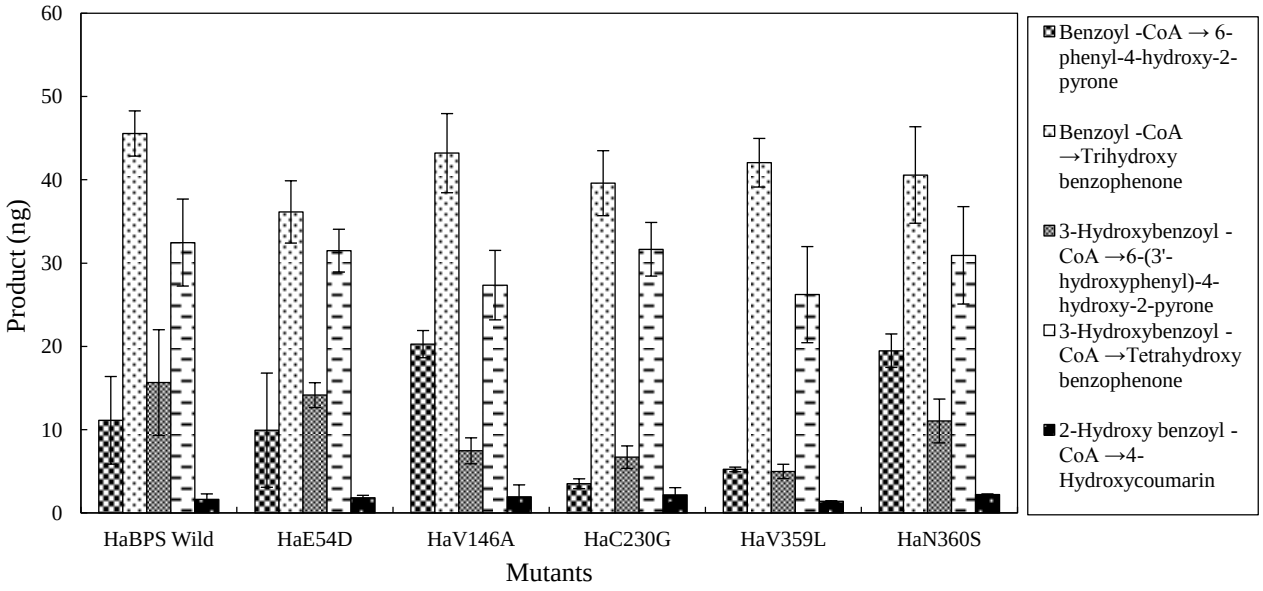

Fig. 57 Substrate and product specificities of HaBPS wild-type and HaE54D, HaV146A, HaC230G, HaV359L and HaN360S mutants.

4.2.2.3 Determination of the kinetic parameters of *H.androsaemum* single mutants

Our target was to find out which of these amino acids may be responsible for the high malonyl-CoA K_m value of HsBPS. Therefore, the kinetic constants of the HaE54D, HaV146A, HaC230G, HaV359L and HaN360S mutants were determined. The increase in reaction rate with increasing concentrations of the substrates benzoyl-CoA and malonyl-CoA obeyed Michaelis-Menten kinetics. Michaelis constants (K_m) of the mutants were calculated from Lineweaver-Burk plots. The kinetic results of *H.androsaemum* five single mutants in comparison with HsBPS and HaBPS wild-types are documented in (Tab. 14) and represented in (Figs. 90, 91, 92, 93 and 94). The determined K_m values of the five single mutants showed 3 - 4.9 fold increase for malonyl-CoA and 2 - 4 fold increase in benzoyl-CoA compared to the wild-type HaBPS (Klundt et al., 2009). These results indicate that, any change in these five amino acid residues (which are away from the active site) decreased the substrates affinity with pronounced effect on malonyl-CoA.

Tab. 14 Steady-state kinetic parameters of HaE54D, HaV146A, HaC230G, HaV359L and HaN360S in comparison to HsBPS and HaBPS wild-types [a]

	Benzoyl-CoA			Malonyl-CoA
Enzyme	**K_{cat} [sec^{-1}]**	**K_m [µM]**	**K_{cat}/K_m [$M^{-1}sec^{-1}$]**	**K_m [µM]**
HsBPS (Huang et al., 2012)	0.391	15.8	25028	92.5
HaBPS (Klundt et al., 2009)	0.055	8.6	6414	31.3
HaE54D	0.141	33.66	4189	154.37
HaV146A	0.082	16.68	6175	128.53
HaC230G	0.111	24.67	4499	120.84
HaV359L	0.143	26.75	5345	140.62
HaN360S	0.096	17.37	5526	100.71

[a] Data are mean values of two independent experiments

4.2.3 Double mutations with the HaBPST135K mutant

As mentioned before (4.2.1) replacement of HaBPS Thr135 with lysine resulted in transformation of HaBPS into HCS. However, the activity of HaT135K was much lower than HsT135K activity. Changing pH, temperature, incubation time, and protein amount failed to improve this activity and thus provoked the idea of double mutations to determine which of the six different amino acids between *H. androsaemum* and *H. sampsonii* BPSs (Fig. 56) will improve the activity of HaT135K with 2-hydroxybenzoyl-CoA. SDM-PCR (3.1.2) was performed using mutated partially overlapping primers designed according to (Zheng et al., 2004). The resulting PCR amplification product (Fig. 95, A) restriction analysis (Fig. 95, B) over-expression (Fig. 95, C and D) and confirmation of these mutants were performed as previously explained.

4.2.3.1 Testing the activities of *H. androsaemum* lysine double mutants

The activities of the affinity-purified mutants with various starter substrates were determined using HPLC analysis (Fig. 58). All the HPLC chromatograms are shown in (Fig. 96, a, b, c, d and e). All the double mutants derived from HaT135K were nearly inactive with benzoyl and 3-hydroxybenzoyl-CoAs while showing a high activity with 2-hydroxybenzoyl-CoA as a starter substrate forming relatively high amounts of 4-hydroxycoumarin which were around 3- times higher than with the HaT135K single mutant.

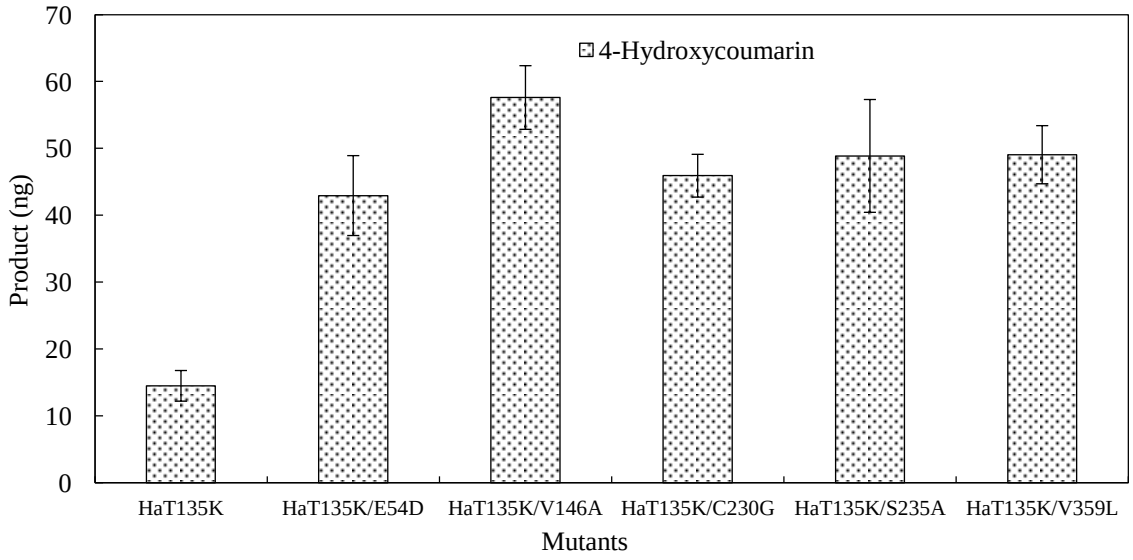

Fig. 58 Catalytic activity with salicoyl-CoA of *H.androsaemum* lysine double mutants, HaE54D/T135K, HaV146A/T135K, HaC230G/T135K, HaS235A/T135K and HaV359L/T135K in comparison to HaT135K single mutant.

4.2.3.2 Determination of the kinetic properties of HaV146A/T135K mutant

From an economical point of view we aimed at finding a 4-hydroxycoumarin synthase (HCS) enzyme mutant with lower malonyl-CoA K_m value due to the expensive price of acyl-CoA esters. We decided to determine the kinetic parameters of the HaV146A/T135K double mutant as it showed the highest activity with salicoyl-CoA. The HaV146A/T135K double mutant showed a K_{cat}/K_m value 4-fold lower than that of HsT135K due to a 3-fold lower K_{cat} value and 1.3 fold higher K_m value for benzoyl-CoA while it showed around 1.3 fold increase in malony-CoA K_m value compared to HsT135K mutant as shown in (Tab. 15 and Fig. 59).

Tab. 15 Steady-state kinetic parameters of the HaV146A/T135K double mutant in comparison with those of above mentioned enzymes.

Benzoyl-CoA				**Salicoyl-CoA**			**Malonyl-CoA**
Enzyme	**K_{cat} [sec^{-1}]**	**K_m [µM]**	**K_{cat}/K_m [$M^{-1}sec^{-1}$]**	**K_{cat} [sec^{-1}]**	**K_m [µM]**	**K_{cat}/K_m [$M^{-1}sec^{-1}$]**	**K_m [µM]**
HaBPS wild-type (Klundt et al., 2009)	0.055	8.6	6414				31.3
HaV146A	0.082	16.68	6175				128.53
HaV146A/T135K				**0.3895**	**56.97**	**6838**	**956.54**
HsBPS wild-type (Huang et al., 2012)	0.391	15.8	25028				92.5
HsT135K				**1.181**	**43.92**	**26889**	**747**

[a] Data are mean values of two independent experiments

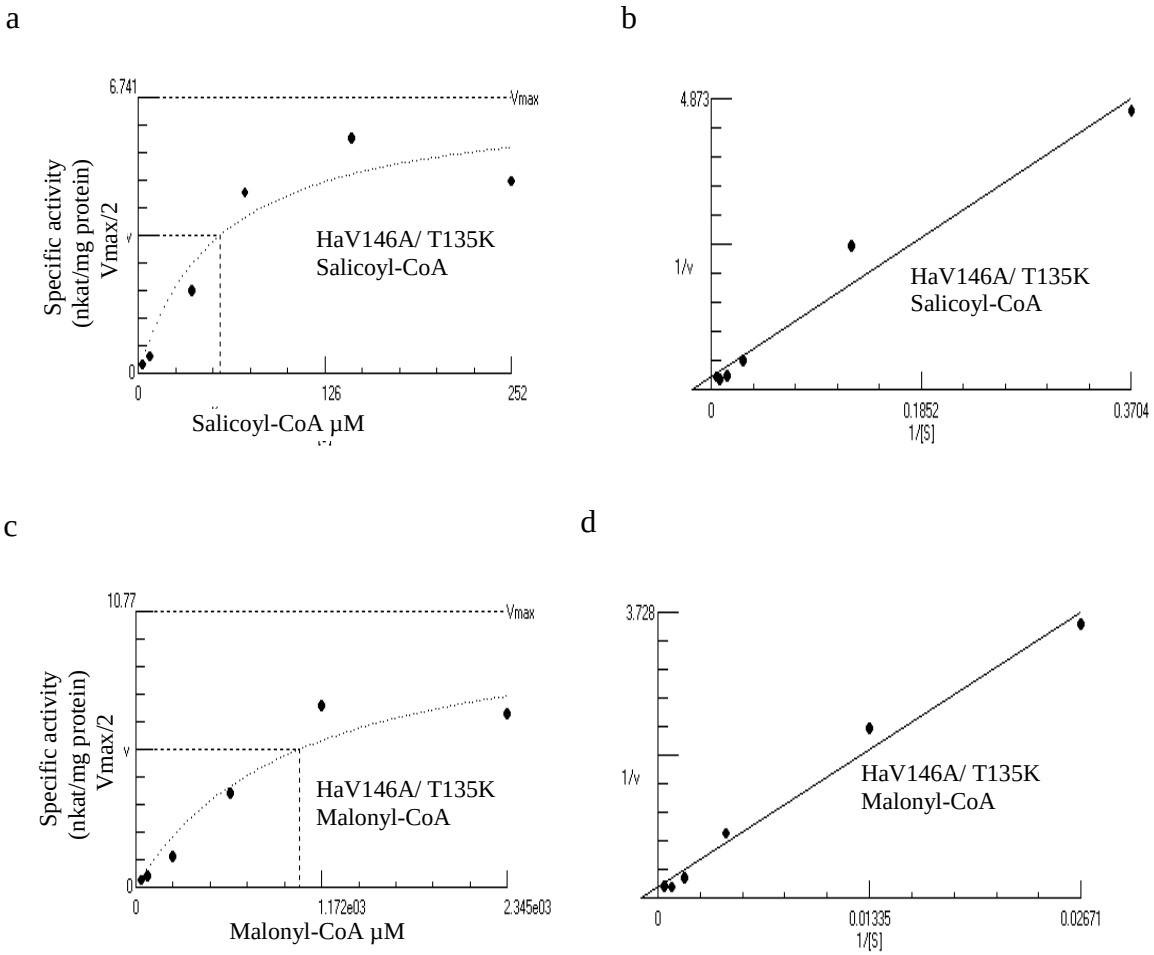

Fig. 59 a: Dependence of HaV146/T135K activity on salicoyl-CoA concentration.
b: Determination of K_m value for salicoyl-CoA via Lineweaver-Burk plot.
c: Dependence of HaV146/T135K activity on malonyl-CoA concentration.
d: Determination of K_m value for malonyl-CoA via Lineweaver-Burk plot.

4.2.4 Double mutations with the HaBPST135I mutant

Replacement of leucine in HaBPS with different amino acids like isoleucine and alanine was not successful (Klundt et al., 2009) but in HsBPS isoleucine in position 135 transformed the enzyme into phenylpyrone synthase (PPS). Recently, our work group cloned two cDNAs from *Centaurium erythraea* for which blasting results showed close homology to type III PKS. One of them functions as PPS (CePKS2/CePPS) (unpublished work) and the most important point is that, position 135 in this natural PPS occupied with isoleucine. It is interesting to find out which of the 6 different amino acids between the HaBPS and HsBPS wild-types are able to recover the isoleucine activity in position 135 in HaBPS. Similarly, the HsT135A mutant was also active and formed around 50% 2,4,6-trihydroxybenzophenone and 50% 6-phenyl-4-hydroxy-2-pyrone with benzoyl-CoA starter substrate. So the same idea is applied to this alanine to explore the effect of the different amino acids between the two genes (HaBPS and HsBPS) on the activity. SDM-PCR was carried out using mutated partially overlapping primers designed according to (Zheng et al., 2004) (Fig. 97, A).The restriction analysis for size confirmation (Fig. 97, B) and expression of the mutants was done (Fig. 97, C) as mentioned before.

4.2.4.1 Testing the activities of *H.androsaemum* isoleucine double mutants

The activities of the affinity-purified double mutants with various starter substrates were determined and compared with those of HaBPS wild-type. The results of the activity tests are represented in (Fig. 60) and the HPLC assays are summarized in (Figs. 98 and 99). The HaE54D/T135I, HaV146A/T135I, HaC230G/T135I, HaS235A/T135I, HaV359L/T135I and HaN360S/T135I double mutants preferred benzoyl-CoA as a starter substrate forming 4-hydroxy-6-phenylpyran-2-on as main product (Fig. 98, a, b, c, d, e and f) they catalyzed iterative condensation of one benzoyl-CoA with two malonyl-CoAs forming triketide intermediate which undergoes cyclization via C-5 keto-enol oxygen→C-1 lactonization into phenylpyrone (Klundt et al., 2009). 3-Hydroxybenzoyl-CoA is the second best substrate for all of the mutants (Fig. 99, a, b, c, d, e and f) forming 4-hydroxy-6-(3-hydroxy) phenylpyran-2-one (Klundt et al., 2009). They also accepted 2-hydroxybenzoyl-CoA forming small amounts of 4-hydroxycoumarin. The HaN360S/T135A double mutant activity results (Fig. 100, a, b and c) were similar to those of the HsT135A single mutant confirming the effect of these six amino acids (which are away from the active site) on the activity. All the results are confirmed by UV spectroscopy and the products were quantified using standard solutions of the respective authentic reference compounds.

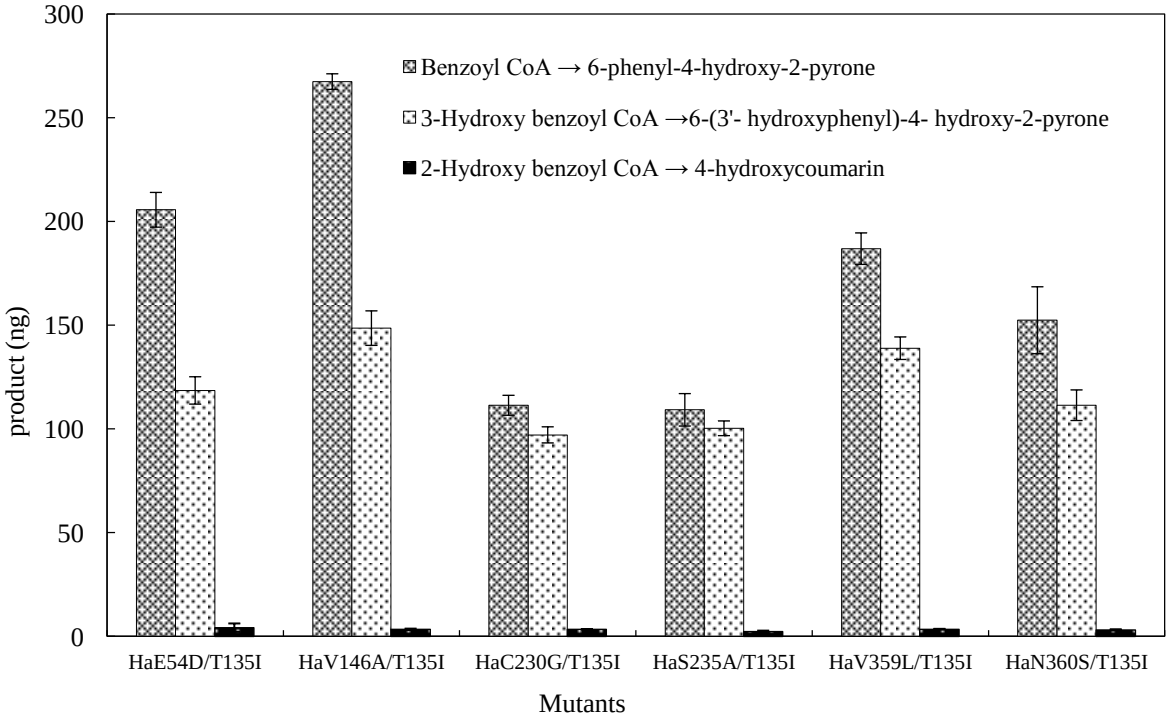

Fig. 60 Catalytic activity with benzoyl, 3-hydroxybenzoyl and salicoyl-CoAs of *H.androsaemum* isoleucine double mutants.

4.3 Site-directed Mutagenesis of *H. calycinum* BPS (HcBPS)

H. calycinum BPS is one of the BPSs which was cloned in our work group (Zodi, 2011). The amino acid sequence alignment (Fig. 56) showed that there are only seven different amino acids between HcBPS and HsBPS wild-types. Screening of different amino acids in position Thr135 of HsBPS revealed that lysine in this position was able to transform HsBPS into a functional 4-hydoxycoumarin synthase (HCS) while Leucine and Isoleucine amino acids were able to convert HsBPS into phenylpyrone synthase (PPS). Our main target was to study the effect of these three amino acids on the activity and specificities when replacing Thr135.

4.3.1 Single mutations of HcBPS

The main problem with the HcBPS cDNA is the low GC content which led to unsuccessful mutation. To overcome this difficulty partially overlapping mutated primers were designed following the protocol of Liu and Naismith, (2008) which is ideal for low GC content genes. Replacement of Thr135 in HcBPS wild-type with lysine, leucine and isoleucine was carried out using SDM-PCR (3.1.2) with the afore-mentioned mutated primers (Fig. 101, A). The resulting PCR amplification product was incubated with *Dpn*I restriction enzyme for 2 h at 37 °C

followed by DH5α transformation (3.1.6.1) and plasmid isolation (3.1.7) and then restriction analysis using *Kpn*I for size confirmation (Fig. 101, B). The successful mutations were confirmed by sequencing.

4.3.1.1 Protein expression of HcThr135Leu, Ile and Lys mutants

Monitoring the over-expression of the HcT135L, HcT135I and HcT135K mutants was done by means of SDS-PAGE analysis (3.1.14) (Fig. 101, C and D). Protein bands were stained with Coomassie brilliant blue. The HcT135L and HcT135I mutants had subunit molecular masses of about ~43 kDa. Unfortunately, due to misfolding of the over-expressed protein (HcT135K) it aggregated to form inclusion bodies which greatly reduced the protein yield to the extent that we were not able to find any soluble protein (Fig. 101, D).

4.3.1.2 Testing the activities of HcBPS wild and HcThr135Leu and Ile mutants

Each PCR-mutated plasmid was transferred to *E.coli* BL21 as described in (3.1.6.2) for protein over-expression. The Ni-NTA system was used for the purification of the His_6-tagged HcBPS wild-type and its mutants (3.1.12). BPSs assay (3.2.2.1) for HcBPS wild-type and its mutants were done to characterize their catalytic activities and specificities. The activity of the affinity-purified wild-type and mutants with various starter substrates were determined (Fig. 61) using HPLC. The HPLC chromatograms are shown in (Fig. 102 and 103). HcBPS wild type accepts and prefers benzoyl-CoA as a starter substrate forming 2,4,6-trihydroxybenzophenone as main product and 4-hydroxy-6-phenylpyran-2-one side product was also detected. Noteworthy is the inactivity of HcBPS wild-type with 2-hydroxybenzoyl-CoA as substrate. Both the HcT135L and HcT135I mutants accepted and preferred benzoyl-CoA as a starter substrate forming 4-hydroxy-6-phenylpyran-2-one as main product and the second best substrate for those mutants is 3-hydroxybenzoyl-CoA which after condensation with 2 malonyl-CoAs forms 4-hydroxy-6-(3-hydroxy) phenylpyran-2-one as main product and also these two mutants did not accept 2-hydroxybenzoyl-CoA.

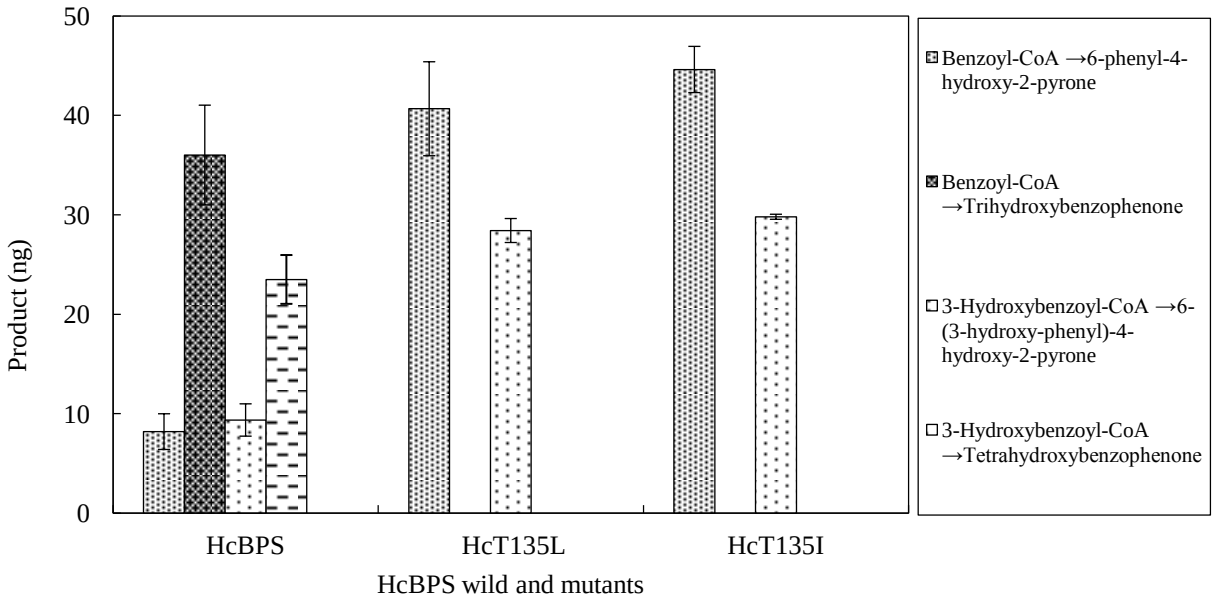

Fig. 61 Catalytic activities and substrate and product specificities of HcBPS wild-type, HcT135L and HcT135I mutants.

4.4 Site-directed mutagenesis of *H. perforatum* ssp *angustifolium* (HpaBPS)

HpaBPS is another BPS cloned in our work group (Tocci, 2013). From amino acid sequence alignment there are 22 different amino acids between HsBPS and HpaBPS and all of them away from the active site so it is very motivating to study the effect of lysine, leucine and isoleucine amino acids instead of Thr135 in HpaBPS on the catalytic activity and substrate specificity.

4.4.1 Single mutation of HpaBPS

SDM-PCR (3.1.2) using partially overlapping mutated primers designed according to (Zheng et al., 2004) was carried out (Fig. 104, A). The resulting PCR amplification product was incubated with *Dpn*I restriction enzyme for 2 h at 37 °C to remove the un-mutated plasmid followed by DH5α transformation (3.1.6.1) and plasmid isolation (3.1.7) and then restriction analysis using *Kpn*I for size confirmation (Fig. 104, B). HpaT135L, HpaT135I and HpaT135K mutation effectiveness was confirmed by sequencing.

4.4.1.1 Protein expression of HpaThr135Leu, Ile and Lys mutants

Monitoring of the over-expression of the HpaT135L, HpaT135I and HpaT135K mutants was done by means of SDS-PAGE analysis (3.1.14) (Fig. 104, C). Protein bands were stained with Coomassie brilliant blue. HpaT135L and HpaT135I mutants have subunit molecular mass

of about ~43 kDa while HpaT135K mutant did not show any over-expression in *E.col* (Fig. 104, D).

4.4.1.2 Testing the activities of HpaBPS wild-type, HpaThr135Leu and Ile mutants

Each PCR-mutated plasmid was transformed in *E. coli* BL21 as described in (3.1.6.2) for protein over-expression. Ni-NTA system was used for the purification of the His_6-tagged HpaBPS wild-type and its mutants (3.1.12). BPSs assay (3.2.2.1) for HpaBPS wild-type and its mutants were done to characterize their catalytic activity and substrate specificity. The activity of the affinity-purified wild and mutants with various starter substrates (Fig. 62) were determined using HPLC. The HPLC chromatograms are shown in (Figs. 105 and 106). HpaBPS wild type accepts and prefers benzoyl-CoA as a starter substrate forming 2,4,6-trihydroxybenzophenone as main product and 4-hydroxy-6-phenylpyran-2-one side product was also detected. Noteworthy is the inactivity of HpaBPS wild with 2-hydroxybenzoyl-CoA substrate. Both of HpaT135L and HcT135I mutants accept and prefer benzoyl-CoA as a starter substrate forming 4-hydroxy-6-phenylpyran-2-one as main product and the second best substrate for those mutants is 3-hydroxybenzoyl-CoA which in the presence of 2 malonyl-CoAs forms 4-hydroxy-6-(3-hydroxy) phenylpyran-2-one as main product and again these 2 mutants did not accepts 2-hydroxybenzoyl-CoA.

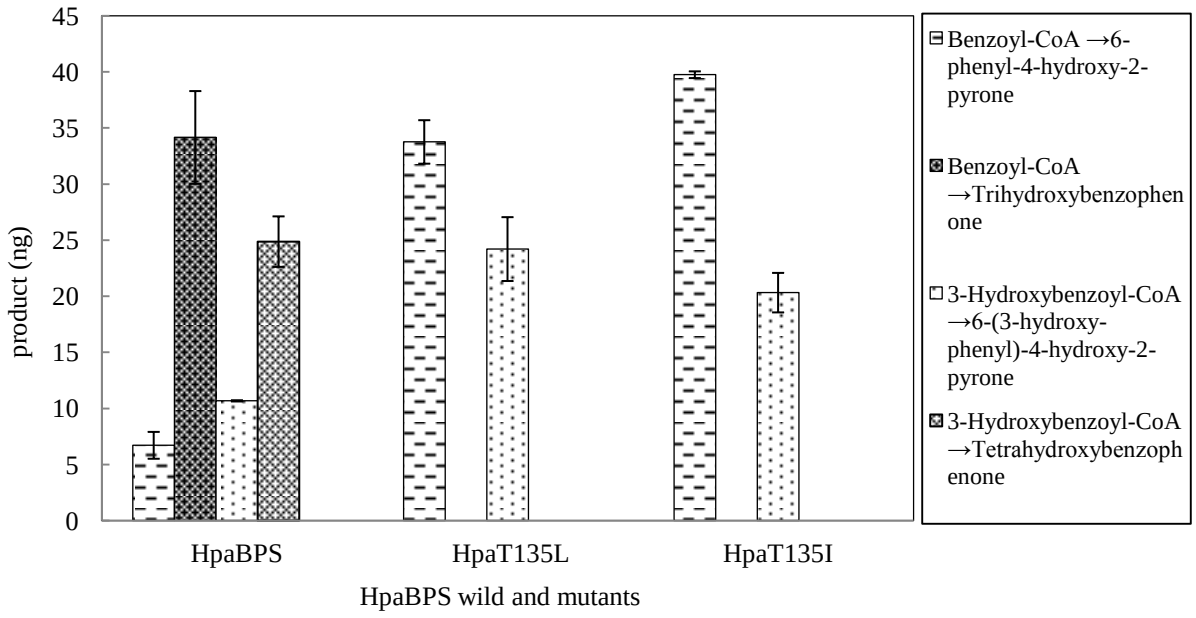

Fig. 62 Catalytic activities and substrate and product specificities of HpaBPS wild-type, HpaT135L and HpaT135I mutants.

4.5 Results of homology modeling

In the current study different amino acids especially those with longer and charged side chains like lysine were tested in *H.sampsonii* in addition to studying BPSs from different *Hypericum* species. The initial model of *H. androsaemum* BPS (Klundt et al., 2009) was created by using the Swiss-Model server (Guex and Peitsch, 1997; Arnold et al., 2006) and contained a single monomer of HaBPS. An updated model of HsBPS was constructed based on the crystal structure of *M. sativa* CHS2 (Ferrer et al., 1999) complexed with resveratrol (Protein Data Bank code 1CGZ) using Yasara Structure (Krieger et al., 2003). The conserved CoA-binding sites and catalytic residues were correctly aligned using SSALN (Qiu and Elber, 2006) which indicates that the generated model is reliable. This new model contains a dimer as an active species. This dimeric quaternary structure is also present in all X-ray crystal structures of related type III PKSs. The homology model of the HsBPS dimer was overlaid with the structure 1EE0 (2-pyrone synthase complexed with acetoacetyl-CoA (Jez et al., 2000). The dimer model contains no acetyl-CoA but can be structurally aligned with the reference structure-1EE0 complexed with acetyl-CoA (Fig. 63). The dimer interface in addition to the different amino acids between *H. sampsonii* and *H. androsaemum* from the amino acid sequence alignment is highlighted.

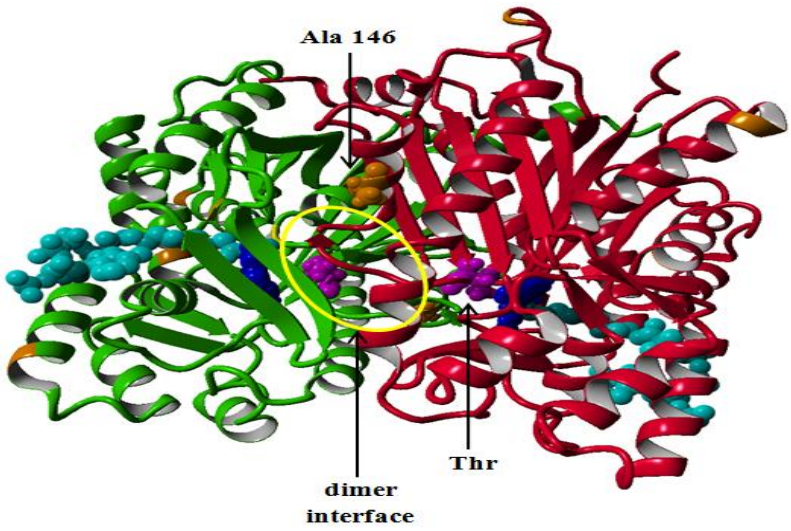

Fig. 63 Homology model of dimeric HsBPS, red: monomer A, green: monomer B, orange: mutations, yellow: active site Cys/His, blue: resveratrol, cyan: acetoacetyl-CoA. The positions 146 and 135 and the dimer interface are also highlighted.

The active site is located very close to the dimer interface and upon mutation of the small Thr135 to the large Lys the side chain is too long to fit easily into the active site and so it is most likely to reorient towards the dimer interface. Thus, its conformation is completely different from

the previous smaller mutations of HaBPS which point directly into the active site as proposed before in the published simple monomer model. In the new model, the lysine residue is pointing away from the active site with its charged end-group and it is most likely in contact with Met 140 of monomer B and Met 267 from the dimer interface (Fig.64).

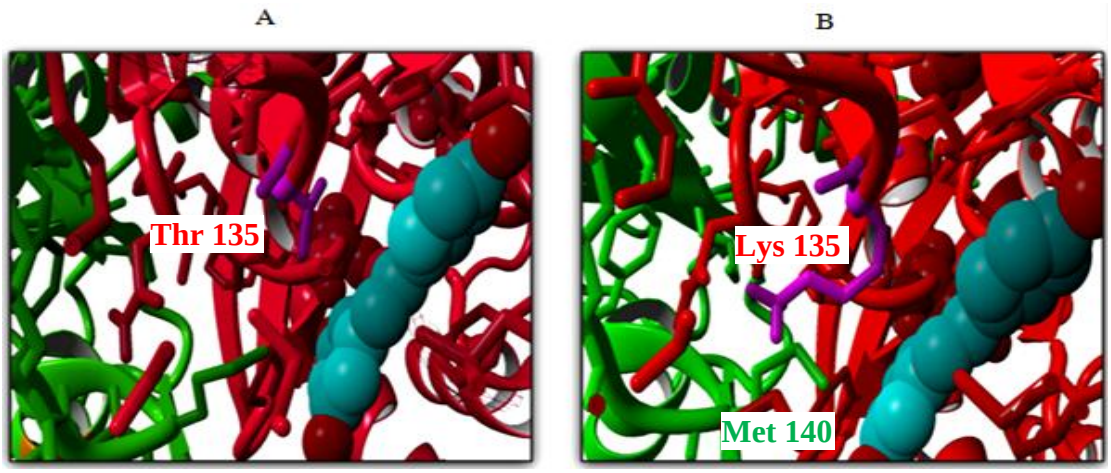

Fig. 64 Thr135 in wild-type HsBPS (A) and Lys135 in the HsBPS T135K mutant (B).

Rationalization of the effect of the six different amino acids between *H.sampsonii* and *H.androsaemum* BPSs was performed in the new model. These six different amino acids are not catalytic residues or involved in the active site but dramatically affect on the enzyme activity and catalysis. In this updated dimer structure the loop from 138 to 144 is part of the dimer interface directly adjacent to the active site mutation in position 135 in the other monomer (Fig. 63). Therefore, it is likely that the combination of residues in position 135 and 146 is independent but will be cooperatively affecting each other. This effect of the adjoining dimer interface will be even more pronounced in *H. calycinum* and *H.perforatum* ssp *angustifolium* BPSs. Where the active site is identical but the dimer interface contains several exchanges and is most likely different. This will result in different orientation of the loop from 138 to 144 which is part of the dimer interface directly adjacent to the active site. To clarify this in more detail an X-ray crystal structure is required as the current model cannot resolve such global conformational changes.

The other two residues (Gly230 and Ala235) are surface residues located adjacent to the N-terminal dimerization helix and thus may be influencing the dimer interface as well (Fig. 65). Interestingly, looking at the alignment (Fig. 56) of *H. calycinum* and *H. perforatum* BPSs in this region, it can be seen that particularly this loop region 230-235 differs in all sequences significantly. When we take the dimer contact residues (N-terminal helix 1 – 20) in this region

into consideration it is second evidence that, despite the high overall sequence identity, exactly this dimer contact region has up to 10 exchanges in *H. perforatum* ssp *angustifolium* and so the dimer interface looks different.

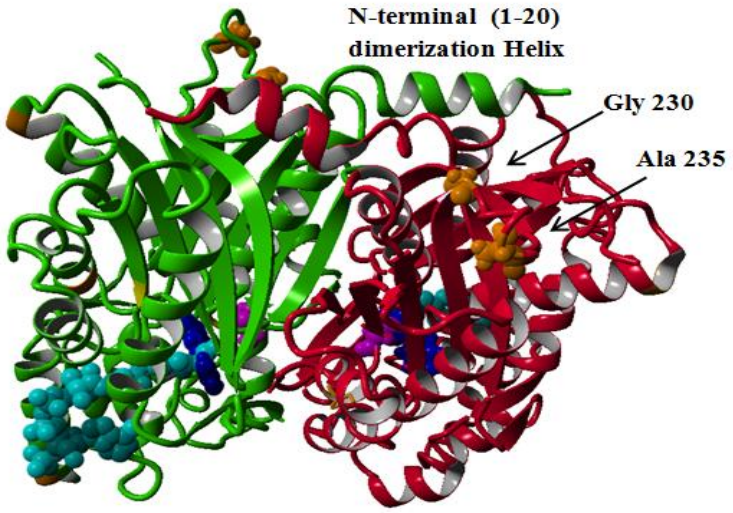

Fig. 65 Homology model of dimeric HsBPS highlighting positions 230 and 235.

Positions 359 and 360 are located at the end of a helix running into the active site. Any conformational changes in this helix from 346 to 360 may impair catalysis globally. Position Ala54 (Fig. 66) is in direct contact with -CoA and therefore may be relevant for its binding. This can easily explain K_m effects if measured on CoA substrates and thus rescue catalysis for the mutants. All other residues seem to be related to CoA binding since they are surface residues and are located not at the dimer interface but close to the CoA binding site.

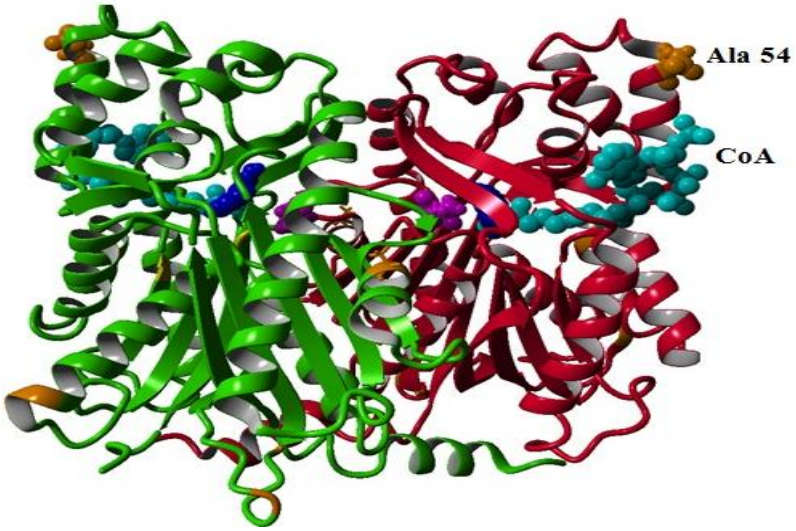

Fig. 66 Homology model of dimeric HsBPS with position 54 highlighted.

5 Discussion

5.1 Significance of type III PKSs

The last couple of years resulted in cloning and characterization of a large number of CHS genes and several new members of the plant type III PKS gene family with novel and unexpected activities and of course future efforts will yield more. These findings confirm the significant role of type III PKSs in generating a wealth of substantially variable molecules by contributing to the biosynthesis of many classes of plant secondary metabolites in spite of using only a small group of biochemical reactions (Abe, 2010; Duckworth, 2012). The first investigated and isolated type III PKS was the CHS from parsley (*Petroselium hortense*) (Reimold et al., 1983) due to its significant role in starting the biosynthesis of flavonoids, known for their wide distribution in higher plants (Austin and Noel, 2003). The crystallographic studies in addition to structure-based mutagenesis investigations of functionally varied type III PKSs started to disclose the structural facts of the reactions catalyzed by this fascinating group of enzymes. As mentioned before, this group of iterative homodimeric enzymes catalyze the sequential condensation of acetyl units derived from the decarboxylation of malonyl-CoA into a developing polyketide chain in a reaction similar to that of fatty acid synthases of the primary metabolism from which the PKSs probably evolved by gene duplication and subsequent refunctionalization of the gene duplicates (Austin and Noel, 2003). PKSs accept a wide range of starter substrates leading to functional and chemical diversity in natural products metabolism of plants. Divergences in the number of malonyl-CoA condensations in addition to the type of the cyclization reactions (Fig. 67) further increase this variation (Austin and Noel, 2003; Flores-Sanchez and Verpoorte, 2009; Abe, 2010).

5.2 Mutation and characterization of type III PKSs

The mutagenic inter-conversion and in vitro characterization of type III PKS enzymes are considered as precious tools for confirming functionally relevant divergences inside this superfamily. Additionally, the solved crystal structures supply answers to points where homology modeling fails to predict the structural and mechanistic effects of vital amino acid substitutions (Austin and Noel, 2003). More insights have been obtained about the steric geometry of the active site of type III PKSs and the molecular basis of their reactions after resolving the first X-ray crystal structure of MsCHS2 (Ferrer et al., 1999) and structures

determination of the following mutagenized forms of MsCHS2 and for 2-pyrone synthase (2PS) from *G. hybrida* (Jez et al., 2000; Jez and Noel, 2002). For example, it was known that, although each of the two active sites in CHS and the closely related stilbene synthase (STS) function independently, dimerization is required for activity (Tropf et al., 1995). It is now clear that this is due to a methionine (Met137) which in each monomer helps to shape the active site cavity of the adjoining monomer (Ferrer et al., 1999). It has also been shown that each active site is buried within the enzyme and the substrates enter through a long CoA-binding tunnel (Ferrer et al., 1999). The three key catalytic residues are located within an initiation/elongation cavity, one lobe of which forms a coumaroyl binding pocket while the other accommodates and determines the length of the developing polyketide chain.

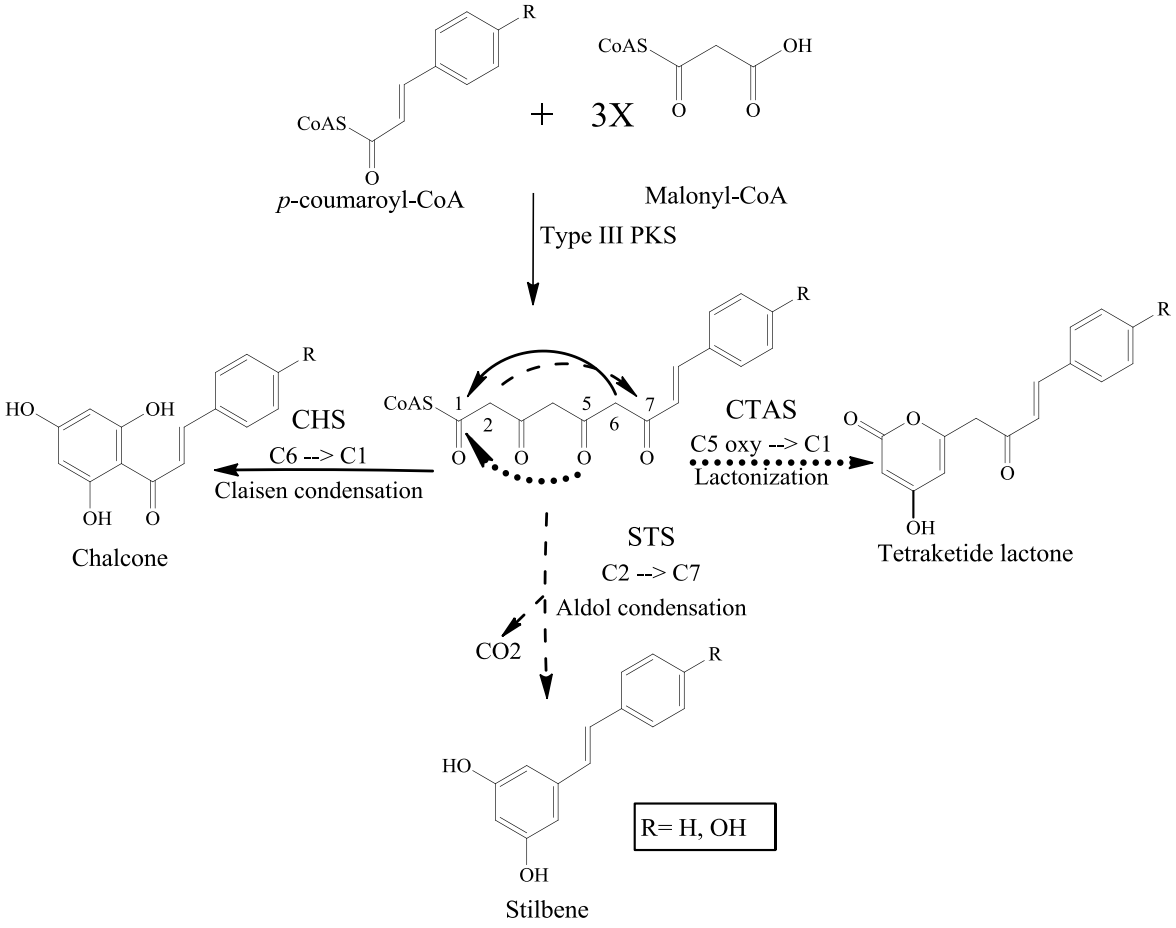

Fig. 67 Cyclization mechanisms catalyzed by plant type III PKSs. The solid arrow illustrates the C6→C1 Claisen condensation; the long dash-dot arrow represents the C2→C7 aldol condensation, and the round-dot arrow demonstrates the C5-oxygen→C1 lactonization modified from; Flores-Sanchez and Verpoorte, (2009).

Although CHS and 2PS use different substrates (*p*-coumaroyl-CoA vs. acetyl-CoA) and form different products (naringenin and triacetic acid lactone respectively) and exhibit only 74%

amino acid sequence identity the three-dimensional overall fold of the two enzymes is almost identical with similar catalytic residues and highly conserved CoA-binding residues. However, the total cavity volume of the active site of 2PS is one-third of that of MsCHS2 (Fig. 68). Remarkably, the steric contraction occurred by alteration of three of the chemically inert residues lining the active-site cavity: Thr197, Gly256, and Ser338 in MsCHS2 are substituted with Leu202, Leu261, and Ile343 in Gh2PS respectively (Eckermann et al., 1998; Jez et al., 2000). Based on the crystal structures of Gh2PS and MsCHS2 these three residues are supposed to play a vital role in controlling starter substrate selectivity and the number of malonyl-CoA condensations by steric modulation of the active-site cavity and providing an illustration for the starter molecule preference of both enzymes.

The reduced 2-PS active site acts as a size-based filter that sterically precludes the bulky *p*-coumaroyl-CoA but allows entrance of the smaller acetyl-CoA into the initiation/elongation cavity. On the other hand, the larger initiation/elongation cavity of CHS allows both binding of different-sized aliphatic and aromatic starter molecules. For example, the CHS active site accepts long aliphatic CoAs like octanoyl-CoA as a starter while smaller CoAs, such as acetyl-CoA fit into the active site but are ineffective starter molecules. The vastness of the CHS active site compared to that of 2-PS grants the acetyl moiety greater conformational flexibility that limits efficient transfer to the catalytic cysteine (Jez et al., 2000). Interestingly, the T197L/G256L/S338I triple mutation in MsCHS2 transformed it into a functional 2PS. These results provided the first structural basis of the effect of the volume and shape of the active site on the functional diversity of type III PKSs (Dana et al., 2006; Abe, 2010).

Remarkably, these three residues are also changed in a number of functionally divergent type III PKSs including pentaketide synthase from *A. arborescens*, PCS (T197M/G256L/S338V), octaketide synthase from *A. arborescens*, OKS (T197G/G256L/S338V) (Abe et al., 2005), and heptaketide synthase from *R. palmatum*, ALS (T197A/G256L/S338T) (Abe et al., 2004). It has been proposed that these inert active site residues control the starter substrate selectivity and polyketide chain length by steric modulation of the initiation/elongation cavity (Abe et al., 2005). Comparison between amino acid residues at position 197 in different PKSs (Fig. 69) reveals that, the more malonyl-CoA units the enzyme adds the smaller the amino acid residue at position 197 tends to be (Ainasoja, 2008).

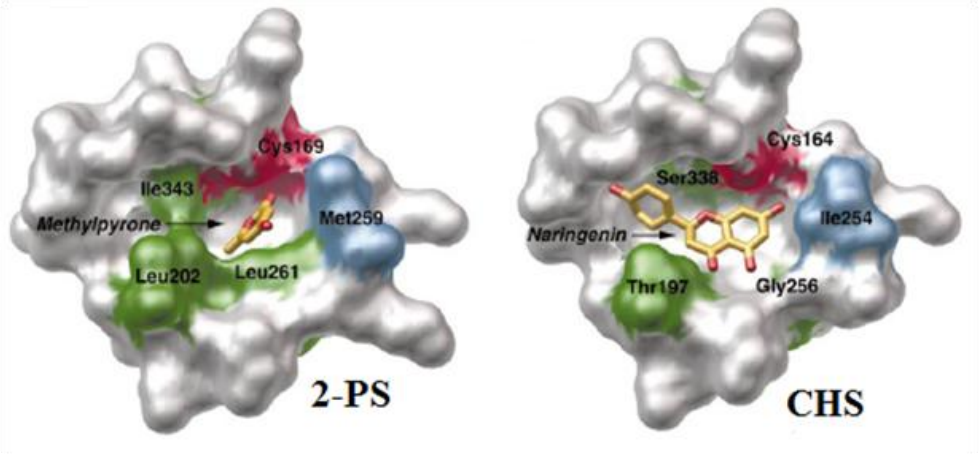

Fig. 68 Comparison of the active site cavities of 2-PS and CHS, the catalytic cysteine (red), the three positions that convert CHS into 2-PS (green) and the substitution which did not affect the product formation (blue) are highlighted modified from; Jez et al., (2000).

Site-directed mutagenesis and X-ray crystallographic studies of AaPCS and AaOKS revealed that the chemically inert single residue 197 determines the polyketide chain length and the product specificity. Replacement of M207 in PCS with glycine transformed PCS into OKS. However, small-to-large substitutions in place of Gly207 in OKS resulted in loss of the octaketide-forming activity and production of shorter chain length polyketides. Structural comparison of AaPCS wild-type and the AaPCSM207G mutant revealed that, the conformations of the residues lining the active-site cavity are almost identical in the mutant but the mutant's active site contains extra new buried pockets which extend into the normal active-site cavity (Fig. 69). This buried pocket was blocked in the wild-type PCS by the presence of the bulky Met207 at its entrance. Replacement of this bulky Met with the small Gly opens a gate to the buried pockets thereby expanding the polyketide elongation cavity.

This is in contrast to the case of 2-PS in which the steric modulation of the active-site cavity by alteration of three chemically inert residues lining the active-site was supposed to play a critical role in controlling starter substrate selectivity and the number of malonyl-CoA condensations (Jez et al., 2000). STS homology models based on the CHS crystal structure showed no significant differences between these two enzymes. Despite of the absence of established clues for a "steric modulation" elucidation for the development of aldol cyclization specificity in STS enzymes, it had been broadly supposed that difference was achieved across folding of the tetraketide intermediate into a different conformation, which leads to aldol condensation. Recently, careful examination of in vitro enzyme reaction products of recombinant *Pueraria lobata* CHS and *Arachis hypogaea* STS revealed that both STS and CHS produce

minor amounts (1–5% of major product yields) of each other's cyclization product in addition to the styrylpyrone side product formation by STS. This cross-reaction between STS and CHS is most likely produced by the conformational flexibility of the active-site of the two enzymes (Yamaguchi et al., 1999).

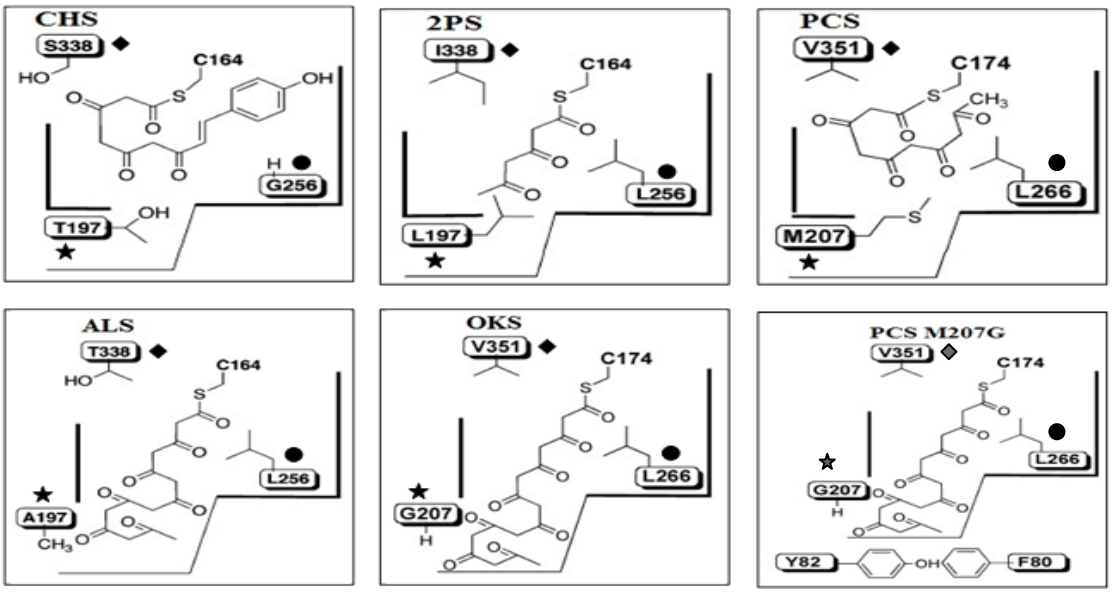

Fig. 69 Schematic representation of the active site architecture of *M. sativa* CHS, *G. hybrid*a 2PS, *A. arborescens* PCS and OKS, *R. palmatum* ALS and *A. arborescens* PCS M207G mutants (numbering in MsCHS). The 'horizontally restricting' G256L substitution controls the starter substrate selectivity, while the 'downward expanding' substitution of T197A (ALS) and T197G (OKS) open a gate to an additional buried pocket that extends into the 'floor' of the active site cavity. On the other hand, the residue T338 (ALS) and V338 (OKS, PCS) located in proximity of the catalytic Cys164 at the 'ceiling' of the active site cavity guides the growing polyketide chain to extend into the buried pocket (Abe et al., 2006).

Crystallographic comparison (of the crystal structures of *P. sylvestris* STS (Austin et al., 2004) and *A. hypogaea* STS (Shomura et al., 2005) with MsCHS2 in addition to structure-guided mutagenic transformation of CHS into STS proved that, STS's different cyclization specificity is occurred by a significant conformational backbone change (Fig. 70). That change occurs on a short buried loop between residues (132 - 136). These residues are located at the dimer interface between the two active sites. This movement is caused by various amino acid substitutions at buried positions adjoining to this loop (significantly the replacement of Val98 with a bulkier side-chain of Met amino acid) and results in a in an altered active site hydrogen-bonding network around the slightly repositioned Thr132 (numbering in MsCHS2). This active site residue (conserved in both CHS and STS) changes its bonding interaction with Glu192 (conserved in all type III PKSs) and based on this change, Thr132 side chain hydroxyl moiety will present within

the hydrogen bonding distance of a water molecule neighboring to the catalytic cysteine. Thr132 in this area is supposed to play a crucial role in balancing competing cyclization specificities in CHS and STS (Austin et al., 2004). whereas Thr132 is a highly conserved in type III PKSs, the positional difference significantly affects the hydrogen bond network around the catalytic Cys164 the so-called ‘‘aldol-switch’’ thioesterase-like electronic hydrogen-bond network involving Ser338-H_2O-Thr132-Glu192 is located adjacent to the catalytic Cys164 in the active-site of STS which is not observed in the structure of CHS (Austin et al., 2004). A three dimensional comparison of the CHS and STS active sites lays doubt upon models that attribute these enzymes cyclization differences to alternative productive conformations of their shared linear tetraketide intermediate achieved by steric differences between the CHS and STS active site cavities. Crystallographic results suggest instead that, those active site changes obviously of an electronic rather than steric nature, favor an alternative cyclization mechanism within the context of a quite similarly folded tetraketide intermediate. This latter model is also consistent with the previously observed cross-reactivity of CHS and STS (Yamaguchi et al., 1999; Austin and Noel, 2003; Abe, 2010).

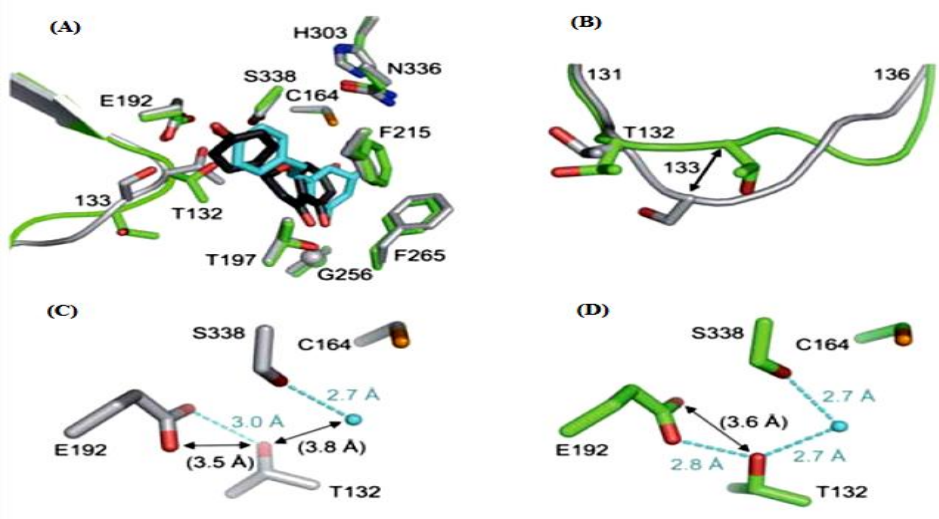

Fig. 70 Active site of *M. sativa* CHS2 (silver) and *P. sylvestris* STS (green). Naringenin and resveratrol complexed with *M. sativa* CHS2 are shown in black and sky-blue respectively. Resveratrol in structure of a CHS mutant which is a functional mutant having the STS activity, is superimposed in A: to demonstrate that the products of both enzymes are attached in an almost identical position. B: Close-up look of the loops between 131–136 in STS and CHS. Close-up look of the hydrogen bond networks in C: CHS and D: STS. The hydrogen bonds and their distances are indicated with parentheses. The putative nucleophilic water molecule in STS and in CHS2 is shown by blue spheres (Abe, 2010).

5.3 Type III PKSs which accepts benzoyl-CoA substrate

In comparison to CHS and STS which both use *p*-coumaroyl-CoA as the starter substrate, PKSs that use benzoyl-CoA as a starter unit is less well studied at the structural and mutational levels. Benzoyl-CoA-derived polyketides such as biphenyls and benzophenones which are the phytoalexins of the Maloideae (apple and pear) and Hypericaceae (St. John's wort) are synthesized by biphenyl synthase (BIS) and benzophenone synthase (BPS) respectively. BIS and BPS are two members of the non-chalcone forming plant type III PKSs. They accept and prefer benzoyl-CoA as a starter substrate, form the same linear tetraketide intermediate after three malonyl-CoA condensations however, catalyze either intramolecular C6→C1 Claisen condensation (BPS) to give 2,4,6-trihydroxybenzophenone or intramolecular C2→C7 aldol condensation followed by decarboxylative elimination of the terminal carboxyl group (BIS) to produce 3,5-dihydroxybiphenyl (Fig. 71) (Liu et al., 2003; Liu et al., 2010).

In addition to benzoyl-CoA as starter these two enzymes also accept 3-hydroxybenzoyl-CoA forming 6-(3-hydroxy-phenyl)-4-hydroxy-2-pyrone after two condensations with malony-CoA in case of BIS while BPS forms 2,3',4,6-tetrahydroxybenzophenone after three malonyl-CoA extensions (Fig. 71). Interestingly, BIS also accepts 2-hydroxybenzoyl-CoA as a substrate and forms 4-hydroxycoumarin after single malonyl-CoA extension while neither HaBPS nor its mutants showed any activity with that substrate (Klundt et al., 2009; Liu et al., 2010). Since recently, GmBPS and HsBPS (Huang et al., 2012; Nualkaew et al., 2012) are the only reported BPSs that accept salicoyl-CoA and form small amounts of 4-hydroxycoumarin. BIS and BPS were first cloned from cell cultures of *S. aucuparia* and *H. androsaemum* respectively. They share 54% amino acid sequence identity (Liu et al., 2003; Liu et al., 2007; Beerhues and Liu, 2009). Using site-directed mutagenesis (Klundt et al., 2009) constructed a large number of mutants based on the amino acids sequence comparison between HaBPS and different members of type III PKSs aiming to transform HaBPS into another polyketide synthase, like CHS, ACS and BAS but all of these trials were not successful. HaT135L is the only mutant that was able to drastically change the substrate and product specificities of HaBPS wild-type and transformed it into a functional phenylpyrone synthase (PPS). PPS was a new PKS variant that was not yet known as a naturally occurring enzyme function. Remarkably, the trials to replace Leu135 with other amino acids like isoleucine and alanine resulted in catalytically inactive proteins (Klundt et al., 2009). Thus, the position 135 in BPS turned out to be highly interesting and based on the above findings provoked the idea of screening different amino acids in this position. In the

current study all of the BPSs which were cloned from selected *Hypericum* species maintained the same amino acid residues along the active site cavity especially Thr135 (numbering from HsBPS) which is also conserved in most of the plant type III PKSs (Tab. 19). In RpBAS, the corresponding residue Thr132 is located within a loop region at the entrance of the coumaroyl binding pocket and the flexibility of this loop was supposed to be essential also for the activity of this enzyme (Shimokawa et al., 2010).

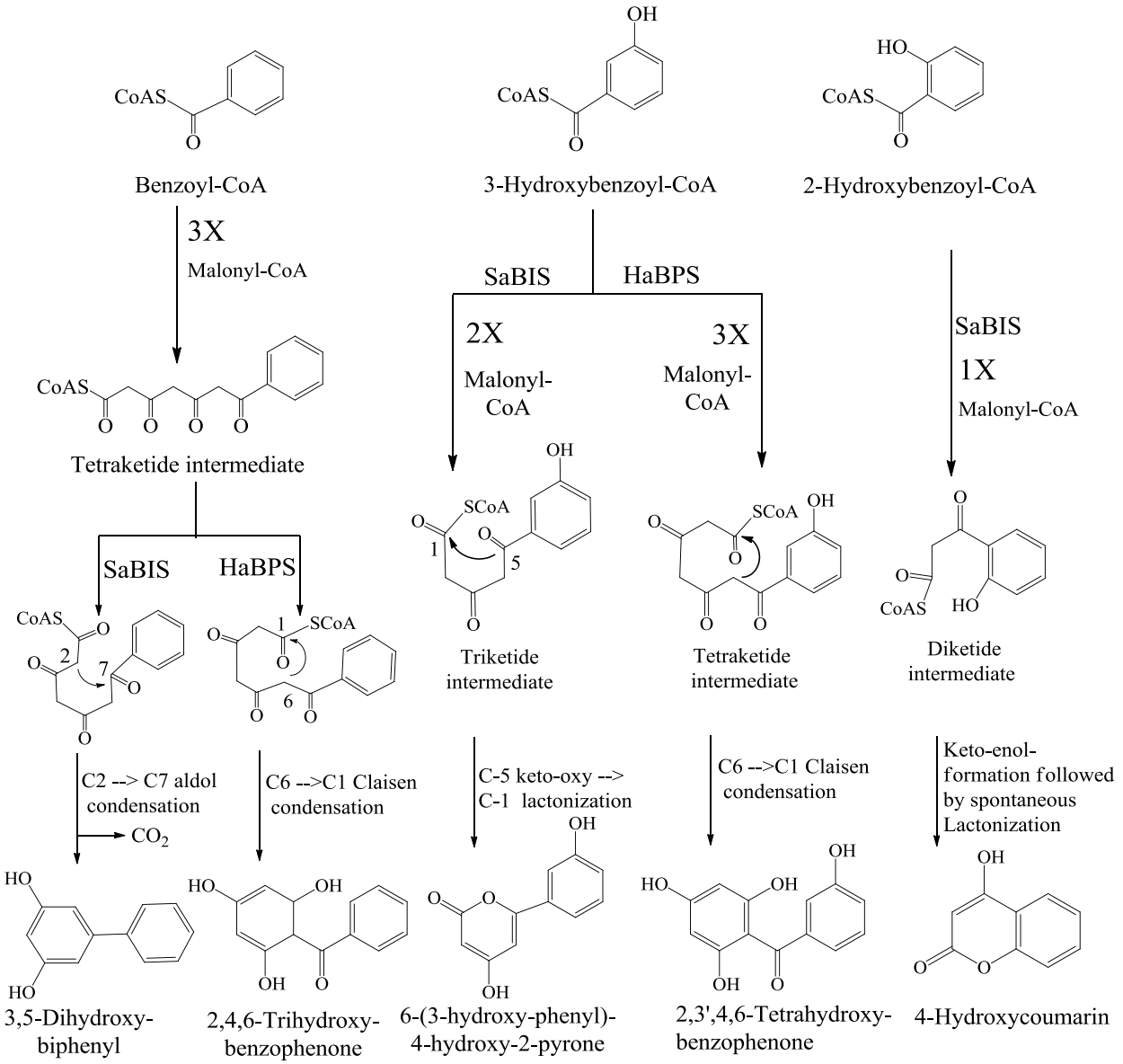

Fig. 71 Reactions of BIS and BPS wild-type enzymes with different substrates.

5.4 *H. sampsonii* benzophenone synthase T135K mutant

Our challenge was to find out if there is any other amino acid that will be able to play the same role like leucine in this critical position or results in a new activity added to the wealth of

type III PKSs activities. Screening of the effects of the other 19 amino acids in position 135 of *H. sampsonii* BPS wild-type revealed that, only the HsT135K mutant, in which Thr was exchanged with Lys, dramatically changed the substrate and the product specificities transforming *H. sampsonii* BPS wild-type (HsBPS) into a functional 4-hydroxycoumarine synthase (HCS). Again, HCS is a new type III PKS variant that has not yet been detected in nature. The main and preferred starter substrate for the interesting enzyme mutant was 2-hydroxybenzoyl (salicoyl)-CoA rather than benzoyl-CoA. Furthermore, the HsT135K mutant catalyzed only a single decarboxylative condensation with malonyl-CoA to form a linear diketide intermediate which then undergoes intramolecular cyclization by nucleophilic attack of the phenol group on the -CoA or cysteine-tethered C1 thioester followed by enolization, spontaneous lactonization and 4-hydroxycoumarin formation. So far, salicoyl-CoA has only been observed as a minor substrate for BPSs from *Garcinia mangostana* and *H. sampsonii*. Interestingly, these results illustrate that a single amino acid substitution in HsBPS impressively shifts the molecular selectivity of this enzyme, resulting in a novel PKS activity and further expansion of the biosynthetic repertoire of the type III PKS superfamily. This novel PKS activity reflects another step toward the modification of the biosynthetic activities of this group of enzymes and confirms their capability in creating a wide range of compounds.

The HsT135K assays contained only 4-hydroxycoumarin and no substituted benzophenone derivative when started with salicoyl-CoA as a starter substrate. We had expected that the HsT135K mutant might also catalyze three malonyl-CoA condensations resulting in formation of an *ortho*-substituted benzophenone which undergoes water elimination, yielding 1,3-dihydroxyxanthone. For comparison, 2'-*O*-ß-D-glucopyranosyl-2,4,5',6-tetrahydroxybenzophenone (hypericophenonoside) was isolated from an *H. annulatum* methanolic extract and subjected to mild acid hydrolysis for sugar release which converted the resulting aglycone spontaneously into 1,3,7 trihydroxyxanthone (Fig. 72). Hypericophenonoside is considered as the second benzophenone-*O*-glycoside found in nature after the previous detection of 2,4',6-trihydroxy-4-methoxybenzophenone-2-*O*-glucoside. Isolation of these compounds supports the hypothesis that some xanthones might be formed in plants by dehydration of 2,2'-dihydroxybenzophenones and the intermediate precursors appear to be benzophenone *O*-glycosides *ortho* to the carbonyl function (Ferrari et al., 2000; Kitanov and Nedialkov, 2001).

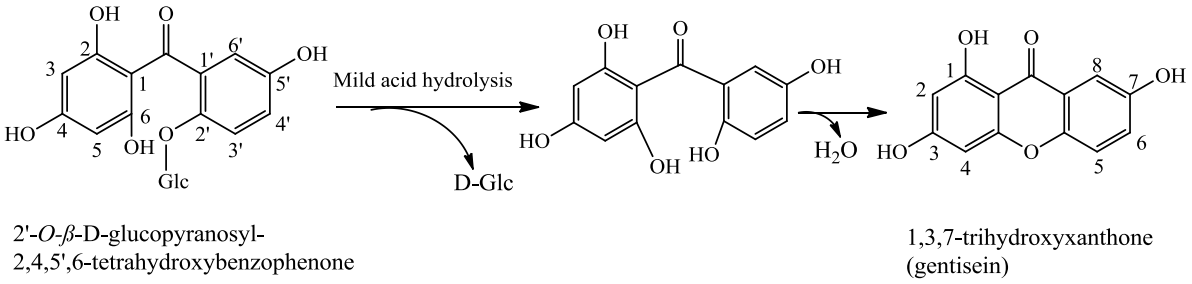

Fig. 72 Hydrolysis and cyclization reactions of 2'-glycosylated benzophenones (Kitanov and Nedialkov, 2001).

A comparable case happened in case of SaBISs which also formed only 4-hydroxycoumarin after a single malonyl-CoA condensation reaction and no *ortho*-substituted biphenyl was detected in the enzymatic reaction. The exclusive 4-hydroxycoumarin formation indicates that the hydroxyl group in the *ortho* position of salicoyl-CoA favors the early intramolecular cyclization and hinders further condensations with other malonyl-CoA molecules (Lin et al., 2013).

The steady state kinetic analysis was carried out to determine the quantitative effect of the introduction of lysine in position 135. The results revealed that the HsT135K mutant showed a K_m = 43.92 µM and a K_{cat} = 1.181 sec^{-1} for salicoyl-CoA (Tab. 16). On the other hand the previously reported 4-hydroxycoumarin forming SaBIS2 and SaBIS3 exhibited K_m values of 2.3 and 3.2 µM and K_{cat} values of 0.0293 and 0.037 sec^{-1}, respectively (Tab. 16) (Liu et al., 2010). It is obvious that the affinity of HsT135K for salicoyl-CoA was 19- and 14-fold lower than that of SaBIS2 and BIS3 however, the mutant showed 40- and 32-fold higher turnover rates compared to the BISs respectively. Finally, a 2-fold higher catalytic efficiency (K_{cat}/K_m) resulted for the HsT135K mutant compared to SaBIS2 and SaBIS3. These results indicate that the single amino acid substitution in the active site cavity of HsBPS mainly affects the catalytic process more than the substrate binding. Notably, the K_m for malonyl-CoA of the HsT135K mutant equals 747 µM which is around 8 fold higher than that of the HsBPS wild-type enzyme (92.5 µM) (Huang et al., 2012). Remarkably, HsBPS wild-type showed the highest malonyl-CoA K_m value compared to other wild-type BPSs e.g. from *H. androsaemum* (K_m 31.3 µM) and *G. mangostana* (K_m 16.38 µM) which on the other side points to subtle differences in the active site structures between BPSs from different *Hypericum* and Clusiaceae species.

Tab. 16 Steady state kinetic values for salicoyl-CoA substrate for HsT135K mutant compared to SaBIS2 and SaBIS3 (Liu et al., 2010)

Enzyme	K_m **µM**	K_{cat} **sec^{-1}**	K_{cat}/K_m **sec^{-1} M^{-1}**
HsT135K	43.92	1.181	26889
SaBIS2	2.3	0.0293	12716
SaBIS3	3.2	0.037	11486

Analogous situations were documented in two cases, a point mutation in position F215 in *Scutellaria baicalensis* CHS (SbCHS) (Abe et al., 2003) and site-directed mutagenesis in *M. sativa* CHS (MsCHS) in position G256 (Jez et al., 2001). Concerning SbCHS point mutations in position F215 (F215W, F215Y, F215S, F215A, F215H and F215C) were constructed and tested for the resulting enzyme activities. When these mutations were compared to the former mutation studies done by (Jez et al., 2000) in the same position of MsCHS many differences in the activities of the mutants resulted. That indicates the presence of different active site structures in each species. For example, MsCHS F215W, F215Y and F215S mutations led to formation of increased levels of derailment products. Also the MsF215S mutant accepted non-physiological *N*-methylanthraniloyl-CoA as a starter to produce an unnatural tetraketide pyrone (Jez et al., 2002) while in SbCHS, the point mutations considerably decreased chalcone formation and modified functional behavior of the enzyme to various levels. Interestingly, the steady state kinetic results of the SbCHS mutants showed a great variation especially in the affinity of the enzyme mutants to the starter and extender substrates. Such as SbF215A, SbF215Y, SbF215C, and SbF215S which showed 6.6, 35.6, 13 and 10.7 µM *p*-coumaroyl-CoA K_m values respectively and 1099, 386, 247 and 117 µM malonyl-CoA K_m values respectively when compared to the wild-type SbCHS with 5.8 and 25.5 µM K_m values for *p*-coumaroyl-CoA and malonyl-CoA respectively.

Tab. 17 *Scutellaria baicalensis* CHS mutants and their *p*-coumaroyl-CoA and malonyl-CoA K_m values (Abe et al., 2003)

Enzyme	***p*-coumaroyl-CoA K_m (µM)**	**Malonyl-CoA K_m (µM)**
SbCHS	5.8	25.5
SbF215A	6.6	1099
SbF215Y	35.6	386
SbF215C	13	247
SbF215S	10.7	117

Those experiments led to 9 - 209-fold decrease in K_{cat}/K_m values for *p*-coumaroyl-CoA and 7 - 2815-fold decreases in K_{cat}/K_m values for malonyl-CoA compared with wild-type CHS (Tab. 17). The previous findings confirm the direct effect of point mutations on the catalytic efficiency of the enzyme with pronounced effect on malonyl-CoA. On the other hand, it was notable that the SbF215Y mutation resulted in almost complete loss of enzyme activity. In contrast, the MsF215Y mutant still saved chalcone-forming activity proposing delicate species-difference of the active site structures between *S. baicalensis* and *M. sativa* (Jez et al., 2000; Abe et al., 2003). In MsCHS, replacement of Gly256 with valine resulted in 3 and 8 fold reduction in the K_{cat} values for *p*-coumaroyl-CoA and malonyl-CoA respectively. The MsG256L and MsG256F mutants showed the greatest variations in the steady-state kinetic parameters. The G256L mutant exhibited 75 and 9 fold decrease in the catalytic efficiency (K_{cat}/K_m) with malonyl-CoA and *p*-coumaroyl-CoA respectively. Replacement of Gly256 with phenylalanine also decreased the catalytic efficiencies with *p*-coumaroyl-CoA and malonyl-CoA by 14 and 47 fold respectively. These kinetic results illustrate that introduction of residues with bulky side chains at position 256 reduces the catalytic efficiency of each mutant enzyme compared to wild-type MsCHS and even the greatest effect was observed for malonyl-CoA (Jez et al., 2001). Ultimately, the right and correct position of substrates at the active site allows the 'catalytic' residues to perform their maximal effect thereby connecting the assistance of binding interactions to catalysis. Therefore, it is tempting to speculate that with active site conformational changes due to introduced mutations for amino acids lining the active site malonyl-CoA may sample a range of conformations at the active site only some of which allow the right interaction with the catalytic residues and so lead to a successful decarboxylation reaction to take place (Jez et al., 2000).

5.4.1 Biosynthesis and anticoagulant activity of 4-hydroxycoumarins

The biosynthesis of 4-hydroxycoumarin is usually related to the effect of molds on *trans*-2-coumaric acid-containing plants such as sweet clover (*Melilotus albus*, Fabaceae). *Trans*-2-coumaric acid is stored as *O*-glucoside and hydrated after sugar release to yield 3-hydroxymelilotic acid which then dehydrogenates to yield 3-oxomelilotic acid (Bye and King, 1970). These acids are found as their -CoA thioesters. Spontaneous lactonization of 3-oxomelilotic acid takes place to produce 4-hydroxycoumarin (Fig. 73). In the presence of formaldehyde produced from microbial degradation two molecules of 4-hydroxycoumarin can form dicoumarol none-enzymatically. Dicoumarol is a natural anticoagulant and acted as a

precursor for the synthetic anticoagulants such as warfarin, acenocoumarol and phenprocoumon (Fig. 74). Notably, some plant species such as *Ferula communis* (Apiaceae) contain 4-hydroxycoumarin derivatives such as ferulenol (Fig. 74) without the molds fermentation effect. Ferulosis is a disease that results from ingestion of ferula plant. It causes hemorrhagic symptoms similar to those caused by sweet clover. Up to date the ferulenol biosynthetic pathway still unclear. Interestingly, precursor-feeding experiments in *Gerbera jamesonii* (Asteraceae) indicated that 4-hydroxy-5-methylcoumarin is synthesized via a pentaketide which is derived from one acetate and four malonates which strongly suggest the involvement of a type III PKS in its formation. (Inoue et al., 1989; Schröder, 2009; Liu et al., 2010).

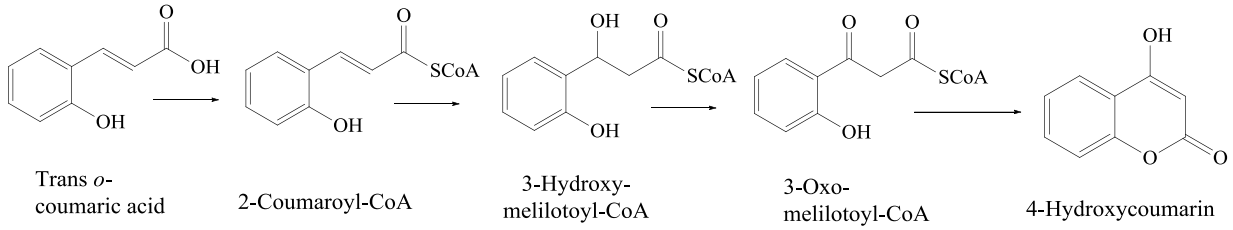

Fig. 73 Proposed biosynthetic pathway of 4-hydroxycoumarin by molds.

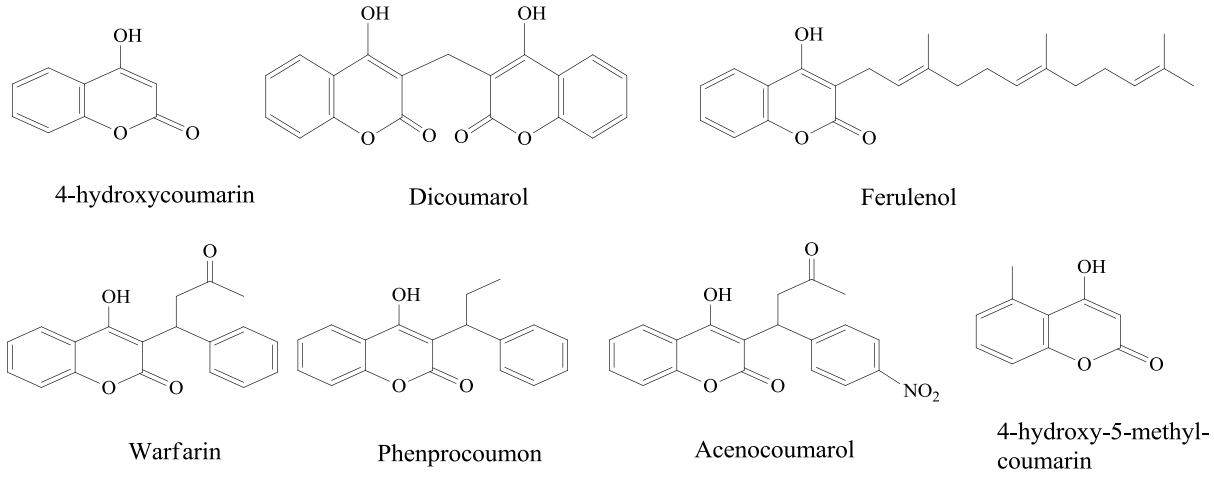

Fig. 74 Structures of 4-hydroxycoumarin and some of its clinically used anticoagulant derivatives.

Interesting are the biosynthesis models of 4-hydroxy-5-methylcoumarin proposed by (Schröder, 2009) especially the second one. In the first model he suggested that the biosynthesis of 4-hydroxy-5-methylcoumarin occurs via a pentaketide intermediate (Fig. 75, A) after a reduction step that results in the elimination of one of the oxygen functions during aromatization of the molecule. This reduction step is very fundamental to get the right product otherwise the derailment products will formed. The second model (Fig. 75, B) proposed that 4-hydroxy-5-methylcoumarin may be synthesized by two reactions, the first reaction includes three

condensations followed by the reduction step which results in the formation of 6-methylsalicylate. This reaction is not known from plants but also well-known from fungi by a type I PKS rather than a type III PKS (Dimroth et al., 1970).

The second reaction would utilize 6-methylsalicoyl-CoA as substrate and perform only one condensation followed by the ring-closure to the pyrone ring of the 4-hydroxy-5-methylcoumarin. The author supposed that the second step of this reaction requires a type III PKS which showed high activity with salicoyl-CoA and catalyzes a single malonyl-CoA extension to form 4-hydroxycoumarin and so this enzyme should accept 6-methylsalicoyl-CoA leading to formation of 4-hydroxy-5-methylcoumarin. It is a fascinating idea that a type III PKS might be involved in the biosynthesis of 4-hydroxy-5-methylcoumarin (Schröder, 2009).

In the current study we have transformed a BPS into a 4-hydroxycoumarin synthase for which salicoyl-CoA is the best substrate. Therefore, it will be promising to figure out the activity of the HsT135K mutant with 6-methylsalicoyl-CoA as a substrate. In fact we synthesized and offered 2-methoxybenzoyl-NAC and 2-mercaptobenzoyl-NAC aiming to get methoxylated benzophenones or thiocoumarins respectively but unfortunately these precursors were accepted by neither the HaT135K mutant nor the wild-type BPS enzyme. HsT135K mutant also did not accept salicoyl-NAC. while HsBPS wild efficiently converted salicoyl and benzoyl-NACs to 4-hydroxycoumarin and trihydroxybenzophenone respectively.

Coumarins involve a huge array of biologically active compounds which have been used in traditional medicine for many years. They constitute a significant category of compounds with numerous pharmacological activities like anticancer, anti-HIV, anticoagulant, spasmolytic, antibacterial and antifungal activities. Antioxidant and antiproliferative activities are the most important and intensively investigated of the numerous coumarin activities (Kostova, 2005; Arif et al., 2009; Schröder, 2009; Kinza Aslam et al., 2010). Recently, a lot of light was shed on coumarins as they show a wide range of effects on tumors. Intensive work is going on to explore the role of these compounds in the treatment of cancer. Several studies revealed that coumarins stimulate the inhibitory effects on cell growth of various carcinoma cell lines and may be potential candidates for cancer therapy (Kostova, 2007). 4-Hydroxycoumarin (4HC) is the precursor of the anticoagulant dicoumarol and the model for the synthesis of warfarin (Fig. 74). The latter is one of the most prescribed oral anticoagulants worldwide and is the best choice for the long-term therapy and prevention of thromboembolic diseases such as deep vein thrombosis.

Warfarin was a top 20 drug by prescription volume in the United States and had a global market value of $300 million in 2008. In Europe the most commonly used oral anticoagulants

are acenocoumarol and phenprocoumon. They share the 4HC skeleton but differ in 3-substitution on the pyrone ring. They can be chemically synthesized using 4-hydroxycoumarin as a direct precursor (Rost et al., 2004; Nicholas and Rettie, 2008; Lin et al., 2013). 4-Hydroxycoumarin derivatives can interfere with blood clotting due to the strong structural similarity of their 4-hydroxycoumarin core to that of vitamin K. Any chemical modulations of the strictly conserved enolic 4-hydroxy group abolish the ability of these drugs to act as inhibitors of VKOR activity (Nicholas and Rettie, 2008). VKOR is a vitamin K epoxide reductase which converts vitamin K 2,3-epoxide to vitamin K which is reduced to vitamin K hydroquinone which is an essential cofactor for posttranslational γ-carboxylation of several blood coagulation factors, such as II (prothrombin) VII, IX and X (Rost et al., 2004) (Fig. 76).

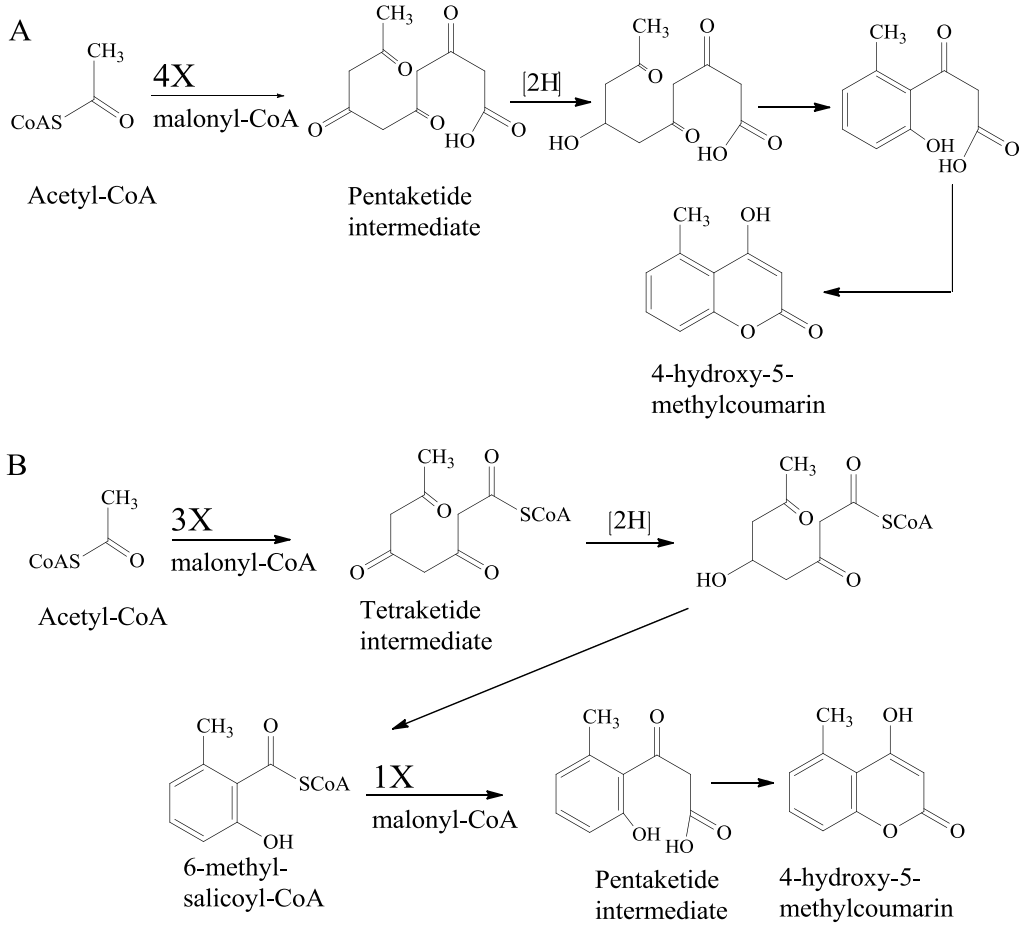

Fig. 75 Models for 4-hydroxyl-5-methylcoumarin biosynthesis A: Biosynthesis via one reaction pentaketide, B: biosynthesis by two reactions modified from; Schröder, (2009).

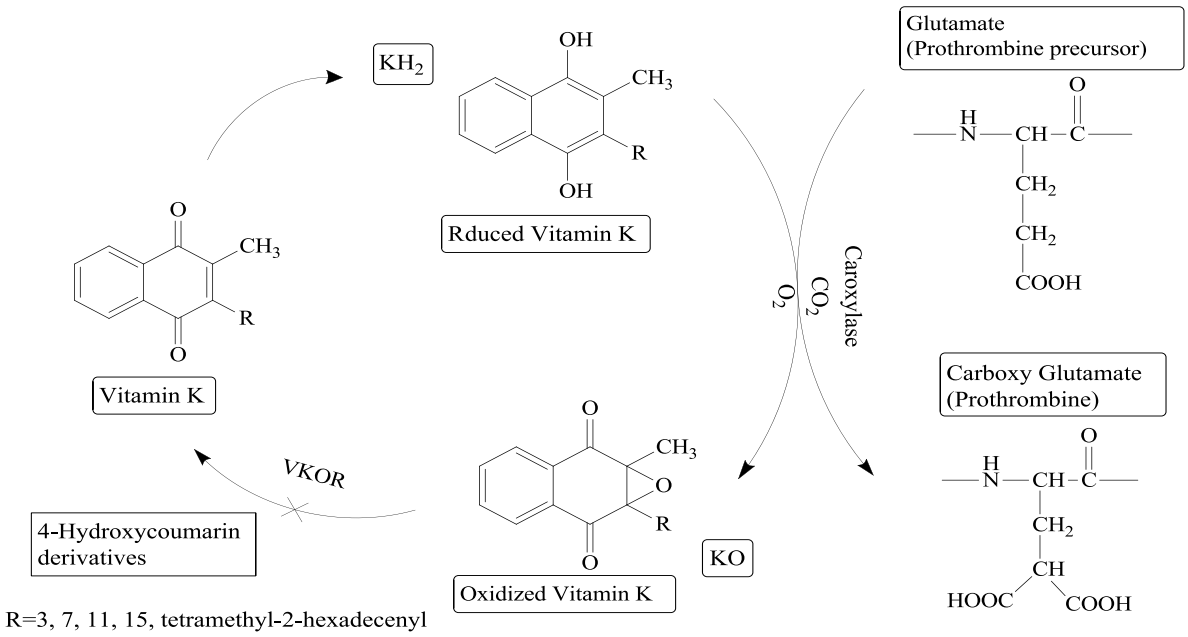

Fig. 76 Mechanism of 4-hydroxycoumarin derivatives such as warfarin as oral anticoagulants modified from; Bhonoah, (2006).

5.4.2 *H.androsaemum* benzophenone synthase T135K single and double mutations

Interestingly, replacement of threonine in position 135 with lysine in the BPS of *H. androsaemum* (HaBPS) was also successful and completely changed the substrate and product specificities of HaBPS wild-type. The new mutant prefers salicoyl-CoA as a substrate catalyzing 4HC formation but with much lower activity compared to the HsT135K variant. Many trials were done to improve the activity of the HaT135K single mutant. The only successful trial was the double mutation including position 135 with other different positions between HaBPS and HsBPS (HaE54D/T135K, HaV146A/T135K, HaC230G/T135K, HaS235A/T135K and HaV359L/T135K), except for position 360, which showed no over-expression in the host cells (Fig. 95, D). These results suggest the difference in the active site architecture between these two *Hypericum* BPSs (HaBPS and HsBPS). Determination of the steady state kinetic characters was calculated for one of these *H. androsaemum* lysine double mutants. The target was to find a mutant which is highly active with salicoyl-CoA and at the same time has a high affinity for malonyl-CoA. The HaV146A/T135K double mutant was selected due to its high activity with salicoyl-CoA. Unfourtionatly, its catalytic effeciency (K_{cat}/K_m) was 4-fold lower than that of the HsT135K single mutant in addition to a 1.3-fold higher malony-CoA K_m value compared to HsT135K mutant. Interestingly, carrying out the same mutation in the same position with two

other *Hypericum* species (HcBPS and HpaBPS) resulted in no over-expression in the host cells in case of HpaT135K mutant and the absence of soluble protein in case of HcT135K mutant as shown by SDS-PAGE analysis of these two mutants (Fig. 104, D and 101 D) respectively. These data propose minor species differences of the active site conformations between different *Hypericum* BPSs despite having the same amino acids lining the active site cavity.

5.5 Effect of Leu and Ile instead of Thr135 in BPSs from different *Hypericum* species

Leucine and isoleucine are another two amino acids that dramatically changed the substrate and product specificities of HsBPS. The replacement of Thr135 in HsBPS with Leu or Ile transformed HsBPS wild-type into phenylpyrone synthase (PPS). Leucine is the only amino acid which results in a dramatically different variant of HaBPS wild type. The functional behavior of the HaT135L mutant was rationalized by using homology modeling based on the crystal structure of chalcone synthase. HaBPS wild-type and the HaT135L mutant catalyze different reaction mechanisms which result in formation of different products (Fig. 77). The modeling explains the difference between them at the diketide and the triketide stages. Up to the diketide stage (Fig. 78) both HaBPS wild-type and the HaT135L mutant do not exhibit dissimilarities in the active site cavities which contain the reaction intermediates. However, at the triketide stage (Fig. 79) there were drastic changes in the guidance and the conformation of the polyketide intermediate. Structural differences in the active sites of wild-type HaBPS and the HaT135L mutant resulted in a change in the product specificity. The phenyl ring from benzoyl-CoA in HaBPS wild-type projects into the elongation cavity where the acetyl moieties resulting from malonyl-CoA decarboxylation are added. This elongation cavity is open because of hydrogen bond formation between the hydroxyl group of Thr135 and the backbone amides of Gln165 and Gly166. In contrast, in the HaBPST135L mutant, leucine projects into the entrance space of the elongation cavity leading to steric hindrance. In addition, the absence of the hydroxyl group which was found in the polar Thr the hydrogen bonding with Gln165 and Gly166 was removed resulting in the formation of a new pocket. Favorable hydrophobic interactions between the lipophilic Leu135 side chain and the benzene ring of benzoyl-CoA result in a new orientation of substrate binding and elongation in the T135L mutant (Baker and Seah, 2012). The catalytic efficiency (K_{cat}/K_m) for the mutant was nearly unchanged compared to the wild-type enzyme as an 8-fold K_{cat} decrease was offset by an 8-fold K_m refinement.

When 3-hydroxybenzoyl-CoA is used as the starter substrate the HaBPS wild-type enzyme catalyzed condensations with three malonyl-CoAs to give a linear tetraketide intermediate which cyclized into 2,3',4,6-tetrahydroxybenzophenone. However, the HaT135L mutant was nearly inactive with 3-hydroxybenzoyl CoA as a starter substrate as the 3-hydroxyl group of the aroyl moiety of the triketide intermediate resides in the position that is occupied in the wild-type enzyme by the hydroxyl group of the Thr135 side chain. Consequently, the 3-hydroxyl group of the triketide now forms hydrogen bonds with the backbone carbonyl and amide groups of Gly166. Thus, the 3-hydroxybenzoyl-primed triketide may be trapped in the new pocket of the active site cavity of the T135L mutant. It acts as an inhibitor explaining why the mutant enzyme is almost inactive with 3-hydroxybenzoyl-CoA as a starter substrate. Thus, the T135L substitution changes both the substrate and the product specificity of BPS (Klundt et al., 2009; Baker and Seah, 2012).

The HsT135I and HsT135L mutants showed some deviation from the previous postulations based on the constructed model for HaBPS wild-type and its mutant. 1- Ile in position 135 in case of HaBPS gave catalytically inactive protein while it transformed HsBPS into PPS. As mentioned before, Ile is the amino acid occupying position 135 in the natural phenylpyrone synthase cloned recently in our group (Gaid, unpublished results). 2- These two mutants (HsT135I and HsT135L) prefer benzoyl-CoA as a starter substrate catalyzing two malonyl-CoA extensions and result in the formation of 6-phenyl-4-hydroxy-2-pyrone. 3-Hydroxybenzoyl-CoA is the second best substrate for these two mutants as they form 6-(3-hydroxyphenyl)-4-hydroxy-2-pyrone as a single product after two malonyl-CoA extensions. Notably, this substrate was a poor starter substrate for HaT135L mutant due to blocking the new pocket by the 3-hydroxybenzoyl-primed triketide intermediate which acts as inhibitor preventing further product formation (Fig. 79) (Klundt et al., 2009). 3- HsT135I and HsT135L mutants showed around 17 and 9% activity respectively, with salicoyl-CoA forming 4-hydroxycoumarin. 4- These two mutants also accept anthraniloyl- and *N*-methylanthraniloyl-CoAs and form 4-hydroxy-2(1*H*)-quinolone and 4-hydroxy-1-methyl-2(1*H*)-quinolone respectively.

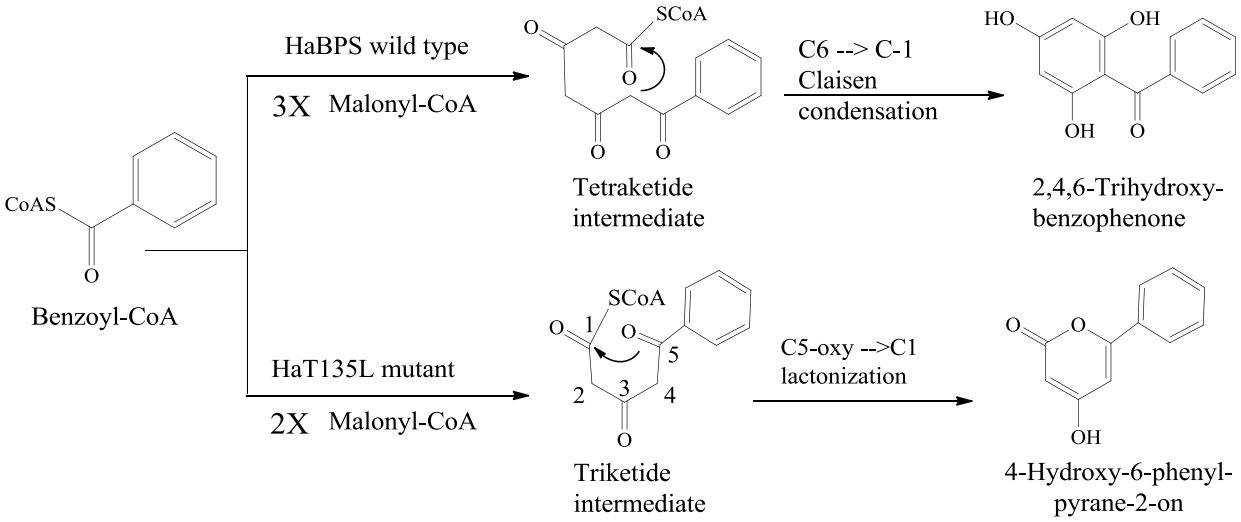

Fig. 77 Reaction mechanisms of *H. androsaemum* BPS wild-type and the HaT135L mutant. The active site structure differences between HaBPS wild-type and HaT135L mutant result in altered product specificities.

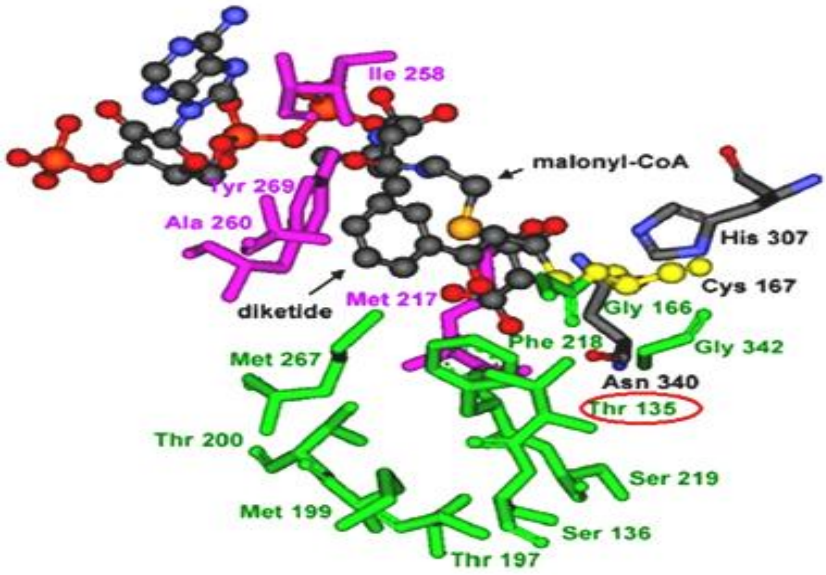

Fig. 78 CHS-based homology model of the HaBPS active site cavity complexed with both the benzoyl-primed diketide that is covalently bound to the catalytic cysteine 167 and malonyl-CoA that is used for the next chain elongation reaction. Amino acids of the initiation and elongation pockets are highlighted in pink and green, respectively. The catalytic triad is displayed in yellow (Cys167) and gray (His307 and Asn340) modified from; Klundt et al., (2009).

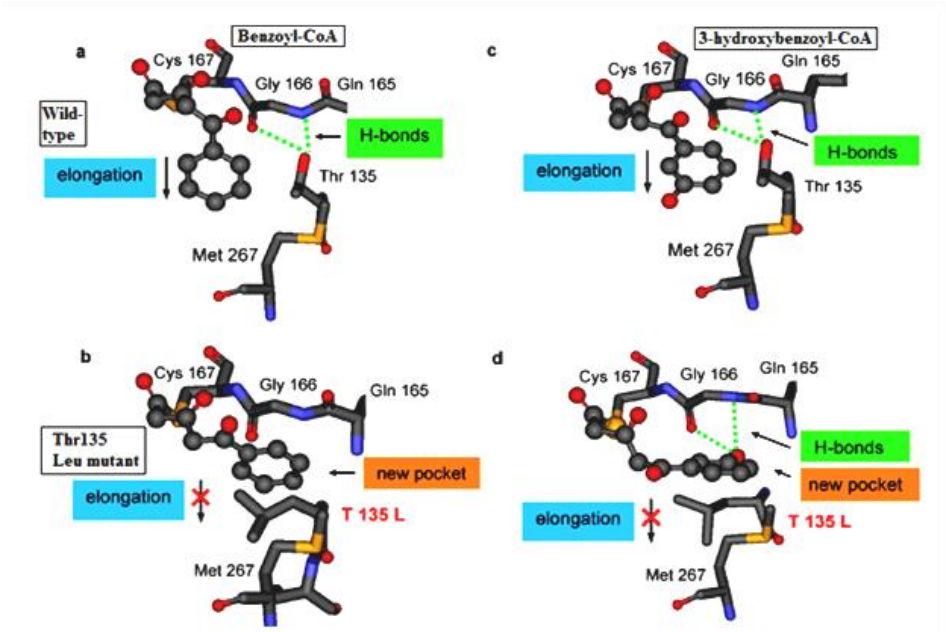

Fig. 79 CHS-based homology models of the active site cavities of wild-type HaBPS (a and c) and the HaT135L mutant (b, d). The benzoyl-primed (a, b) and 3-hydroxybenzoyl-primed triketides (c and d) are covalently attached to the catalytic cysteine 167. The wild-type enzyme catalyzes another acetyl addition to the intermediate triketides. In the mutant enzyme, however, the triketides may be redirected into a new pocket where no further chain elongation takes place (Klundt et al., 2009).

5.6 Anthraniloyl and *N*-methylanthraniloyl-CoAs substrates

Remarkably, HsBPS wild type showed around 7 and 12% activities with anthraniloyl and *N*-methylanthraniloyl-CoAs respectively. While the three mutants (HsT135K, Hst135I and HsT135L) showed 15, 20 and 43% activities with anthraniloyl-CoA and 6, 5, and 8% activities with *N*-methylanthraniloyl-CoA respectively. These findings are differing from *R. palmatum* benzalacetone synthase (RpBAS) and *Aegle marmelos* quinolone synthase (AmQNS) which showed highest activity with *N*-methylanthraniloyl-CoA (Abe et al., 2006; Resmi et al., 2013). RpBAS is a diketide-producing PKS and can efficiently catalyze condensation of *N*-methylanthraniloyl-CoA (or anthraniloyl-CoA) with malonyl-CoA (or methylmalonyl-CoA) to produce 4-hydroxy-2(1*H*)-quinolone and the activity with *N*-methylanthraniloyl-CoA and anthraniloyl-CoA was 80% and 4% respectively (Abe et al., 2006). AmQNS accepts different starter substrates forming triketide and tetraketide lactones while *N*-methylanthraniloyl-CoA is the best substrate for this new type III PKSs member (Resmi et al., 2013). Transformation of AmQNS to CHS was carried out by (Resmi et al., 2013) *via* two amino acid substitutions S132T/A133S (numbering from MsCHS). It will be interesting to transform HsBPS into QNS especially since we already have HsT135S as a single mutant. Ultimately, leucine is present

naturally in RpBAS in position 132 (numbering from MsCHS). Notably, this active-site residue (Leu132) is located at the entrance of the coumaroyl binding pocket and it was supposed that it also plays a crucial role in the benzalacetone forming activity besides Ile214/Leu215 residues which are located at the junction between the active-site cavity and the CoA binding tunnel.

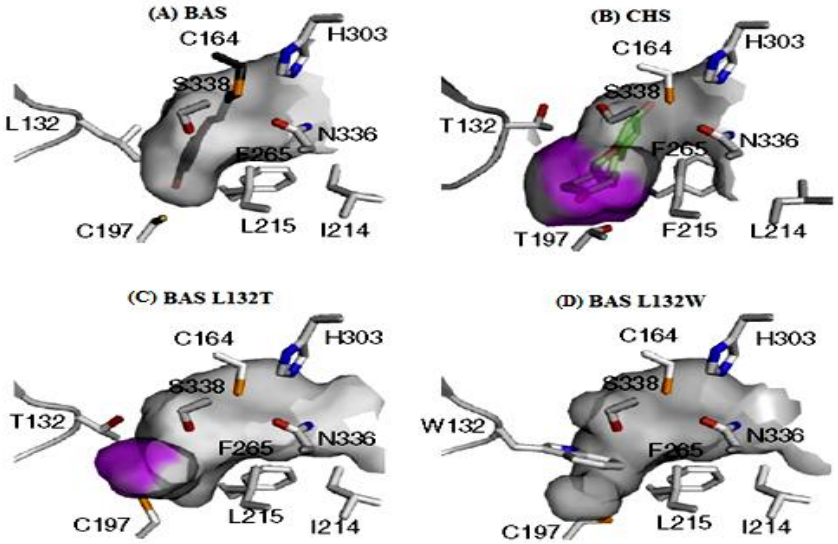

Fig. 80 Active-site architecture comparisons of RpBAS A: wild-type, B: MsCHS, C: L132T and D: L132W mutants. Surface models illustrate the active sites. The coumarate that covalently binds to the active site Cys in BAS and the naringenin molecules are shown as black and green stick models respectively. The bottoms of the 'coumaroyl binding pocket' are highlighted in purple modified from; Shimokawa et al., (2010).

The distinctive substitution of Thr132 (numbering in MsCHS2), which is highly conserved in most type III PKSs, with Leu causes steric contraction of the BAS active-site to form the diketide instead of the tetraketide intermediate. Only replacement of L132 with Thr (like MsCHS) restored the chalcone-forming activity in RpBAS. The homology models predicted that the L132T mutant restored the coumaroyl binding pocket in the active-site cavity (Fig. 80). It was previously proposed that Thr132 in CHS forms a hydrogen bond with the neighboring Glu192 and is thought to control the folding of the tetraketide intermediate so that the Claisen-type cyclization results in chalcone formation (Austin et al., 2004). These observations suggest that the L132T substitution in RpBAS opens a gate to the buried coumaroyl-binding pocket thereby increasing the polyketide chain elongation by up to three condensations with malonyl-CoA and leading to the formation of chalcone (Shimokawa et al., 2010). Natural phenylpyrone derivatives were isolated from some *Aloe* species (Rebecca et al., 2003; Durì et al., 2004). Previously, psilotinin that is 4'-hydroxylated phenylpyrone was found in

Psilotum nudum (Whisk fern) which is the most primitive vascular plant (Mclnnes et al., 1965). Feeding experiments proposed that psilotinin results from condensation of single malonyl-CoA with coumaroyl-CoA followed by lactonization (Leete et al., 1982). Several type III PKSs such as CHS, STS and VPS were cloned from this species but nothing was reported about PPS activity despite of extensive work. Ultimately, The K_{cat}/K_m values of the HsT135I and HsT135L mutants are 2.5 and 3.5-fold higher respectively compared to the HaT135L mutant from *H. androsaemum* (Klundt et al., 2009). However, they are more or less similar to those of the HsBPS wild-type (Huang et al., 2012). Both HsT135I and HsT135L showed 10 and 4 fold higher K_m values for malonyl-CoA compared to HsBPS wild-type (Huang et al., 2012). Replacement of Thr135 with leucine or isoleucine in case of HcBPS and HpaBPS gave the same results like HsBPS mutants. They transformed HcBPS and HpaBPS into PPSs. All the previous results suggest the active site architectural differences between these *Hypericum* BPSs. Pyrone compounds such as 5,6-dihydro-4-hydroxy-6-phenylpyran-2-one and its derivatives like those which have thiophenyl and thiobenzyl side chains at C-3 (Fig. 81) are used as small nonpeptide protease inhibitors of the human immunodeficiency virus (HIV). Inhibition of HIV protease is an important target for antiviral therapy. It was reported that HIV which lacks this protease is non-infectious (Tait et al., 1997).

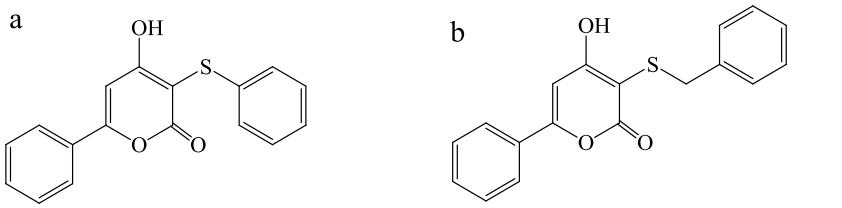

3-(phenylthio)-
4-hydroxy-6-phenyl-2*H*-pyran-2-one

3-(benzylthio)-
4-hydroxy-6-phenyl-2*H*-pyran-2-one

Fig. 81 Structures of 5,6-dihydro-4-hydroxy-6-phenylpyran-2-one derivatives, which block HIV protease.

Generally, mutations of type III PKSs that have a single active site are characterized by unforeseen results. For example, transformation of PCS to OKS by single amino acid substitution in position M207G while large to small substitutions in place of Gly207 in OKS resulted in loss of the octaketide forming activity and production of shorter chain-length polyketides ranging from triketide to heptaketide as mentioned before (Abe, 2008). In addition to identifying new enzymes and biosynthetic pathways, the challenge now is how to use these results in industrial and medicinal fields. Considerable research works are now devoted to understanding type III PKSs and engineering this fascinating group of enzymes. The objective is

to develop new compounds with significant and distinct biological activities (U.Nair et al., 2010). One of the most essential properties in the engineering of an enzyme for selective catalysis is changing the substrate specificity either by shifting the specificity towards novel substrates or expanding and narrowing substrate specificity. Type III PKSs are promiscuous enzymes accepting a wide range of starter substrates. Engineering of an enzyme to have a narrow substrate range is a challenge. Site-directed mutagenesis (SDM) plays a crucial role in this area. In the present study by using SDM a single amino acid substitution (HsT135K) switched the substrate specificity of HsBPS wild-type from benzoyl-CoA and 3-hydroxybenzoyl-CoA to salicoyl-CoA.

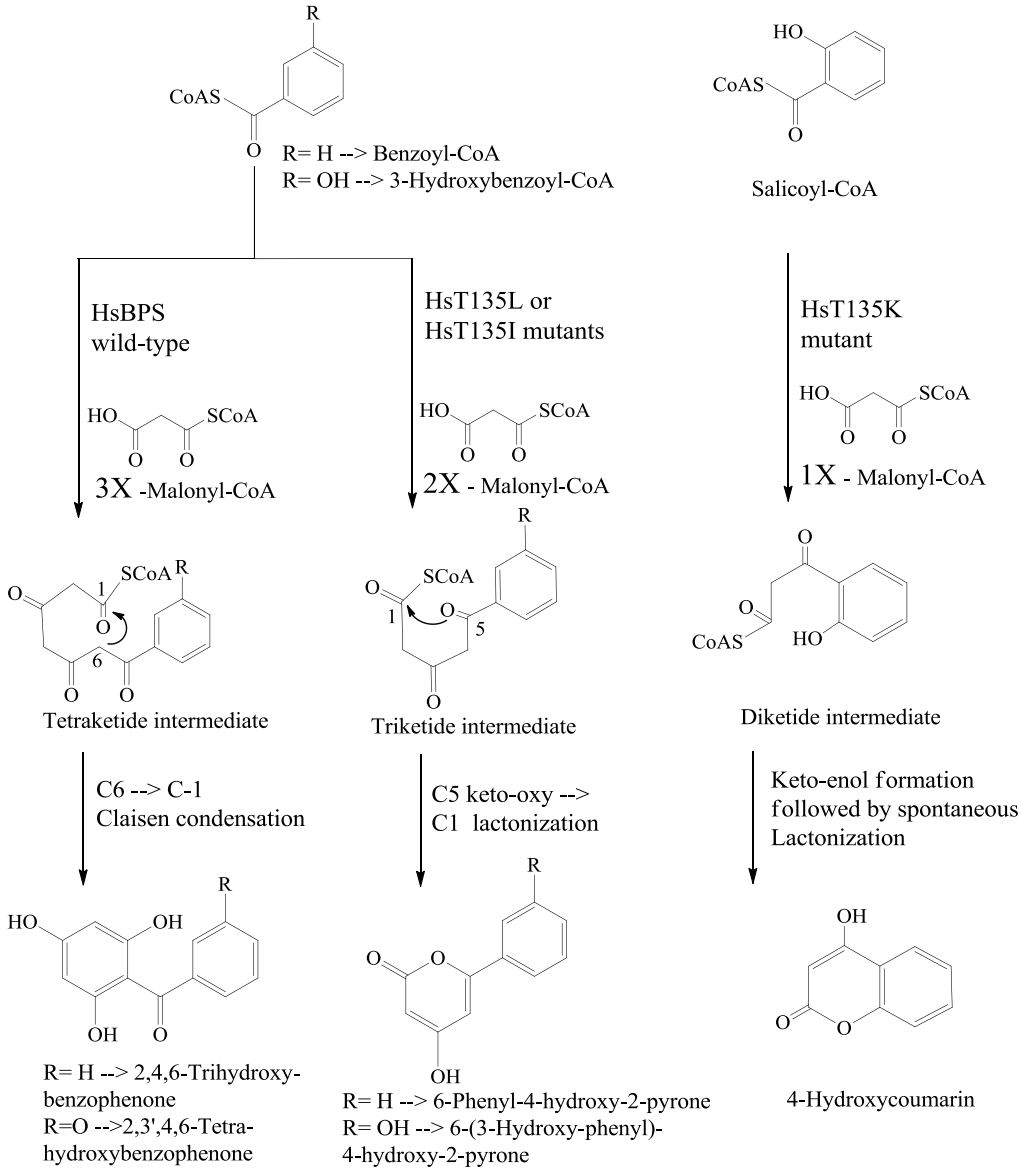

Fig. 82 Proposed reaction mechanisms of HsBPS wild-type, HsT135L, HsT135I and HsT135K enzyme mutants.

Not only the substrate specificity changed but there was also a dramatically altered product specificity from tri and tetrahydroxybenzophenones after three malonyl-CoA extensions and Claisen condensation to 4-hydroxycoumarin after only one malonyl-CoA extension and spontaneous lactonization (Fig. 82). However, leucine or isoleucine in the same position result in formation of phenylpyrone after two malonyl-CoA extensions and lactonization, which is a drastic change in the product specificity as HsT135I and HsT135L, still accept benzoyl and 3-hydroxybenzoyl-CoAs as substrates (Fig. 82).

5.7 Amino acids which did not dramatically change the activity

Other amino acids in position135 (Thr135) instead of threonine gave variable results. Aspartic acid, glutamine and proline showed no expression in the host cells as shown by SDS-PAGE analysis (Fig. 23). It was reported that most of the expression problems are due to protein toxicity. No expression in the host cells is one of these problems which indicate that these proteins are too toxic to the host cells and results in cell death (Inc., 2009). Normally, in biological systems any specific protein is expressed only in a specific place or tissue in a specific period and in the required amount. That is named spatial, temporal and quantitative expression which is not harmful to the cell. Expression of recombinant proteins usually results in introduction of a strange protein in the host cell. This introduced protein is expressed in higher levels and in unwanted time. If this over-expressed recombinant protein is formed as a soluble one it will carry out certain functions which are not required by the host and may be destructive to the host cells. These effects could be observed as decreased growth rates and cell density and sometimes cell death. Recombinant proteins which result in the previous effects are called toxic proteins. Around 80% of all soluble proteins possess a particular degree of toxicity to their hosts. Nearly 10% of all proteins are extremely toxic to host cells. Insoluble proteins showed no toxicity to the host cell. It is tempting to speculate that a single amino acid substitution may results in a toxic protein which leads to cell death and so no expression could be detected (Inc., 2009). Replacement of Thr135 in HsBPS wild-type with glutamic acid, argenine, tryptophane, tyrosine in addition to glycine decreased the activity so much compared to the wild-type HsBPS. These mutants resulted in formation of very low amounts of the products mainly phenylpyrone with benzoyl and 3-hydroxybenzoyl-CoAs and 4-hydroxycoumarin with 2-hydroxybenzoyl-CoA. Recently, replacement of Leu132 in RpBAS with tryptophane blocked the entrance of the coumaroyl-binding pocket. The RpT132W mutant has a smaller cavity volume than the RpBAS wild-type, as expected from homology modeling (Fig. 80). This smaller volume of the active site

cavity of the RpL132W mutant cannot support the formation of bisnoryangonin (BNY) after two malonyl-CoA extensions but an increase in the formation of benzalacetone after one malonyl-CoA extension. Tyrosine in the same position in RpBASL132 also increases the benzalacetone formation while the L132G mutant was similar to the wild-type RpBAS (Shimokawa et al., 2010). Alanine instead of Thr135 in HsBPS results in the formation of nearly the same amounts of 2,4,6-trihydroxybenzophenone and 6-phenyl-4-hydroxy-2-pyrone from benzoyl-CoA. When 3-hydroxybenzoyl-CoA is used as a substrate, the HsT135A mutant forms around 77% 6-(3-hydroxy-phenyl)-4-hydroxy-2-pyrone and about 22% 2,3',4,6-tetrahydroxybenzophenone. Valine gave nearly the same result but with lower activity than alanine. The HsT135S mutant is the most similar one to the HsBPS wild-type albeit with the formation of higher amounts of the side products with both benzoyl and 3-hydroxybenzoyl-CoAs substrates. Cysteine and asparagine still form tri- and tetrahydroxybenzophenones but with much lower activities compared to the wild-type. HsT135F and T135H mutants increased the activity with salicoyl-CoA and formed only smaller amounts of phenylpyrone with benzoyl and 3-hydroxybenzoyl-CoAs. No benzophenones were detected with these two mutants. Methionine showed good activity with benzoyl-CoA but mainly formed 6-phenyl-4-hydroxy-2-pyrone in addition to lower amounts of 2,4,6-trihydroxybenzophenone. With 3-hydroxybenzoyl-CoA it forms only 6-(3-hydroxy-phenyl)-4-hydroxy-2-pyrone and no 2,3',4,6-tetrahydroxy-benzophenone. Finally, it also forms higher amounts of 4-hydroxycoumarin when salicoyl-CoA was used as a substrate.

Physiological product formation in type III PKS-catalyzed reactions needs a specific conformation of the polyketide intermediate which results in an effective cyclization reaction. After solving the X-ray crystal structure of MsCHS2 it was suggested that the active site (initiation/elongation/cyclization) cavity is considered as a structural model stabilizing a specific conformation of the linear tetraketide intermediate which permits the Claisen condensation to take place (Ferrer et al., 1999). However, derailment product (CTAL) or other lactone side products formed either in solution or in the enzyme active site via C5 keto-enolization which is followed by nucleophilic attack on the C1 keton by a hydroxyl group in solution or the cysteine thiolate (enzyme bound) as the leaving group results in CTAL. Any structural modification of the elongation/cyclization cavity of CHS will sway the ratio of Claisen-formed products against lactone products with physiological and nonphysiological substrates (Jez et al., 2001). Interestingly, most CHS mutagenesis experiments that showed increased formation of coumaroyltriacetic acid lactone (CTAL) proposed that the structural variations at different positions in the initiation/elongation/cyclization pockets results in conformational changes in the

formed tetraketide intermediate (Jez et al., 2000; Suh et al., 2000). For example, replacement of MsCHSThr197 with Leu results in the formation of only CTAL as a single product after three malonyl-CoA extension with *p*-coumaroyl-CoA (Jez et al., 2000). Ultimately, it was demonstrated that there is a direct relationship between the structural variations in the active site cavity and functional changes in the cyclization reaction (Jez et al., 2001). Briefly, the 3D structure of the active site in addition to the shape and size of the starter substrates are two important factors for the optimal stabilization of the tetraketide intermediate's conformation that permits the Claisen condensation reaction to proceed effectively before side products formation (Jez et al., 2001). Remarkably, larger starter molecules prevent the polyketide intermediate from taking over the conformation required for the correct cyclization reaction. Comparable effects have been stated with 4-substituted analogues of *p*-coumaroyl-CoA and other aliphatic starter substrates (Zuurbier et al., 1998; Morita et al., 2000).

5.8 Malonyl-CoA K_m values of HsBPS and HaBPS enzymes

Despite of the high similarity between HsBPS and HaBPS their malonyl-CoA K_m values are very different. The malonyl-CoA K_m value of HsBPS is around three fold higher than that of HaBPS 92.5 µM and 31.3 µM respectively (Liu et al., 2003; Huang et al., 2012). Only six amino acids are different between these two BPSs. So six single mutants were constructed for HaBPS wild-type towards HsBPS. Studying the effect of these positions, which are away from the active site, on the activity was performed using different starter substrates. Five mutants (HaE54D, HaV146A, HaC230G, HaV359L and HaN360S) are active where the sixth mutant (HaS235A) did not show any over-expression in the host cells as shown by SDS-PAGE analysis (Fig. 89, D). The five active mutants are more or less similar to the wild-type HaBPS in their activity with the tested starter substrates (benzoyl, 3-hydroxybenzoyl and 2-hydroxybenzoyl-CoAs) as shown in (Fig. 57). Steady state kinetic parameters of these five single HaBPS mutants were calculated to determine which amino acid would switch the K_m value of malonyl-CoA. All of these five positions showed a direct effect on the affinities for both the starter and extender substrates with profound effect on malonyl-CoA. The K_m values for these mutants varied by factor 2 and 1.5 for benzoyl-CoA and malonyl-CoA respectively. They also showed 3 - 4.9 and 2 - 4 fold increase in the malonyl-CoA and benzoyl-CoA K_m values respectively compared to HaBPS wild-type. Notably, it was reported that residues which are not involved in the active site but influencing close to responsive areas of the three dimensional structure can modify enzyme specificities probably through modulating protein conformations (Ketterman et al., 2001). Mutational studies

of six Arg (non-active site) residues in *Pueraria lobata* CHS showed that some of these residues are essential for providing significant interactions to sustain the three dimensional structure of the enzyme. Some others showed significant effects on the enzyme activity. These residues are supposed to play important roles in placing the active site residues in the right catalytic positions. The previous findings demonstrate that residues away from the active site can have remarkable effects on the catalytic activity of the enzyme (Fukuma et al., 2007). At the same time replacement of Thr135 with Ile in *H. sampsonii, H. calycinum, and H. perforatum* ssp *angustifolium* resulted in three active mutants (HsT135I, HcT135I and HpaT135I) and transformed the wild-type BPSs of these *Hypericum* species into functional phenylpyrone synthases. While HaT135I mutant gave in active protein (Klundt et al., 2009).

From the amino acid sequences alignment there are only six different amino acids between *H. androsaemum* and *H. sampsonii* BPSs. Thus provoked the idea of constructing six double mutants of HaT135I with the six different amino acids towards *H.sampsonii*. The target was to find which of these six positions will regain the activity of the HaT135I mutant. The six double mutants (HaE54D/T135I, HaV146A/T135I, HaC230G/T135I, HaS235A/T135I, HaV359L/T135I and HaN360S/T135I) were active with different substrates (benzoyl, 3-hydroxybenzoyl and 2-hydroxybenzoyl-CoAs) resulting in the formation of 4-hydroxy-6-phenylpyran-2-one, 4-hydroxy-6-(3-hydroxy)-phenylpyran-2-one and small amounts of 4-hydroxycoumarin respectively (Fig. 60). Interestingly, the HaS235A single mutant showed no over-expression in the host cells while the HaS235A/T135I double mutant was active. These results suggest the presence of cooperation between these six non-active site residues and the conserved Thr135 amino acid. Ultimately, point mutations of amino acid residues which are not involved in the active site may change the tertiary structure of the enzyme either by modifying the mobility and positioning of a number of significant residues at different locations in the enzyme or changing the conformation of key side chains in the active site. These effects may drastically influence the enzyme activity (Dana et al., 2006).

5.9 Comparative homology dimer model of HsBPS

An updated comparative homology model was constructed to clarify many points obtained in the present study. The most important and interesting point is the dramatic functional variation of HsT135K mutant which completely changed the substrate and product specificity of *H. sampsonii* BPS wild-type. As previously shown in (Fig. 64) lysine residue has a long charged side chain which is in contact with the adjoining monomer and the dimer interface therefore,

lysine in position 135 not only acts as an active site residue but also extended to the other monomer and the dimer interface. This makes the explanation of the effect of this residue on the enzyme activity is not so easy and needs a crystal structure of the enzyme and the mutant to compare. The published model of *H. androsaemum* BPS (HaBPS) (Klundt et al., 2009) was monomeric for simplicity as all the former smaller mutations pointed directly into the active site. Therefore, this simple monomer model was sufficient to clarify the previous HaBPS mutations and so dimer stability or higher oligomers (tetramer) were neglected. Interestingly, after calculating the folding stability of the published model using FoldX (first turning all amino acids of the initial model into standard rotamers) the result indicated that Thr135Leu is only marginally destabilizing, in contrast to glycine, alanine, valine, isoleucine, asparagine and tyrosine which gave significantly more destabilized proteins which is in agreement with the experimental mutation results of *H.androsaemum*. Despite of the high sequence identity between the BPSs of the tested *Hypericum* species the different dimer interface results in different behavior of each enzyme. In case of *H.sampsonii* and based on the updated model the different dimer interface will result in a different orientation of the amino acids side chains and so a different behavior with different substrates. For example, 3-hydroxybenzoyl-CoA which is the second best substrate for HaBPS wild-type was not accepted by its leucine mutant HaT135L. In contrast, 3-hydroxybenzoyl-CoA still is the second best substrate for *H.sampsonii*, *H .calycinum* and *H. perforatum* ssp *angustifolium* BPSs wild types and their leucine mutants. Ultimately, six different positions ‘54, 146, 230, 235, 359, and 360’ between *H. sampsonii* and *H. androsaemum* are a way from the active site but they affect the enzyme activity as shown from the updated model.

6 Summary

- Understanding the structure and function of type III polyketide synthases (PKSs) increased in the past years due to cloning and characterization of novel enzymes which expand the biosynthetic repertoire of this fascinating group of enzymes. Crystallographic studies and site-directed mutagenesis play an essential role in illustrating the active site structural details. Type III PKSs share a common three-dimensional fold and absolutely conserved catalytic triad Cys-His-Asn. Minor changes in the active site architecture in addition to steric modulation are responsible for the amazing functional diversity of this superfamily of enzymes.
- Benzophenone synthase (BPS) is a relatively new member of type III PKSs cloned from some *Hypericum* species such as *H. androsaemum*, *H. sampsonii*, *H. calycinum* and *H. perforatum* ssp *angustifolium*. This enzyme is responsible for the formation of the C_{13} skeleton of benzophenone derivatives and xanthones which are classes of phenolic natural products with interesting pharmacological activities. BPS catalyzes iterative condensation of benzoyl-CoA or 3-hydroxybenzoyl-CoA with three molecules of malonyl-CoA to form a linear tetraketide intermediate which undergoes C6→C1 Claisen condensation and aromatization to form tri and tetrahydroxybenzophenones respectively. Recently, *H. androsaemum* BPS was transformed into a functional phenylpyrone synthase (PPS) by single amino acid substitution in the active site i.e. replacement of Thr135 with Leu.
- In the present study, various site-directed mutagenesis approaches were used to exchange Thr135 in *H. sampsonii* BPS (HsBPS) for the other 19 amino acids. Only three of these residues (lysine, isoleucine and leucine) dramatically changed the substrate and product specificities of HsBPS. Lysine in position 135 transformed HsBPS into a functional 4-hydroxycoumarin synthase (HCS) a novel PKS variant. The preferred starter substrate for HCS is 2-hydroxybenzoyl (salicoyl)-CoA rather than benzoyl-CoA. Furthermore, there is only a single chain extension with malonyl-CoA which results in formation of 4-hydroxycoumarin as a single product.
- Leucine and isoleucine in the same position convert HsBPS into functional PPSs. The two mutants catalyze two malonyl-CoA extensions leading to formation of 6-phenyl-4-hydroxy-2-pyrone. In contrast to the above *H. androsaemum* BPS-derived PPS both mutant enzymes showed relatively high activity with 3-hydroxybenzoyl-CoA forming 6-

(3-hydroxyphenyl)-4-hydroxy-2-pyrone. They also accepted 2-hydroxybenzoyl-CoA forming small amounts of 4-hydroxycoumarin.

- Three mutants containing proline, aspartic acid and glutamine in position 135 did not yield over-expression in *E. coli*. Glutamic acid, argenine, tryptophane, tyrosine and glycine strongly decreased the catalytic activity compared to the wild-type. Mutants with the other amino acids (alanine, valine, serine, cysteine, asparagine, methionine, phenylalanine and histidine) were more or less similar to the wild-type albeit with formation of higher amounts of the side products.
- Testing the three mutants HsT135K, HsT135I and HsT135L with different starter substrates such as 2-aminobenzoyl (anthraniloyl)-CoA, 2-methoxybenzoyl- and 2-mercaptobenzoyl-NACs which were chemically synthesized and *N*-methylanthraniloyl-CoA revealed that anthraniloyl-CoA and *N*-methylanthraniloyl-CoA led to formation of 4-hydroxy-2(1*H*)-quinolone and 4-hydroxy-1-methyl-2(1*H*)-quinolone respectively while 2-methoxybenzoyl- and 2-mercaptobenzoyl-NACs were not converted.
- Characterization of the three mutants revealed that the HsT135K mutant showed 40 and 32 fold higher turnover rate (K_{cat}) when compared to *Sorbus aucupar*ia BISs (Sa BIS2 and SaBIS3) which can also form 4-hydroxycoumarin. The HsT135L and HsT135I mutants showed 3.5 and 2.5 fold higher catalytic efficiencies (K_{cat}/K_m) respectively when compared to the T135L mutant of *H. androsaemum* BPS. However, the three HsBPS mutants showed 10, 8 and 4 fold higher K_m values for malonyl-CoA than HsBPS wild-type. The pH and temperature optima of the mutants were 7 and 30 °C respectively.
- Replacement of Thr135 with Lys in *H. androsaemum* BPS also generated HCS but with much lower catalytic activity in comparison to the HsT135K mutant.
- HsBPS had an around 3 fold higher malonyl-CoA K_m value than *H. androsaemum* BPS (HaBPS) although only six amino acids differ. To check for position-specific effects the six single mutants HaE54D, HaV146A, HaC230G, HaS235A, HaV359L and HaN360S were constructed, of which HaS235A failed to be over-expressed. Steady-state kinetic analysis of the five active mutants elucidated that all five positions directly affected the affinities for both starter and extender substrates. The K_m values for malonyl-CoA and benzoyl-CoA were increased 3 - 4.9 and 2 - 4 times compared to wild-type.
- Six double mutants (HaE54D/T135K, HaV146A/T135K, HaC230G/T135K, HaS235A/T135K, HaV359L/T135K and HaN360S/T135K) were constructed of which HaN360S/T135K failed to be over-expressed. The five residual double mutants showed

good activity with salicoyl-CoA and formed 4-hydroxycoumarin. As an example, steady state kinetic parameters were determind for HaV146A/T135K. Its catalytic efficiency (K_{cat}/K_m) was 4 fold lower than that of HsT135K in addition to a 1.3 fold higher malonyl-CoA K_m value.

- Isoleucine instead of Thr135 in HaBPS resulted previously in catalytically inactive proteins. The double mutants HaE54D/T135I, HaV146A/T135I, HaC230G/T135I, HaS235A/T135I, HaV359L/T135I and HaN360S/T135I were constructed to investigate the effect of these non-active-site amino acids on regaining activity. All these six double mutants showed good activity with benzoyl and 3-hydroxybenzoyl-CoAs and resulted in formation of 6-phenyl-4-hydroxy-2-pyrone and 6-(3-hydroxyphenyl)-4-hydroxy-2-pyrone, respectively.
- *H. calycinum* and *H. perforatum* ssp *angustifolium* BPSs also contain Thr135 with few different amino acids away from the active site. Replacement of Thr135 with Lys resulted in no over-expression in case of HpaT135K and no soluble protein in case of HcT135K. Leucine and isoleucine in the same position transformed both BPSs into PPSs which also exhibited good activities with 3-hydroxybenzoyl-CoA, forming 6-(3-hydroxy-phenyl)-4-hydroxy-2-pyrone.
- Finally, an updated homology model of HsBPS was constructed as a dimer based on the crystal structure of *Medicago sativa* chalcone synthase to rationalize the dramatic functional variation of HsT135K mutant. The modeling showed that lysine residue has a long charged side chain which is in contact with the adjoining monomer and the dimer interface. Lysine in position 135 does not only act as an active site residue but also extends to the other monomer and the dimer interface due to its long charged side chain. This makes the explanation of the effect of this residue on the enzyme activity not so easy and needs a crystal structure of the enzyme and the mutant to compare.
- In addition, it showed that the loop from aa 138 to 144 is part of the dimer interface directly adjacent to the active site mutation in position 135. This effect of the adjoining dimer interface is even more pronounced in *H. calycinum* and *H. perforatum* ssp *angustifolium* BPSs where the active sites are identical but the dimer interfaces look different. Clarification in more detail needs an X-ray crystal structure as the current model cannot resolve such global conformational changes.
- The following flow chart (Fig. 83) summarizes all *Hypericum* BPSs tested and all mutations constructed.

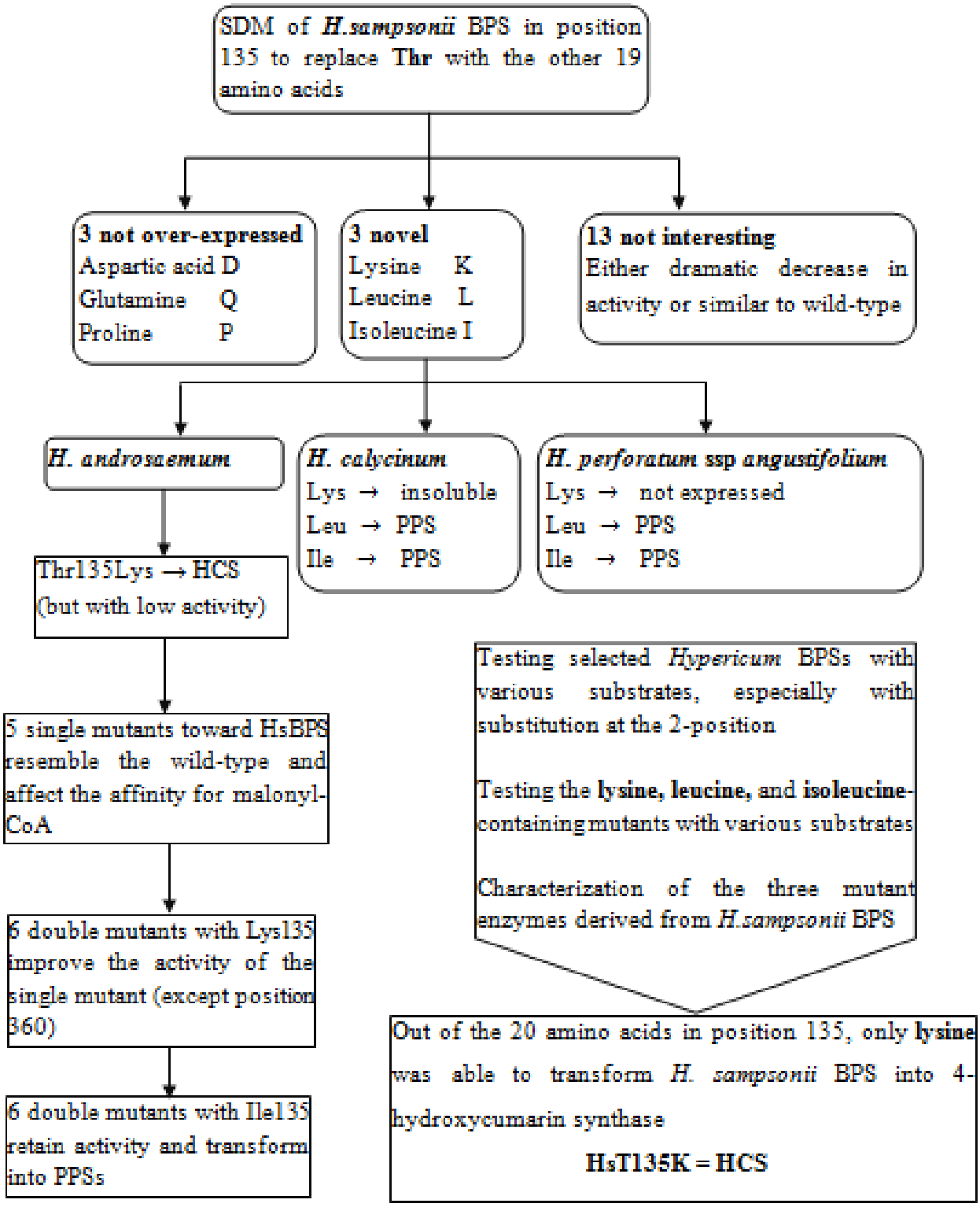

Fig. 83 Flow chart of all *Hypericum* BPSs tested and all mutations constructed

7 References

Abe I (2008) Engineering of plant polyketide biosynthesis. Chem Pharm Bull (Tokyo) **56:** 1505-1514

Abe I (2010) Engineered biosynthesis of plant polyketides: structure-based and precursor-directed approach. Top Curr Chem **297:** 45-66

Abe I (2012) Benzalacetone synthase. Frontiers in Plant Science **3**

Abe I, Abe T, Wanibuchi K, Noguchi H (2006) Enzymatic formation of quinolone alkaloids by a plant type III polyketide synthase. Org Lett **8:** 6063-6065

Abe I, Morita H (2010) Structure and function of the chalcone synthase superfamily of plant type III polyketide synthases. *In* Natural Product Reports, Vol 27. The Royal Society of Chemistry, pp 809-838

Abe I, Oguro S, Utsumi Y, Sano Y, Noguchi H (2005) Engineered biosynthesis of plant polyketides: chain length control in an octaketide-producing plant type III polyketide synthase. Journal of the American Chemical Society **127:** 12709-12716

Abe I, Sano Y, Takahashi Y, Noguchi H (2003) Site-directed mutagenesis of benzalacetone synthase: The role of Phe215 in plant type III polyketide synthases. Journal of Biological Chemistry **278:** 25218-25226

Abe I, Takahashi Y, Morita H, Noguchi H (2001) Benzalacetone synthase. A novel polyketide synthase that plays a crucial role in the biosynthesis of phenylbutanones in *Rheum palmatum*. Eur J Biochem **268:** 3354-3359

Abe I, Takahashi Y, Noguchi H (2002) Enzymatic formation of an unnatural C6−C5 aromatic polyketide by plant type III polyketide synthases. Organic Letters **4:** 3623-3626

Abe I, Utsumi Y, Oguro S, Morita H, Sano Y, Noguchi H (2005) A plant type III polyketide synthase that produces pentaketide chromone. J Am Chem Soc **127:** 1362-1363

Abe I, Utsumi Y, Oguro S, Noguchi H (2004) The first plant type III polyketide synthase that catalyzes formation of aromatic heptaketide. FEBS Lett **562:** 171-176

Abe I, Watanabe T, Lou W, Noguchi H (2006) Active site residues governing substrate selectivity and polyketide chain length in aloesone synthase. FEBS J **273:** 208-218

Abe I, Watanabe T, Lou W, Noguchi H (2006) Active site residues governing substrate selectivity and polyketide chain length in aloesone synthase. FEBS Journal **273:** 208-218

Abe T, Morita H, Noma H, Kohno T, Noguchi H, Abe I (2007) Structure function analysis of benzalacetone synthase from *Rheum palmatum*. Bioorg Med Chem Lett **17:** 3161-3166

Abe T, Noma H, Noguchi H, Abe I (2006) Enzymatic formation of an unnatural methylated triketide by plant type III polyketide synthases. Tetrahedron Letters **47:** 8727-8730

Ainasoja M (2008) Secondary metabolites in *Gerbera hybrida*. Doctoral Thesis. Helsinki Graduate School in Biotechnology and Molecular Biology,University of Helsinki, Finland

Al-Arif A, Blecher M (1969) Synthesis of fatty acyl CoA and other thiol esters using *N*-hydroxysuccinimide esters of fatty acids. J Lipid Res **10:** 344-345

Arif T, Bhosale JD, Kumar N, Mandal TK, Bendre RS, Lavekar GS, Dabur R (2009) Natural products--antifungal agents derived from plants. J Asian Nat Prod Res **11:** 621-638

Arnold K, Bordoli L, Kopp J, Schwede T (2006) The SWISS-MODEL workspace: a web-based environment for protein structure homology modelling. Bioinformatics **22:** 195-201

Austin MB, Bowman ME, Ferrer J-L, Schröder J, Noel JP (2004) An Aldol Switch Discovered in Stilbene Synthases Mediates Cyclization Specificity of Type III Polyketide Synthases. Chemistry & Biology **11:** 1179-1194

Austin MB, Izumikawa M, Bowman ME, Udwary DW, Ferrer J-L, Moore BS, Noel JP (2004) Crystal structure of a bacterial type III polyketide synthase and enzymatic control of reactive polyketide intermediates. J Biol Chem **279:** 45162-45174

Austin MB, Noel JP (2003) The chalcone synthase superfamily of type III polyketide synthases. Natural Product Reports **20:** 79-110

Baker P, Seah S (2012) Rational approaches for engineering carbon-carbon bond forming enzymes,

Beerhues L (1996) Benzophenone synthase from cultured cells of *Centaurium erythraea*. FEBS Lett **383:** 264-266

Beerhues L, Liu B (2009) Biosynthesis of biphenyls and benzophenones--evolution of benzoic acid-specific type III polyketide synthases in plants. Phytochemistry **70:** 1719-1727

Beuerle T, Pichersky E (2002) Enzymatic synthesis and purification of aromatic coenzyme A esters. Analytical Biochemistry **302:** 305-312

Bhonoah Y (2006) Warfarin. *In*. http://www.ch.ic.ac.uk/local/projects/bhonoah/home.html

Birnboim HC, Doly J (1979) A rapid alkaline extraction procedure for screening recombinant plasmid DNA. Nucleic Acids Res **7:** 1513-1523

Borejsza-Wysocki W, Hrazdina G (1996) Aromatic polyketide synthases (purification, characterization, and antibody development to benzalacetone synthase from raspberry fruits. Plant Physiology **110:** 791-799

Bradford MM (1976) A rapid and sensitive method for the quantitation of microgram quantities of protein utilizing the principle of protein-dye binding. Analytical Biochemistry **72:** 248-254

Brand S, Hölscher D, Schierhorn A, Svatoš A, Schröder J, Schneider B (2006) A type III polyketide synthase from *Wachendorfia thyrsiflora* and its role in diarylheptanoid and phenylphenalenone biosynthesis. Planta **224:** 413-428

Bruni R, Pellati F, Bellardi MG, Benvenuti S, Paltrinieri S, Bertaccini A, Bianchi A (2005) Herbal drug quality and phytochemical composition of *Hypericum perforatum* L. affected by ash yellows phytoplasma infection. Journal of Agricultural and Food Chemistry **53:** 964-968

Bye A, King HK (1970) The biosynthesis of 4-hydroxycoumarin and dicoumarol by *Aspergillus fumigatus* Fresenius. Biochem J **117:** 237-245

Cholewinski G, Dzierzbicka K, Kolodziejczyk AM (2011) Natural and synthetic acridines/acridones as antitumor agents: their biological activities and methods of synthesis. Pharmacol Rep **63:** 305-336

Chothia C, Lesk AM (1986) The relation between the divergence of sequence and structure in proteins. EMBO J **5:** 823-826

Çirak C, Ayan AK, Kevseroglu K, Özen T (2006) Variation of hypericin in St. John's Wort (*Hypericum perforatum)* from wild populations of Northern Turkey. Acta Botanica Hungarica **48:** 55-64

Cohen SN, Chang AC, Hsu L (1972) Nonchromosomal antibiotic resistance in bacteria: genetic transformation of *Escherichia coli* by R-factor DNA. Proc Natl Acad Sci U S A **69:** 2110-2114

Crockett SL, Robson NK (2011) Taxonomy and chemotaxonomy of the genus *Hypericum*. Med Aromat Plant Sci Biotechnol **5:** 1-13

Czygan FC (2003) [From a 2500 year old apotropic comes a current antidepressive. The cultural history and mistique of St. John's wort]. Pharm Unserer Zeit **32:** 184-190

Dagert M, Ehrlich SD (1979) Prolonged incubation in calcium chloride improves the competence of *Escherichia coli* cells. Gene **6:** 23-28

Dana CD, Bevan DR, Winkel BSJ (2006) Molecular modeling of the effects of mutant alleles on chalcone synthase protein structure. J Mol Model **12:** 905-914

Decosterd LA, Hoffmann E, Kyburz R, Bray D, Hostettmann K (1991) A new phloroglucinol derivative from *Hypericum calycinum* with antifungal and *in vitro* antimalarial activity. Planta Med **57:** 548-551

Decosterd LA, Stoeckli-Evans H, Chapuis J-C, Sordat B, Hostettmann K (1989) New cell growth-inhibitory cyclohexadienone derivatives from *Hypericum calycinum* L. Helvetica Chimica Acta **72:** 1833-1845

Dewick PM (2002) Medicinal natural products- a biosynthetic approach. *In*, Ed 2nd. John Wiley & Sons Ltd,, England

Dimroth P, Walter H, Lynen F (1970) Biosynthese von 6-methylsalicylsäure. European Journal of Biochemistry **13:** 98-110

Duckworth P (2012) The synthesis of intermediates to probe the biosynthesis of bacillaene. Master Thesis. University of Bristol,Cantock's Close, Bristol, BS8 1TS, U.K.

Dukovčić I, Kreft S, Beerhues L (2012) Approaches to optimization of hyperforin production in *Hypericum Perforatum* shoot cultures. Master Thesis. University of Ljubljana,Slovenia / Technische Universitat, Braunschweig, Germany.

Durì L, Morelli CF, Crippa S, Speranza G (2004) 6-Phenylpyrones and 5-methylchromones from Kenya aloe. Fitoterapia **75:** 520-522

Eckermann S, Schröder G, Schmidt J, Streck D, Edrada RA, Helariutta Y, Elomaa P, Kotilainen M, Kilpeläinen I, Proksch P, Teeri TH, Schröder J (1998) New pathway to polyketides in plants. Nature **396:** 387-390

Ferrari J, Terreaux C, Sahpaz S, Msonthi JD, Wolfender J-L, Hostettmann K (2000) Benzophenone glycosides from *Gnidia involucrata*. Phytochemistry **54:** 883-889

Ferrer J-L, Jez JM, Bowman ME, Dixon RA, Noel JP (1999) Structure of chalcone synthase and the molecular basis of plant polyketide biosynthesis. Nature Structural Biology **6:** 775-784

Flicksi (2011) *Hypericum calycinum*. *In*. http://flicksi.deviantart.com/art/Hypericum-calycinum-234611076

Flores-Sanchez IJ, Verpoorte R (2009) Plant polyketide synthases: A fascinating group of enzymes. Plant Physiology and Biochemistry **47:** 167-174

Frandsen R (2010) Polyketide synthases. *In*. http://www.rasmusfrandsen.dk/polyketide_synthases.htm

Fu H, Ebert-Khosla S, Hopwood DA, Khosla C (1994) Engineered biosynthesis of novel polyketides: dissection of the catalytic specificity of the *act* ketoreductase. Journal of the American Chemical Society **116:** 4166-4170

Fukuma K, Neuls ED, Ryberg JM, Suh D-Y, Sankawa U (2007) Mutational analysis of conserved outer sphere arginine residues of chalcone synthase. J Biochem **142:** 731-739

Germer J (2008) *Hypericum androsaemum* L. *In*. http://www.virboga.de/Hypericum_androsaemum.htm, Botanical Garden Hohenheim, Germany

Gleason F, K. , Chollet R (2012) Plant biochemistry. Jones & Bartlett Learning, http://samples.jbpub.com/9780763764012/64012_Ch08_0148_rev.pdf, Sudbury, Mass.

Guex N, Peitsch MC (1997) SWISS-MODEL and the Swiss-PdbViewer: an environment for comparative protein modeling. Electrophoresis **18:** 2714-2723

Habib AM, Ho DK, Masuda S, McCloud T, Reddy KS, Aboushoer M, McKenzie A, Byrn SR, Chang CJ, Cassady JM (1987) Structure and stereochemistry of psorospermin and related cytotoxic dihydrofuranoxanthones from *Psorospermum febrifugum*. The Journal of Organic Chemistry **52:** 412-418

Healthcare (2011) *Hypericum sampsonii*. *In*. http://www.aqnovel.com/mytag.php?id=52775

Helariutta Y, Elomaa P, Kotilainen M, Griesbach R, Schröder J, Teeri T (1995) Chalcone synthase-like genes active during corolla development are differentially expressed and encode enzymes with different catalytic properties in *Gerbera hybrida* (Asteraceae). Plant Molecular Biology **28:** 47-60

Herbarium HK (2013) *Hypericum sampsonii* (Sampson's St. Johnswort). *In*. http://www.hkherbarium.net/herbarium/20/Plant_of_month.asp?Year=2013&Month=6

Higdon J (2008) Resveratrol *In*. http://lpi.oregonstate.edu/infocenter/phytochemicals/resveratrol/

Hobbs C (1998) St. John's Wort (*Hypericum Perforatum* L.). *In*. www.christopherhobbs.com/website/library/articles/article_files/st_johnswort_01.html

Hobbs C (2013) Information on St. John's Wort. *In*. http://christopherhobbs.com/database/?details&type=herbs&name=St.%20John's%20Wort

Hu L-H, Sim K-Y (2000) Sampsoniones A–M, a unique family of caged polyprenylated benzoylphloroglucinol derivatives, from *Hypericum sampsonii*. Tetrahedron **56:** 1379-1386

Huang L, Wang H, Ye H, Du Z, Zhang Y, Beerhues L, Liu B (2012) Differential expression of benzophenone synthase and chalcone synthase in *Hypericum sampsonii*. Nat Prod Commun **7:** 1615-1618

Inc. ET (2009) Toxic protein cloning and expression. *In*. http://www.exptec.com/Expression%20Technologies/Toxic%20protein%20cloning%20and%20expression.htm

Inoue T, Toyonaga T, Nagumo S, Nagai M (1989) Biosynthesis of 4-hydroxy-5-methylcoumarin in a *Gerbera jamesonii* hybrid. Phytochemistry **28:** 2329-2330

Izumikawa M, Shipley PR, Hopke JN, O'Hare T, Xiang L, Noel JP, Moore BS (2003) Expression and characterization of the type III polyketide synthase 1,3,6,8-tetrahydroxynaphthalene synthase from *Streptomyces coelicolor* A3(2). J Ind Microbiol Biotechnol **30:** 510-515

Jeya M, Kim T-S, Kumar Tiwari M, Li J, Zhao H, Lee J-K (2012) A type III polyketide synthase from *Rhizobium etli* condenses malonyl CoAs to a heptaketide pyrone with unusually high catalytic efficiency. Molecular BioSystems **8:** 3103-3106

Jez JM, Austin MB, Ferrer J-L, Bowman ME, Schroder J, Noel JP (2000) Structural control of polyketide formation in plant-specific polyketide synthases. Chem Biol **7:** 919-930

Jez JM, Austin MB, Ferrer J-L, Bowman ME, Schröder J, Noel JP (2000) Structural control of polyketide formation in plant-specific polyketide synthases. Chemistry & Biology **7:** 919-930

Jez JM, Bowman ME, Noel JP (2001) Structure-guided programming of polyketide chain-length determination in chalcone synthase. Biochemistry **40:** 14829-14838

Jez JM, Bowman ME, Noel JP (2002) Expanding the biosynthetic repertoire of plant type III polyketide synthases by altering starter molecule specificity. Proceedings of the National Academy of Sciences **99:** 5319-5324

Jez JM, Ferrer J-L, Bowman ME, Austin ME, Schröder J, Dixon RA, Noel JP (2001) Structure and mechanism of chalcone synthase-like polyketide synthases. Journal of Industrial Microbiology and Biotechnology **27:** 393-398

Jez JM, Ferrer J-L, Bowman ME, Dixon RA, Noel JP (2000) Dissection of malonyl-coenzyme A decarboxylation from polyketide formation in the reaction mechanism of a plant polyketide synthase. Biochemistry **39:** 890-902

Jez JM, Noel JP (2000) Mechanism of chalcone synthase. pKa of the catalytic cysteine and the role of the conserved histidine in a plant polyketide synthase. J Biol Chem **275:** 39640-39646

Jez JM, Noel JP (2002) Reaction mechanism of chalcone isomerase: pH dependence, diffusion control, and product binding differences. Journal of Biological Chemistry **277:** 1361-1369

Karppinen K, Hokkanen J, Tolonen A, Mattila S, Hohtola A (2007) Biosynthesis of hyperforin and adhyperforin from amino acid precursors in shoot cultures of *Hypericum perforatum*. Phytochemistry **68:** 1038-1045

Ketterman AJ, Prommeenate P, Boonchauy C, Chanama U, Leetachewa S, Promtet N, Prapanthadara L (2001) Single amino acid changes outside the active site significantly affect activity of glutathione S-transferases. Insect Biochem Mol Biol **31:** 65-74

Kinza Aslam K, Khosa MK, Jahan N, Nosheen S (2010) Short communication: synthesis and applications ofcoumarin. Pak J Pharm Sci **23:** 449-454

Kitanov GM, Nedialkov PT (2001) Benzophenone O-glucoside, a biogenic precursor of 1,3,7-trioxygenated xanthones in *Hypericum annulatum*. Phytochemistry **57:** 1237-1243

Klingauf P, Beuerle T, Mellenthin A, El-Moghazy SA, Boubakir Z, Beerhues L (2005) Biosynthesis of the hyperforin skeleton in Hypericum calycinum cell cultures. Phytochemistry **66:** 139-145

Klingauf P, Beuerle T, Mellenthin A, El-Moghazy SAM, Boubakir Z, Beerhues L (2005) Biosynthesis of the hyperforin skeleton in *Hypericum calycinum* cell cultures. Phytochemistry **66:** 139-145

Klundt T (2008) Ortsgerichtete mutagenese der benzophenon synthase von *Hypericum androsaemum*. Doctoral thesis. Technischen Universität Carolo-Wilhelmina zu Braunschweig, Germany

Klundt T, Bocola M, Lutge M, Beuerle T, Liu B, Beerhues L (2009) A single amino acid substitution converts benzophenone synthase into phenylpyrone synthase. J Biol Chem **284:** 30957-30964

Krieger E, Nabuurs SB, Vriend G (2003) Homology modeling. Methods Biochem Anal **44:** 509-523

Kostova I (2005) Synthetic and natural coumarins as cytotoxic agents. Curr med chem anticancer agents **5:** 29-46

Kostova I (2007) Studying plant-derived coumarins for their pharmacological and therapeutic properties as potential anticancer drugs. Expert Opinion on Drug Discovery **2:** 1605-1618

Kwok Y, Hurley LH (1998) Topoisomerase II site-directed alkylation of DNA by psorospermin and its effect on topoisomerase II-mediated DNA cleavage. J Biol Chem **273:** 33020-33026

Laemmli UK (1970) Cleavage of structural proteins during the assembly of the head of bacteriophage T4. Nature **227:** 680-685

Lapidot Y, Rappoport S, Wolman Y (1967) Use of esters of *N*-hydroxysuccinimide in the synthesis of N-acylamino acids. J Lipid Res **8:** 142-145

Lausanne U (2013) Homology modeling. *In*. http://www.unil.ch/pmf/page48308.html

Leete E, Muir A, Towers GHN (1982) Biosynthesis of psilotin from [2′,3′-^{13}C2,1′-^{14}C,4-^{3}H]phenylalanine studied with ^{13}C-NMR. Tetrahedron Letters **23:** 2635-2638

Li X, Liu S, Huang H, Liu N, Zhao C, Liao S, Yang C, Liu Y, Zhao C, Li S, Lu X, Liu C, Guan L, Zhao K, Shi X, Song W, Zhou P, Dong X, Guo H, Wen G, Zhang C, Jiang L, Ma N, Li B, Wang S, Tan H, Wang X, Dou QP, Liu J (2013) Gambogic acid is a tissue-specific proteasome inhibitor in vitro and in vivo. Cell Reports **3:** 211-222

Lin Y, Shen X, Yuan Q, Yan Y (2013) Microbial biosynthesis of the anticoagulant precursor 4-hydroxycoumarin. Nat Commun **4:** 2603

Liu B, Beuerle T, Klundt T, Beerhues L (2004) Biphenyl synthase from yeast-extract-treated cell cultures of *Sorbus aucuparia*. Planta **218:** 492-496

Liu B, Falkenstein-Paul H, Schmidt W, Beerhues L (2003) Benzophenone synthase and chalcone synthase from *Hypericum androsaemum* cell cultures: cDNA cloning, functional expression, and site-directed mutagenesis of two polyketide synthases. Plant J **34:** 847-855

Liu B, Raeth T, Beuerle B, Beerhues L (2010) A novel 4-hydroxycoumarin biosynthetic pathway. Plant Mol Biol **72:** 17-25

Liu B, Raeth T, Beuerle T, Beerhues L (2007) Biphenyl synthase, a novel type III polyketide synthase. Planta **225:** 1495-1503

Liu H, Naismith JH (2008) An efficient one-step site-directed deletion, insertion, single and multiple-site plasmid mutagenesis protocol. BMC Biotechnology **8:** 1-10

Lleida Pd (2010) *Hypericum perforatum* var. *angustifolium*. (Pericó) *In*. http://flponent.atspace.org/flora/flo/fam/guttiferes/hypericum_gut.htm

Loening A (2005) Site Directed Mutagenesis Protocol. *In*. http://www.stanford.edu/~loening/protocols/Site_Directed_Mutagenesis.pdf

Lukacin R, Schreiner S, Matern U (2001) Transformation of acridone synthase to chalcone synthase. FEBS Lett **508:** 413-417

Lukacin R, Schreiner S, Silber K, Matern U (2005) Starter substrate specificities of wild-type and mutant polyketide synthases from Rutaceae. Phytochemistry **66:** 277-284

Lukacin R, Springob K, Urbanke C, Ernwein C, Schroëder G, Schroëder J, Matern U (1999) Native acridone synthases I and II from *Ruta graveolens* L. form homodimers. FEBS Lett **448:** 135-140

Ma L-Q, Guo Y-W, Gao D-Y, Ma D-M, Wang Y-N, Li G-F, Liu B-Y, Wang H, Ye H-C (2009) Identification of a *Polygonum cuspidatum* three-intron gene encoding a type III polyketide synthase producing both naringenin and *p*-hydroxybenzalacetone. Planta **229:** 1077-1086

Ma L-Q, Pang X-B, Shen H-Y, Pu G-B, Wang H-H, Lei C-Y, Wang H, Li G-F, Liu B-Y, Ye H-C (2009) A novel type III polyketide synthase encoded by a three-intron gene from *Polygonum cuspidatum*. Planta **229:** 457-469

Males Z, Brantner AH, Sovic K, Pilepic KH, Plazibat M (2006) Comparative phytochemical and antimicrobial investigations of *Hypericum perforatum* L. subsp. *perforatum* and *H. perforatum* subsp. *angustifolium* (DC.) Gaudin. Acta Pharm **56:** 359-367

Mallika V, Sivakumar KC, Soniya EV (2011) Evolutionary implications and physicochemical analyses of selected proteins of type III polyketide synthase family. Evol Bioinform Online **7:** 41-53

Mandel M, Higa A (1970) Calcium-dependent bacteriophage DNA infection. J Mol Biol **53:** 159-162

Mclnnes AG, Yoshida S, Towers GHN (1965) A phenolic glycoside from *psilotum nudum* (L) griseb. Tetrahedron **21:** 2939-2946

Menichini G, Alfano C, Marrelli M, Toniolo C, Provenzano E, Statti GA, Nicoletti M, Menichini F, Conforti F (2013) *Hypericum perforatum* L. subsp. *perforatum* induces inhibition of free radicals and enhanced phototoxicity in human melanoma cells under ultraviolet light. Cell Prolif **46:** 193-202

Mizuuchi Y, Shi S-P, Wanibuchi K, Kojima A, Morita H, Noguchi H, Abe I (2009) Novel type III polyketide synthases from *Aloe arborescens*. FEBS Journal **276:** 2391-2401

Moore BS (2005) Biosynthesis of marine natural products: microorganisms (Part A). Natural Product Reports **22:** 580-593

Morita H, Kondo S, Abe T, Noguchi H, Sugio S, Abe I, Kohno T (2006) Crystallization and preliminary crystallographic analysis of a novel plant type III polyketide synthase that produces pentaketide chromone. Acta Crystallogr Sect F Struct Biol Cryst Commun **62:** 899-901

Morita H, Kondo S, Kato R, Wanibuchi K, Noguchi H, Sugio S, Abe I, Kohno T (2007) Crystallization and preliminary crystallographic analysis of an acridone-producing novel multifunctional type III polyketide synthase from *Huperzia serrata*. Acta Crystallogr Sect F Struct Biol Cryst Commun **63:** 576-578

Morita H, Kondo S, Oguro S, Noguchi H, Sugio S, Abe I, Kohno T (2007) Structural insight into chain-length control and product specificity of pentaketide chromone synthase from *Aloe arborescens*. Chem Biol **14:** 359-369

Morita H, Noguchi H, Schröder J, Abe I (2001) Novel polyketides synthesized with a higher plant stilbene synthase. European Journal of Biochemistry **268:** 3759-3766

Morita H, Takahashi Y, Noguchi H, Abe I (2000) Enzymatic formation of unnatural aromatic polyketides by chalcone synthase. Biochem Biophys Res Commun **279:** 190-195

Nicholas A, Rettie AE (2008) Pharmacogenomics of 4-hydroxycoumarin anticoagulants. Drug Metabolism Reviews **40:** 355-375

Nielsen H, Arends P (1979) Xanthone Constituents of *Hypericum androsaemum*. Journal of Natural Products **42:** 301-304

Nualkaew N, Morita H, Shimokawa Y, Kinjo K, Kushiro T, De-Eknamkul W, Ebizuka Y, Abe I (2012) Benzophenone synthase from *Garcinia mangostana* L. pericarps. Phytochemistry **77:** 60-69

Nürk N (2011) Phylogenetic analyses in St. John's wort (*Hypericum*) Inferring character evolution and historical biogeography. Doctoral Thesis. der Freien Universität

Ocak A, Erkara İ, Koyuncu O, Osoydan K, Yaylaci Ö, Özgişi K, Kurt F (2013) Palynological investigations on some Hypericum taxa (Hypericaceae) growing naturally in Turkey. Plant Systematics and Evolution **299:** 379-388

Oguro S, Akashi T, Ayabe S-i, Noguchi H, Abe I (2004) Probing biosynthesis of plant polyketides with synthetic N-acetylcysteamine thioesters. Biochem Biophys Res Commun **325:** 561-567

Ozturk Y (1997) Testing the antidepressant effects of *Hypericum* species on animal models. Pharmacopsychiatry **30 Suppl 2:** 125-128

Peters S, Schmidt W, Beerhues L (1997) Regioselective oxidative phenol couplings of 2,3′,4,6-tetrahydroxybenzophenone in cell cultures of *Centaurium erythraea* RAFN and *Hypericum androsaemum* L. Planta **204:** 64-69

Pietta P-G (2000) Flavonoids as antioxidants. Journal of Natural Products **63:** 1035-1042

Pignatti S (1982) Flora d'Italia, Vol 1-3. Il Sole 24 Ore Edagricole

Price NC, Stevens L (1982) Fundamentals of enzymology. *In*, Ed Third. Oxford University Press

Qiu J, Elber R (2006) SSALN: an alignment algorithm using structure-dependent substitution matrices and gap penalties learned from structurally aligned protein pairs. Proteins **62:** 881-891

Radhakrishnan EK SK, Soniya EV (2009) Molecular characterization of novel form of type III polyketide synthase from *Zingiber Officinale* Rosc. and its Analysis using bioinformatics method. . J Proteomics Bioinform **2:** 310-315

Raja Abdul Rahman RNZ, Zakaria II, Salleh AB, Basri M (2012) Enzymatic properties and mutational studies of chalcone synthase from *Physcomitrella patens*. International Journal of Molecular Sciences **13:** 9673-9691

Ralser M, Querfurth R, Warnatz HJ, Lehrach H, Yaspo ML, Krobitsch S (2006) An efficient and economic enhancer mix for PCR. Biochem Biophys Res Commun **347:** 747-751

Rebecca W, Kayser O, Hagels H, Zessin KH, Madundo M, Gamba N (2003) The phytochemical profile and identification of main phenolic compounds from the leaf exudate of *Aloe secundiflora* by high-performance liquid chromatography-mass spectroscopy. Phytochem Anal **14:** 83-86

Reimold U, Kroger M, Kreuzaler F, Hahlbrock K (1983) Coding and 3' non-coding nucleotide sequence of chalcone synthase mRNA and assignment of amino acid sequence of the enzyme. EMBO J **2:** 1801-1805

Resmi MS, Verma P, Gokhale RS, Soniya EV (2013) Identification and characterization of a type III Polyketide synthase involved in quinolone alkaloid biosynthesis from *Aegle marmelos* Correa. Journal of Biological Chemistry **288:** 7271-7281

Rodnina MV, Wintermeyer W, Greenstein MR (2011) Ribosomes structure, function, and dynamics. Springer, Wien; New York, http://dx.doi.org/10.1007/978-3-7091-0215-2

Rost S, Fregin A, Ivaskevicius V, Conzelmann E, Hortnagel K, Pelz HJ, Lappegard K, Seifried E, Scharrer I, Tuddenham EG, Muller CR, Strom TM, Oldenburg J (2004) Mutations in VKORC1 cause warfarin resistance and multiple coagulation factor deficiency type 2. Nature **427:** 537-541

Schmidt W, Abd el-Mawla AMA, Wolfender J-L, Hostettmann K, Beerhues L (2000) Xanthones in cell cultures of *Hypericum androsaemum*. Planta Med **66:** 380-381

Schröder J (2008) Hyperforin biosynthesis in *Hypericum perforatum*. *In*. http://www.biologie.uni-freiburg.de/data/bio2/schroeder/Hyperforin_Syn.html

Schröder J (2008) Pyrone Synthase from *Gerbera hybrida*. *In*. http://www.biologie.uni-freiburg.de/data/bio2/schroeder/Gerbera_2PS.html

Schröder J (2009) Acridone synthase (ACS) from *Ruta graveolens*. *In*. http://www.biologie.uni-freiburg.de/data/bio2/schroeder/Acridone_Syn.html

Schröder J (2009) Biosynthesis of 4-hydroxy-5-methylcoumarin in *Gerbera*. *In*. http://www.biologie.uni-freiburg.de/data/bio2/schroeder/Methylcoumarin_Syn.html

Schröder J (2009) Four condensation reactions: pentaketide chromone synthase (PCS). *In*. http://www.biologie.uni-freiburg.de/data/bio2/schroeder/Chromone_Syn.html

Schröder J (2009) Plant Type III PKS: One Condensation Reaction (Type III PKS in 4-Hydroxycoumarin Biosynthesis). *In*. http://www.biologie.uni-freiburg.de/data/bio2/schroeder/Plants_TypeIII_1_Condensation.html

Schröder J (2009) Six condensation reactions: Aloesone synthase (ALS). *In*. http://www.biologie.uni-freiburg.de/data/bio2/schroeder/Aloesone_Syn.html

Schröder J (2009) Type III PKS in 4-hydroxycoumarin biosynthesis. *In*. http://www.biologie.uni-freiburg.de/data/bio2/schroeder/4-Hydroxycoumarin_Biosynthesis.html

Shakirova KK, et al. (1970) Antimicrobial properties of some species of St. John's wort cultivated in Uzbekista Mikrobiol. Zh. (Kiev) **32:** 494-497 (CA 474:34570d).

Shimokawa Y, Morita H, Abe I (2010) Structure-based engineering of benzalacetone synthase. Bioorg Med Chem Lett **20:** 5099-5103

Shomura Y, Torayama I, Suh D-Y, Xiang T, Kita A, Sankawa U, Miki K (2005) Crystal structure of stilbene synthase from *Arachis hypogaea*. Proteins: Structure, Function, and Bioinformatics **60:** 803-806

Smith GF, Neubauer BL, Sundboom JL, Best KL, Goode RL, Tanzer LR, Merriman RL, Frank JD, Herrmann RG (1988) Correlation of the in vivo anticoagulant, antithrombotic, and antimetastatic efficacy of warfarin in the rat. Thrombosis Research **50:** 163-174

Southwell IA, Campbell MH (1991) Hypericin content variation in *Hypericum perforatum* in Australia. Phytochemistry **30:** 475-478

Spengler T (2013) *Hypericum Calycinum*. *In*. http://www.ehow.com/about_7232729_hypericum-calycinum-habitat.html, eHow

Srikanth G., Rajesh Babua Y., Bhagavan Raju M. (2013) Acridone derivatives in reversing multidrug resistance in cancer cells – where are we now? World Journal of Pharmaceutical research **2:** 308-318

Staunton J, Weissman KJ (2001) Polyketide biosynthesis: a millennium review. Natural Product Reports **18:** 380-416

Stevens PF (2007) Clusiaceae-Guttiferae. *In* K Kubitzki, ed, Flowering Plants · Eudicots, Vol 9. Springer Berlin Heidelberg, pp 48-66

Stöckigt J, Zenk MH (1975) Chemical syntheses and properties of hydroxycinnamoyl-coenzyme A derivatives. Z Naturforsch C **30:** 352-358

Stratagene (2005) QuikChange®site-directed mutagenesis kit *In*, United States and Canada, http://research.pomona.edu/jane-liu/files/2012/08/Stratagene-Quikchange-mutagenesis.pdf

Suh D-Y, Fukuma K, Kagami J, Yamazaki Y, Shibuya M, Ebizuka Y, Sankawa U (2000) Identification of amino acid residues important in the cyclization reactions of chalcone and stilbene synthases. Biochem J **350 Pt 1:** 229-235

Suo Z, Chen H, Walsh CT (2000) Acyl-CoA hydrolysis by the high molecular weight protein 1 subunit of yersiniabactin synthetase: mutational evidence for a cascade of four acyl-enzyme intermediates during hydrolytic editing. Proc Natl Acad Sci U S A **97:** 14188-14193

Suo Z, Chen H, Walsh CT (2000) Acyl-CoA hydrolysis by the high molecular weight protein 1 subunit of yersiniabactin synthetase: Mutational evidence for a cascade of four acyl-enzyme intermediates during hydrolytic editing. Proceedings of the National Academy of Sciences **97:** 14188-14193

Tait BD, Hagen S, Domagala J, Ellsworth EL, Gajda C, Hamilton HW, Vara Prasad JVN, Ferguson D, Graham N, Hupe D, Nouhan C, Tummino PJ, Humblet C, Lunney EA, Pavlovsky A, Rubin J, Gracheck SJ, Baldwin ET, Bhat TN, Erickson JW, Gulnik SV, Liu B (1997) 4-Hydroxy-5,6-dihydropyrones. 2. potent non-peptide inhibitors of HIV protease. Journal of Medicinal Chemistry **40:** 3781-3792

The University of California MoP (2010) Understanding evolution. *In*. http://evolution.berkeley.edu/evolibrary/article/mutations_03

Tocci N (2013) *Hypericum perforatum* subsp. *angustifolium*: study of xanthone biosynthesis in planta and in *in vitro* systems. Doctoral Thesis. Università "Sapienza" di Roma, Italy /Technische Universitat, Braunschweig, Germany

Tropf S, Karcher B, Schröder G, Schröder J (1995) Reaction mechanisms of homodimeric plant polyketide synthase (stilbenes and chalcone synthase). A single active site for the condensing reaction is sufficient for synthesis of stilbenes, chalcones, and 6'-deoxychalcones. J Biol Chem **270:** 7922-7928

U. Nair N, A. Denard C, Zhao H (2010) Engineering of enzymes for selective catalysis. Current Organic Chemistry **14:** 1870-1882

Usai M, Leggio B, Grappi S, Nanni G, Gambarana C, Tolu P, Giachetti D, De Montis MG (2003) *Hypericum perforatum* subspecies *angustifolium* shows a protective activity on the consequences of unavoidable stress exposure at lower doses than *Hypericum perforatum perforatum*. Pharmacopsychiatry **36:** 283-287

Valentão P, Dias A, Ferreira M, Silva B, Andrade PB, Bastos MdL, Seabra RM (2003) Variability in phenolic composition of *Hypericum androsaemum*. Nat Prod Res **17:** 135-140

Valentão P, Fernandes E, Carvalho F, Andrade PB, Seabra RM, Bastos MdL (2002) Antioxidant activity of *Hypericum androsaemum* infusion: scavenging activity against superoxide radical, hydroxyl radical and hypochlorous acid. Biol Pharm Bull **25:** 1320-1323

Valentão P, Carvalho M, Fernandes E, Carvalho F, Andrade PB, Seabra RM, Bastos MdL (2004) Protective activity of *Hypericum androsaemum* infusion against tert-butyl hydroperoxide-induced oxidative damage in isolated rat hepatocytes. Journal of Ethnopharmacology **92:** 79-84

Wanibuchi K, Zhang P, Abe T, Morita H, Kohno T, Chen G, Noguchi H, Abe I (2007) An acridone-producing novel multifunctional type III polyketide synthase from *Huperzia serrata*. FEBS Journal **274:** 1073-1082

Wikipedia (2013) Hypericaceae. *In*. http://en.wikipedia.org/wiki/Hypericaceae

Woelk H (2000) Comparison of St John's wort and imipramine for treating depression: randomised controlled trial. BMJ **321**

Xiao ZY, Mu Q, Shiu WKP, Zeng YH, Gibbons S (2007) Polyisoprenylated benzoylphloroglucinol derivatives from *Hypericum sampsonii*. J Nat Prod **70:** 1779-1782

Xiao ZY, Zeng YH, Mu Q, Shiu WKP, Gibbons S (2010) Prenylated benzophenone peroxide derivatives from *Hypericum sampsonii*. Chem Biodivers **7:** 953-958

Xin W-B, Jin G-L, Mao Z-J, Qin L-P (2011) Two unusual phenolic substances and one new xanthone from *Hypericum sampsonii*. Helvetica Chimica Acta **94:** 686-692

Xin W-b, Man X-h, Zheng C-j, Jia M, Jiang Y-p, Zhao X-x, Jin G-l, Mao Z-j, Huang H-q, Qin L-p (2012) Prenylated phloroglucinol derivatives from *Hypericum sampsonii*. Fitoterapia **83:** 1540-1547

Xin W-B, Mao Z-J, Jin G-L, Qin L-P (2011) Two new xanthones from *Hypericum sampsonii* and biological activity of the isolated compounds. Phytother Res **25:** 536-539

Yamaguchi T, Kurosaki F, Suh D-Y, Sankawa U, Nishioka M, Akiyama T, Shibuya M, Ebizuka Y (1999) Cross-reaction of chalcone synthase and stilbene synthase overexpressed in *Escherichia coli*. FEBS Letters **460:** 457-461

Zeng J-Z, Sun D-F, Wang L, Cao X, Qi J-B, Yang T, Hu C-Q, Liu W, Zhang X-K (2006) *Hypericum sampsonii* induces apoptosis and nuclear export of retinoid X receptor-alpha. Carcinogenesis **27:** 1991-2000

Zha W, Rubin-Pitel SB, Zhao H (2006) Characterization of the substrate specificity of PhlD, a Type III Polyketide synthase from *Pseudomonas fluorescens*. Journal of Biological Chemistry **281:** 32036-32047

Zhang S, Yang X, Morris ME (2004) Combined effects of multiple flavonoids on breast cancer resistance protein (ABCG2)-mediated transport. Pharm Res **21:** 1263-1273

Zheng D, Hrazdina G (2008) Molecular and biochemical characterization of benzalacetone synthase and chalcone synthase genes and their proteins from raspberry (*Rubus idaeus* L.). Arch Biochem Biophys **470:** 139-145

Zheng L, Baumann U, Reymond J-L (2004) An efficient one-step site-directed and site-saturation mutagenesis protocol. Nucleic Acids Research **32:** e115

Zodi R (2011) Molecular cloning of benzophenone synthase from *Hypericum calycinum* cell cultures and attempts toward transformation of *Hypericum perforatum*. Doctoral Thesis. Technische Universitat, Braunschweig, Germany.

Zuurbier KW, Leser J, Berger T, Hofte AJ, Schröder G, Verpoorte R, Schröder J (1998) 4-Hydroxy-2-pyrone formation by chalcone and stilbene synthase with nonphysiological substrates. Phytochemistry **49:** 1945-1951

Zuurbier KWM, Leser J, Berger T, Hofte AJP, Schröder G, Verpoorte R, Schröder J (1998) 4-hydroxy-2-pyrone formation by chalcone and stilbene synthase with nonphysiological substrates. Phytochemistry**:** 1945-1951

8 Appendix

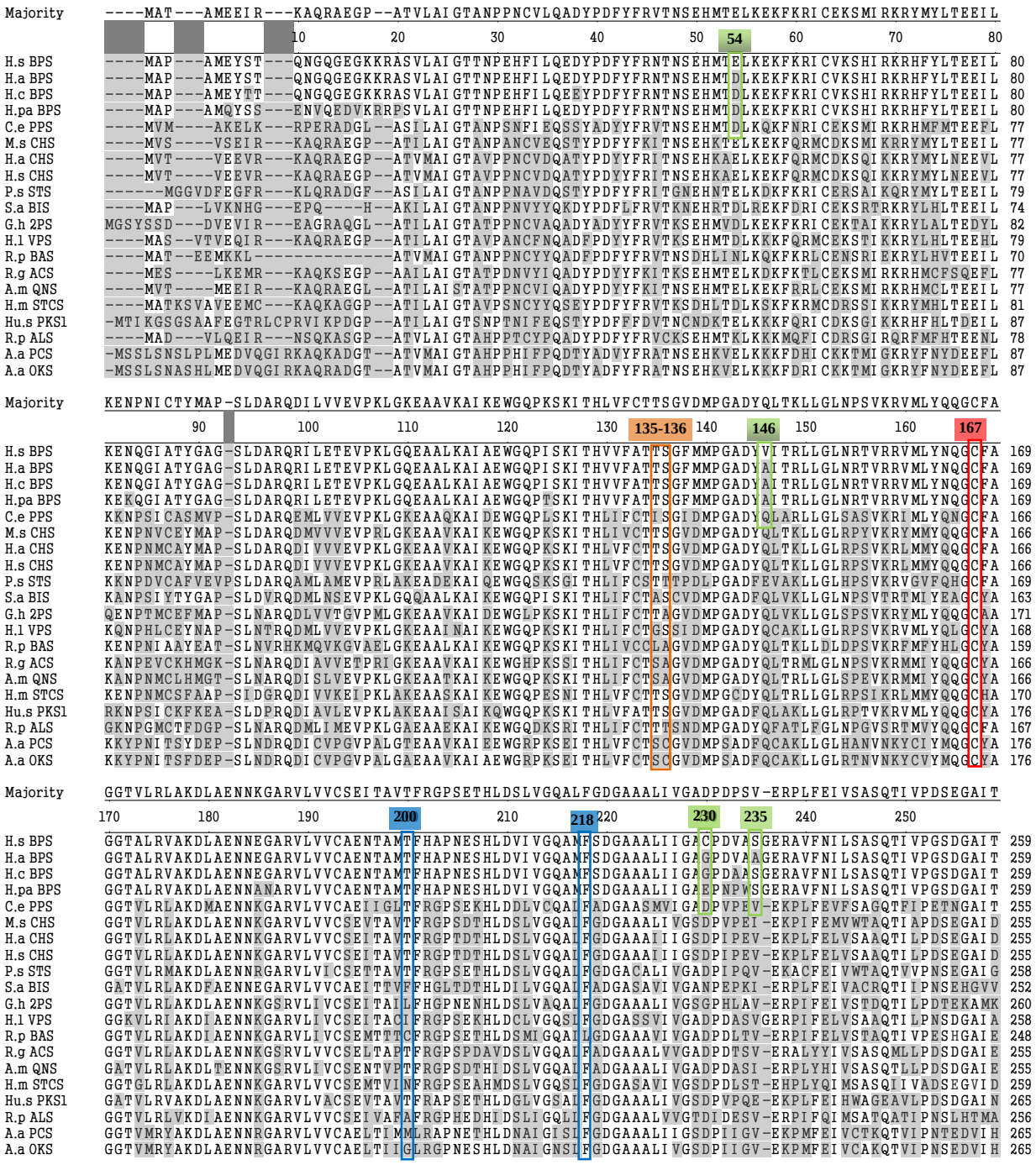
Majority
H.s BPS
H.a BPS
H.c BPS
H.pa BPS
C.e PPS
M.s CHS
H.a CHS
H.s CHS
P.s STS
S.a BIS
G.h 2PS
H.l VPS
R.p BAS
R.g ACS
A.m QNS
H.m STCS
Hu.s PKS1
R.p ALS
A.a PCS
A.a OKS
54
135-136
146
167
200
218
230
235

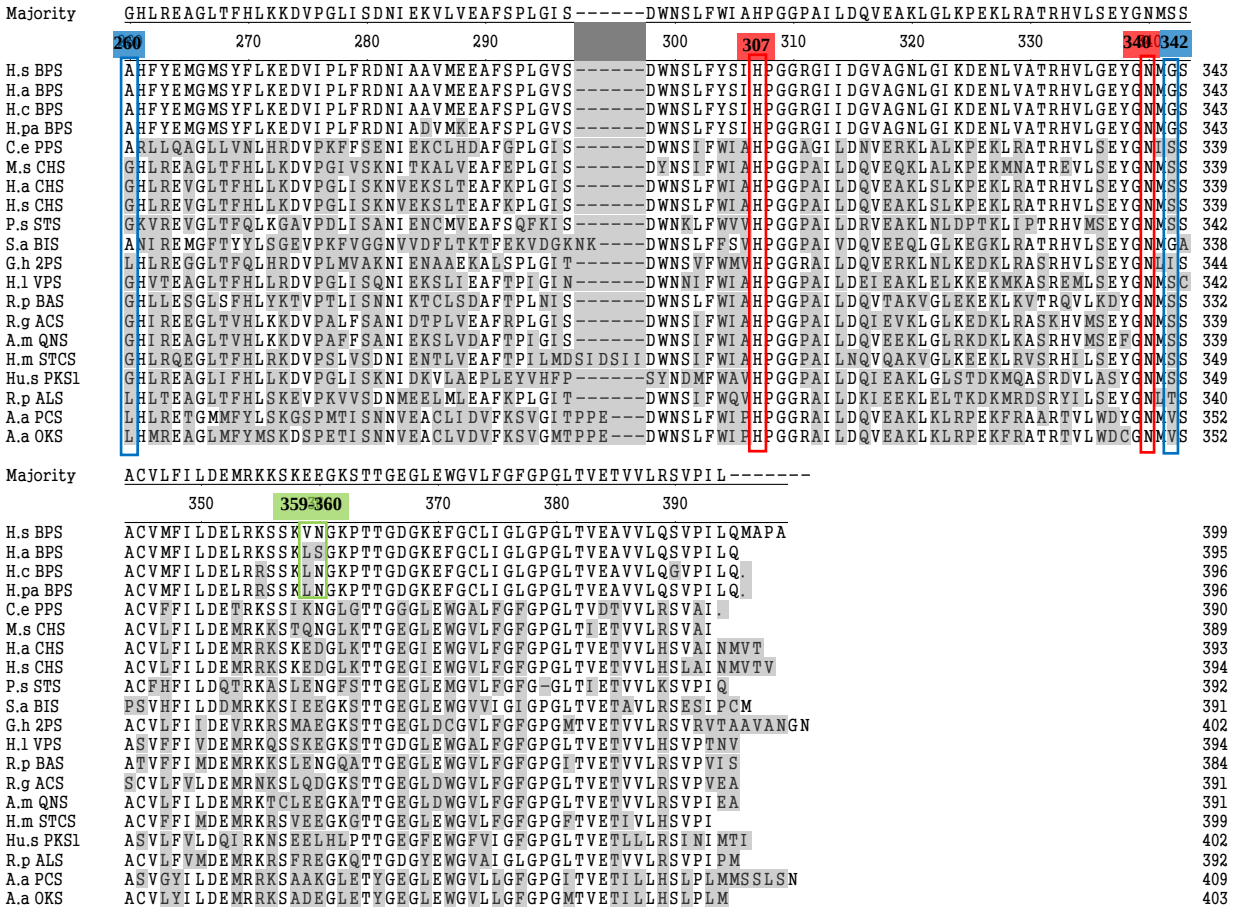

Fig. 84 Alignment of the amino acid sequences of plant type III PKSs. The catalytic triad Cys-His-Asn is colored in red. The residues lining the active-site which are important for the functional diversity of type III PKSs are highlighted in blue and orange colors. The green color represents the different amino acid residues between *H. sampsonii*, *H .androsaemum*, *H. calycinum*, and *H. perforatum* ssp *angustifolium* BPSs (numbering in *H. sampsonii* BPS). Abbreviations are summarized in (Tab. 18).

Tab. 18 Specification of PKSs used in the alignment illustrated in (Fig. 84).

Abbreviation	**Name**	**accession numbers**
H.s BPS	*Hypericum sampsonii* BPS	JQ670939
H.a BPS	*Hypericum androsaemum* BPS	AAL79808
H.c BPS	*Hypericum calycinum* BPS	
H.pa BPS	*Hypericum perforatum spp angustifolium* BPS	
C.e PPS	*Centaurium erythraea PPS*	
P.s STS	*Pinus sylvestris* STS	AAB24341
M.s CHS	*Medicago sativa* CHS2	P30074
H.s CHS	*Hypericum sampsonii* CHS	JQ670940
H.a CHS	*Hypericum androsaemum* CHS	AAG30295
S.a BIS	*Sorbus aucuparia* BIS	ABB89212
R.g ACS	*Ruta graveolens* ACS	CAC14058
A.m QNS	*Aegle. Marmelos* QNS	JX679860
G.h 2PS	*Gerbera hybrida* 2-PS	P48391
H.l VPS	*Humulus lupulus* VPS	BAA29039
R.p BAS	*Rheum palmatum* BAS	AAK82824
Hu.s PKS1	*Huperzia. serrata* PKS1	DQ979827
R.p ALS	*Rheum palmatum* ALS	AY517486
A.a PCS	*Aloe arborescens* PCS	AY823626
A.a OKS	*Aloe arborescens* OKS	AY567707

Tab. 19 Amino acid residues lining the active sites of CHS from *Medicago sativa* and BPSs from *H. sampsonii, H. androsaemum, H. calycinum,* and *H. perforatum* ssp *angustifolium*.

***M. sativa* CHS**		***Hypericum* BPSs**		***M. sativa* CHS**		***Hypericum* BPSs**	
Initiation Pocket				**Elongation Pocket**			
Leucine	214	Methionine	217	Threonine	132	Threonine	135
Isoleucine	254	Isoleucine	258	Serine	133	Serine	136
Glycine	256	Alanine	260	Threonine	194	Threonine	197
Phenylalanine	265	Tyrosine	269	Valine	196	Methionine	199
Catalytic Triad				Threonine	197	Threonine	200
Cysteine	164	Cysteine	167	Glycine	216	Serine	219
Histidine	303	Histidine	307	Leucine	263	Methionine	267
Aspragine	336	Aspragine	340	Serine	338	Glycine	342

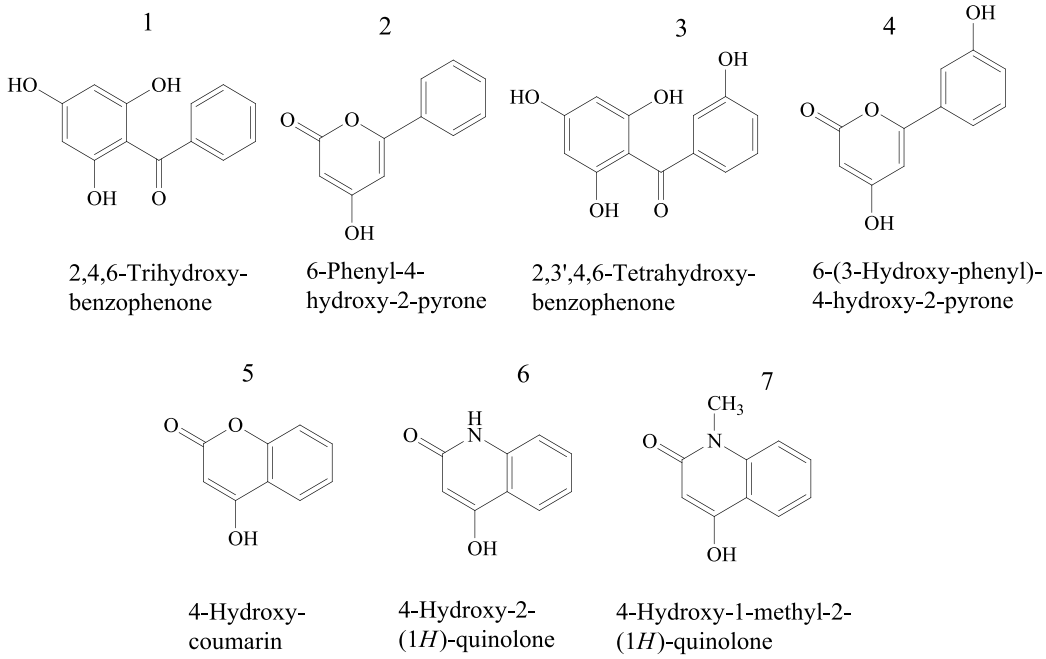

Fig. 85 Structures of the enzymatic products obtained in the present study.

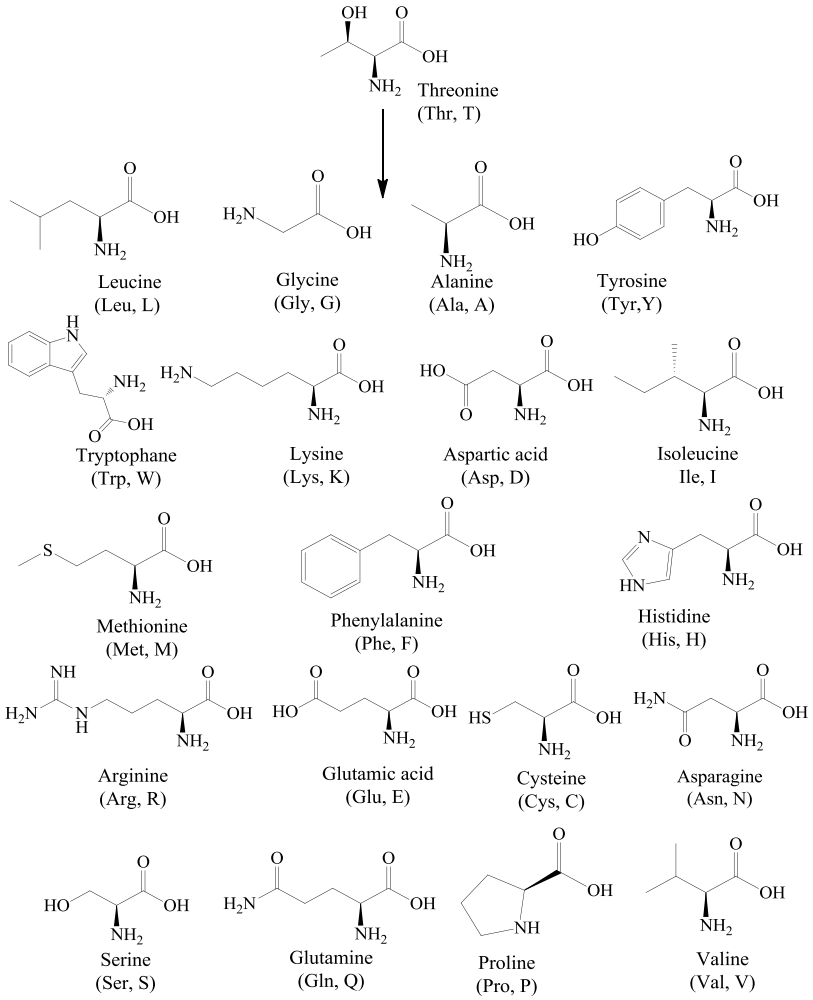

Fig. 86 Structures of the amino acids tested in HsBPS.

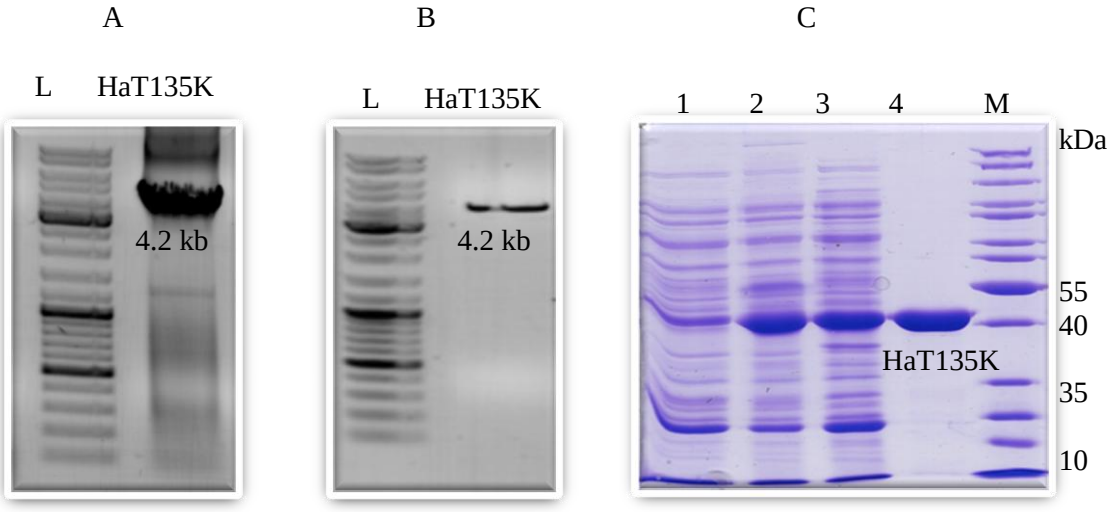

Fig. 87 Agarose gel electrophoresis of, the SDM-PCR amplification product of HaBPS lysine single mutant (A), the enzyme mutant after *Kpn*I digestion (B), L: DNA Ladder Mix (Thermo Scientific). SDS-PAGE demonstrating production in *E.col* and purification of the HaT135K mutant (C).
M: protein marker, 1: pre-induction, 2: post-induction, 3: soluble protein, 4: affinity-purified protein.

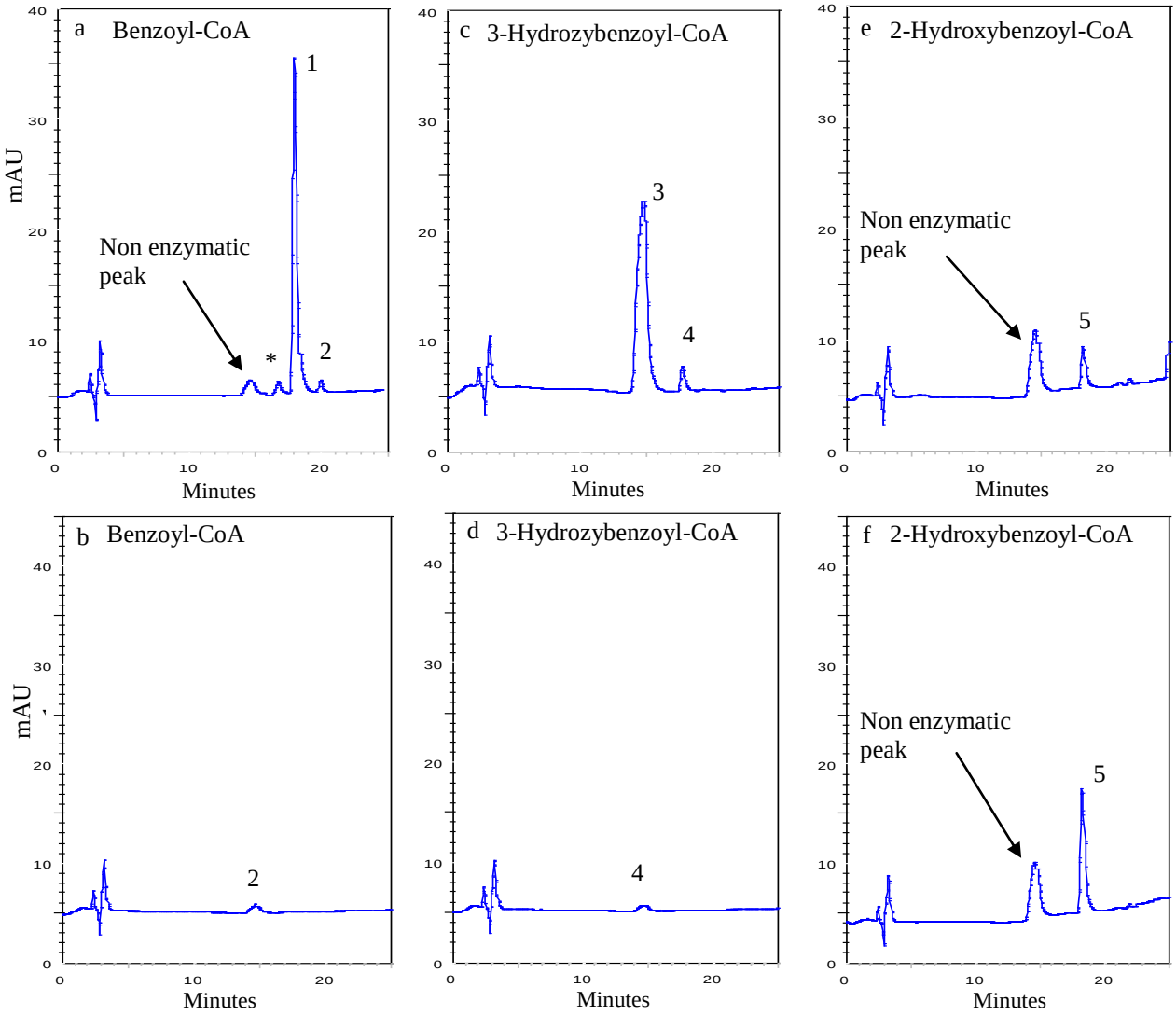

Fig. 88 HPLC chromatograms of assays of HaBPS wild-type and HaT135K with, a, b: benzoyl-CoA, c, d: 3-hydroxybenzoyl-CoA, e, f: 2-hydroxybenzoyl-CoA.
1: 2,4,6-trihydroxybenzophenone. 2: 6-phenyl-4-hydroxy-2-pyrone,
3: 2,3',4,6-tetrahydroxybenzophenone, 4: 6- (3-hydroxy-phenyl)-4-hydroxy-2-pyron,
5: 4-hydroxycoumarin.

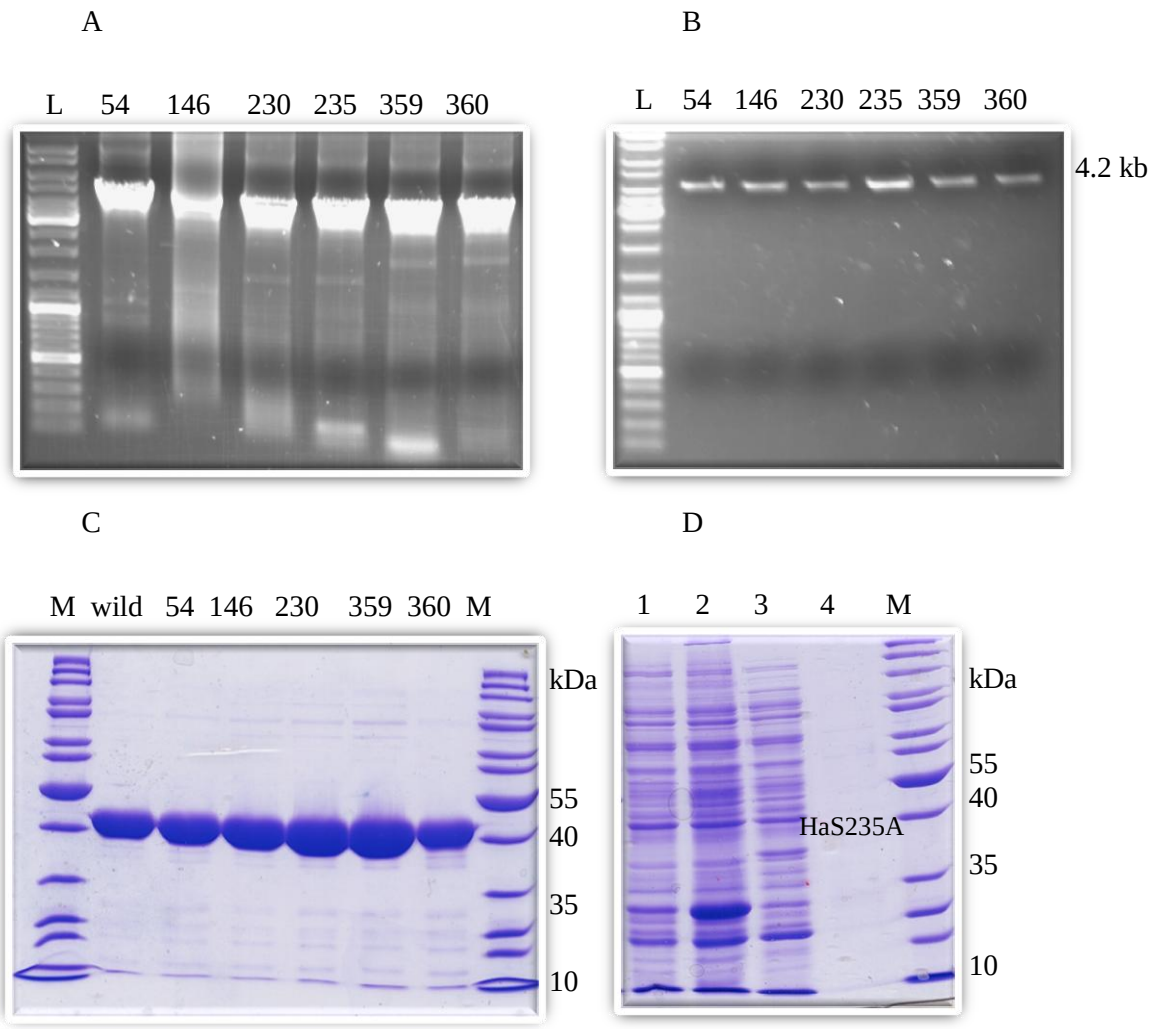

Fig. 89 A: Agarose gel electrophoresis of the SDM-PCR amplification products of HaBPS single mutants, 54: HaE54D, 146: HaV146A, 230: HaC230G, 235: HaS235A, 359: HaV359L, 360: HaN360S, B: Agarose gel electrophoresis of the HaBPS single mutants after *Kpn*I digestion, L: DNA Ladder Mix (Thermo Scientific). C: SDS-PAGE demonstrating the purification of His_6-HaBPS wild-type and mutants, wild: HaBPS wild-type, 54: HaE54D, 146: HaV146A, 230: HaC230G, 359: HaV359L, 360: HaN360S. D: SDS-PAGE for HaS235A.
M: protein marker, 1: pre-induction, 2: post-induction, 3: soluble protein, 4: affinity-purified protein.

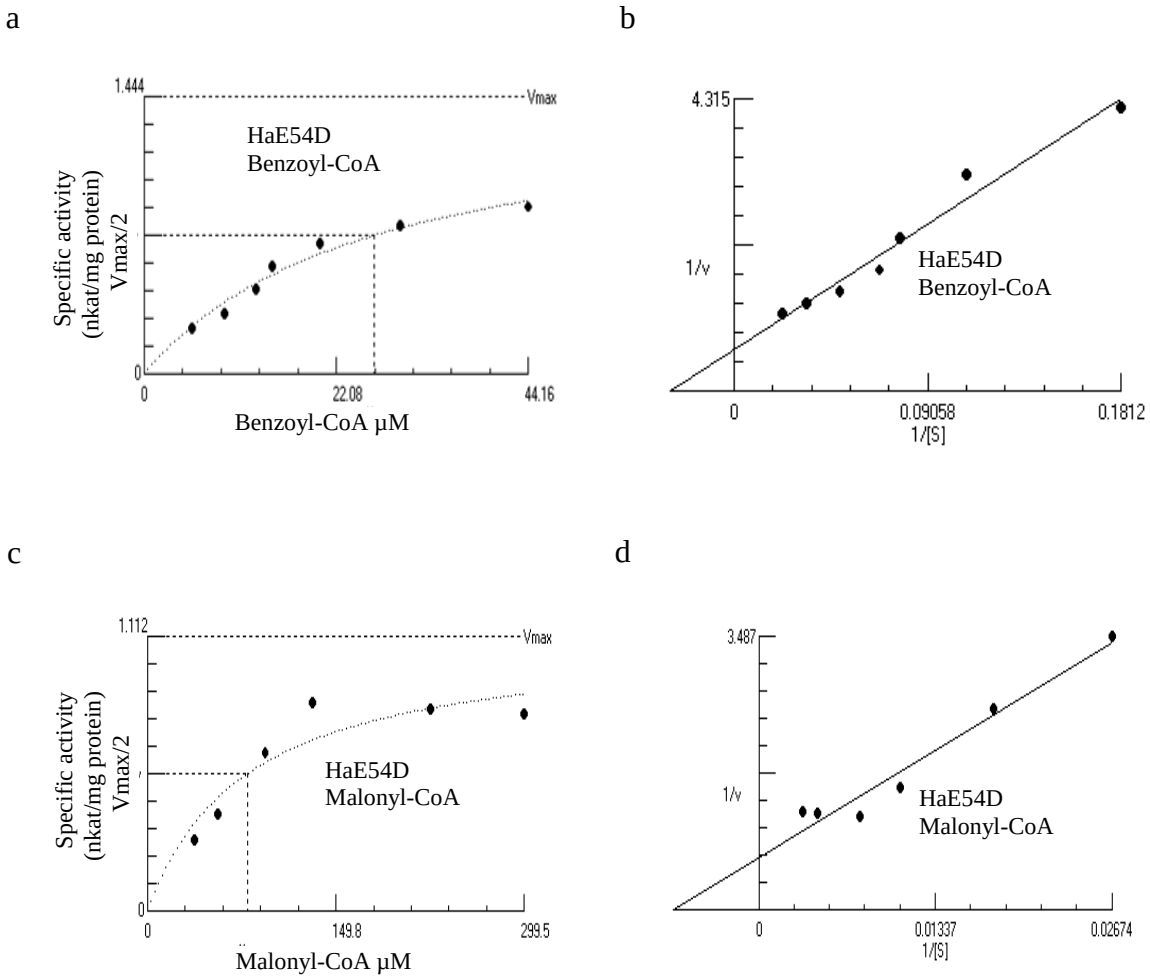

Fig. 90 a: Dependence of HaE54D activity on benzoyl-CoA concentration.
b: Determination of the K_m value for benzoyl-CoA via Lineweaver-Burk plot.
c: Dependence of HaE54D activity on malonyl-CoA concentration.
d: Determination of K_m value for malonyl-CoA via Lineweaver-Burk plot.

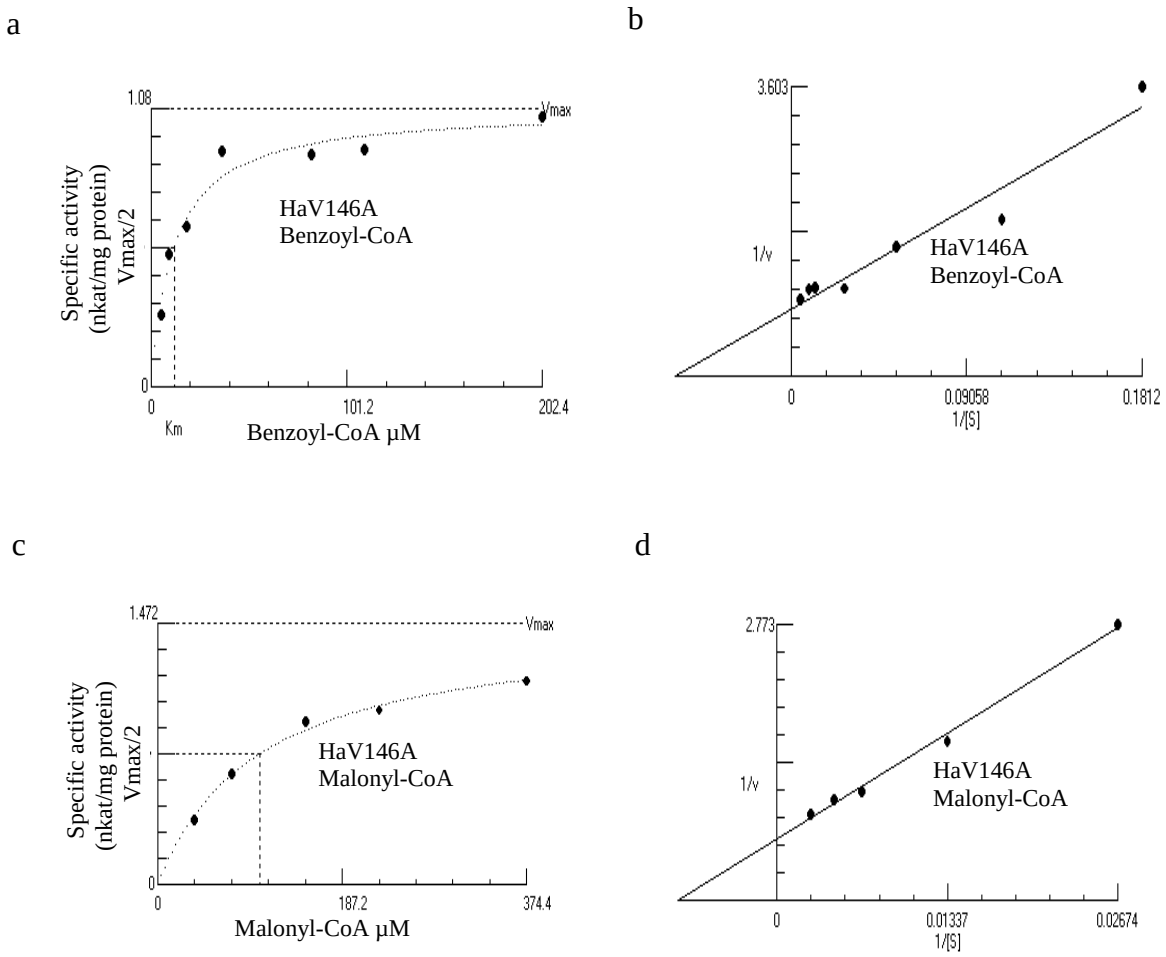

Fig. 91 a: Dependence of HaV146A activity on benzoyl-CoA concentration.
b: Determination of K_m value for benzoyl-CoA *via* Lineweaver-Burk plot.
c: Dependence of HaV146A activity on malonyl-CoA concentration.
d: Determination of K_m value for malonyl-CoA *via* Lineweaver-Burk plot.

.

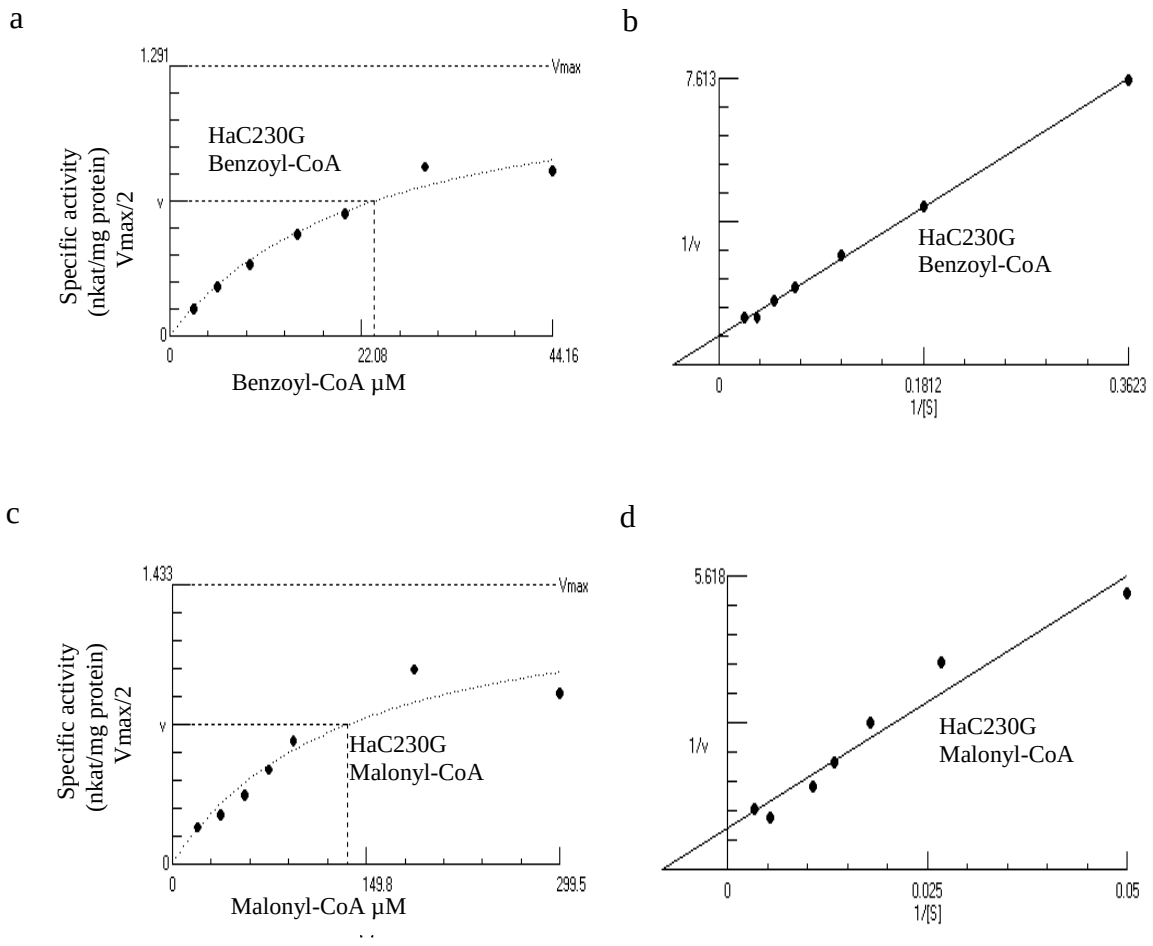

Fig. 92 a: Dependence of HaC230G activity on benzoyl-CoA concentration.
b: Determination of K_m value for benzoyl-CoA *via* Lineweaver-Burk plot.
c: Dependence of HaC230G activity on malonyl-CoA concentration.
d: Determination of K_m value for malonyl-CoA *via* Lineweaver-Burk plot.

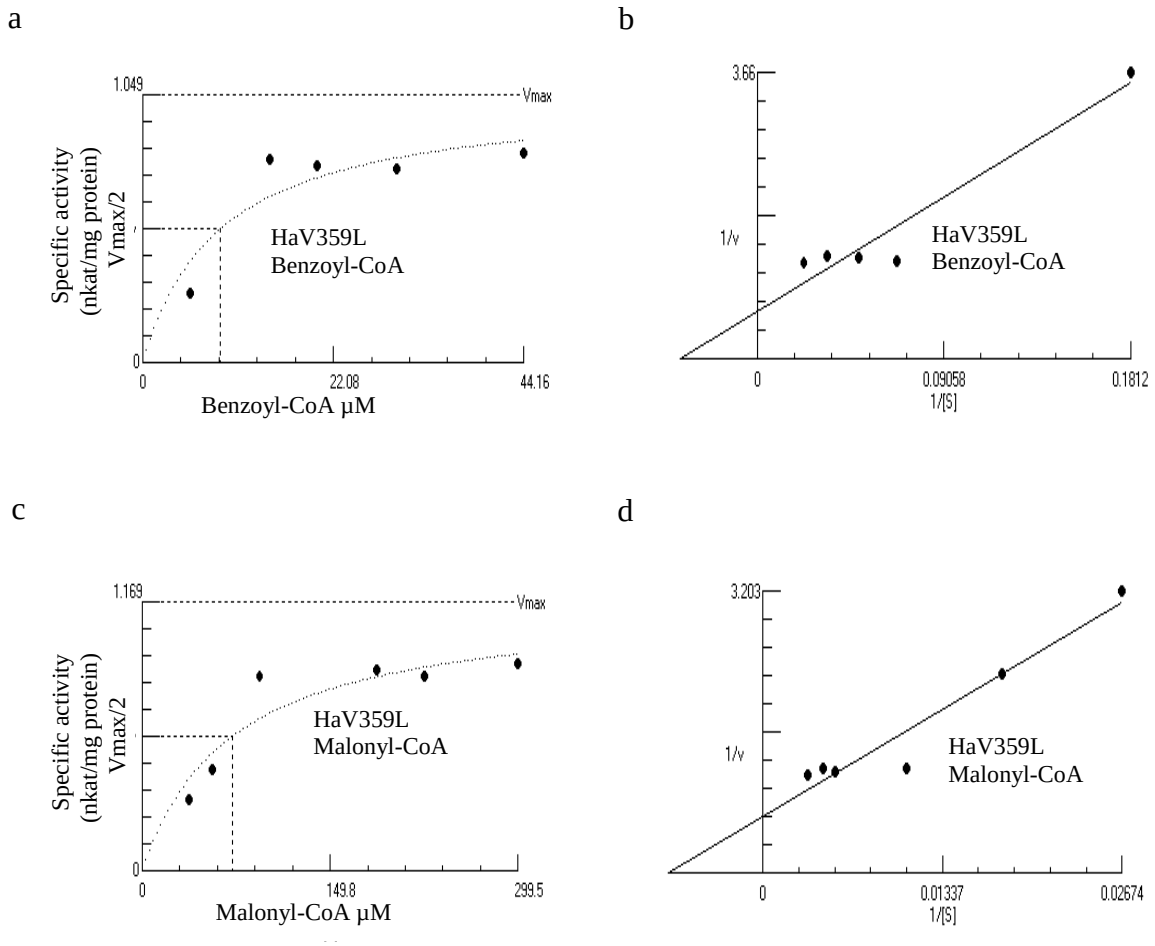

Fig. 93 a: Dependence of HaV359L activity on benzoyl-CoA concentration.
b: Determination of K_m value for benzoyl-CoA *via* Lineweaver-Burk plot.
c: Dependence of HaV359L activity on malonyl-CoA concentration.
d: Determination of K_m value for malonyl-CoA *via* Lineweaver-Burk plot.

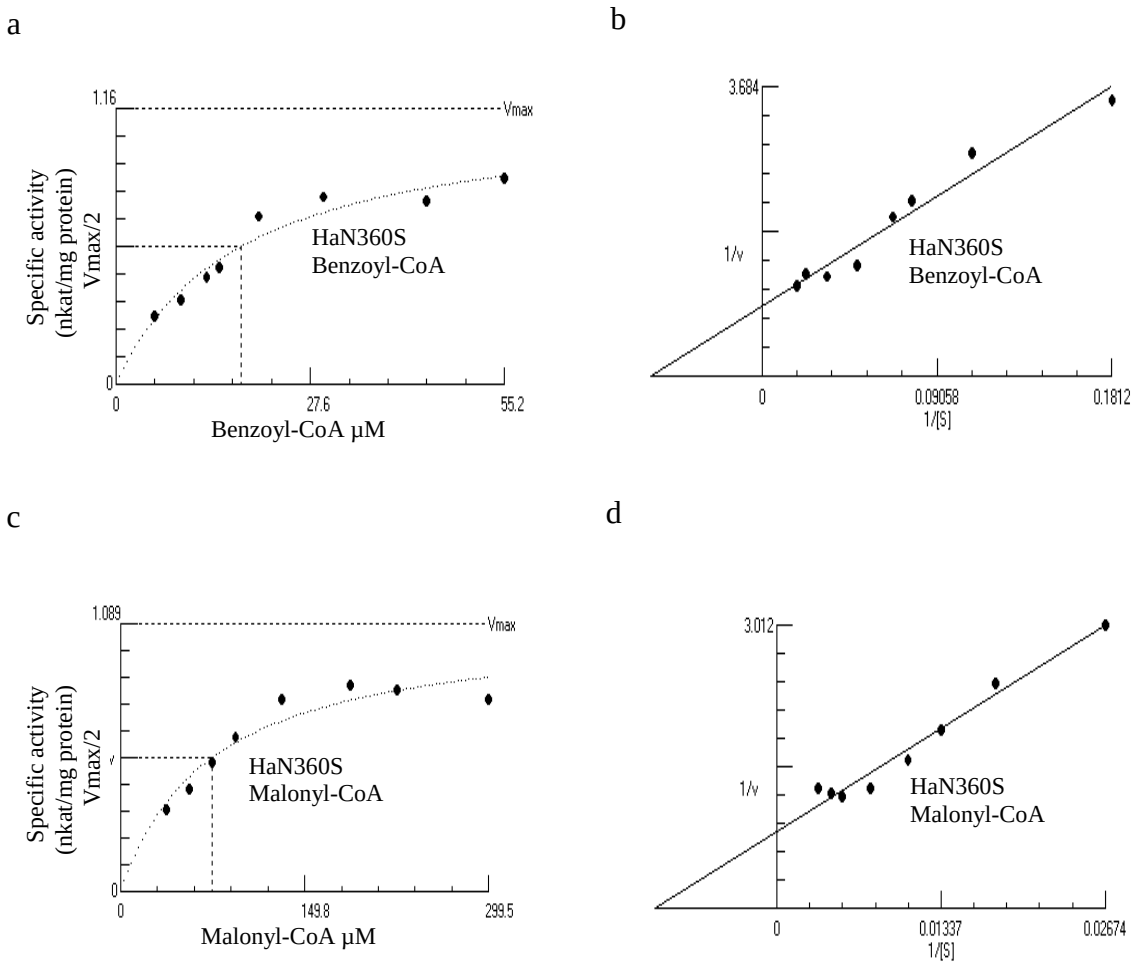

Fig. 94 a: Dependence of HaN360S activity on benzoyl-CoA concentration.
b: Determination of K_m value for benzoyl-CoA *via* Lineweaver-Burk plot.
c: Dependence of HaN360S activity on malonyl-CoA concentration.
d: Determination of K_m value for malonyl-CoA *via* Lineweaver-Burk plot.

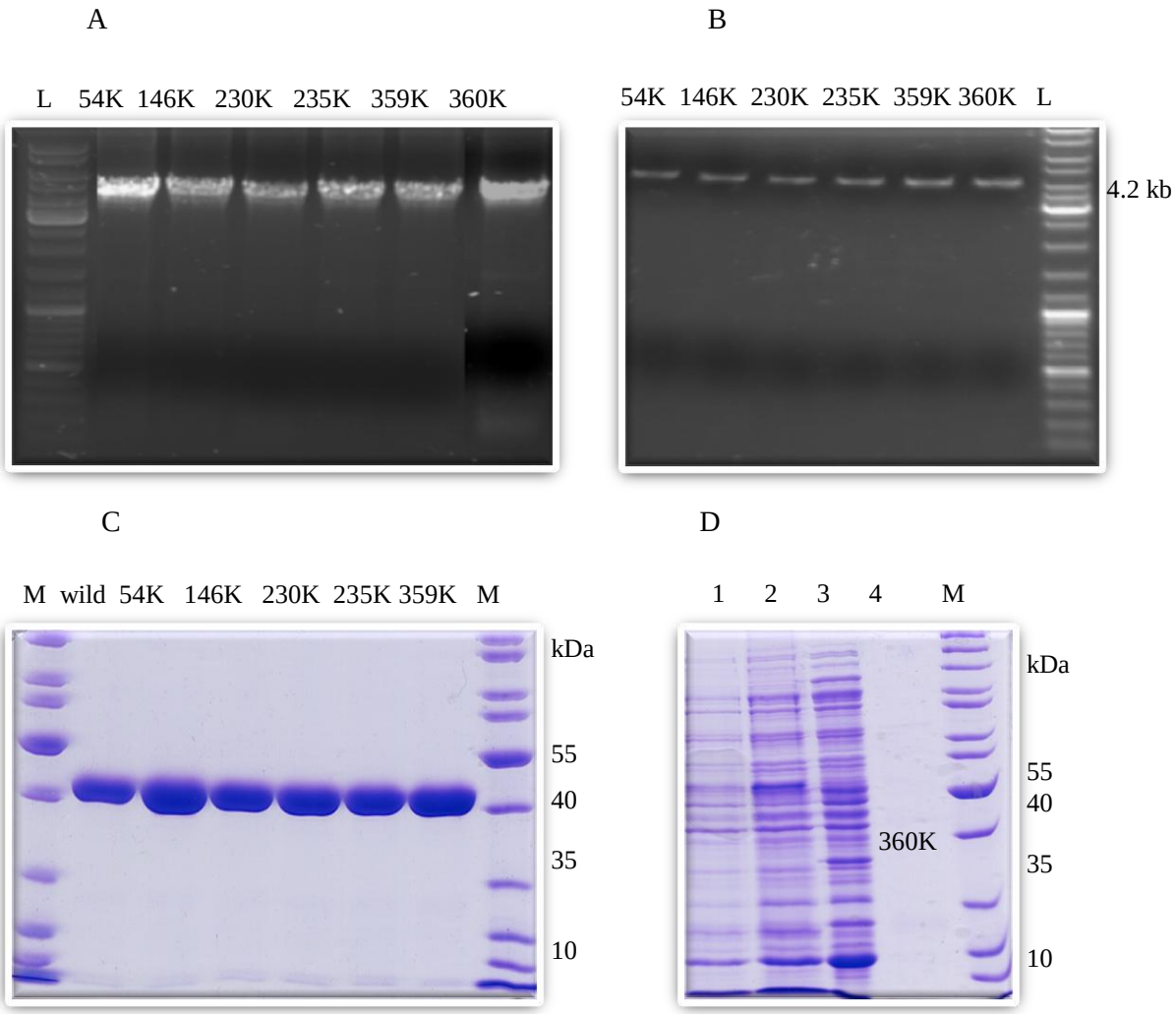

Fig. 95 A: Agarose gel electrophoresis of SDM-PCR amplification products of HaBPS lysine double mutants, 54K: HaE54D/T135K, 146K: HaV146A/T135K, 230K: HaC230G/T135K, 235K: HaS235A/T135K, 359K: HaV359L/T135K 360K: HaN360S/T135K, B: Agarose gel electrophoresis of the enzyme mutants after *Kpn*I digestion, L: DNA Ladder Mix (Thermo Scientific). C: SDS-PAGE of affinity-purified proteins, wild: HaBPS, 54K: HaE54D/T135K, 146K: HaV146A/T135K, 230K: HaC230G/T135K, 235K: HaS235A/T135K, 359K: HaV359L/T135K, D: SDS-PAGE of Ha N360S/T135K double mutant.

M: protein marker, 1: pre-induction, 2: post-induction, 3: soluble protein, 4: affinity-purified protein.

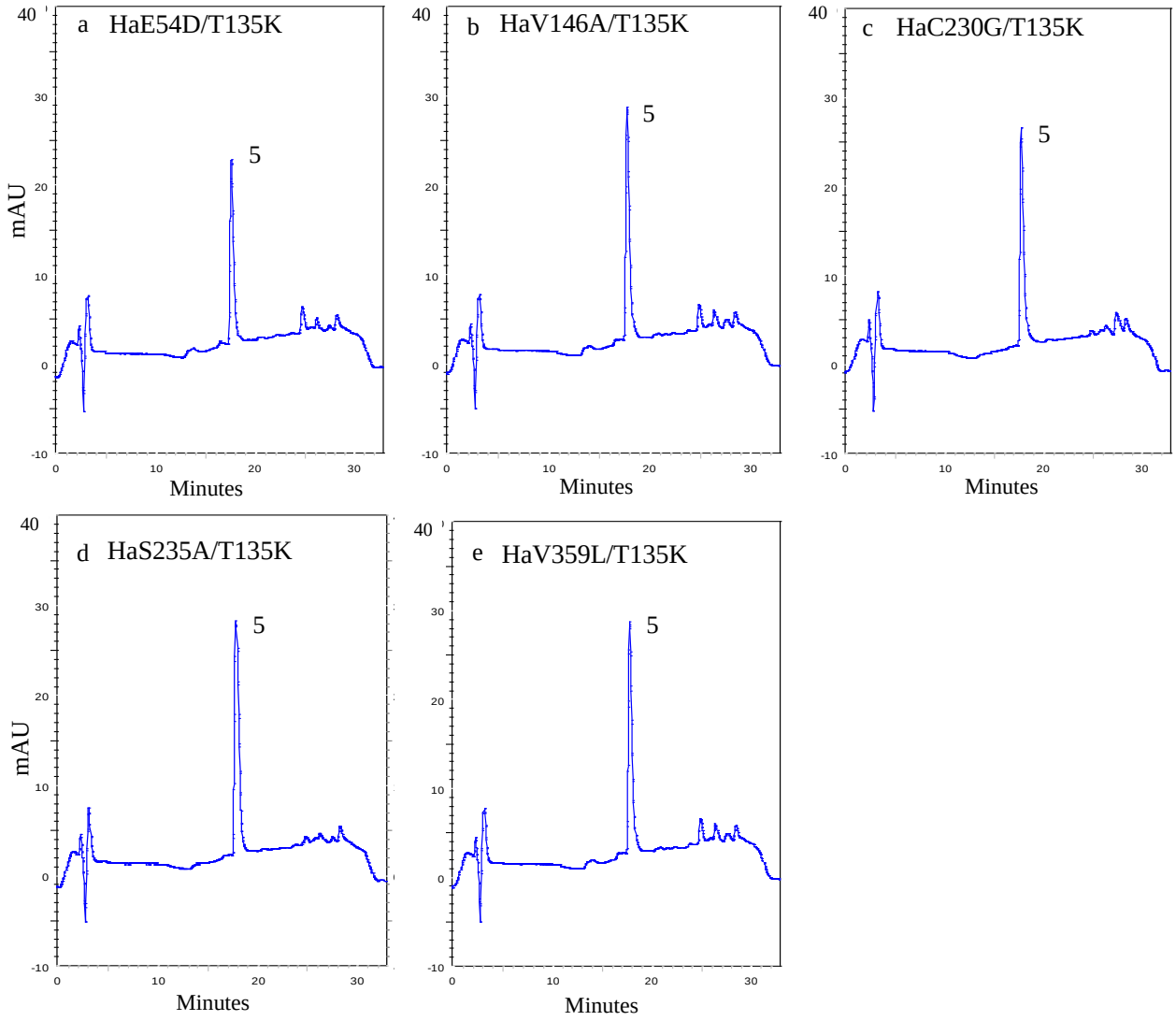

Fig. 96 HPLC chromatograms of assays of HaBPS lysine double mutants with salicoyl-CoA a: HaE54D/T135K, b: HaV146A /T135K, c: HaC230G/T135K, d: HaS235A/T135K,
e: HaV359L/T135K.
5: 4-hydroxycoumarin.

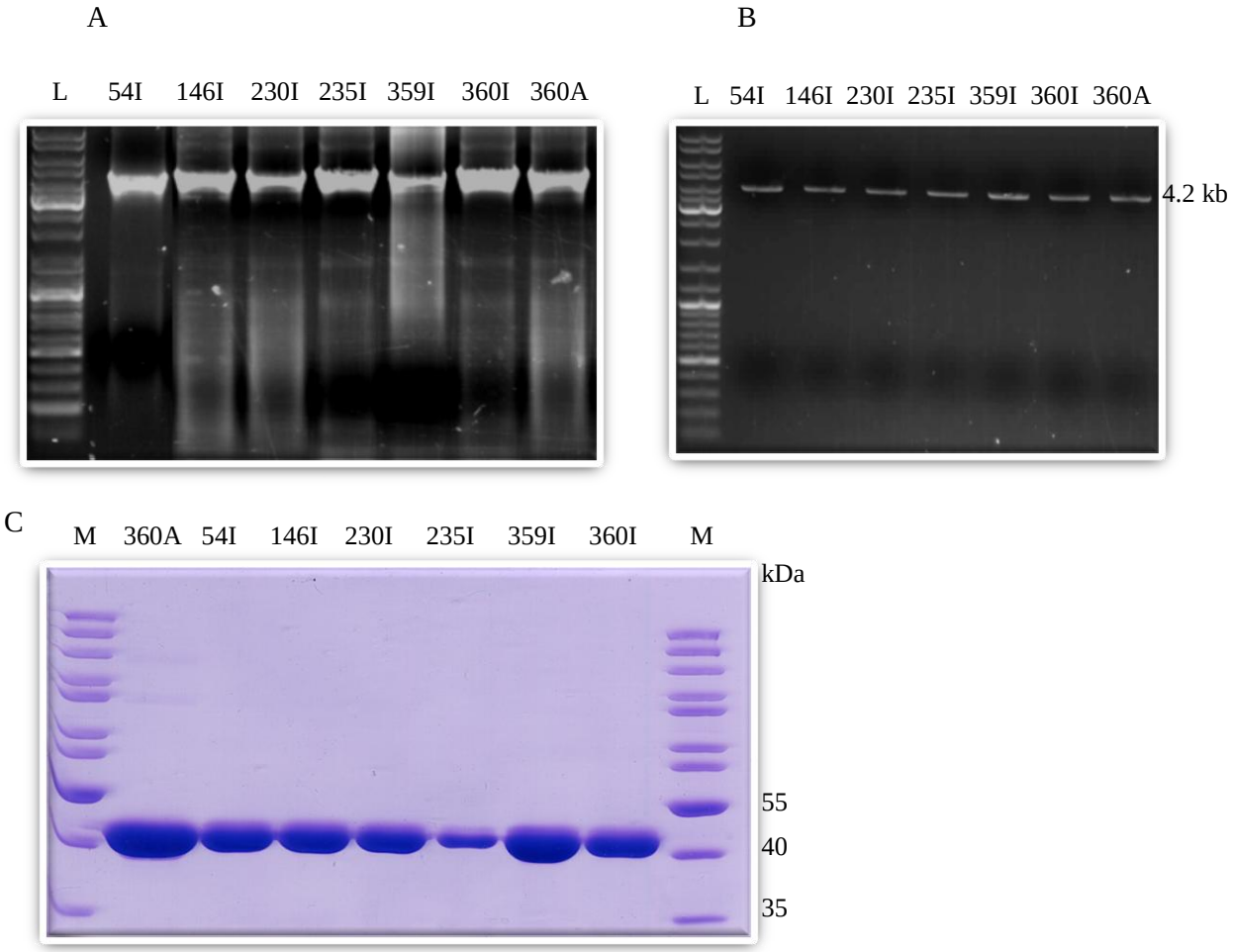

Fig. 97 Agarose gel electrophoresis of, A: SDM-PCR amplification products of isoleucine double mutants, B: the mutants after *Kpn*I digestion, L: DNA Ladder Mix (Thermo Scientific). C: SDS-PAGE of affinity-purified proteins, 360A: Ha N360S/T135A, 54I: HaE54D/T135I, 146I: HaV146A/T135I, 230I: HaC230G/T135, 235I: HaS235A/T135I, 359I: HaV359L/T135I, 360I: HaN360S/T135I.
M: protein marker, 1: pre-induction, 2: post-induction, 3: soluble protein, 4: affinity-purified protein.

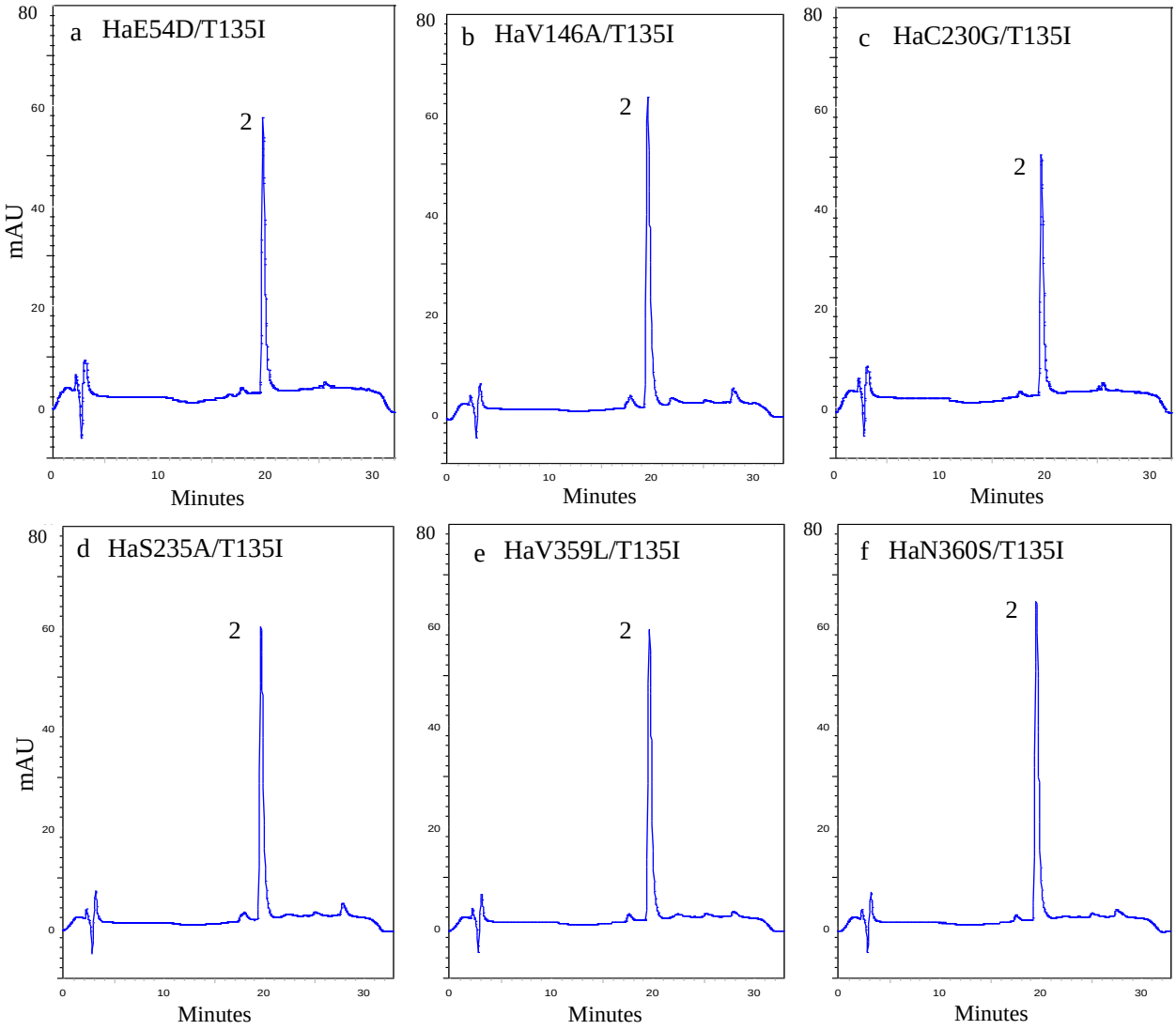

Fig. 98 HPLC chromatograms of assays of isoleucine double mutants with benzoyl-CoA a: HaE54D/T135I, b: HaV146A/T135I, c: HaC230G/T135I, d: HaS235A/T135I, e: HaV359L/T135I, f: HaN360S/T135I double mutants.
2: 6-phenyl-4-hydroxy-2-pyrone.

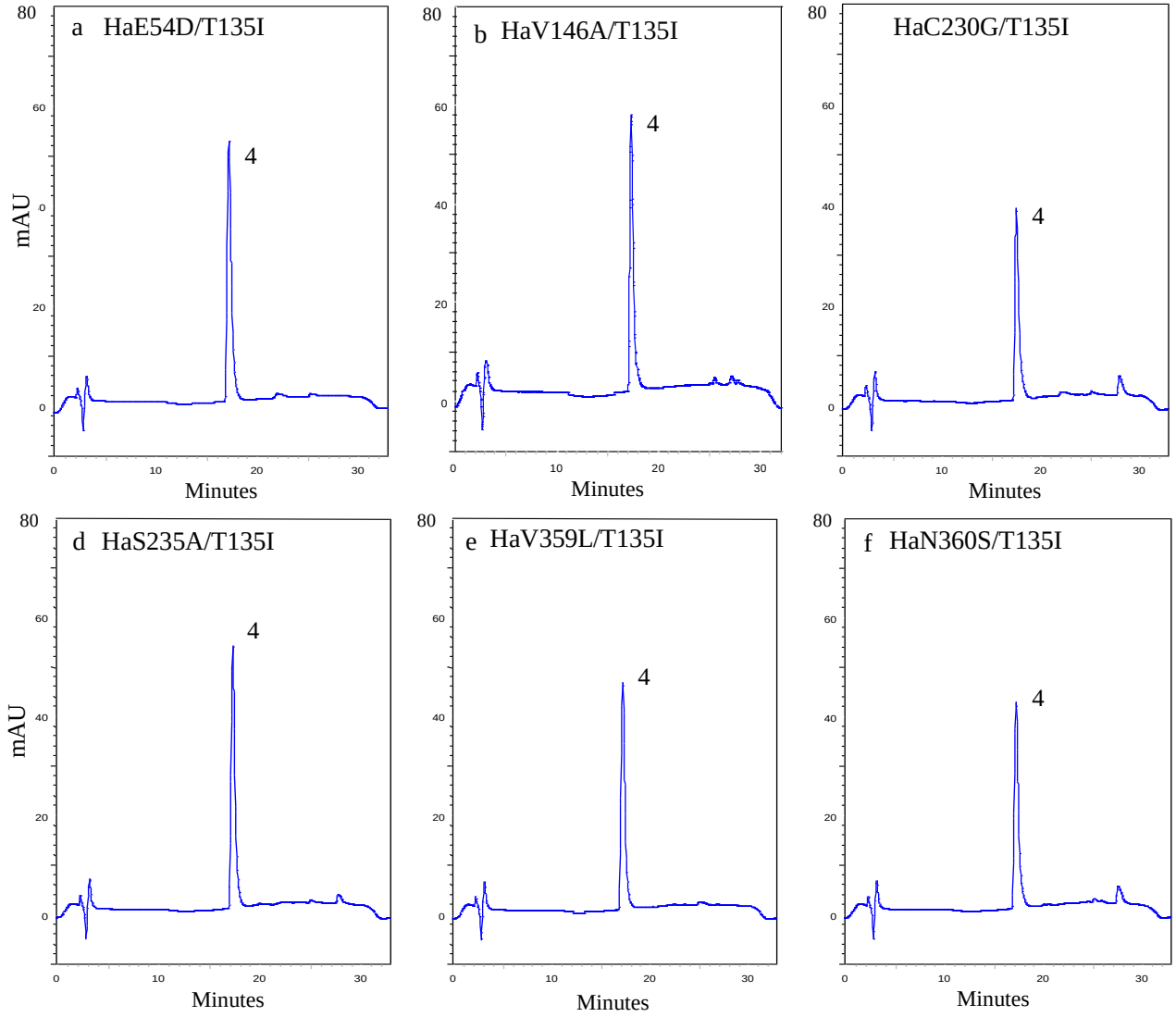

Fig. 99 HPLC chromatograms of assays of isoleucine double mutants with 3-hydroxybenzoyl-CoA, a: HaE54D/T135I, b: HaV146A/T135I, c: HaC230G/T135I, d: HaS235A/T135I, e: HaV359L/T135I, f: HaN360S/T135I double mutants.
4: 6- (3-hydroxy-phenyl)-4-hydroxy-2-pyron.

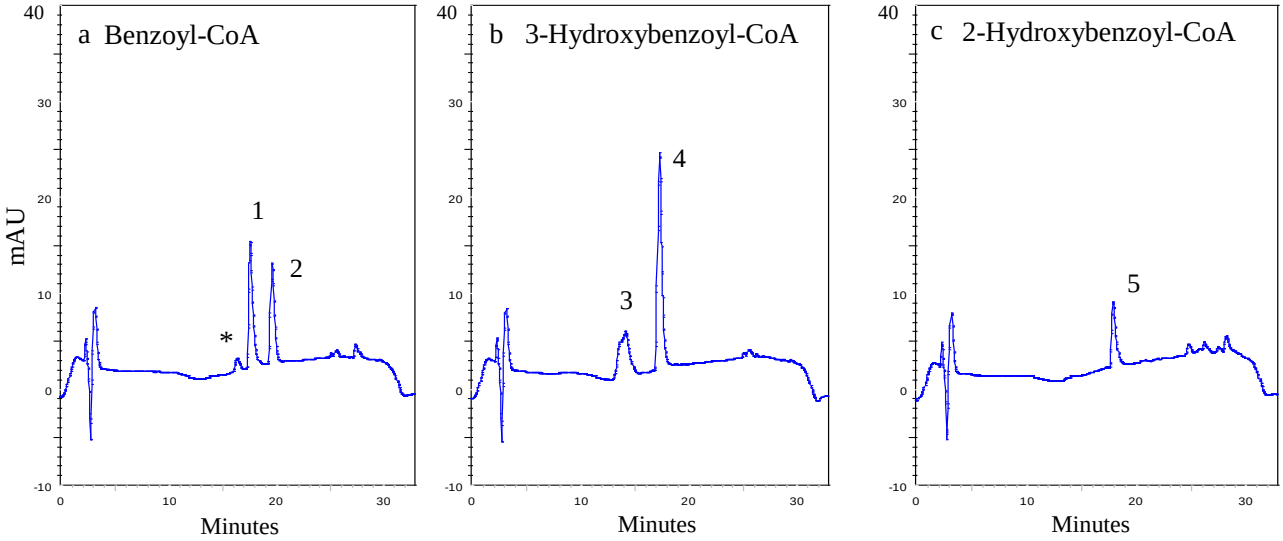

Fig. 100 HPLC chromatograms of assays of HaN360S/T135A with, a: benzoyl-CoA.
b: 3-hydroxybenzoyl-CoA.c: 2-hydroxybenzoyl-CoA.
1: 2,4,6-trihydroxybenzophenone. 2: 6-phenyl-4-hydroxy-2-pyrone, *: unidentified peak.
3: 2,3',4,6-tetrahydroxybenzophenone, 4: 6-(3-hydroxy-phenyl)-4-hydroxy-2-pyrone,
5: 4-hydroxycoumarin.

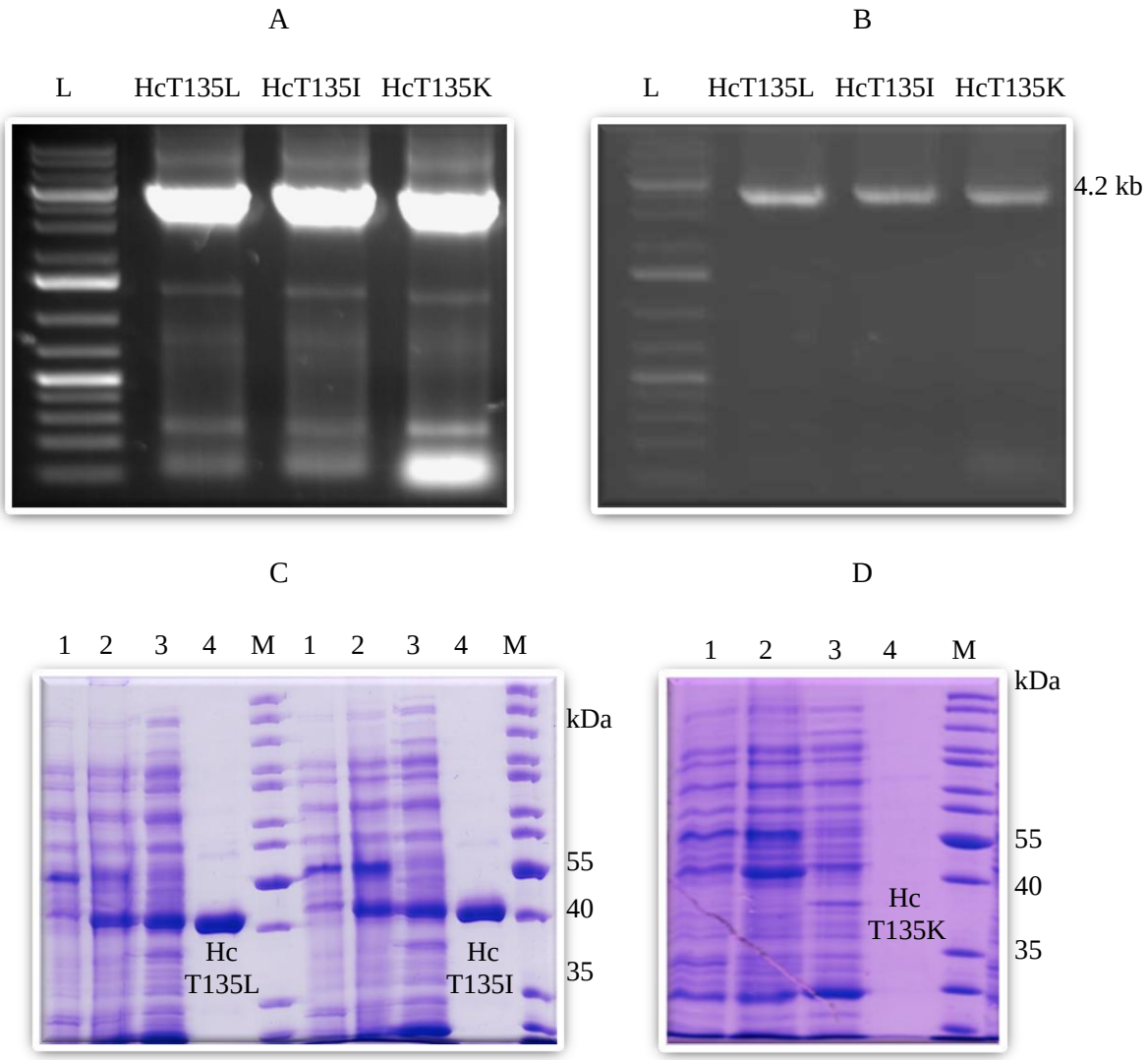

Fig. 101 Agarose gel electrophoresis of, A: SDM-PCR amplification products of HcBPS mutants, B: the enzyme mutants after *Kpn*I digestion, L: DNA Ladder Mix (Thermo Scientific), C: SDS-PAGE demonstrating His_6- HcT135L and HcT135I mutants, D: SDS-PAGE demonstrating His_6-HcT135K mutant.
M: protein marker, 1: pre-induction, 2: post-induction, 3: soluble protein, 4: affinity-purified protein.

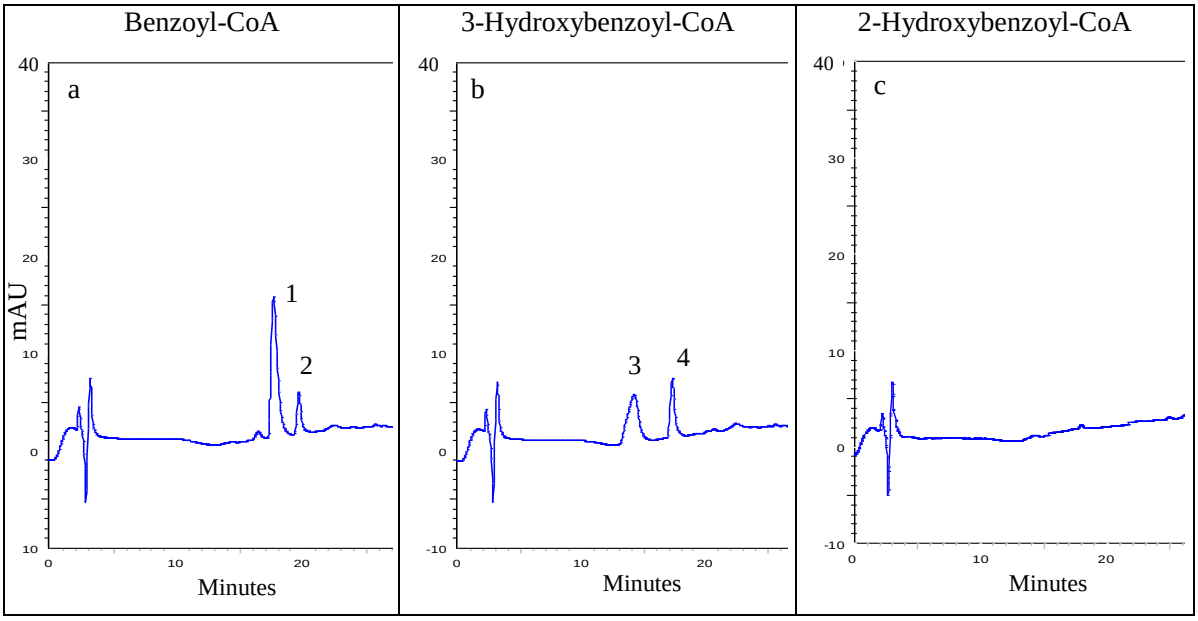

Fig. 102 HPLC chromatograms of assays of HcBPS wild-type with, a: benzoyl-CoA.
b: 3-hydroxybenzoyl-CoA. c: 2-hydroxybenzoyl-CoA.
1: 2,4,6-trihydroxybenzophenone, 2: 6-phenyl-4-hydroxy-2-pyrone,
3: 2,3',4,6-tetrahydroxybenzophenone, 4: 6-(3-hydroxy-phenyl)-4-hydroxy-2-pyrone.

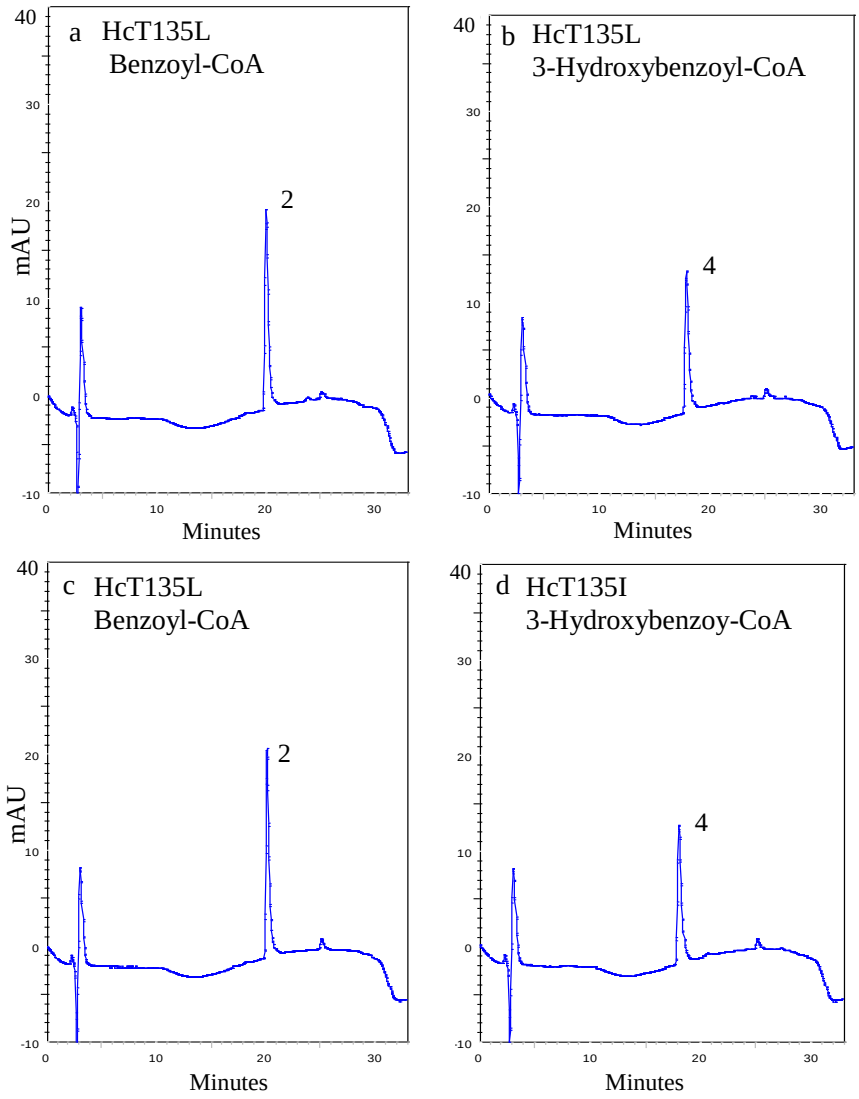

Fig. 103 HPLC chromatograms of assays of HcT135L and HcT135I mutants with a, c: benzoyl-CoA. b, d: 3-hydroxybenzoyl-CoA.

2: 6-phenyl-4-hydroxy-2-pyrone, 4: 6-(3-hydroxy-phenyl)-4-hydroxy-2-pyrone.

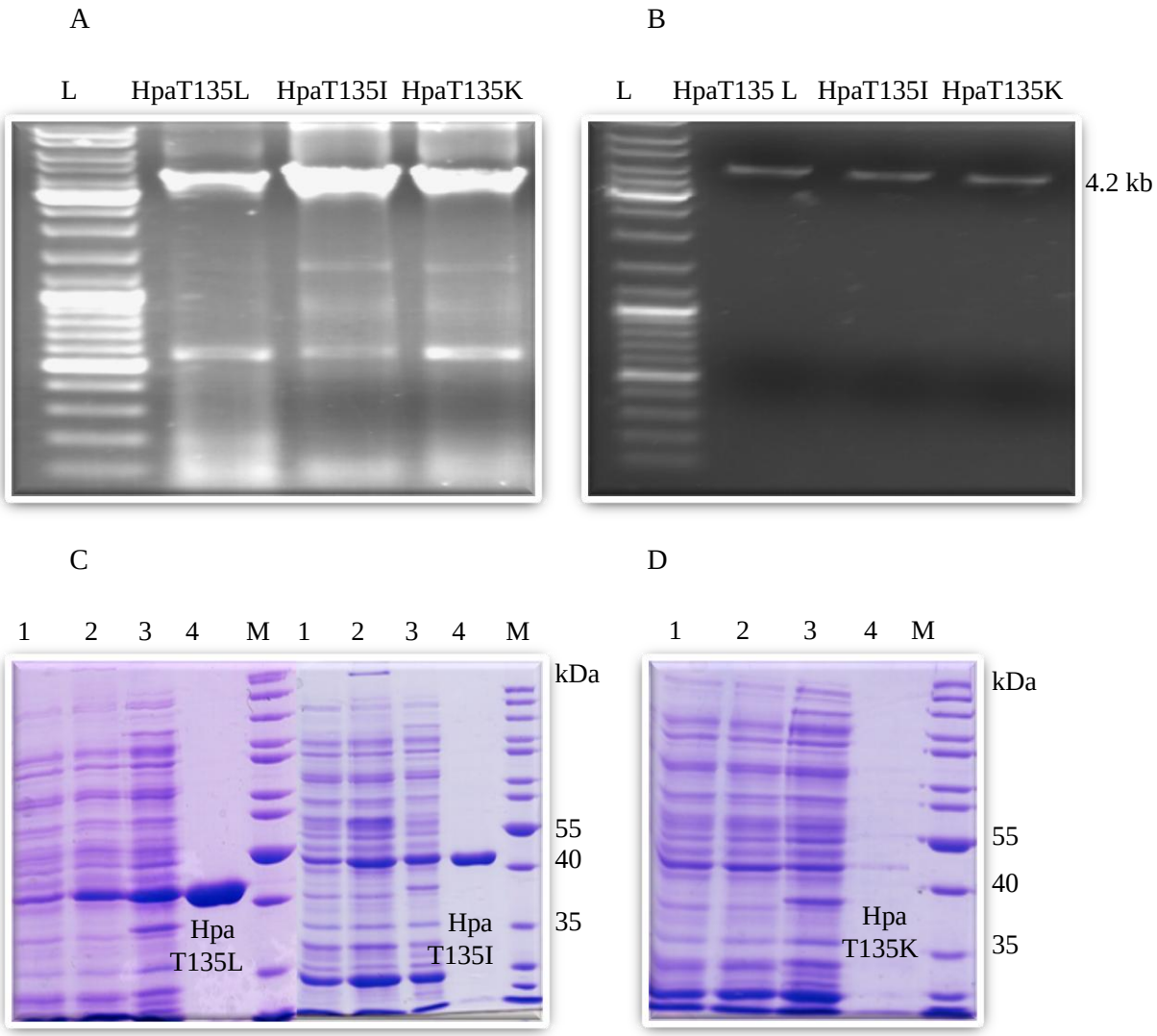

Fig. 104 Agarose gel electrophoresis of, A: SDM PCR amplification products of HpaBPS mutants, B: the mutants after *Kpn*I digestion, L: DNA Ladder Mix (Thermo Scientific). C: SDS-PAGE demonstrating HpaT135L and HpaT135I enzyme mutants, D: SDS-PAGE illustrating HpaT135K mutants.
M: protein marker, 1: pre-induction, 2: post-induction, 3: soluble protein, 4: affinity-purified protein.

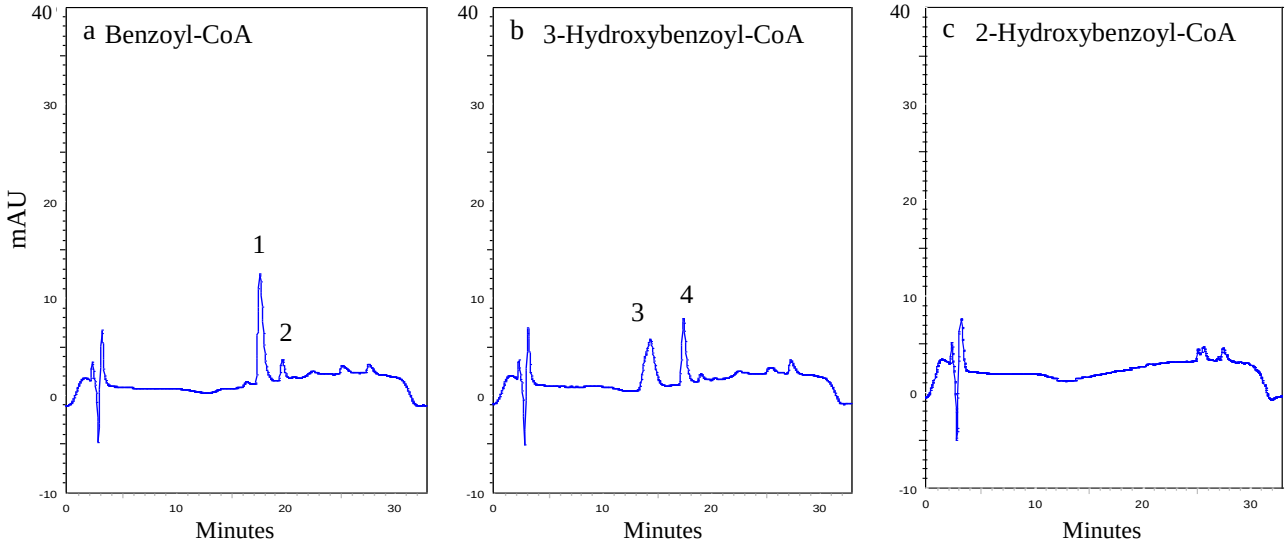

Fig. 105 HPLC chromatograms of assays of HpaBPS wild-type with, a: benzoyl-CoA. b: 3-hydroxybenzoyl-CoA. C: 2-hydroxybenzoyl-CoA.

1: 2,4,6-trihydroxybenzophenone.2: 6-phenyl-4-hydroxy-2-pyrone,

3: 2,3',4,6-tetrahydroxybenzophenone, 4: 6-(3-hydroxy-phenyl)-4-hydroxy-2-pyrone.

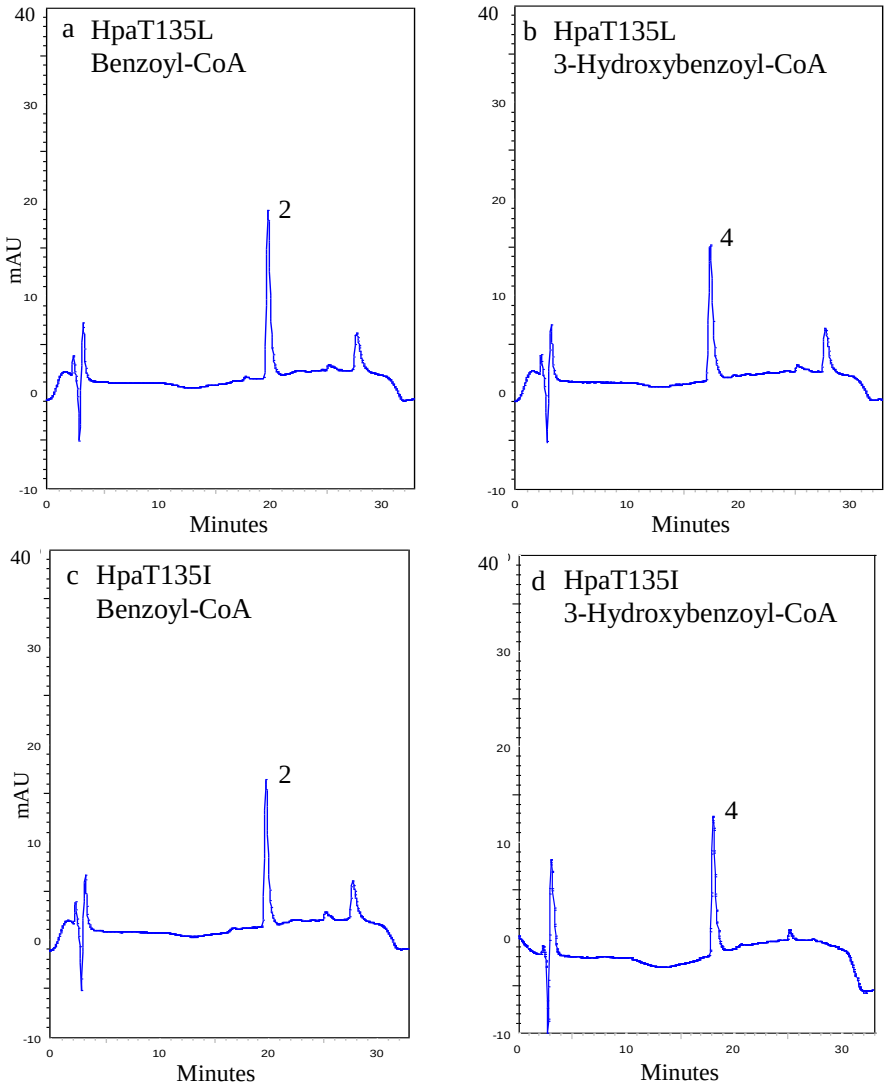

Fig. 106 HPLC chromatograms of assays of HpaT135L and HpaT135I mutants with a, c: benzoyl-CoA. b, d: 3-hydroxybenzoyl-CoA.

2: 6-phenyl-4-hydroxy-2-pyrone, 4: 6-(3-hydroxy-phenyl)-4-hydroxy-2-pyrone.

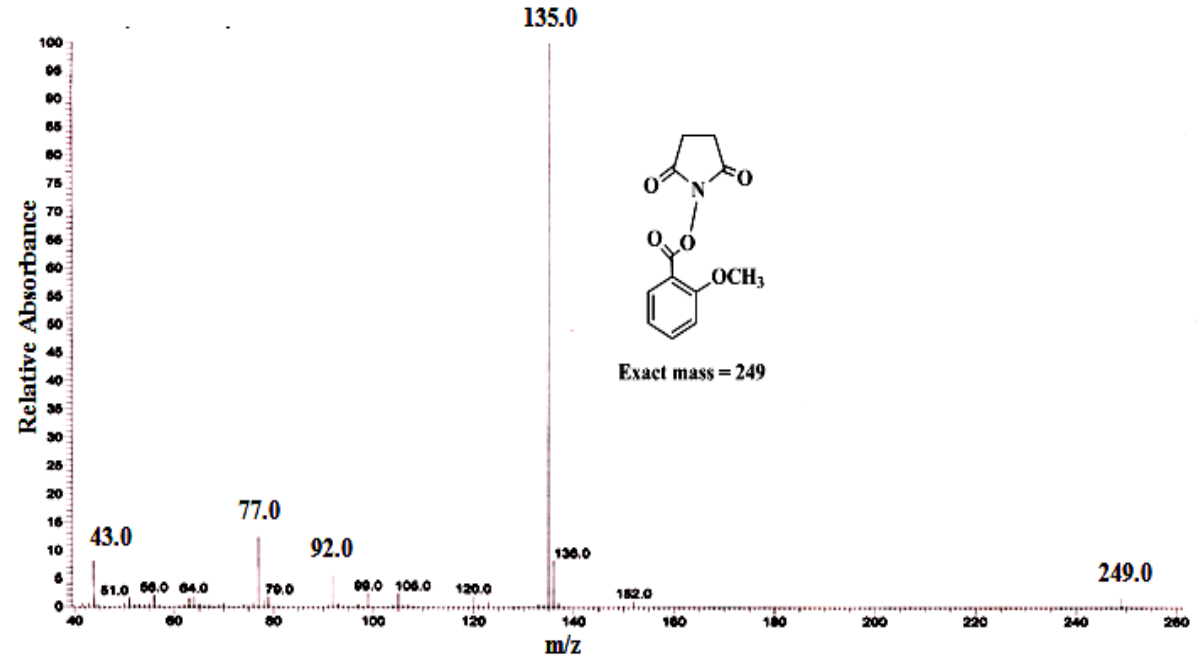

Fig. 107 Mass spectra of 2-methoxybenzoyl-*N*-hydroxysuccinimide ester.

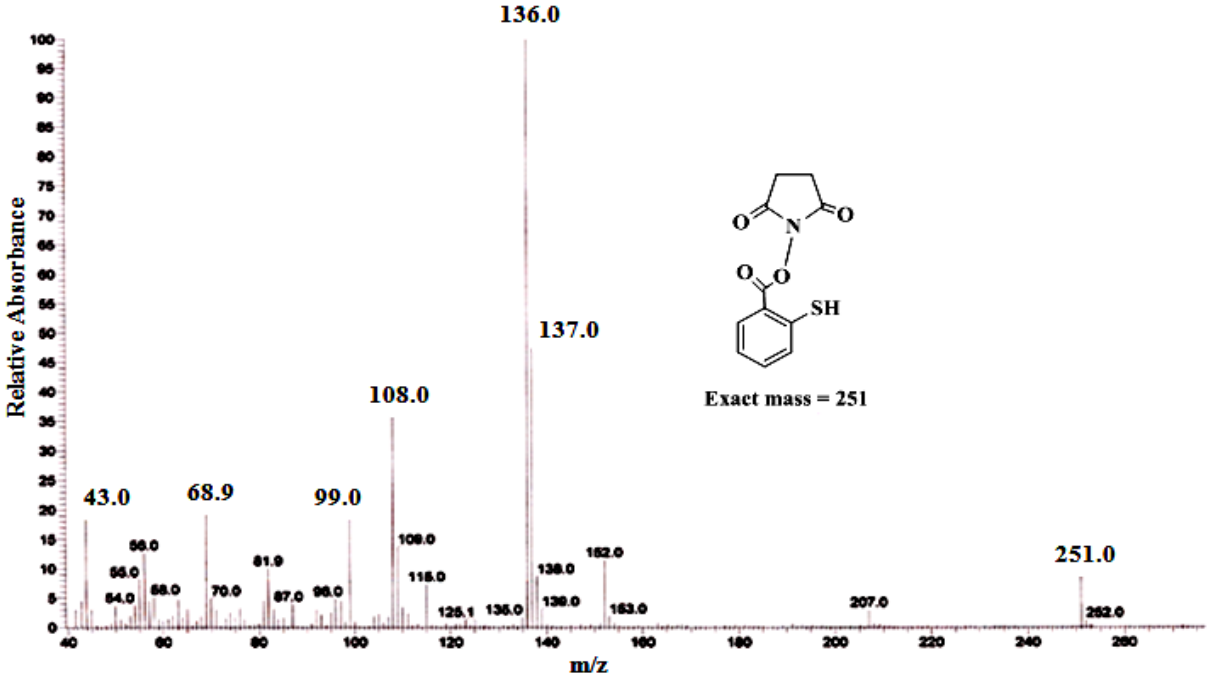

Fig. 108 Mass spectra of 2-mercaptobenzoyl-*N*-hydroxysuccinimide ester.